The University of Sheffield

Prediction, Diagnosis and Prevention of Fouling in Seawater Reverse Osmosis Membrane Systems

A Thesis Submitted to the University of Sheffield

By

Ibrahim M. El-Azizi

For the Degree of Doctor of Philosophy

Project Supervisor:

Dr. Robert G. J. Edyvean

Chemical and Process Engineering Department

October - 2009

ABSTRACT

The performance of pre-treatment and reverse osmosis (RO) membrane systems of a reverse osmosis (SWRO) desalination plant was evaluated using both in-*situ* fouling monitoring methods and theoretical standardisation and normalisation methods. The results showed that overall performance of the plant deteriorated after 6 months of operation due to fouling. In order to determine the identity and cause of the fouling two SWRO membranes were subjected to destructive membrane autopsy. The results showed formation of severe fouling on the surface of both membranes. Microscopic studies using atomic force microscopy (AFM) and scanning electron microscopy (SEM) with Energy Dispersion X-ray spectrometer (EDX), elucidated this layer. AFM, SEM and EDX results showed different types of fouling includes scaling, colloidal and biological fouling. The presence of these foulants on the membrane surfaces indicates malfunctions in the pre-treatment systems used in the plant, ultimately resulting in the formation of composite fouling. The effect of this composite fouling on the performance of the RO membrane systems was investigated using a laboratory-scale RO unit and raw seawater samples from the Mediterranean and the North Seas. A rapid flux decline was observed. In order to eliminate the formation of the composite fouling in the RO membrane systems, a novel fouling prevention method was examined. This was a depth filter (Disruptor^{TM}) made of nanoalumina fibres upstream to the RO membranes. The results show that this depth filter removes the majority of substances which cause the fouling on the RO membranes. Results are discussed in relation to the practicalities of desalination plant operation.

ACKNOWLEDGEMENTS

I would like to express my sincerest gratitude to my academic supervisor, Dr. Robert J. G. Edyvean for his support, guidance, and friendship during this research.

I am deeply grateful to Dr Bashir Ashhuby for his support and advice, Achim Schmalenberger, Dr. Robert Bachman, Jesus Ojeda, Kieran Baker, John Heneghan and Andrew Fairburn from Kroto Institute for their assistance in FTIR, contact angle and ICP-MS measurements.

I would like to expresses my sincerest appreciation to the head of the Tajoura Research Centre and Rodney Komlenic from Ahlstrom Company for their help and support. I am also grateful to all the staff of the Tajoura SWRO desalination plant, Libya for providing data, membranes and information.

I would like to acknowledge to Ahlstrom Filtration LLC, USA and Amazon Filtration Ltd, UK for providing filters, Disruptors and supporting this study.

I would like to express my special thanks to my wife and children for their patience and support. Finally I will be forever grateful to Allah.

Thank You All

TABLE OF CONTENTS

LIST OF FIGURES

List of Tables

Nomenclature

A	= membrane surface area
AFM	= Atomic force microscopy
ASTM	= the American Standard for Testing Materials (ASTM)
ATR-FTIR	= attenuated total reflection-Fourier transform infrared spectroscopy.
a_i	= the activity of i species in solution
BWRO	= Brackish water reverse osmosis
CA	= Cellulose acetate
C_f	= Feed water concentration ($mg.L^{-1}$)
C_p	= Permeate water concentration ($mg.L^{-1}$)
C_c	= Concentrate water concentration ($mg.L^{-1}$)
C_B	= Bulk concentration ($mg.L^{-1}$)
C_p	= Permeate concentration ($mg.L^{-1}$)
C_w	= concentration at the membrane wall
C_{fcs}	= Standard feed – concentrate concentration ($mg.L^{-1}$)
C_{fa}	= Actual feed concentration ($mg.L^{-1}$)
C_{fs}	= Feed concentration ($mg.L^{-1}$)
C_{fc}	= average feed and concentrate concentration ($mg.L^{-1}$).
C_i	= concentration of all constituents in a solution ($g.mol.\ m^{-3}$)
CF	= Cartridge filter
CF	= Concentration factor
CFU	= Colony forming unit
cm^2	= Square Centimetre
D	= Diffusion coefficient ($m.s^{-1}$)
EDX	= the energy dispersive X-ray spectrometer.
EPS	= Extra cellular polysaccharides
FTIR	= Fourier Transformation Infrared Spectrophotometer
FA	= Fulvic acid
HA	= Humic acid
HSDM	= Homogenous Solution Diffusion method
ICP-MS	= inductively coupled plasma spectrometer

IC = Ion chromatography

ID = Inside diameter

I_f = Ionic strength of feed water

I_c = Ionic strength of concentrate water

IP_C = Ion product

J_N = Normalized permeate flux ($ml.cm^{-2}.ml^{-1}$).

J = Membrane flux ($l.m^{-2}.h^{-1}$)

J_0 = Initial permeate flux ($ml.cm^{-2}.ml^{-1}$).

J_a = Actual permeate flux ($ml.cm^{-2}.ml^{-1}$).

J_S = Standard permeate flux ($ml.cm^{-2}.ml^{-1}$).

J_s = Salt flux through the membrane ($m.s^{-1}$)

J_w = Permeate flux produced by reverse osmosis membrane ($l.m^{-2}.hr^{-1}$)

K = Mass transfer coefficient

Kev = Kilo electron volt

K_w = Membrane permeability coefficient for water ($m^3.hr^{-1}.m^{-2}.bar^{-1}$)

K_S = Membrane permeability coefficient for salt ($m.s^{-1}$)

K_{sp} = Thermodynamic solubility product

LSI = Langelier Saturation Index

MF = Microfiltration

MMF = Multimedia filter

m_i = Molal concentration of ion ($mol.kg^{-1}$)

MW_i = Molecular weight of ion

NDP = Net driving pressure (bar)

NDP_a = Net driving pressure at the actual condition (bar)

NDP_s = Net driving pressure at the standard condition (bar)

NF = Nano-filtration

NTU = Nephlometric Turbidity Unit

OD = Outside diameter

PA = Polyamide

PCA = Plate count agar

P_f = feed pressure (bar)

P_c = Concentrate pressure (bar)

P_p = Permeate pressure (bar)

pH = Power of hydrogen

PSI = Pound per square inch

Q_p = Product flow rate ($m^3.h^{-1}$)

Q_f = Feed flow rate ($m^3.h^{-1}$)

Q_c = Concentrate flow rate ($m^3.h^{-1}$)

Q_{NPF} = the normalized permeate flow ($m^3.d^{-1}$)

R_a = the arithmetic surface roughness

R_{ms} = the geometric mean of surface roughness

R = Universal gas constant 8.314 kPa $m^3.g^{-1}$ mol^{-1}.

R2A = agar medium

RO = Reverse osmosis

SDI = Silt Density index

SEM = Scanning electron microscopy

SR = Salt rejection (%)

SP = Salt passage (%)

SP_a = the actual salt passage (%)

S&DSI = Stiff and Davis stability index

Sr = Supersaturation ratio

SUVA = Specific ultraviolet absorbance ($l.m^{-1}.mg^{-1}$)

SWRO = Seawater reverse osmosis

t_0 = Initial time to collect 500 ml of water sample

t_f = Time to collect 500 ml of water sample

T = Time of the test (min).

T = Temperature (^oK or ^oC))

TFC = Thin film composite

TFC = temperature correction factor (dimensionless)

TCF_a = Temperature correction factor at the actual condition

TCF_s = Temperature correction factor at the standard condition

TDS = Total dissolved solids ($mg.L^{-1}$)

TEP	= Transparent exopolymers particles ($mg.L^{-1}$)
TOC	= Total organic carbon ($mg.L^{-1}$)
TSS	= Total suspended solids ($mg.L^{-1}$)
U	= Temperature coefficient depending on the membrane material.
UF	= Ultrafiltartion
UV	= Ultraviolet absorbance (m^{-1})
Y	= Recovery or conversion (%)
XPS	= X-Ray photoelectron Spectroscopy
XRD	= X-Ray Diffract meter
W_0	= the weight of empty crucible
W_{T1}	= the weight of crucible and sample heated at 100 °C.
W_{T2}	= the weight of crucible and sample heated at 550 °C.
Z_i	= Number of ions formed if the solute dissociates (dimensionless)

Greek letters

μS	= microsiemens
μm	= micrometer
ΔP	= the hydraulic pressure differential across the membrane (bar)
ΔC	= Salt concentration differential across the membrane ($mg.L^{-1}$)
$\Delta\pi$	= osmotic pressure differential across membrane
π	= osmotic pressure
π_p	= permeate osmotic pressure (bar)
π_{fc}	= average feed-concentrate water osmotic pressure (bar)
μ_i	= the chemical potential non-ideal solution
μ_0	= the chemical potential of pure ions at standard state
σ	= the Staverman reflection coefficient.
δ	= Thickness of the boundary layer

Subscription

a	= actual operating data
b	= bulk
c	= Concentrate
f	= feed
fc	= Feed – concentrate
i	= ion
N	= Normalised
p	= Permeate
s	= Salt permeability
s	= standard operating data
w	= membrane wall
w	= water permeability

CHAPTER 1

INTRODUCTION

1.1 Background

Reverse osmosis (RO) is widely applied to purify brackish water, seawater and the production of ultra-pure water for industrial and pharmaceutical applications. Despite the advantages of RO membrane technology, membrane fouling is always considered as a serious operational problem that deteriorates the performance of the membrane filtration systems (Hu, *et al.*, 2005 and Flemming, *et al.*, 1997). Fouling is "a condition resulting in loss of performance of a membrane due to the deposition of suspended and/or dissolved substances on its surface, at its pore openings or within its pores" (Lee, *et al.*, 2000; Koros, *et al.*, 1996; Lin, *et al.*, 2005).

During the operation of an RO membrane plant, several types of fouling can occur on the membrane surfaces such as inorganic fouling, organic fouling, colloidal fouling and biological fouling "biofouling" (Herzbereg and Elimelech, 2007; Schaule, *et al.*, 1999; Kumar, *et al.*, 2006). Fouling causes a need to increase operating pressure, and chemical cleaning which both reduce the membrane life. There is also an increase in energy consumption and thus the cost of RO plant operation (Vrouwenvlder and Van der Kooij, 2002; Pontie, *et al.*, 2005; Xu, *et al.*, 2006). In order to maintain the operating performance of a full scale seawater reverse osmosis (SWRO) plant, it is essential to control fouling, which demands an establishment of a comprehensive and practical program of testing and checking of fouling and scaling potential under normal operation conditions (Saad, 2004; Vrouwenvelder, *et al.*, 2003). Destructive autopsy of RO membranes has been very important to identify the type and cause of membrane fouling and to evaluate alternative cleaning procedures (Al-Amoudi and Farooque, 2005; Darton, *et al.*, 2004; Schneider, *et al.*, 2005; Shon, *et al.*, 2009).

In order to control fouling in RO membrane systems it is necessary to understand the individual system. This requires the establishment of a comprehensive and practical program of testing and checking of fouling and scaling potential under normal operation conditions (Vrouwenvelder and van der Kooij, 2001). This program should include

measurements of turbidity and silt density index (SDI) on a regular basis as well as physical inspection and culturing techniques (e.g. incubation and direct count methods) to monitor biological activity in a plant system. Operating data normalisation and destructive study (autopsy) on RO membranes is very important to identify the type and cause of membrane fouling and evaluate altenative cleaning procedures (Saad, 2002; Vrouwenvelder, *et al.*, 2003)

Numerous studies have been carried out for fouling reduction in SWRO desalination plants; however membrane fouling is still far from being solved. In absence of effective pre-treatment practices, different types of fouling may occur and deteriorate the performance of RO membrane systems in short operating periods. Various *in Situ* and theoretical techniques have been suggested by many researchers to predicate fouling in full scale SWRO desalination plants. The research described here therefore, aims to study the accuracy of the commonly used *in Situ* and theoretical methods in predicting fouling, determining its true identity by carrying out a membrane autopsy and to develop an appropriate method for its prevention. The Tajoura SWRO desalination plant was selected as case-study for this research.

1.2 The Tajoura Seawater Reverse Osmosis Desalination Plant

The Tajoura seawater reverse osmosis (SWRO) desalination plant is the biggest RO deslaination plant in Libya and located about 30 km east of Tripoli, Figure 1.1.

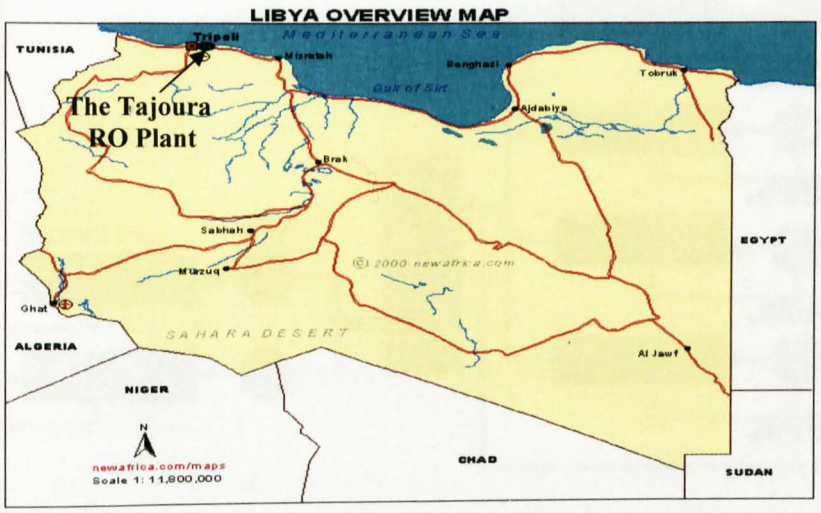

Figure 1.1: Location of the *Tajoura SWRO desalination Plant.*

The plant was designed and built by a German Company (Deutscher Verfahrenstechink) in 1983, to produce high quality waters for drinking and industrial purposes. It utilises a double pass of spiral wound polyamide thin film composite RO membranes. The first pass utilises polyamide SWRO membranes to desalt seawater while the second pass utilised BWRO membranes for further desalt the product from the first pass to produce high quality industrial water. The plant uses two SWRO membrane passes and one BWRO membrane pass during the period between 1984 and 1999. Since, 1999 and thereafter the first pass of SWRO membranes was directly used for converting seawater to potable water with conductivity in the average of 500 $\mu S\ cm^{-1}$, while the second pass was kept to be used to produce higher purity water. The plant consists of the following main components; intake system, pre-treatment unit, main treatment system, post-treatment system and storage reservoir (El-Azizi and Omran, 2002; Abufayed, 2003) (Figure 1.2).

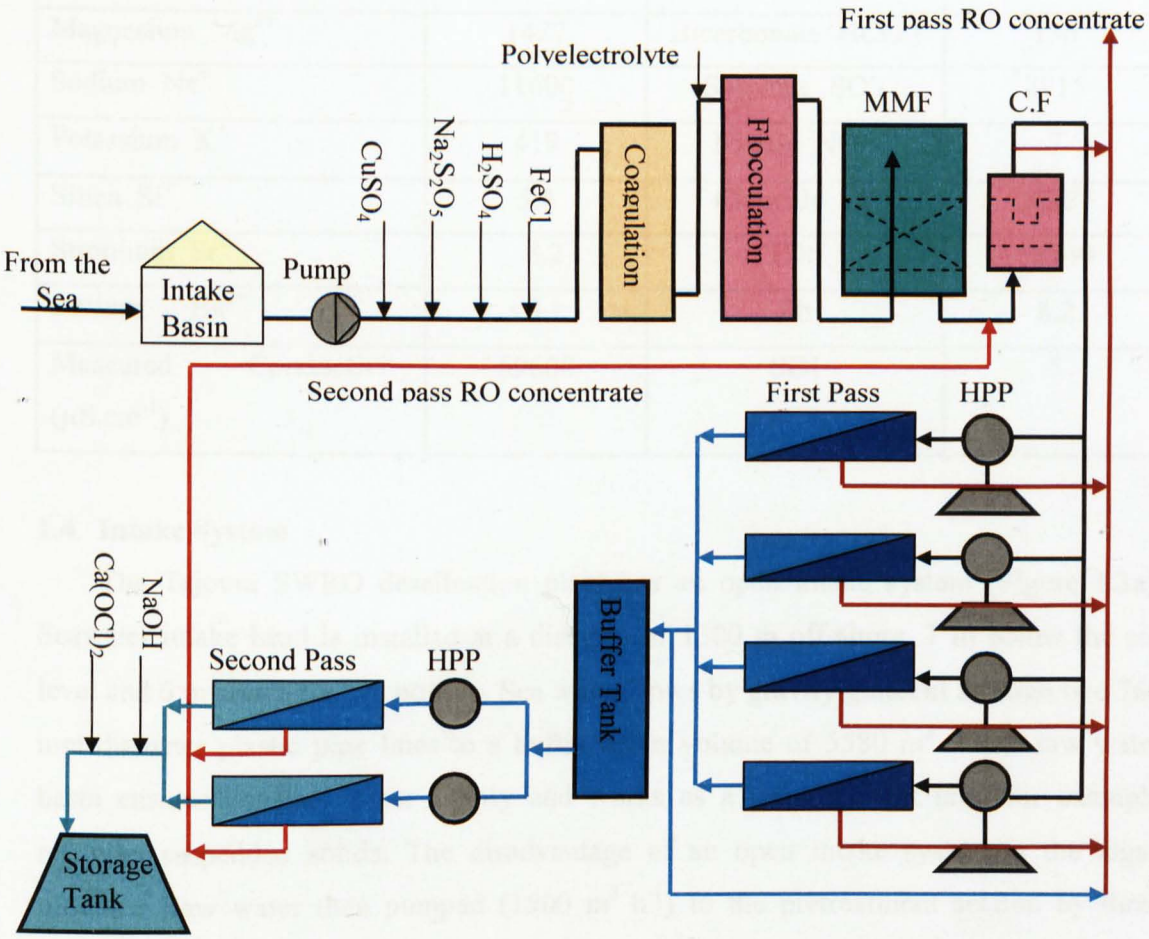

Figure 1.2: Schematic diagram of the main design features of the Tajoura Plant.

1.3 Water Source

The water source of the Tajoura SWRO desalination plant is the Mediterranean Sea. Even though, the intake is located far enough from chemical or industrial contamination inputs. However, impurities in suspended, colloidal, and dissolved forms are present in the raw seawater. Chemical composition of the water source of the Tajoura plant is shown in Table 1.1.

Table 1.1: Chemical composition of the Mediterranean Sea raw seawater (El-Azizi and Omran, 2002).

Component	Composition ($mg.L^{-1}$)	Component	Composition ($mg.L^{-1}$)
Calcium Ca^{2+}	455	Fluoride	1.2
Magnesium Mg^{2+}	1427	Bicarbonate HCO^{-}_{3}	136
Sodium Na^{+}	11600	Sulphate SO^{-}_{4}	2915
Potassium K^{+}	419	Nitrate NO^{-}_{3}	7
Silica Si^{+}	5.4	Chloride Cl^{-}	20987
Strontium Sr^{2+}	8.2	TDS	38740
Barium Ba^{2+}	<0.1	Ph	8.2
Measured Conductivity ($\mu S.cm^{-1}$)	59600	SDI	5

1.4 Intake System

The Tajoura SWRO desalination plant has an open intake system (Figure 1.3a). Seawater intake head is installed at a distance of 1300 m off shore, 7 m below the sea level and 6 m above the sea bottom. Sea water flows by gravity gradient through two 760 mm diameter plastic pipe lines to a buffer basin volume of 5580 m^3. This raw water basin ensures constant water supply and works as a pre-treatment unit, for example reducing suspended solids. The disadvantage of an open intake system is the algae growth. Raw water then pumped (1500 $m^3\ h^{-1}$) to the pretreatment section by three controlled seawater pumps (Figure 1.3b).

Figure 1.3 – Photographs of the (a) intake basin and (b) pump station of the Tajoura SWRO desalination plant.

1.5 Pre-treatment Systems

The role of the pre-treatment in RO desalination plant is to purify raw seawater to a quality acceptable to the RO membranes. The pre-treatment was designed to reduce the contents of suspended and dissolved materials, such as inorganic and organic suspended particles as well as iron, manganese and colloidal dissolved substances. Different types

of treatment processes are applied in the pre-treatment stage such as biological, chemical, and physical treatment.

1.5.1 Biological Treatment

Biological treatment is applied to disinfect the raw seawater in order to minimise the biofouling potential in the pre-treatment and the RO membrane systems. In the Tajoura RO plant two chemicals: sodium metabisulphite ($Na_2S_2O_5$) and copper sulphate ($CuSO_4$) are used as disinfectants, and are dosed to the raw seawater prior to the pre-treatment units in order to prevent any biological growth in the treatment systems of the plant. Moreover, $Na_2S_2O_5$ is used to remove the residual chlorine from RO feed water. When $Na_2S_2O_5$ is dissolved in water, sodium bisulphite is formed as it is shown the following reaction (Equation 1.1):

$$Na_2S_2O_5 + H_2O \rightarrow 2NaHSO_3 \qquad (1.1)$$

The produced sodium bisulphite then reduces the hypocholorous acid according to the following reaction (Equation 1.2):

$$NaHSO_3 + HOCl \rightarrow HCl + NaHSO_4 \qquad (1.2)$$

Sodium metabisulphite is added to ensure that all residual chlorine molecules are swept from the water before reaching the RO membranes. Also, it is very important to stick to the recommended dosing limit of sodium metabisulphite to prevent the consumption of the dissolved oxygen in the RO feed water by excess $NaHSO_3$ and to create anaerobic conditions for anaerobic bacteria (e.g. sulphate reducing bacteria).

1.5.2 Chemical Treatment

Chemical treatment can be accomplished using various types of chemicals in the pre-treatment stage in order to treat raw seawater before reaching the RO membranes.
Photograph of chemical dosing units is shown in Figure 1.4.

Figure 1.4 – Photographs of chemical dosing units of the Tajoura SWRO desalination plant.

1.5.2.1 Acid Dosing

Concentrated sulphuric acid (H_2SO_4) solution is dosed into the feed water to adjust pH from 8.3 to 7 in order to control the alkaline scaling in the pipelines and RO membranes.

$$H_2SO_4 + 2HCO^-_3 \rightarrow 2H_2O + CO_2 + SO^{2-}_4 \quad (1.3)$$

$$Ca^{2+} + HCO^-_3 \leftrightarrow H^+ + CaCO_3 \quad (1.4)$$

Due to the low turbidity and SDI values of the water source at the Tajoura SWRO desalination plant, no online coagulation / flocculation systems have been applied in this plant.

1.5.2.2 Anti-Scalant Dosing

Anti-Scalant is also added to the raw seawater to prevent precipitation of sparingly soluble salts such as calcium sulphate, barium sulphate and silica on the RO membrane surfaces. Anti-Scalant is introduced ahead of the cartridge filters. Types of chemicals that

are used in the pre-treatment process and their specific dosages are summarised in Table 1.2.

Table 1.2: Specific dosage of the applied chemicals in the pre-treatment at the Tajoura plant.

Chemical	Denomination	Specific dosage	Concentration
Copper sulphate	Disinfectant	4 mg. L^{-1}	98% (w/v)
Sodium Metabisulphite	De-Oxidation	3 mg.L^{-1}	98% (w/v)
Ferric Chloride Sulphate	Coagulant	2 – 4 mg.L^{-1}	41% (v/v)
Sulphuric acid	pH adjustment	40 mg.L^{-1}	98% (v/v)
Polyelectrolyte	Flocculant	0.78 mg.L^{-1}	25% (v/v)
Perm care 191	Anti-Scalant	4 mg.L^{-1}	60% (v/v)

1.5.3 Physical Treatment

Physical treatment consists mainly of multimedia filters and fine cartridge filters.

1.5.3.1 Multimedia Filters (MMF)

Media filters use a filtration bed consist of three layers of media granules which are gravel, sand and anthracite. The multimedia filters are provided to reduce the suspended solids in the raw seawater and to ensure that the silt density index (SDI) values are maintained less than 3 as recommended by the supplier of RO membranes (Bonnelye, *et al.*, 2008). A multimedia filter is designed to make better use of the bed depth to remove a greater volume of suspended solids. The Tajoura plant has 8 dual media filters, where each 4 filters are arranged in one array. The major design parameters of dual media filters, the media depth and grain size are shown in Table 1.3.

Table 1.3: The major design parameters of dual media filters of the Tajoura plant (El-Azizi and Omran, 2002).

Specification	Design parameter
Number of dual media filters	8
Filtration velocity	11.7 m h^{-1}
Water flow rate through each filter	187 m^3 h^{-1}
Design pressure	4.5 bar
Filter tank diameter and length	4.5m / 2.9m
Supporting gravel layer (Depth / grain size)	0.3 m / 4 – 5 mm
Quartz sand layer (Depth / grain size)	0.85 m / 0.7 – 1.2 mm
Hydro Anthracite layer (Depth / grain size)	0.85 m / 1.4 – 2.5 mm

The Tajoura plant has 8 dual media filters, where each 4 filters are arranged in one array (Figure 1.5).

Figure 1.5 – Photographs of multimedia filters of the Tajoura SWRO desalination plant

1.5.3.2 Cartridge Filters

Cartridge filters or fine filters are the final filtration step in the pre-treatment stage, which are located a head of RO membrane units. Cartridge filters are made of polypropylene, and are used in the pre-treatment process if the sizes of particles to be removed from the feed water are in range of 5 – 20 μm. The major design parameters of cartridge filters are shown in Table 1.4.

Table 1.4: The major design parameters of the cartridge filters (El-Azizi and Omran, 2002).

Specification	Design parameter
Number of cartridge filters	5
Nominal filtration size	5 μm
Capacity of each filter	300 $m^3 h^{-1}$
Design pressure	4 bar

Figure 1.6shows photograph of cartridge filters casings of the Tajoura SWRO desalination plant.

Figure 1.6: Photograph of cartridge filters casing of the Tajoura SWRO desalination plant.

1.6 Main Treatment

The main treatment of the Tajoura RO plant consists of four seawater RO membrane racks in the first pass and two brackish water RO membranes racks in the second pass. The membrane racks are arranged in two lines to run the plant either with 50% or 100% production capacity. The specification of the first and second pass RO membranes are shown in Table 1.5.

Table 1.5: Specification of seawater/brackish water RO membranes.

Component	First pass	Second pass
Number of racks	4	2
Pressure vessels configuration	One stage	Three stages
Membrane diameter and length	20 / 100 (cm)	20 / 100 (cm)
Design salt rejection	99.6% / 99.8 (%)	99.4 (%)
Design permeate TDS	500 ($mg.L^{-1}$)	10 ($mg.L^{-1}$)
Membranes material	Thin film composite polyamide	Thin film composite polyamide
Membranes models	- TFC 2822SS-360 SU-820	- TFC 8600 PA SU-720
Membranes type	Fluid System / Toray	Fluid System / Toray

Figure 1.7 shows photograph of reverse osmosis membrane racks of the Tajoura SWRO desalination plant.

Figure 1.7: Photograph of reverse osmosis membrane trains of the Tajoura SWRO desalination plant.

1.7 Post-Treatment

Post-Treatment is used for further adjustments of the product water pH as well as the addition of chlorine to prevent any biological growth in the distribution system. The following chemicals are added in the post-treatment at the Tajoura RO plant.

1.7.1 Sodium Hydroxide for pH Adjustment

Sodium Hydroxide (NaOH) is added to the product water to maintain pH of 8 (Equation 1.5). 16 $mg.L^{-1}$ of NaOH is dosed to the permeate water to prevent aggressiveness by the formation of carbonic acid at low pH values, which causes corrosion in the pipelines.

$$NaOH + CO_2 \rightarrow NaHCO_3 \qquad (1.5)$$

1.7.2 Chlorination

Calcium hypochlorite $Ca(OCl)_2$ is added to the product water to prevent any biological growth in the pipeline and in the product water storage reservoir. The operating dosing rate is kept at 0.61 mg l^{-1} in order to maintain the residual chlorine level at about 0.5 mg $.L^{-1}$ (Equation 1.6).

$$Ca(OCl)_2 + H_2O \rightarrow 2HOCl + Ca(OH)_2 \qquad (1.6)$$

Hypochlorous acid dissociates in water to hydrogen ions and hypochlorite ions (Equation 1.7).

$$HOCl \leftrightarrow H^+ + OCl^- \qquad (1.7)$$

The specific chemicals dosages that are applied in the post-treatment phase at the Tajoura RO plant are summarised in Table 1.6.

Table 1.6: Specific dosages of the applied chemicals in the post-treatment at the Tajoura RO plant.

Chemical	Denomination	Specific dosage	Concentration
Sodium hydroxide	pH adjustment	16 $mg.L^{-1}$	50% (w/v)
Calcium hypochlorite	Disinfectant	0.61 $mg.L^{-1}$	65% (w/v)

Since 1984 the Tajoura SWRO desalination plant was operated at less than 50% of its maximum production capacity. Non-continuous operation of the plant causes a lot of problems, particularly fouling and scaling. This mode of operation greatly affects the performance of the plant, and in order to improve performance it was essential to carry out a comprehensive study on the plant performance by evaluating the pre-treatment and the RO membrane systems.

1.8 Objectives

The main goal of this research was to study the accuracy of the conventional *in-Situ* experimental and theoretical fouling monitoring methods used to predict the fouling type. Also to determine the identity of the fouling that caused deterioration in the performance of the Tajoura desalination plant by carrying out a destructive study (membrane autopsy) on two SWRO membranes. In order to apply these understandings more practically, and to develop a fouling prevention method, the following objectives were formulated:

I- To evaluate the performance of the pre-treatment and the RO membrane systems at the Tajoura SWRO desalination plant using the conventional *in-Situ* fouling monitoring methods and the theoretical and software standardisation approaches. Also to find out whether these methods are applicable to predict the types of fouling.

II- To characterise membrane fouling of the RO membrane systems at the Tajoura SWRO desalination plant by carrying out a destructive study (membrane autopsy).

III- To investigate the effect of the composite fouling on the permeate flux and to determine the composition of fouling materials in the absence of pre-treatment using raw seawater.

IV-To apply a novel fouling prevention method in order to improve SWRO desalination plant performance.

1.9 Research Significance

The RO membrane technology is widely applied in the desalination of sea and brackish waters, however fouling deteriorates its performance and causes a decline in the quality and quantity of the permeate flux, which leads to detrimental increases in the operational and maintenance costs. Different fouling monitoring methods has been applied in the RO desalination systems, however little literature has been reported in regards the limitations of the theoretical methods and software standardisation packages and their accuracy in the prediction of various fouling types. Also to determine the fouling identity in full scale SWRO desalination plants.

In this research, four standardisation methods were used to evaluate the performance of RO membrane systems of the Tajoura desalination plant which was selected as a case study. The true identity of fouling that deteriorated the performance of the Tajoura plant was determined through carrying out a destructive study (membrane autopsy) on two different commercial SWRO membranes.

Another important engineering issue is that the introduction of a fouling prevention procedure by the application of a novel pre-treatment technique. Studies showed that conventional and membrane filtration techniques have limitations in preventing RO membranes from fouling. In this research, a novel pre-treatment system was applied to prevent fouling.

1.10 Thesis Approach

This thesis is comprised of eight chapters. Chapter 1 includes a general introduction about the treatment systems of the Tajoura SWRO desalination plant. Chapter 2 includes a general literature review of various pressure driven membrane processes, RO membrane materials, definitions and background theory of the reverse osmosis, types of fouling and fouling monitoring methods. In Chapter 3, the experimental

rigs and materials and different analytical methodologies and procedures are presented. Chapter 4 discusses the fouling prediction methods (objective I) including SDI, biological growth, and theoretical and software RO data standardisation methods. Chapter 5 discusses the characterisation and the identification of membrane fouling (objective II), through carrying out membrane autopsies on two 8 inch (20 cm) diameter and 40 inch (100 cm) length commercial SWRO membranes using different microscopic visualisation techniques including AFM, SEM, X-Ray and FTIR. Whilst Chapter 6 includes studies on the effect of composite fouling on the RO membrane performance (objective III) using two types of raw seawaters. Chapter 7 presents the application of the Disruptor^{TM} media (objective IV) as a novel fouling prevention method in the RO membrane systems. Finally, Chapter 8 summarises the most important findings and conclusions of the research study, as well as some important recommendations and future studies are included.

CHAPTER 2

LITERATURE REVIEW

2.1 Pressure – Driven Membrane Processes

In the past, membrane separation techniques were not often considered important technologies due to their operational problems and high investment costs. Nowadays these technologies are used in a wide range of applications especially in water and waste water treatment. The advantages of membrane separation technology include; low energy consumption, ease of design, simplicity and that separation process can be carried out continuously (Goosen, *et al.,* 2004). However, disadvantages include membrane fouling, low flux and short membrane lifetime (Van der Burggen, *et al.*, 2003; Sediel and Elimelech, 2002). The most common types of membrane processes used in water industries are microfiltration (MF), ultrafiltration (UF), nanofiltration (NF) and reverse osmosis (RO).

2.1.1 Microfiltration (MF)

Microfiltration (MF) utilises a micro porous membrane with pore size ranging from 0.1 μm to 10 μm (Baker, 2004). Systems have high permeability at low operating pressure (1–7 bar). In general, suspended particles, many microorganisms and large colloidal particles are rejected while macromolcules, many bacteria, viruses and dissolved solids pass through the membrane (van der Bruggen, *et al.,* 2003 and Scott and Hughes, 1996), (Figure 2.1).

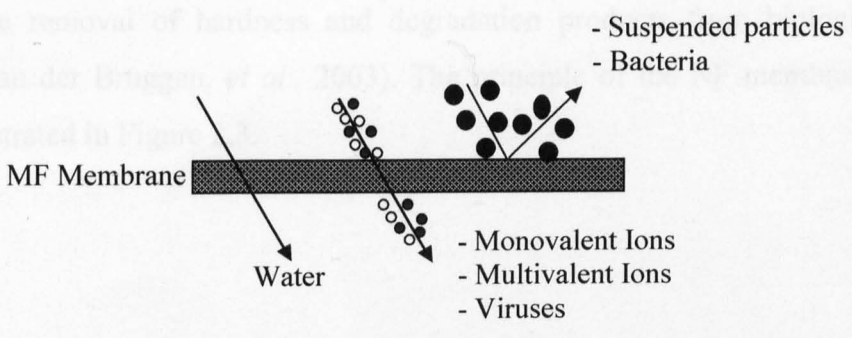

Figure 2.1: Microfiltration (MF) membrane separation, (van der Bruggen, *et al.,* 2003).

2.1.2 Ultrafiltration (UF)

Ultrafiltration (UF) utilises a micro porous membrane with pore size smaller than MF. In UF, the pore size range from 0.02 μm to 0.001 μm. The separation mechanism is selective sieving through the membrane pores. UF membranes are used to remove large particles, microorganisms and soluble macromolecules such as protein, while small particles will pass through (Tansel, *et al.*, 2000; Scott and Hughes, 1996), (Figure 2.2). UF has the advantage of low operating pressure (1–7 bar) to overcome the viscous resistance of liquid permeation through the membrane pores.

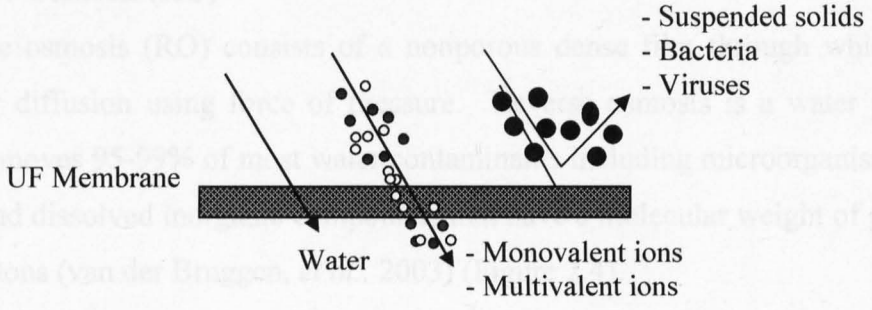

Figure 2.2: Ultrafiltration (UF) membrane separation, (van der Bruggen, *et al.*, 2003).

2.1.3 Nanofiltration (NF)

Nanofiltration (NF) is a pressure-driven process. In NF the pore size is smaller than UF, typically around 0.001 μm, which corresponds to dissolved compounds with a molecular weight of about 300 Daltons (Da) (Mulder, 2003). NF membranes are suitable for the removal of relatively small organics such as organic micropollutants and colour from surface water, and the removal of hardness and degradation products from biologically treated wastewater (van der Bruggen, *et al.*, 2003). The principle of the NF membrane separation process is illustrated in Figure 2.3.

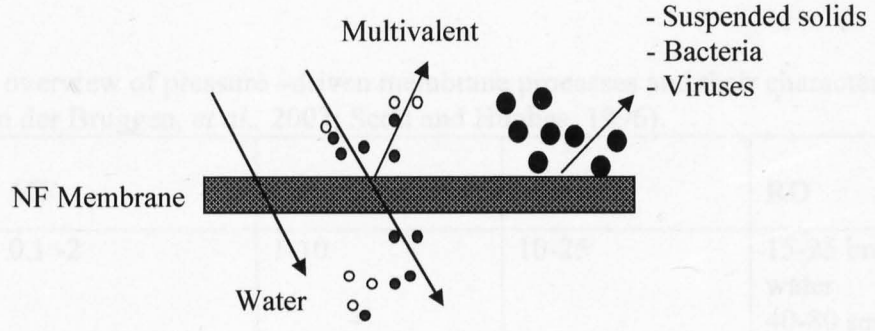

Figure 2.3: Nanofiltration (NF) membrane separation, (van der Bruggen, *et al.,* 2003).

2.1.4 Reverse Osmosis (RO)

Reverse osmosis (RO) consists of a nonporous dense film through which water is transported by diffusion using force of pressure. Reverse osmosis is a water purification process that removes 95-99% of most water contaminants including microorganisms, organic compounds, and dissolved inorganic compounds that have a molecular weight of greater than 150 – 250 Daltons (van der Bruggen, *et al.,* 2003) (Figure 2.4).

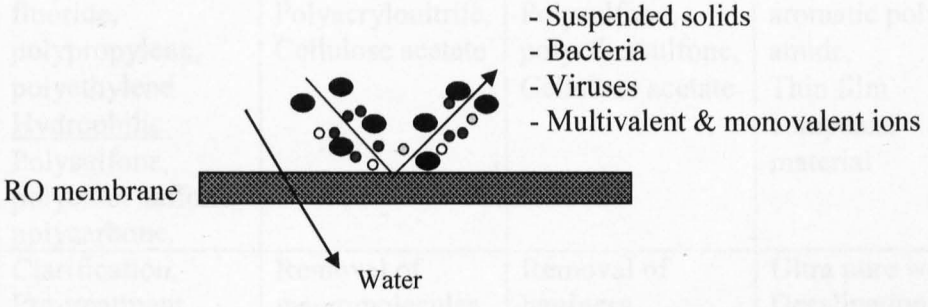

Figure 2.4: Reverse osmosis (RO) membrane separation, (van der Bruggen, *et al.,* 2003).

The RO membranes are either asymmetric or composite with a thick and dense rejection layer (0.2 μm) supported by a porous layer. Characteristics of pressure-driven membrane processes are summarised in Table 2.1.

Table 2.1: An overview of pressure –driven membrane processes and their characteristics (van der Bruggen, *et al.*, 2003; Scott and Hughes, 1996).

	MF	**UF**	**NF**	**RO**
Pressure (bar)	0.1 -2	1-10	10-25	15-25 brackish water 40-80 seawater
Pore size (μm)	0.05 – 10	0.001 – 0.01	<0.00 2	0.0001
Thickness (μm)	10 – 150	150	Sub-layer – 150 Top layer - 1	Sub-layer – 150 Top layer – 0.2
Morphology	Symmetric	Asymmetric	Composite	Composite
Rejection Ability	Particles	Particles Macromolecules, Bacteria	Particles Macromolecules, Bacteria Multivalent,	Particles Macromolecules, Bacteria Multivalent Monovalent
Separation mechanism	Sieving	Sieving	Solution diffusion	Solution diffusion
Material	Hydrophobic: polyvinylidene fluoride, polypropylene, polyethylene Hydrophilic: Polysulfone, polyether sulfone, polycarbone.	Polysulfone, polyethersulfone, Polyacrylonitrile, Cellulose acetate	Aromatic polyamide, Polysulfone, polyethersulfone, Cellulose acetate	Cellulose triacetate, aromatic poly amide, Thin film composite material
Application	Clarification, Pre-treatment, Removal of bacteria	Removal of macromolecules, Bacteria	Removal of hardness, Small organics	Ultra pure water, Desalination

2.2 Reverse Osmosis Membrane Materials

The most popular reverse osmosis membranes used in the water treatment industries are cellulose acetate (CA), cellulose triacetate (CTA) and polyamide (PA).

2.2.1 Cellulose Acetate

The first asymmetric Cellulose Acetate (CA) membrane was demonstrated by Leob and Sourirajan in 1963 and commercially used in desalination of seawater in 1970 (Glater, *et*

al., 1994; Khulbe, *et al.*, 2004). CA membrane is made from acetylated cellulose and consists of a very dense and thin active layer (0.1–1 μm) on the top of a highly porous and thick substrate (100–200 μm) and display the important feature of combining high salt rejection with high water permeability (Dais, *et al.*, 1998). CA reverse osmosis membranes have good mechanical properties and can tolerate up to 5 $mg.l^{-1}$ of free chlorine (Murphy, *et al.*, 2001). CA membranes are extremely sensitive to changes in pH and are stable only in pH ranges of 4 to 6. Change in feed water pH causes damage to CA membranes and this process of chemical attack is called hydrolysis (Duarte *et al.*, 2008). Hydrolysis usually strips acetate molecules off of the polymeric cellulose which reduces the salt rejection of the membrane. In addition microorganisms such as fungal and bacteria damage CA RO membranes (Murphy, *et al.*, 2001). The mechanical stability and resistance to hydrolysis of CA reverse osmosis membranes can be improved when the CA is blended with cellulose triacetate (CTA), however the membrane permeability decreases (El-Saied, *et al.*, 2003; Duarte, *et al.*, 2008).

2.2.2 Polyamide Thin Film Composite (TFC)

The polyamide thin film composite (TFC) reverse osmosis membranes were first used in 1972 in desalination of seawater (Kurihara, *et al.*, 1985). The TFC polyamide membrane consists of a top ultra-thin skin polyamide layer coated on a middle polysulfone porous support and bottom non-woven fabric polyester layer (Singh, *et al*, 2006). The coating provides the salt rejection properties of the membrane. This aromatic polyamide active layer, made via interfacial polymerization though the reaction between meta-phenylene diamine in aqueous phase and trimesoyl chloride in organic phase (Singh, *et al.*, 2006; Kurihara, *et al.*, 1994). Variations of this chemistry are still used today to produce cross-linked membranes for commercial RO membranes. Commercially, the spiral wound polyamide thin film composite (TFC) RO membranes are the most successful membrane that are used in full scale desalination plants (Ng, *et al.*, 2008). A comparison of cellulose acetate (CA), cellulose triacetate (CTA) and polyamide thin film composite (TFC) RO membranes is shown in Table 2.2.

Table 2.2: Comparison of CA, CTA and TFC RO membranes (Khulbe, *et al.*, 2004; Hanra and Ramachandharn, 1996).

Parameter	CA	CTA	TFC
Operating Pressure (bar)	28.3 – 41	28.3 – 41	13.8 – 55.4
Operating Temperature (°C)	5 – 30	5 – 35	5– 45
Operating pH	4 – 8	4 – 9	2 – 11
Permeate flux ($l.m^{-2}.h^{-1}$)	0.78		1.6
Salt Rejection (%)	85% - 92%	92% - 95%	95% – 99%
Stability to Free Chlorine	1.0 mg/l	3 mg/l	0.1 mg/l
Resistance to biofouling	Poor	Good	Excellent
Membrane Degradation Potential	Hydrolyses at low and high pH	Hydrolyses at low and high pH	Stable over broad pH range
Cost	Low	Medium	High

2.3 Classification of Reverse Osmosis Membranes

Reverse osmosis membranes are classified as asymmetric and/or composite membranes (Figures 2.5a and 2.5b). Asymmetric membranes can be micro-porous, or micro-porous with a non-porous top layer. They have non-uniform pores over the membrane cross section and have a very dense top layer with a thickness of 0.1– 0.5 μm supported by a porous sub-layer with a thickness of 50 – 150 μm (Singh, *et al*, 2006). The asymmetric membranes give high permeate flow due to very thin selective top layer and a reasonable mechanical stability resulting from the underlying porous structure (Baker, 2004). Asymmetric membranes can be divided into cellulose acetate and thin film composite membranes, (Figures 2.5a and 2.5b).

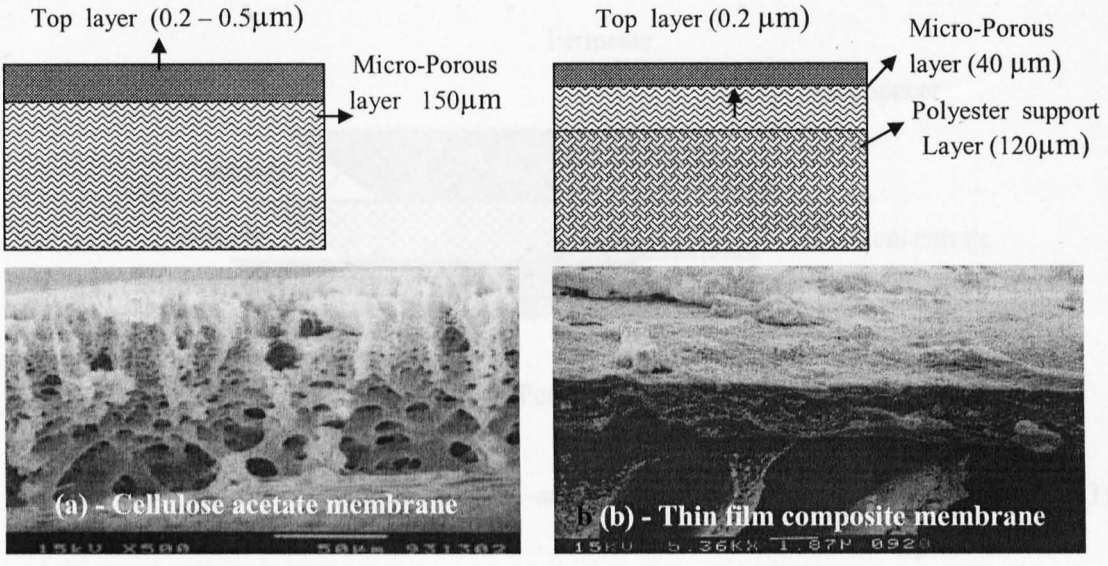

Figure 2.5: Schematic diagrams and SEM images of a cross-section of a cellulose acetate (a) and thin film composite membranes (b), (Reproduced from Mulder, 2003).

2.4 Membrane Configurations

According to their configuration, membranes are classified as plate-and-frame, hollow fibre, spiral wound and tubular membranes. In this project, flat sheet and spiral wound membranes modules were used for filtration experiments and autopsy visualisations, respectively.

2.4.1 Plate-and-Frame Module

The plate-and-frame module is the simplest configuration, consisting of two end plates, the flat sheet membrane, and feed spacers (Figure 2.6) (Mulder, 2003). Plate and frame membranes are very limited in the desalination applications due to high cost and lower recovery rates compared to spiral wound and hollow fibre modules. However, they are used in the food and beverage industries.

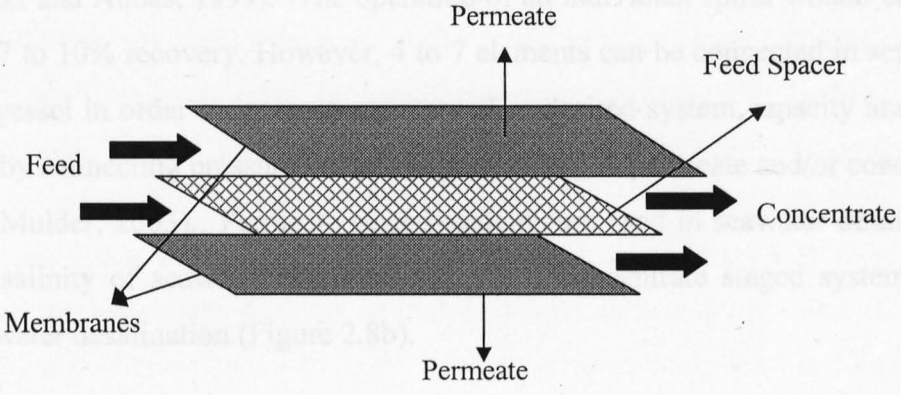

Figure 2.6: Schematic diagram of plate–and–frame membrane module (Mulder, 2003).

2.4.2 Spiral Wound Module

The spiral wound membrane configuration is widely used in the desalination of brackish and seawaters. These modules have been subjected to numerous improvements since their development in the mid-1960s and modifications included increasing applied pressure and spacer design (Mulder, 2003; Kurihara, *et al.,* 1994). However, other materials such as cellulose triacetate and polyamide/polysulfone composites are also used. Figure 2.7 shows a schematic diagram of spiral wound module.

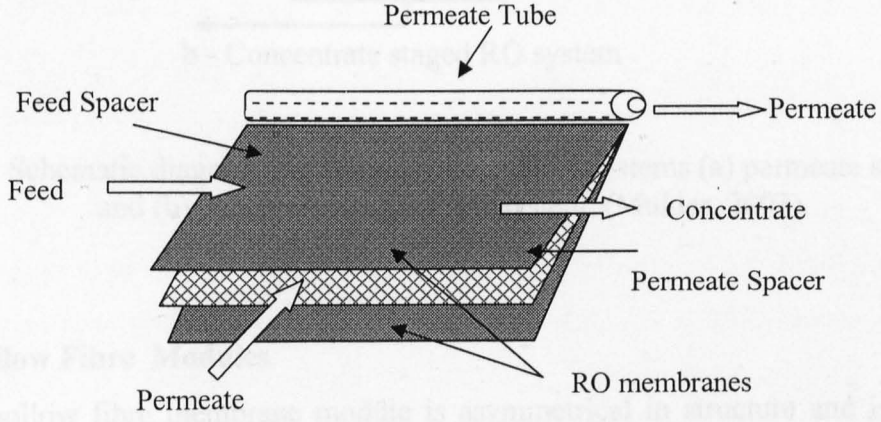

Figure 2.7: Schematic drawing of a spiral-wound module (Mulder, 2003).

In spiral-wound modules, the presence of concentrate spacers helps to create more turbulence of the solution at the concentrate side, and thus reduces the concentration polarisation effects (Al-Bastaki and Abbas, 1999). The operation of an individual spiral wound element usually provides 7 to 10% recovery. However, 4 to 7 elements can be connected in series in a single pressure vessel in order to increase recovery. The desired system capacity and recovery are achieved by connecting pressure vessels in parallel and in permeate and/or concentrate staged systems (Mulder, 2003). Permeate staged systems are used in seawater desalination due to the high salinity of seawater (Figure 2.8a), while concentrate staged systems are used in brackish water desalination (Figure 2.8b).

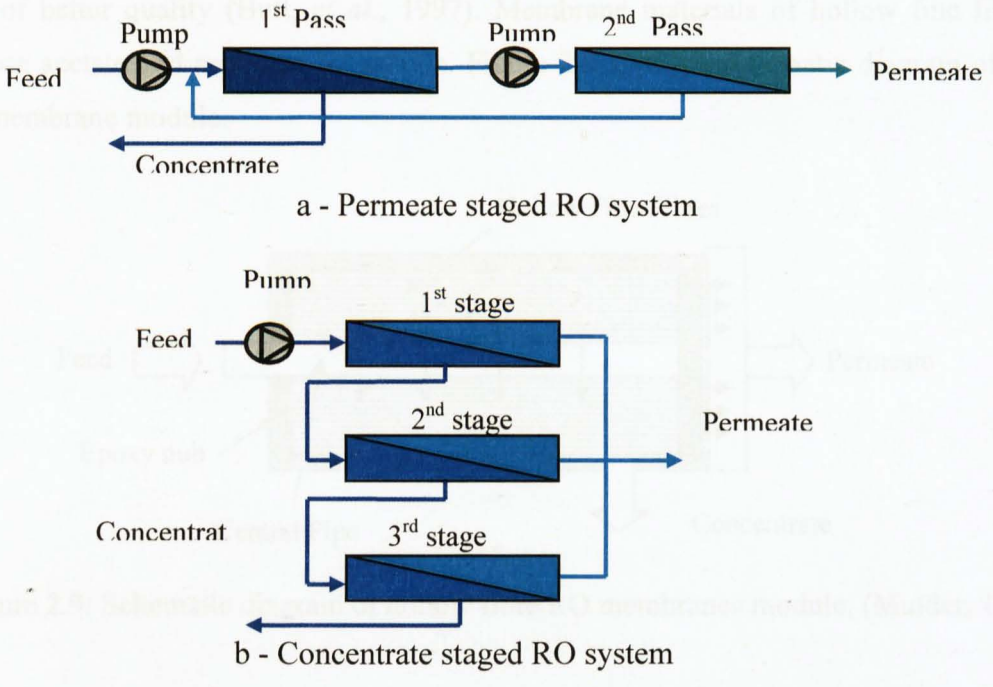

Figure 2.8: Schematic diagram of RO membrane staged systems (a) permeate staged system and (b) concentrate staged RO system, (Mulder, 2003).

2.4.3 Hollow Fibre Modules

A hollow fibre membrane module is asymmetrical in structure and is as fine as a human hair, about 42 μm I.D and 85 μm O.D (El-Dessouky and Ettoueny, 2002; Mulder, 2003). Millions of these fibres are formed into a bundle and folded in half to a length of approximately 120 cm. The hollow fibre membrane bundle, 10 cm to 20 cm in diameter is

contained in a cylindrical housing or shell approximately 137 cm long and 15 – 30 cm in diameter (El-Dessouky and Ettoueny, 2002). A plastic tube is inserted in the centre to serve as a feed water distributor. The feed solution can enter inside the fibre (inside – out) or to the outside (outside – in). One of the disadvantages of the outside-in type is that channelling may occur, in which feed has a tendency to flow along a fixed path thus reducing the effective membrane surface area. With a central pipe the feed solution is more uniformly distributed throughout the modules so that the whole surface are is more effectively used. Hollow fibre membranes are very sensitive to colloidal fouling therefore, they require feed water of better quality (Butt, *et al.*, 1997). Membrane materials of hollow fine fibres are cellulose acetate and aromatic polyamide. Figure 2.9 shows a schematic diagram of hollow fibre membrane module.

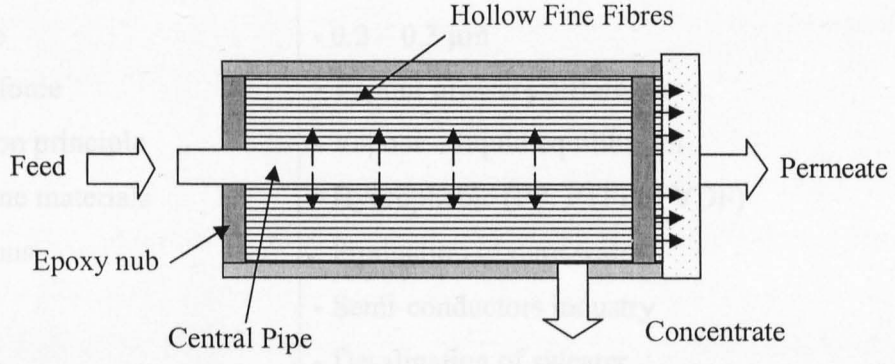

Figure 2.9: Schematic diagram of hollow fibre RO membranes module, (Mulder, 1996).

2.5 Membrane Distillation

Membrane distillation is a water separation process where a porous hydrophobic membrane is used to separate contaminants from water (Bahar, *et al.*, 2009; Mulder, 2003). The first membrane distillation patent was obtained by Bodell in 1963 (Bahar, *et al.*, 2009). By early 1980s, the research on membrane distillation became very active, and various types of membranes were developed (Bahar, *et al.*, 2009; Al-Obaidani, *et al.*, 2008). Membrane distillation is a combination of evaporation of water from saline solution and diffusion of vapour through a hydrophobic membrane. The main requirement in this process is that the membrane must not be wetted because if wetting occurs, the water will pass into the pores of

the membrane. In order to avoid wetting the maximum pore size must be small (0.2 to 0.3 μm), the porosity should be between 70% and 80%, the surface tension should be high and the membrane should be as thin as possible (Scott and Hughes, 1996). The membrane materials are typically polypropylene (PP), polytetrafluoroethylene (PTEF) and polyvinylidenedifluoride (PVDF). A summary of membrane distillation is present in Table 2.3.

Table 2.3: A Summary of membrane distillation (Scott and Hughes,1996).

Parameter	Description
- Membranes	- Symmetric or asymmetric porous
- Membrane Thickness	- 20 – 10 μm
- Pore size	- 0.2 – 0.3 μm
- Driving force	- Vapour pressure difference
- Separation principle	- Vapour – liquid equilibrium
- Membrane materials	- Hydrophobic (PP, PTFE, PVDF)
Applications	- Production of pure water
	- Semi-conductors industry
	- Desalination of sweater
	- Production of boiler feed water for power plants.

The major advantages of membrane distillation are:

- Compact modules equipped with hollow fibres
- A high surface area per unit liquid volume
- High overall permeation rates.
- Requirement of low energy associated with ambient pressure for evaporation.

Membrane distillation can handle higher salt concentration without substantial decrease in membrane performance and the permeate quality is independent of the feed concentration. However, major practical limitations in membrane distillation applications include low water flux and shortage of long-term performance data due to the wetting of the hydrophobic

microporous membrane. Moreover, the required pressure upstream of the membrane must be less than the penetration pressure of the membrane. The required pressure can be calculated using Laplace Equation (2.1) (Mulder, 2003).

$$\Delta P = \frac{2r\gamma}{r}\cos\theta \qquad (2.1)$$

Where:

r – Pore size (μm).

γ - Surface tension of the liquid ($N.m^{-1}$).

θ – Contact angle.

If the contact angle is greater than 90°, the water does not wet the membrane surface, while if the contact angle $\theta = 0$ the water spreads on the surface.

With development of hydrophobic membranes at a cheap cost, membrane distillation has drawn significant attention in water research. Al-Obaidani, *et al.* 2008 reported that the total water production cost by membrane distillation is about $1.23\$.m^{-3}$ without using waste heat. However, with using the waste heat and utilising the energy from condensing steam, the production cost can be reduced (Meindersma, *et al.*, 2006).

2.6 Reverse Osmosis

2.6.1 Definition and Background Theory

The principle of osmosis and reverse osmosis processes is that if two solutions containing different concentrations of dissolved salts are separated by a semi-permeable membrane, solvent will spontaneously move across the membrane to the side with the greater solute concentration until the pressure gradient across the membrane reaches an equilibrium value. The process is called osmosis and the equilibrium pressure gradient is called osmotic pressure (El-Dessouky and Ettoueny, 2002). Osmotic pressure attempts to equalise the solute concentration by driving solvent from the side with the lower concentration of solute to the other side. By applying pressure greater than the osmotic pressure to the more concentrated

solution, solvent will flow in the reverse direction, a process known as reverse osmosis (RO). The driving force for the water transport across the membrane is the pressure difference between the operating pressure and the osmotic pressure (Net driven pressure). A schematic illustration of the principles of osmosis and reverse osmosis processes are shown in Figure 2.10. Transport of solute and solvent across the membrane takes place because of a difference in chemical potential ($\Delta\mu$) (El-Dessouky and Ettoueny, 2002; Mulder, 2003; Atkins, 2001).

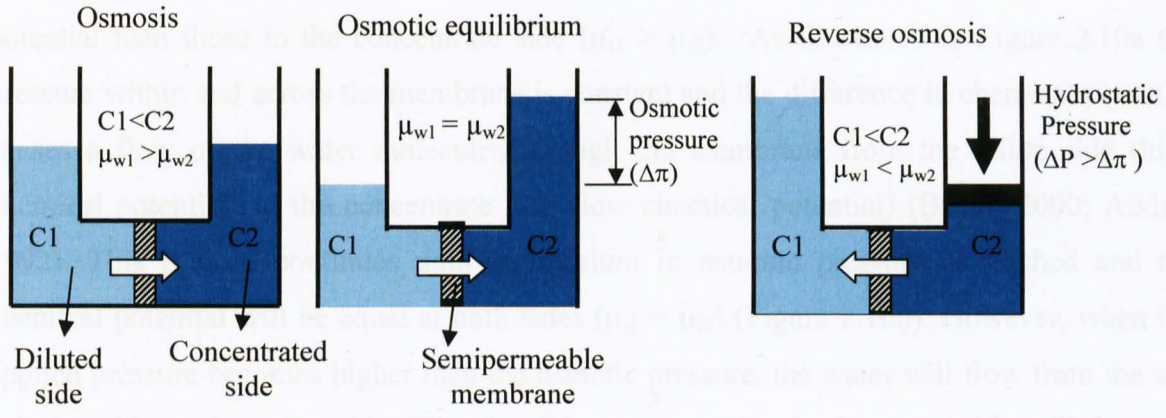

Figure 2.10: Schematic diagram of principles of osmosis (a), osmotic equilibrium (b) and reverse osmosis (c) processes where, π = is the osmotic pressure and P = is the hydrostatic pressure, (El-Dessouky and Ettoueny, 2002).

As in reverse osmosis, membrane pressure and salt concentration are involved as driving forces and can be included in one parameter, the chemical potential (μ). At constant temperature, the chemical potential of the pure water ($\mu_{i,1}$) and the chemical potential of the salt solution ($\mu_{i,2}$) are given by Equations 2-3 and Equation 2-4, respectively (Mulder, 2003; Atkins, 1992).

$$\mu_{i,1} = \mu_{i,1}^{\ 0} + RT\ln(\gamma_i C_i)_1 + V_i P_1 \qquad (2\text{-}2)$$

$$\mu_{i,2} = \mu_{i,2}^{\ 0} + RT\ln(\gamma_i C_i)_2 + V_i P_2 \qquad (2\text{-}3)$$

Where:

μ_i – is the chemical potential

μ_i^0 – is the chemical potential of pure i at a reference pressure P^0_i.

C_i – is the molar concentration of component i ($mol.mol^{-1}$).

γ_i – is the activity coefficients of i component in solution.

P – is the pressure (bar).

V_i – is the molar volume of component i.

According to the solution diffusion model (Wijmans and Baker, 1995) and due to the effect of osmosis (Mulder 2003), the water molecules in the dilute side have higher chemical potential than those in the concentrate side ($\mu_{i1} > \mu_{i2}$). As illustrated in Figure 2.10a the pressure within and across the membrane is constant and the difference in chemical potential causes a flow of the water molecules through the membrane from the dilute side (high chemical potential) to the concentrate side (low chemical potential) (Baker, 2000; Atkins, 1992). This process continues until equilibrium in osmotic pressure is reached and the chemical potential will be equal at both sides ($\mu_{i1} = \mu_{i2}$) (Figure 2.10b). However, when the applied pressure becomes higher than the osmotic pressure, the water will flow from the salt solution side to the water side. Therefore, the concentration in the water side will decrease and leads to reduction in chemical potential, while the ion concentration in the salt solution will increase leading to increasing chemical potential (Figure 2.10c).

According to the solution diffusion model the pressure across the membrane is uniform and the chemical potential gradient across the membrane is expressed only as a concentration gradient.

2.6.2 Osmotic Pressure

The simple relationship between the osmotic pressure (π) and the solute concentration (C_i), is called the van't Hoff equation (2-4) (Mulder, 2003).

$$\pi = RT\sum C_i(Z_i)^2 \qquad (2.4)$$

Where:

π - is the osmotic pressure (bar)

$\sum c_i$ - is the concentration of all constituents in a solution ($g.mol.m^{-3}$)

Z_i - is the number of ions formed if the solute dissociates (dimensionless)

R - is the universal gas constant 8.314 kPa $m^3.g^{-1}$ mol^{-1}.

T - is the absolute temperature (Kelvin)

It can be seen that osmotic pressure is proportional to the concentration as, when dissociation occurs, the number of moles increases and hence the osmotic pressure increases, while in the case of association the number of moles decreases as does the osmotic pressure. Van't Hoff equation (2.4) dictates an ion by ion calculation to determine osmotic pressure, the data for which is not available every month.

Typically only conductivity data is available from RO membrane systems and the following equation is used to convert conductivity to concentration in terms of total dissolved solids (TDS):

$$TDS\ (mg.l^{-1}) = A \times (\mu S.cm^{-1}) \qquad (2\text{-}5)$$

Where:

A – is a conversion factor depends on the salt concentration in the water.

Therefore, osmotic pressure as a function of the feed water temperature (T) and feed concentration (concentration of dissolved solids) (C) can be calculated using the following equation (Zhao, 2005; Lu, *et al.*, 2006):

$$\pi = \frac{0.2654 \times C \times (T + 273.15)}{1000 - \frac{C}{1000}} \qquad (2.6)$$

Where:

π - is the osmotic pressure (kpa) (1 bar = 100 kpa)

C – is the feed concentration ($mg.L^{-1}$).

T - is the absolute temperature (Kelvin)

An approximation for (π) may be made by assuming that 1000 mg.L^{-1} of total dissolved solids (TDS) equals to 0.76 bar of osmotic pressure (a rough rule of thumb) (El-Dessouky and Ettoueny, 2002).

$$\pi = \frac{TDS\ (mg.L^{-1}) \times 0.76}{1000\ (mg.L^{-1})} \qquad (2.7)$$

From equations (2.4. 2.6), it can be seen that osmotic pressure is proportional to the feed concentration and temperature and depends on the dissociation and association of solute. If dissociation occurs, the number of moles increases and the osmotic pressure will increase, while in case of association the number of mole decreases as does the osmotic pressure (Mulder, 2003).

2.6.3 Differential Pressure (ΔP)

Differential pressure can be defined as the resistance to the passage of feed water though the pressure vessel of an RO unit due to build up of foulants on the surface of the membranes as well as in the feed spacer material. As these foulants accumulate, the resistance to flow of feed water increases. This resistance to water flow may be measured as a differential pressure across the membrane and/or pressure vessel. Differential pressure is calculated using Equation (2.8).

$$\Delta P = P_f - P_c \qquad (2.8)$$

Where:

ΔP – Differential pressure (bar)

P_f - Feed pressure (pressure vessel inlet) (bar)

P_c - Concentrate pressure (pressure vessel outlet) (bar)

2.6.4 Water Transport (K_w)

The solvent and solute fluxes through the RO membrane is characterised by two phenomena; solvent transport in terms of water permeability coefficient (K_w) and solute transport in terms of the salt permeability coefficient (K_s) (Voros *et al.*, 1996). Permeate flux is the rate of water passage through the membrane surface and can be calculated as follows:

$$J_w = \frac{Q_p}{A} \tag{2.9}$$

The permeate flux (J) produced by RO membrane is proportional to net driven pressure differential (NDP) across the membrane as shown in the following equations (Kimura, 1995; Zhao and Taylor, 2005).

$$J_w = K_w[\Delta P - \sigma * \Delta \Pi] \tag{2.10}$$

$$\Delta P = \frac{(P_f + P_c)}{2} \tag{2.11}$$

$$\Delta \pi = \pi_{fc} - \pi_p \tag{2.12}$$

Where:

J_w - is the permeate flux produced by reverse osmosis membrane ($l.m^{-2}.h^{-1}$)

K_w - is the membrane permeability coefficient for water ($m^3.h^{-1}.m^{-2}.bar^{-1}$)

ΔP - is the hydraulic pressure differential across the membrane (bar).

P_f – is the feed pressure (bar).

P_c - is the concentrate pressure (bar).

$\Delta \pi$ - is the osmotic pressure differential across the membrane (bar).

π_{fc} - is the feed – concentrate osmotic pressure (bar).

π_p - is the permeate osmotic pressure (bar).

σ - is the reflection coefficient.

Q_p - is the permeate flow ($m^3.h^{-1}$)

A - is the membrane surface area (m^2)

The reflection coefficient (σ) which represents the rejection capability of a membrane, whose values are between 0 and 1. A reflection coefficient of 1 corresponds to ideal semi permeable membranes and 0 for entirely unselective membranes (Taniguchi and Kimura, 2000; Kimura, 1995).

2.6.5 Salt Transport

The rate of salt flow through the RO membrane is defined by the following equation (Zhao and Taylor, 2005; Pais, *et al.*, 2007):

$$J_S = K_S \times \Delta C = J_w \times C_P \qquad (2.13)$$

Where:

J_S - is the flow rate of salt through the membrane ($mg.s^{-1}$)

K_S - is the membrane permeability coefficient for salt ($m.s^{-1}$)

ΔC – is the salt concentration differential across membrane =($C_f - C_p$) ($mg.L^{-1}$)

J_w - is the flow rate of water through the membrane ($l.m^{-2}.h^{-1}$)

C_f and C_p - are the feed and permeate concentration ($mg.L^{-1}$)

Rate of salt flow is proportional to the concentration differential across the membrane and is independent of applied pressure. The transport of salt across a membrane is commonly expressed as salt passage or salt rejection.

2.6.6 Salt Passage (%)

Salt passage (SP) is defined as the percentage of dissolved constituents in the feed water that pass through the membrane. Salt passage (SP) is the ratio of concentration of salt on the permeate (C_p) side of the membrane relative to the average feed – concentrate concentration (C_{fc}) and mathematically, it is expressed as: (Kimura, 1995; Taniguchi and Kimura, 2000).

$$SP(\%) = 100 \times \frac{C_p}{C_{fc}} \qquad (2.14)$$

Where:

SP – is the salt passage (%)

C_p – is the salt concentration in the permeate ($mg.L^{-1}$)

C_{fc} – is the average feed – concentrate concentration ($mg.L^{-1}$)

2.6.7 Salt Rejection (%)

Salt rejection (SR) refers to the ability of the membrane to reject the dissolved solids (salts) in the feed water. It can be defined as 100% minus the percentage of salt passage (Mulder, 2003). There are different ways to calculate salt rejection and it illustrated in Eq. (1.15) and Eq. (2.16).

$$SR(\%) = 100\% - SP(\%) \tag{2.15}$$

$$SR(\%) = 100 - SP(\%)\left(\frac{C_p}{C_{fc}}\right) \times 100\% \tag{2.16}$$

2.6.8 Recovery (%)

Recovery / Conversion can be defined as the ratio of the product flow rate to the feed flow rate and can be calculated using the following equation (Mulder, 2003; Scott and Hughes, 1996):

$$Y(\%) = \frac{Q_p}{Q_f} \times 100\ \% \tag{2.17}$$

Where:

Y – is the percent recovery or conversion (%)

Q_p – is the permeate flow rate ($m^3.h^{-1}$)

Q_f - is the feed flow rate ($m^3.h^{-1}$)

2.6.9 Concentration Factor (CF)

The degree of concentration of the concentrate is given by the concentration factor (CF), and defined by the ratio of the concentration of component *i* in the concentrate (C_{ic}) to

the concentration of the same component in the feed (C_{if}) and it is related to the recovery rate (Y) by the following equation:

$$CF = \frac{(C_i)_c}{(C_i)_f} = \frac{1}{1-Y} \qquad (2.18)$$

2.7 Reverse Osmosis Desalination Plants.

Historically, most of the installed seawater desalination capacity has been produced through thermal distillation. However, since the late 1990s, reverse osmosis (RO) membrane systems have become the fastest growing segment of the seawater desalination market. Reverse osmosis desalination technology is an attractive desalination technique after improvement of RO membrane performance and reduction of capital and operation costs. The result is that large SWRO desalination plants are being constructed to reduce the unit cost of desalinated water in various parts of the world that suffer from shortage of freshwater. Table 2.4 shows examples of the world's largest SWRO desalination plants.

Table 2.4: The world's largest sea and brackish waters RO desalination plants. Source, Stover, *et al.*, (2007); Gustave, (2004).

Name of the plant	**Country**	**Capacity ($m^3.d^{-1}$)**	**Year**
- Ashkelon SWRO desalination plant	Israel	330, 000	2003
- Perth SWRO desalination plant	Australia	144,000	2005
- The Torrenieja SWRO desalination plant	Spain	440,000	2008
- Hamma Seawater Desalination plant	Algeria	200,000	2007
- Palm Jumeirah	UAE	71,000	2003
- Bahia de Palma	Spain	68,500	1995
- Laranca SWRO desalination plant	Cyprus	54,000	2006
- Fukuoka	Japan	50,000	2005
- Jeddah SWRO desalination Plant	Saudi Arabia	52,000	2006

Generally every SWRO desalination plant consists of six components: an intake to provide a consistent supply of feed water; a pretreatment system to properly condition the feed water; a high-pressure pumping system to provide the energy necessary for fresh water to pass through the membrane; a membrane module which performs the desalination process by rejecting the salt; post-treatment to condition the product water; and product storage and distribution (Figure 2.11). The performance of the RO membrane system is dependent upon the proper design and operation of each component.

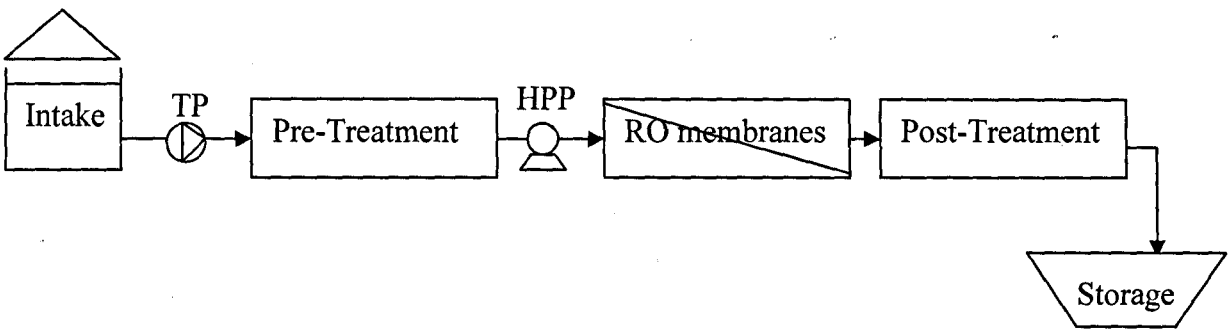

Figure 2.11: Schematic diagram of reverse osmosis desalination plant components.

2.8 Factors Affecting Reverse Osmosis Membrane Performance

There are several factors that affect the performance of RO membranes. These factors include recovery, feed water temperature, feed pressure, feed water salinity and concentration polarisation.

2.8.1 System Recovery

Increasing system recovery (the amount of treated water obtained) above the design criteria will increase the salt concentration near the membrane surface and in the bulk solution and causes an increase in osmotic pressure of the concentrate stream (Bartels, *et al.*, 2005 and Mulder, 2003). The permeate flow will stop through the membrane if the osmotic pressure becomes as high as the applied feed pressure. Increasing osmotic pressure in the system will also increase the salt passage through the membrane (Elimelech, *et. al*, 1997).

2.8.2 Feed Water Temperature

Temperature change can result in both osmotic pressure (π) and water flux (J_w) changes. As indicated in Equation 2.5, the osmotic pressure and water flux (K_w) is directly proportional to temperature. Water viscosity can also be affected with variations in water temperature. It is estimated that an increase of one degree Celsius in feed water temperature can cause an increase of 3% in permeate flux but salt passage will increase as well (Al-Bastaki and Al-Qahtani,1994).

2.8.3 Feed Pressure

Feed pressure is created by high pressure pumps supplying feed water to the RO membranes. As a general rule, any increase in transmembrane pressure (ΔP) results in an increase in water flux (J_w) of a given set of feed conditions. With increasing feed pressure the permeate flux will increase.

2.8.4 Feed Water Salinity

Feed water salinity affects the quality and quantity of permeate water because it causes a decrease in water flux, an increase in osmotic pressure and an increase in salt passage through a reverse osmosis membrane (Bartels, *et al.*, 2005). However, increasing salt passage through an RO membrane can be attributed to many factors including feed water temperature, feed water concentration, fouling, membrane pore size and charge density. While RO membranes have the capability to reject up to 99.6% of ions, this strongly depends on the surface charge of each membrane. RO membranes are negatively charged and strong negatively charged membranes have better rejection than weak negatively charged membranes (Figure 2.12).

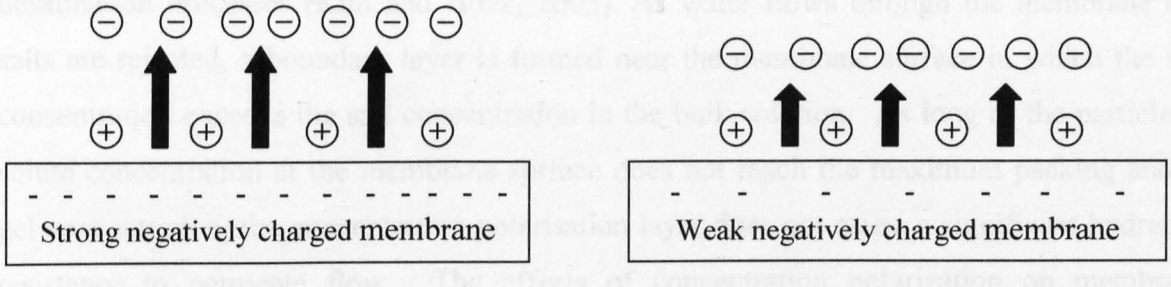

Figure 2.12: Repulsion and attraction of cations and anions by negatively charged RO membrane (Bartels *et al.*, 2005).

When cations and anions come in contact with the negatively charged RO membrane, an electrical potential "Donnan potential" is created at the boundary layer between the bulk solution and the membrane surface. The Donnan potential attracts the cations to the membrane surface and repels anions away to the bulk solution, thus increasing the rejection of anions. According to this theory, the overall salt rejection of the membrane is dependent on the rejection of anions. Therefore, the overall salt rejection of the membrane increases at a higher Donnan potential (Bartels, *et al.*, 2005; Peeters *et al.*, 1998). The Donnan potential can be neglected at low salinity (TDS<300 $mg.l^{-1}$) because of low cation and anion concentration. Increasing water salinity beyond 3000 $mg.l^{-1}$ weakens the Donnan potential and reduces the salt rejection by the membrane. Higa, *et al,* (1998) reported that the presence of a high concentration of divalent cations in solution weakens the Donnan potential because they accumulate on the membrane surface and shield the membranes repulsive force on the anions in the bulk solution (Figure 2.13).

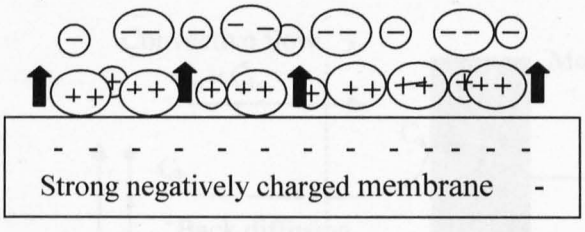

Figure 2.13: Accumulation of divalent cations at the membrane surface shield the repulsive force between the negatively charged membrane and the anions in the bulk solution (Bartels, *et al.*, 2005).

2.8.5 Concentration Polarisation

The phenomenon of concentration polarisation is very common in membrane desalination processes (Kim and Hoek, 2005). As water flows through the membrane and salts are rejected, a boundary layer is formed near the membrane surface in which the salt concentration exceeds the salt concentration in the bulk solution. As long as the particle or solute concentration at the membrane surface does not reach the maximum packing and/or gel concentration, the concentration polarisation layer does not cause a significant hydraulic resistance to permeate flow. The effects of concentration polarization on membrane performance are; an increase in osmotic pressure at the membrane surface, which results in

lowering the trans-membrane pressure driving force, reduction in permeate flow and an increase in salt passage across the membrane. Consequently, the probability of exceeding solubility limits of sparingly soluble salts at the membrane surface will increase and membrane scaling will occur (Bhattacharyya and Hwang, 1997).

The increase in solute concentration continues until a steady state condition is reached (Lin, *et al.*, 2004). The convective flow of solutes towards the membrane can be written as J_w x C_f where; J_w is membrane flux ($l.m^{-2}.hr^{-1}$) and C_f is the feed solute concentration ($mg.L^{-1}$). As the RO membrane capability to reject ion salts is not 100%, solute flow and concentration through the membrane can be written as J_w. C_p. The retained solutes accumulate at the membrane surface and their concentration increases and creates a diffusive flow back to the bulk of the feed. The back diffusion of salt concentration can be written as Ddc/dx (Fick's law), where D is the diffusion coefficient (Figure 2.14).

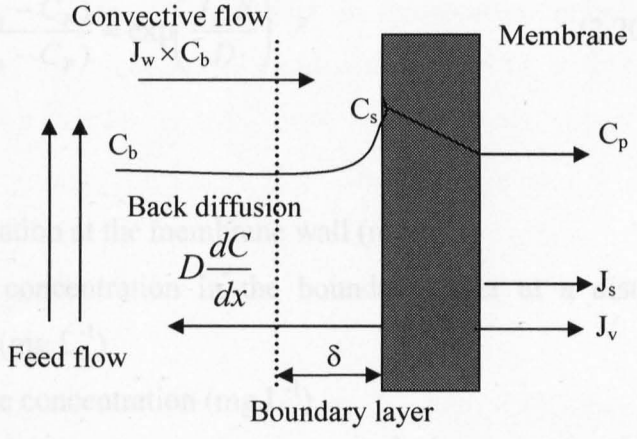

Figure 2.14: Schematic representation of concentration polarisation phenomenon (Lisdonk, *et al.*, 2001).

Increasing the boundary layer (δ) due to an increasing in solute concentration at the membrane wall increases the resistance to flow and causes flux decline. At steady state conditions, transport to the membrane is equal to the sum of the permeate flux plus the diffusive back transport of the solute (Mulder, 2003; Lin, *et al.*, 2005).

$$J_w \times C - D\frac{dC}{dx} = Jv \times C_p \qquad (2.19)$$

Where:

J_w – is the permeate flux ($l.m^{-2}.s^{-1}$).

C – is the solute concentration in the boundary layer at a distance x from the membrane surface ($mg.L^{-1}$).

J_v – is the permeate flux ($l.m^{-2}.s^{-1}$).

C_p – is the permeate solute concentration ($mg.L^{-1}$)

D – is the solute diffusion coefficient ($m^2.s^{-1}$).

dC /dx – is the solute concentration gradient.

x – is the coordinate perpendicular to the membrane surface (m).

With the boundary layer conditions at x = 0, C = C_S and at x = δ, C = C_b and integration of equation (2-19), the concentration polarisation can be written as follows:

$$\frac{(C_s - C_P)}{(C_b - C_P)} = \exp\left(\frac{J_w.\delta}{D}\right) \qquad (2.20)$$

Where:

C_s – is the concentration at the membrane wall ($mg.L^{-1}$)

C_b – is the bulk concentration in the boundary layer at a distance x from the membrane surface ($mg.L^{-1}$).

C_p – is the permeate concentration ($mg.L^{-1}$).

D – is the solute diffusion coefficient in water ($m^2.s^{-1}$).

δ - is the thickness of the boundary layer (m).

Because the thickness of the boundary layer (δ) is unknown, one can instead use the mass transfer coefficient (K) defined as the ratio of diffusion coefficient (D) to thickness of the boundary layer (δ) and can be determined as following:

$$K = \frac{D}{\delta} \qquad (2.21)$$

Substituting the mass transfer coefficient in Equation 2.21, gives:

$$\frac{(C_S - C_P)}{(C_B - C_P)} = \exp\left(\frac{J_w}{K}\right) \qquad (2.22)$$

The ratio of the concentration on the wall (C_s) to the concentration in the bulk (C_b) is defined as the concentration polarisation modulus (CP). Since the value of the permeate concentration (C_p) is so small, it can be neglected and the concentration polarisation (CP) can be determined by the permeate flux (J_w) and mass transfer coefficient K (Baker 2004).

$$CP = \frac{C_s}{C_b} = \exp\left(\frac{J_w}{K}\right) \qquad (2.23)$$

The concentration (C_s) at the membrane surface increases exponentially with increasing water flux, with increasing salt rejection (SR) and with decreasing mass transfer coefficient (K). The concentration polarisation modulus depends only on the solute characteristics (D and C_s) and the boundary layer thickness (δ). When the value of C_s is 1.0, then no concentration polarisation occurs. For reverse osmosis membrane, the concentration polarisation factor (C_s) is normally between 1.1 – 1.5 (Baker, 2004).

For RO membranes, concentration polarisation can be determined by measuring the permeate flux (J_w) and the mass transfer coefficient (K) (Sutzkover 2000). Permeate flux (J_w) produced by RO membrane is linked to the applied and osmotic pressure (Eq. 2.24):

$$J_w = K_w\left[\Delta P - (\pi_{fc} - \pi_p)\right] \qquad (2.24)$$

The value of the mass transfer coefficient (K) at a given pressure can be determined by measuring the fluxes for pure water and saline water respectively (Eq. 2.25).

$$K = \frac{(J_W)_{Salt}}{\ln\left\{\frac{\Delta P}{\pi_{fc} - \pi_p} \times \left[1 - \frac{(J_w)_{salt}}{(J_w)_{H_2O}}\right]\right\}} \quad (2.25)$$

Where:

K_w – is the water permeability coefficient ($l.m^{-2}.h^{-1}.bar^{-1}$).

ΔP – is the applied pressure (bar).

π_{fc} – is the feed-concentrate osmotic pressure (bar).

π_p – is the permeate osmotic pressure (bar).

$(J_w)_{salt}$ – is the permeate flux of saline water ($l.m^{-2}.h^{-1}$).

$(J_w)_{H2O}$ – is the permeate flux of pure water ($l.m^{-2}.h^{-1}$).

However, the simplest procedure for reducing the concentration polarization is to increase membrane cross flow velocity in order to hinder deposition of solute onto membrane. However, the cross flow velocity which can be used is limited due to high pressure drop (Scott and Highes, 1996).

2.9 Membrane Problems

There are different operational problems that can affect membrane filtration systems. These include membrane compaction, membrane degradation and membrane fouling.

2.9.1 Membrane Compaction

Compaction can be defined as a change in the physical structure of RO membranes caused by exposure to excessive pressure and/or temperature which reduces the ability of the membrane to produce permeate. Thin film composite RO membranes suffer from compaction effects under high operating pressure and temperature. As the water pressure increases, the polymers are slightly reorganized into a tighter fitting structure that results in a lower porosity which limiting the efficiency of the membrane. Generally the higher the feed pressure, the greater the membrane compaction.

2.9.2 Membrane Degradation

Degradation of membranes may occur due to agents such as chlorine, detergents, solvents, and high temperature. The extent to which these factors affect the membrane depends on the properties of the particular membrane. Degradation leads to an increase in permeate flow, a lower rejection of contaminants and a lower quality of the permeate. For example, change in pH affects the cellulose acetate membrane performance and causes hydrolysis. Hydrolysis usually strips acetate molecules off the polymeric cellulose which reduces the salt rejection of the membrane. In the case of polyamid thin film composite membranes, chlorine tolerance by these membranes dose not exceeds 0.1 $mg.l^{-1}$ of Cl_2 (Glater, *et al.*, 1994). Chemical attacks by Cl_2 cause membrane failures because certain change in the polymer structure is occurred. The chemical structure of TFC RO membrane shows that there are numerous carbon, hydrogen, oxygen and nitrogen atoms bounded together. The oxygen and nitrogen functional groups enhance hydrophilicity of the membrane. The attack by chlorine, bromine, or ozone will break the bounds between atoms and increase the salt passage (Glater, *et al.*, 1994). The chemical composition of TFC RO membranes can be seen in laboratory by using dyes.

2.9.3 Membrane Fouling

Membrane fouling is a frequent problem in most seawater reverse osmosis systems, particularly when raw water is drawn from an open sea intake. Membrane fouling is a complex phenomenon involving the deposition of foulants such as particles, colloids, salts, oil, humic acids and microorganisms on the membrane surface (Xu, *et al.*, 2006; Feng, *et al.*, 2006). Several types of fouling can occur on RO membranes, which include: inorganic fouling that is caused by precipitation of inorganic salts such as $CaCO_3$, $CaSO_4$, $BaSO_4$ and silica (Lisdonk, *et al.* 2000; Tzotzi, *et al.*, 2007) organic fouling that is caused by natural and synthetic organic matterial (Hong, *et al.*, 1997); colloidal fouling that is caused by deposition of clays, silts and colloidal silica (Elimelech, *et al.*, 1997) and biological fouling that caused by the growth of microorganisms on the membrane surface (Vrouwenvelder and Van der Kooij D., 2002). Metal fouling including aluminum hydroxide $Al(OH)_3$ and iron hydroxide $Fe(OH)_3$ are very common in RO membrane systems because iron and aluminum are

naturally present at low levels in most water sources, as well as using of aluminum sulphate $Al_2(SO_4)_3$ and ferric chloride ($FeCl_3$) as coagulants in conventional pretreatment systems (Darton, *et al.*, 2004; Gabelich, *et al.*, 2002). Moreover, iron oxide or hydroxide can be formed and foul the RO membranes as a result of corrosion of metal pipes and pumps (Darton, *et al.*, 2004; Lopez, *et al.*, 2005). Location of fouling in RO desalination plant is summarised in Table (2.5).

Table 2.5: Location of fouling in RO desalination plants (Hutting, *et al.*, 2001).

Fouling	**Where it does occur first**
Scaling	Last membranes in last stage
Metal oxides	First membranes in first stage
Colloids	First membranes in first stage
Organic	First membranes in first stage
Biofouling (Rapid) (Slow)	- First membranes in first stage - Through out the whole RO systems

Ng and Elimelceh, (2004) and Verijenhoek *et al.*, (2001) stated that membrane fouling results in several effects including a decrease in permeat flow due to a gradual decline in flux, an increase in applied pressure to maintain a constant productivity, an increase in salt passage which results in low permeate quality.

2.10 Mechanism of Membrane Fouling

The major modes of membrane fouling include: cake formation, pore blocking, chemical interaction (concentration polarization), and adsorption. The rate of fouling is influenced by water quality, concentration of treated water, membrane type, hydrodynamics and surface characteristics of the membrane (Mulder, 2003). Cake formation normally occurs when particles larger than the average pore size accumulate on the membrane surface, forming a cake layer. Moreover, during filtration particles are deposited on top of one another leading to cake growth. As a result, the cake may increase the particle removal efficiency; however it also increases the filter's resistance.

Complete pore blockage can occur when particles arriving at the membrane participate in blocking the membrane pores. The most serious mechanism is internal pore blockage in which particles are adsorbed or trapped on the pore walls leading to a decrease in the pore volume. Reducing the volume of the membrane pores greatly reduces water flux and makes membrane cleaning very difficult (Tansel, *et al.*, 2000; Scott and Huges, 1996). Fouling of membrane filtration systems can be either reversible or irreversible. Reversible fouling refers to deposition of retained solutes on the membrane surface that generally exist as a gel cake layer (Figure 2.15a). Irreversible fouling tends to refer to adsorption or pore plugging of solutes within the membrane pore matrix (Figure 2.15b, and 2.15c).

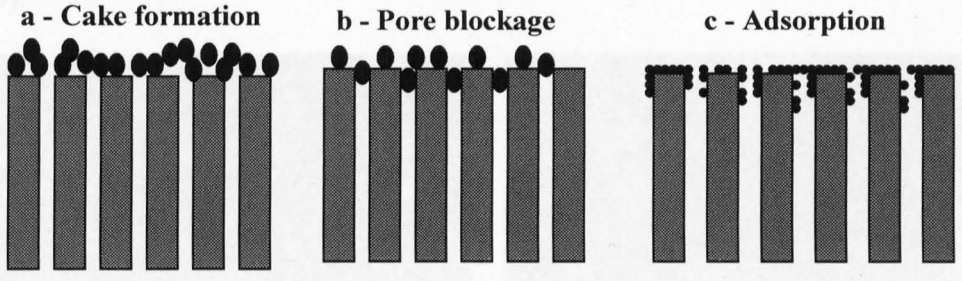

Figure 2.15: Mechanisms of membrane fouling, (Mulder, 2003; Scott and Huges, 1996).

Reversible fouling can be removed by chemical cleaning, backwashing "reversing of flow with a pressure higher than the feed pressure" and flashing "passing water at low pressure through the membranes" processes, however irreversible fouling is difficult to remove and requires extensive chemical cleaning and/or membrane replacement (Zularism, *et al.*, 2006).

2.11 Types of Membrane Fouling

Membrane fouling can be classified into five groups including inorganic, organic, colloidal, biological and composite fouling.

2.11.1 Inorganic Fouling (Scaling)

Scaling refers to precipitation of sparingly soluble salts such as $CaCO_3$, $CaSO_4$, $BaSO_4$ and Silica on the surface of RO membranes. As product water recovery increases, sparingly soluble salts become oversaturated in the concentrate stream and near the membrane surface due to concentration polarization (CP). Mineral salts can then precipitate

in the bulk solution near the membrane surface and crystallize directly at the membrane surface, thereby scaling the membrane resulting in flux decline, and necessitating an increase in energy consumption, chemical cleaning frequency and eventually shortening of membrane life (Lisdonk, *et al.*, 2001; Jawor and Hoek, 2009). Scaling can be avoided by adding acids and anti-scalants which work to inhibit the growth of crystal and/or lowering recovery. However, antiscalants are expensive and may be biodegradable, potentially leading to biological and organic fouling. Lowering recovery is not economically desirable as less water is produced and more concentrate is disposed off. Figure 2.16 shows an SEM image of calcium carbonate, calcium sulphate, barium sulphate and strontium sulphate scaling (Lopez, *et al*, 2005).

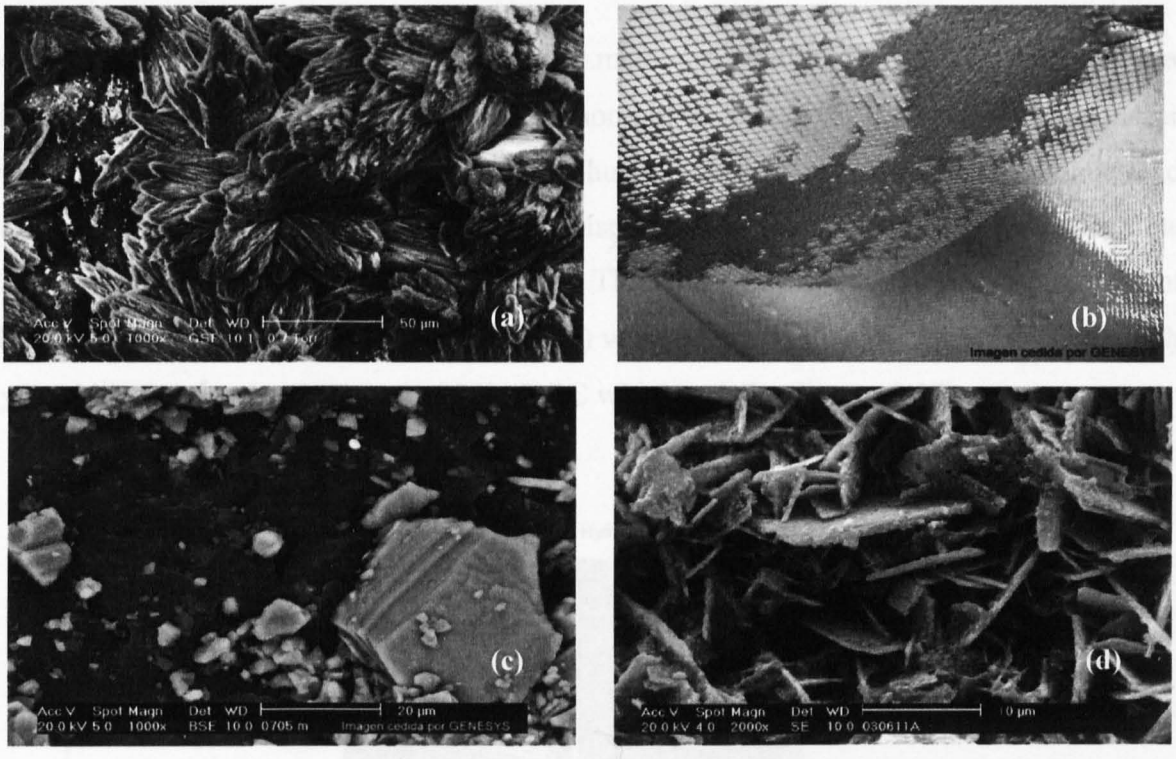

Figure 2.16: SEM image of calcium carbonate (a), calcium sulphate (b), barium sulphate (c) and strontium sulphate (d) scaling on RO membrane surface and feed spacer, (Reproduced from Lopez *e,t al.*, 2005)

Calcium sulphate and barium sulphate scaling are particularly troublesome in reverse osmosis due to low solubility. If they are not detected at an early stage and age into a hard deposit, it is difficult to remove them by conventional cleaning chemicals (Boeralge, *et al.*, 2002).

2.11.2 Organic Fouling

If the water source contains high natural organic matter (NOM), organic fouling could occur and would cause flux decline and increase in differential pressure in the RO membrane system. Research on membrane fouling has shown that NOM in the feed water can irreversibly be adsorbed onto the membrane surface and causes fouling. NOM reacts with free chlorine, which is used as a disinfectant in water treatment processes, and it is found to have a tendency to form disinfection by-products (DBPs) such as trihalomenthanes, haloacetics and other halogenated organics (Zularisam, *et al.*, 2006). DBPs are extremely harmful, and direct exposure to DBPs can lead to cancer, miscarriages and nervous system complications.

NOM is a complex mixture of organic materials, with varying concentration and characteristics, containing both humic and non-humic fractions. The humic fractions are more hydrophobic in character and comprise humic and fulvic acids. The non-humic acids are hydrophilic in character and mainly comprise of amino acids, proteins, and carbohydrates (Owen, *et al.*, 1995; Zularisam, *et al.*, 2006). The hydrophobic fraction of NOM represents about 49% of dissolved organic carbon (DOC) with large molecular weight (MW), while the hydrophilic fraction is composed of 30% DOC with low MW (Figure 2.17).

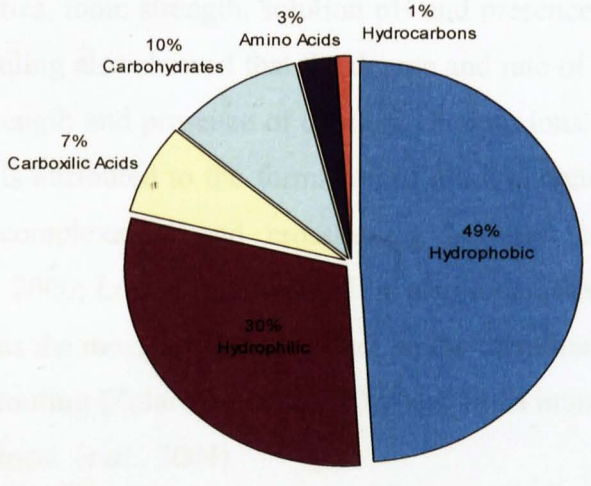

Figure 2.17: Fraction of NOM in surface water based on dissolved organic carbon (DOC) (Zularisam *et al.*, 2006).

NOM is basically divided into three categories: humic acid (HA), fulvic acid (FA) and humin. HA and FA are anionic polyelectrolytes with negative charged carboxylic acid ($COOH^-$), methoxyl carbonyls (C = O) and phenolic (OH^-) functional groups. HA is soluble in water at high pH values, whilst FA is soluble in water at any pH. Hummin has a black colour, and it is not soluble in water at any pH (Zularisam, *et al.*, 2006). Physical and chemical characteristics of fulvic acid, humic acid, and humans are summarised in Table 2.6.

Table 2.6: Physical and chemical characteristics of humic substances (Zularisam, *et al.*, 2006)

Fulivic acid	**Humic acid**	**Humin**
Light yellow Yellow brown	Dark brown Grey black	Black

The humin fraction of NOM has been found to cause more fouling than any other NOM component due to its adsorptive capacity on the membrane surface. Research on membrane fouling has shown that the NOM fraction in the feed water can irreversibly be adsorbed or deposited on to the membrane surface and causes fouling (Yuan *et al.*, 1999; Jones, *et al.*, 2000). The adsorption mechanism happens much quicker compared to cake formation process. However, this mechanism basically depends on many factors including, the membrane properties, ionic strength, solution pH and presence of divalent cations. Research on memebrane fouling also showed that the degree and rate of fouling are accelerated at low pH, high ionic strength and presence of divalent calcium ions. Increasing of fouling in the presence of Ca^{2+} is attributed to the formation of a thick, dense gel layer on the membrane surface due to complexation and crosslinking between calcium and macromolecules (Zularisam, *et al.*, 2006; Lee, *et al.*, 2004). It is also found that the dissolved organic matter (DOM) fraction has the most detrimental effect on the membrane performance as it can result in an irreversible fouling (Zularisam, *et al.*, 2006). A SEM image of organic fouling is shown in Figure 2.18 (Darton, *et al.*, 2004).

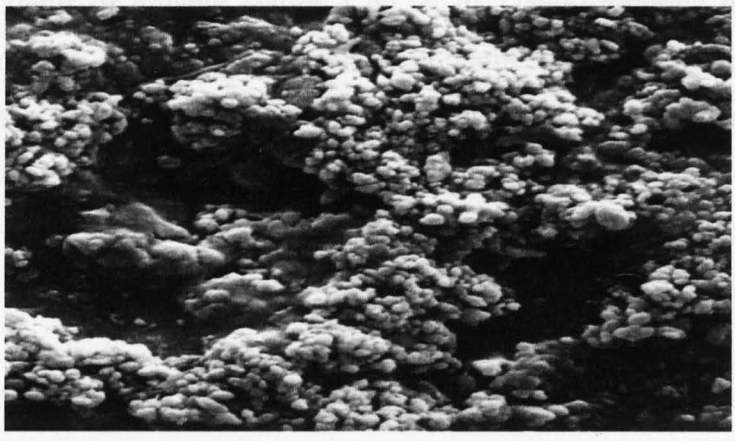

Figure 2.18: SEM image of organic fouling on RO membrane surface, (Reproduced from Darton, *et al.*, 2004)

Mo and Huang, (2003) investigated the surface of fouled membrane, observed that the fouling layer was a combination of microorganisms and inorganic materials. They found that organic foulants were mainly composed of low MW substances and Ca^{2+} was the primary inorganic substance. In another study, Cho, *et al.* (2000) reported that the hydraulic resistance of HA increased at low pH and high ionic strength and in the presence of calcium ions because calcium ions, reduced the HA solubility and canceled the negative charge effect (protonation) of the functional group. Similarly, this finding was also, supported by Hong and Elimelech, (1997) who found that the organic fouling rate increased with increasing ionic strength, and decreasing pH as well as with the addition of calcium ions to feed water. Several studies (Hong and Elimelech 1997; Yuan and Zydeny, 2000; Seidel and Elimelech, 2002) showed that fouling by NOM promoted by low pH, high divalent ion concentration (Ca^{2+} and Mg^{2+}), high ionic strength, and low cross-flow velocity. They attributed flux decline at this condition to reduction in electrostatic repulsion between humic acid molecules and between humic acid and membrane surface.

Ultraviolet absorbance has been used as an indicator to identify both humic and fulvic acids in solution as it is very sensitive to aromatic compounds. The specific UV absorbance (SUVA) which defines as the UV_{254} absorbance (expressed as per meter of absorbance in m^{-1} per unit concentration of DOC in $mg.l^{-1}$) gives an indication about the hydrophilicity and

hydophobicity extents of organic matter. Cho, *et al.* (1998) reported that higher values of SUVA indicated that greater fraction of hydrophobic organic materials in water, thus suggesting a greater potential for organic membrane fouling. On the other hand Zularisam, *et al.* (2006) reported that SUVA of NOM adsorped from natural waters was in the range of 2.4 – 4.4 $L.mg^{-1}.m^{-1}$. Organic matter with SUVA values less than 3 units are hydrophilic in nature, while NOM with SUVA values higher than 3 units are hydrophobic in nature.

2.11.3 Colloidal Fouling

Colloids are present in all natural and process waters in different forms such as clays, colloidal silica, iron oxyhydroxide, large organic macromolecules, organic colloids suspended matter, and calcium carbonate precipitates. Colloids that cause fouling in RO membrane systems range between 0.05 to 0.1 microns because they can easily pass through multimedia filters and 5 microns cartridge filters (Ning, *et al.*, 2005). During cross-flow membrane filtration suspended particles and colloids are transported to the feed spacer and membrane surface. Because of the finite size of colloidal particles, concentration on the membrane surface reaches its maximum after a short period of time and a cake layer starts to form. The accumulation of colloidal particles at the membrane surface increases the hydraulic resistance to water flow through the membrane and thus reduces permeate flow and increases salt passage (Hong, *et al.*, 1997; Faibish, *et al.*, 1998; Park, *et al.*, 2008). The fundamental mechanisms controlling the colloidal fouling of RO membranes are complex and not well understood (Elimelech, *et al.*, 1997). Iron fouling is very common in RO membrane systems because it is added as a flocculant (Ferric chloride or ferrous sulphate) or occurs as the iron oxide or hydroxide form as a result of corrosion of metal pipes and pumps (Lopez, *et al.*, 2005) (Figure 2.19).

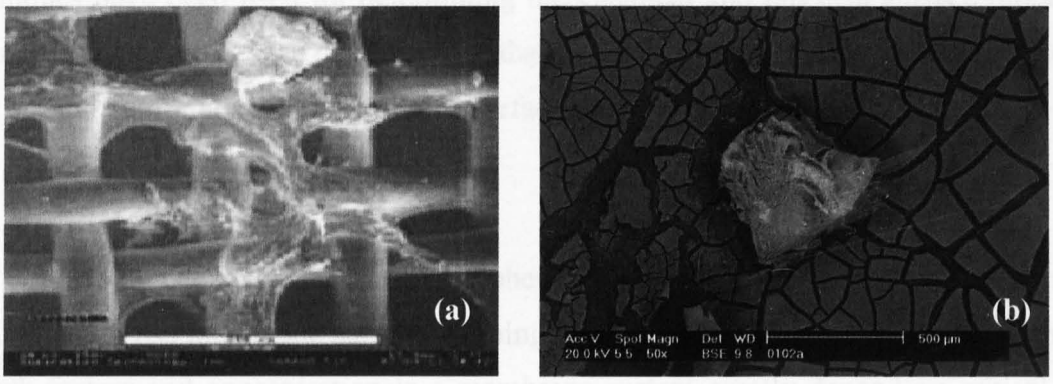

Figure 2.19: SEM image of colloidal (a) and iron (b) fouling on RO feed spacer and membrane surface (Reporduced from Lopez, *et al.*, 2005).

Hoek, *et al.* (2002) found that flux declines in colloidal fouling of RO and NF membranes due to cake-enhanced osmotic pressure. They suggested that a severe flux decline was observed because the colloidal cake layer limits back diffusion of salt ions from the membrane surface to the bulk solution, thus significantly elevating the salt concentration. Ng and Flimelech, (2004) investigated the influence of colloidal fouling on salt rejection by RO membranes and it was found that salt rejection decline was lower in the case of low colloid concentration and higher in the case of high colloid concentration in RO feed water. Similar results have been observed by Hoek, *et al.* (2002) and Elimelech, *et al.* (1997) in which the buildup of a cake layer at the membrane surface hinders back diffusion of solute from the membrane surface to the bulk solution and increases the salt concentration at the membrane surface. The increase in salt concentration creates greater salt concentration gradient across the membrane, causing an increase in salt passage and decrease in salt rejection by the RO membrane. Vrijenhoek, *et al.* (2001) reported that colloidal fouling of RO and NF membranes is correlated with membrane surface roughness and AFM images clearly show that more particles are deposited on rough membranes than on the smooth membranes. Particles accumulate in the "valley" of rough membranes, resulting in valley clogging which causes more flux decline than in smooth membranes. Several fundamental investigations of membrane fouling have explored the effects of membrane surface properties such as pore size and pores distribution, surface roughness and structure, electro-kinetic characteristics (zeta potential) and chemical properties (hydrophilic/hydrophobic). Various analytical

techniques have been used for determining the chemical and physical surface properties of RO membranes. It has been demonstrated that colloidal fouling of RO and NF membranes is only strongly correlated with membrane surface roughness.

2.11.4 Biological Fouling

Biological fouling refers to the phenomenon in which bacteria tend to adhere and accumulate to RO membrane surface, forming a biofilm. The types of micro-organisms, their growth factors and concentration in a membrane system greatly depend on critical factors, such as temperature, pH and the presence of organic and inorganic nutrients in feed water (Hu, *et al.*, 2005; Chen, *et al*, 2005). In order to control biological fouling in RO membrane systems, an efficient pre-treatment is required. Appling of conventional and membrane filtration as pre-treatment for RO membranes does not solve the biofouling problem because in practice, entering of a single viable bacterium to an RO membrane system could result in biofilm development. The available and mostly used technology for prevention of biofouling is addition of biocides agents to the RO feed water (Ridgway and Safarik, 1990; Flemming and Tamachkiarow, 2003). Table 2.6 gives a list of some chemical biocides which have been used to prevent biofouling in RO membrane systems.

However, biofouling and its control remains a major problem for many RO plants particularly those in tropical and sub-tropical regions (Baker and Dudley, 1998). Formation of a biofilm on RO membranes starts by transport of microorganisms to the membrane surface, attachment, and growth at the surface (Gossen, *et al.*, 2004; Ridgway and Safarik, 1990). Flemming *et al.,* (1997) reported that the attachment of bacterial cells to the membrane surface occurs after a few minutes of contact between a membrane and raw water and a biofilm can cover a RO membrane surface within three days. Ridgway and Safarik, (1990) reported that the adhesion of bacteria on the RO membrane surface depends on the hydrophobic interaction. They found that bacteria which exhibit a strongly hydrophobic cell surface, such as *mycobacteria*, display more rapid adhesion than hydrophilic bacteria.

Table 2.7: Chemical agents which are used for preventing of biofouling in RO membrane systems (Ridgway and Safarik, 1990).

Biocide agent	Compatibility with:		
	Typical concentration	CA membrane	TFC Membrane
Free chlorine	0.5 – 1.0 $mg.l^{-1}$	Yes	no
Chlorine oxide	0.5 – 2.0 $mg.l^{-1}$	yes	no
Formaldehyde	5.0 – 25 $g.l^{-1}$	yes	yes
Bisulfite	10 – 100 $mg.l^{-1}$	yes	yes
UV irradiation	>99.00% kill	1	1
Hydrogen peroxide	0.1 – 2.0 $g.l^{-1}$	yes	no
Ozone	0.5 – 2.0 $g.l^{-1}$	2	2
Peracetic acid	0.1 – 2.0 $g.l^{-1}$	yes	yes
EDTA	0.1 – 5.0 $g.l^{-1}$	yes	yes
pH extremes	pH 2 – pH 12	no	yes

[1] UV irradiation has an effect on RO feed water, however no active disinfectant residual will be left on the RO membrane surface.
[2] Ozone it can be used to disinfect the RO feed water only because it damages most RO membrane polymers.

Development of biofilm on the RO membrane surface causes a gradual decline in permeate flux, an increase in the differential pressure in the RO module and an increase in salt passage (Ridgway and Safarik, 1990; Flemming, *et al*, 1997). Furthermore, biofouling of the feed spacer and surfaces of spiral wound RO membranes causes a significant increase in differential pressure due to increasing of hydraulic resistance and deterioration of product water quality (Hu, *et al.*, 2005, Ridgway and Safarik, 1990; Flemming, *et al*, 1997). Therefore, understanding of the mechanism of bacterial attachment on the RO membrane surface and membrane feed spacer is a very important step in the development of antifouling methods (*Goosen, et al.*, 2004; Flemming, *et al.*, 1997). Different techniques are used in order to control biofouling including disinfection using hypochlorite, ozone, bromine, chlorine dioxide and ultraviolet light (Griebe and Flemming, 1998; Hu, *et al.*, 2005).

2.11.5 Microbial Biofilm

A microbial biofilm is a surface associated community that creates its own microenvironmental niches by forming a complex structure of bacteria embedded in a matrix of extracellular polysaccharides (EPS) (Schaule, *et al.*, 1999). Biofilm formation starts with attachment of microbes to the membrane surface, utilising the inorganic matter rejected by the membrane and retained in the fouling matrix (EPS). Pang, *et al.* (2005) investigated the biofilm formation of bacteria isolates retrieved from a RO membrane and found that the transition from planktonic to sessile on the membrane surface is high. Biofilm formation develops by initial cell adhesion, cell aggregation into microocolonies and cell reproduction. Figure 2.20 illustrates the development of biofilm on a cellulose acetate RO membrane surface.

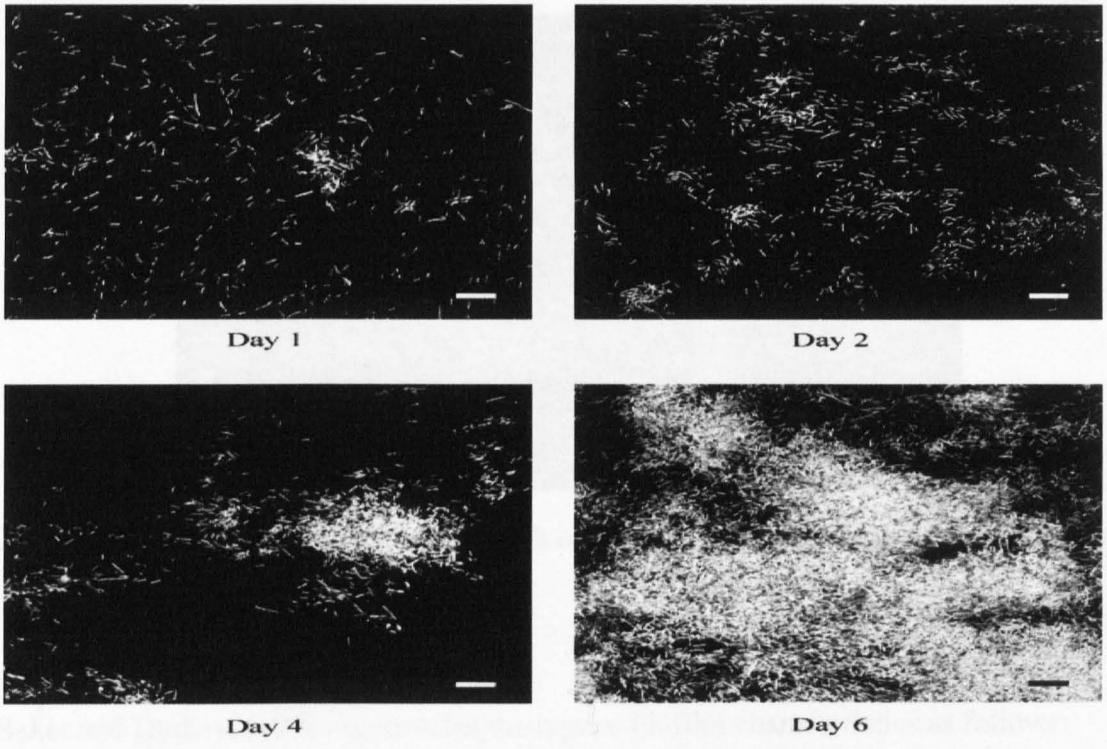

Figure 2.20: Development of biofilm on CA RO membrane surface during 6 days of experimental run (Reproduced from Pang, *et al.*, 2005).

The biofilm matrix contains polysaccharides, proteins and lipids and can absorb organic and inorganic molecules and entrap other biotic and abiotic particles as well as acting as a nucleation site for the formation of inorganic crystals. Bacteria embedded in biofilm are more resistant to biocides than the same bacteria in a dispersed state (Schaule, *et al.*, 1998).

The biocide only affects the top layer of the biofilm, and viable bacteria deep in the biofilm will quickly re-contaminate the membrane system and high bacteria levels would be seen again within a few days.

The main important influences on the rate of biofilm development are the presence of nutrients such as carbon, nitrogen, and phosphorus and temperature (Flemming, *et al*, 1997). In full scale RO plants it is difficult to eliminate the presence of nutrients and control the feed water temperature. Biofilms are involved from the very beginning (after few hours of operation). Figure 2.21 shows biofilm bacteria attached to a cellulose acetate RO membrane operated for a period of six days on a pre-treated municipal wastewater (Ridgway and Safarik, 1990).

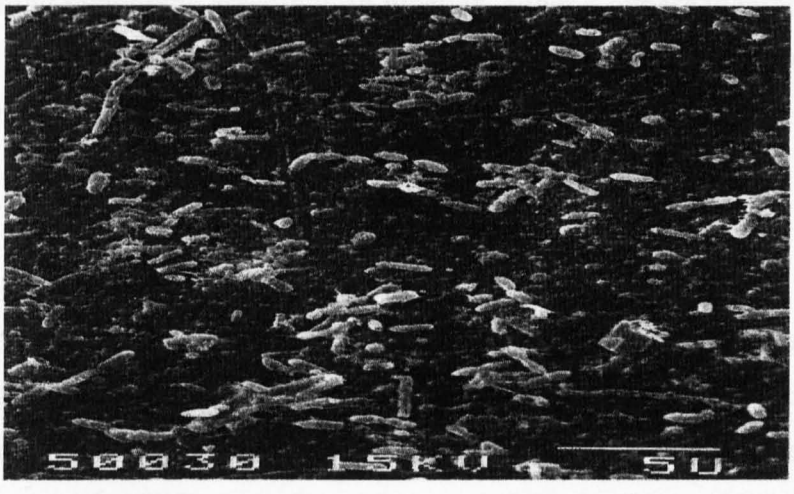

Figure 2.21: Scanning electron micrograph of biofilm bacteria (Reproduced from Ridgway and Safarik, 1990).

Baker and Dudley, (1998) summarise the typical biofilm characteristics as follows:

- More than 90% water,
- Of the dried content, more than 50% is total organic matter,
- Up to 40% humic substances as a percentage of total organic matter in high coloured waters,
- Low inorganic content,
- More than 5% Fe as iron oxide when treating brackish water,

- High microbiological counts (more than10^6 cfu.cm^{-2}) including bacteria, fungi, and sometimes yeasts.

Ridgway and Safarik, (1990) reported that development of biofilm in RO membrane systems forms a boundary layer on the membrane surface, where dissolved salts tend to accumulate, thereby a leading to an enhanced opportunity for concentration polarization. The process of biofilm formation on many substrata has been investigated, however the possible mechanisms involved in bacterial transport and attachment onto water purification RO membranes have not been thoroughly explored, and the different adhesion mechanisms between bacterial cells and the membrane surface is not well understood (Pang, *et al.,* 2005). Moreover, there is still no technology available to take biofilm samples non-destructively from an operating membrane assembly. In practice, either a bypass membrane device is used from which membranes can be removed and investigated destructively, or other representative surfaces are sampled which are accessible, such as cartridge filters (Flemming, *et al*, 1997).

2.12 Transparent Exopolymers Particles (TEP)

The presence of organic colloidal material and other unknown components of natural organic matter in water sources play an important role in the preconditioning of surfaces for biofilm development (Flemming, 1997; Kumar, *et. al.,* 2006). Other undetected transparent exopolymers particles (TEP) were found in sea and fresh water. Alldredge, *et al.* (1993) during staining of seawater using Alcian Blue which is a specific dye use for acid mucopolysaccharides, found a high abundance of undetected transparent micro-particles (~ 10^3 to 10^7 particles per liter). They range from ~1μm to ~200μm and exist as individual particles rather than as cell coating or dissolved limes (Passow and Alldrage, 1995). Alldredge, *et al.*, (1993) and Villacorte, *et al.*, (2009) reported that TEPs are hydrophilic substances that can exist in different shapes (blobs, clouds, sheets and filaments) and sizes (~0.4 to 400 μm). TEPs can be defined as deformable gel-like particles suspended in the water mass (Breman and holenberg, 2005; *Bar-Zeev et al.*, 2009). The presence of polysaccharides in TEP makes them more sticky than phytoplankton or mineral particles (Figure 2.22).

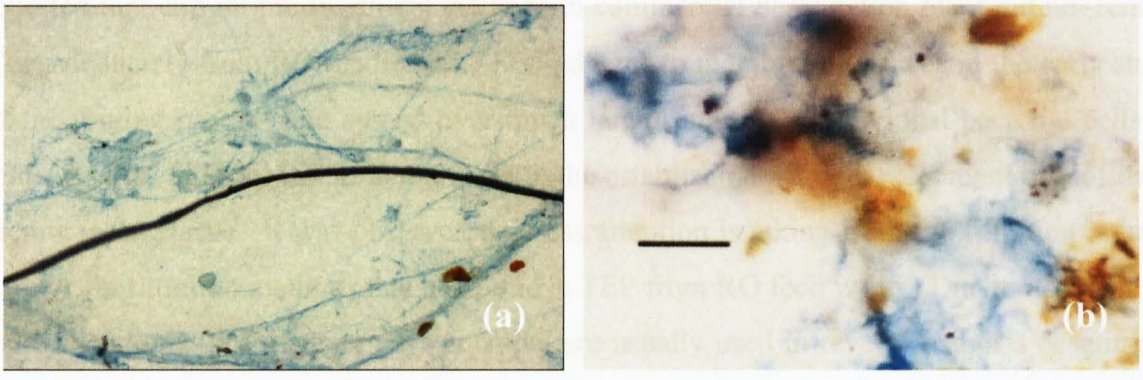

Figure 2.22: Fresh water TEP (a) together with inorganic particles (Lake Kinneret) and marine TEP (b) near surface (Southren Ocean), (Reprduced from Breman and Holenberg, 2005).

It has been reported that TEP are produced from the gelatinous envelopes surrounding diatoms, bacterial mucous and other algae (Passo,w *et al.*, 2001; Breman and Holenberg, 2005). Villacorte, *et al.*, (2009) reported that the majority of TEP are formed from colloidal polysaccharides 1-3 nm in diameter by hundreds of nm long and they are flixble enough to pass through 8 kDa pore size membranes. TEP often colonised by bacteria and other micro-organisms because they are rich in surface active acidic polysaccharides and other substances including proteins and nucleic acids (Figure 2.23).

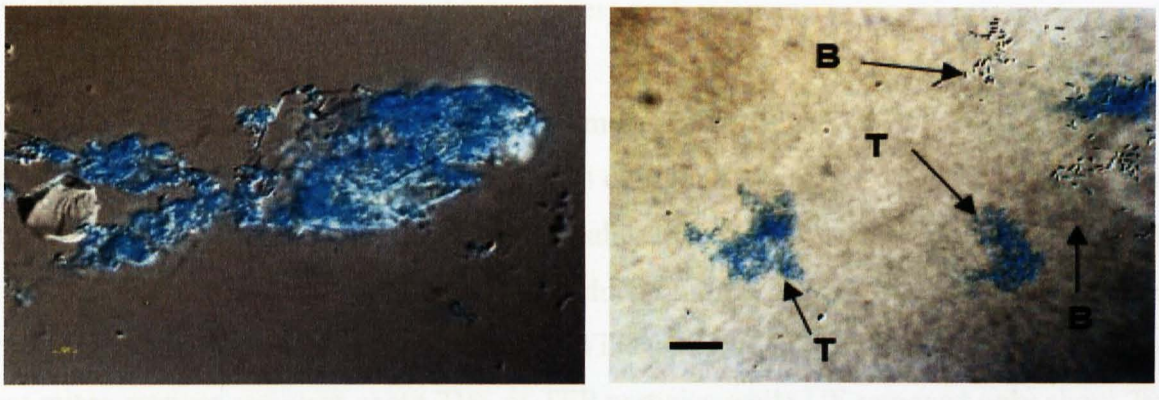

Figure 2.23: TEP with attached bacteria (Combined DAPI with Alcian Blue Stain), (Reproduced from Bar-Zeev, *et. al.*, 2009).

TEP play a major role in biofilm formation and development on membrane and other surfaces. Breman and Holenberg, (2005) described the potential link of TEP with RO membrane fouling. They consider TEP as a "major initiation" in biofilm formation and its

subsequent build up in RO membrane systems. In another study Bar-Zeev, *et al*, (2009) reported that current pre-treatment methods in commercial desalination plant did not remove TEP adequately from RO feed water. TEP adheres to membrane surfaces in the early stages of the fouling process and spread over much larger areas than individual bacterial cells. It indicates that TEP play an important role in the establishment and development of biofilm on membrane surfaces. It was observed that less attention is taking from the filtration industry to develop filtration methods that can remove TEP from RO feed water. Due to its small size the conventional pre-treatment systems that are usually used in reverse osmosis desalination plants do not adequately remove them. Bar-Zeev, *et al.*, (2009) investigated the removal efficiency of sand filters and 5 micron cartridges filters at Adom Desalination Plant, Ashkelon in removing of TEP from seawater, they found that the concentration of TEP did not decrease after sand filters and even they tended to increase after passing through the cartridge filters. They attributed the increase of TEP concentration after cartridge filters due to turbulence in the water stream passing through the cartridge filters. As TEP have very small size and glue like characteristics they can entrap or bind organic and inorganic colloids in the feed water onto membrane surfaces. In this way, presence of TEP can be a risk not only to cause biofouling but organic and particulate fouling as well. There are several papers in the literature about TEP however people in filtration industry may be are as yet unaware of the effect of these particles on membrane process performance.

MF and UF are used as pre-treatment for RO membranes (Teuler, *et al.*, (1999; Glueckstren, *et al.*, 2002). However, this technology has its own limitations in treating low quality water and in removing of acidic polysaccharides smaller than 0.4μm. According to oceanographic literature TEP are present in colloidal form which possibly can not be removed completely from RO feed water by MF.UF membranes. Villacorate, *et al,* (2009) in recent study found that micro-strainer removed about 21% of TEP particles while UF removed only about 28%. Therefore, an adequate filtration technique should be developed and applied to remove TEP and protect RO membranes from biofouling.

The promising filtration technique that can be used to remove substances that foul membranes including, TEP is using of Disruptor^{TM}. As TEP contain very small and sticky

negatively charged polysaccharides which many of them already carry resident bacterial populations, they could easily be removed by the novel nanoalumina depth filter "Disruptor^{TM}". This depth filter has naturally positive charge and has capability to remove the majority of substances that cause membrane fouling. The efficiency of this filter in removing the substances that responsible for fouling RO membranes including TEPs has been thoroughly investigated in this study.

2.13 Composite Fouling

Composite fouling is common in RO membrane desalination process. Composite fouling involves more than one foulant or more than one fouling mechanism working simultaneously (Sheikholeslami, 2005). The complexity of the fouling process itself restricted fouling research to single fouling. In general, there is complete lack of attention to the presence, mechanism, modelling and mitigation of composite fouling in RO membrane systems (Sheikholeslami, 1999).

2.14 Fouling Monitoring Techniques

2.14.1 Measuring of turbidity

Particulate and colloidal fouling in the RO plant can be monitored by measuring turbidity and silt density index (SDI) in the raw seawater and pre-treated seawater (RO feed water). Turbidity is an indicator of the rate of RO membrane fouling by suspended solids. On line turbidity meters are used to measure the scattering of light caused by suspended solids in the water. A water sample having a turbidity reading greater than one Nephlometric Turbidity Unit (NTU) will foul the RO membrane elements.

2.14.2 Silt Density Index (SDI)

Silt density index (SDI) is described in American Society Testing Methods (ASTM D 4189-95). The following equation is used to calculate the SDI.

$$SDI = \left(\frac{1 - \frac{T_0}{T_1}}{15} \right) \times 100\% \qquad (2.26)$$

Where:

T_0 = is the initial time necessary to filter 500 ml of sample water

T_1 = is the time necessary to filter 500ml of water sample after 15 minutes of experiment run.

SDI is the most commonly used methods for prediction of particulate fouling in RO membrane systems. Membrane manufacturers have put a lot emphasis on the silt density index (SDI) standard method ASTM D 4189-95 as an important parameter for design and operation of RO membrane systems (Choules, *et al.*, 2008; Mosset, *et al.*, 2008). However, Borlage, *et al.* (2002) has reported that SDI does not provide any information regarding the nature of the foulants passing through a 0.45 micron filter and regarding the risk of biofouling. Furthermore, fouling problems have been reported even with very low SDI values. Boerlage, *et al.* (2002) and Rodriguez, *et al.* (2009) found that the modified fouling index (MFI) developed by Schippers and Verdouw in 1980, has many advantages over SDI including a linear relation between the concentration of colloidal particles and MFI and cake filtration is assumed to be the dominating filtration mechanism. Particles smaller than 0.45 μm in size can not be captured by the 0.45μm membrane, while the MFI using membranes with a pore size of 0.05μm. In 2003, Boerlage *et al.* has introduced the application of MFI-UF to fresh water sources however, since that MFI-UF has not yet been tested and evaluated for seawater. Rodriguez, *et al.* (2009) reported that MFI-UF method has limitations in predicting fouling in RO membranes, because RO membrane systems are operated in a cross flow mode while the MFI-UF is operated in a dead-end filtration test. Therefore the cake layer formed on surface of RO membrane has different characteristics from that formed in dead-end filtration mode. That is why in the majority of large scale RO desalination plants still use SDI as indicator for particulate fouling.

2.14.3 Calculation of Scaling Potential

Monitoring and prediction of scaling is very important in RO plants. Depending on the type of scaling, different scaling calculation procedures can be applied. These are adapted from the ASTM standards methods (D3739 and D4582) and can predict whether the sparingly soluble salts present in RO feed water will cause a scaling problem. Scaling usually

occurs in the last element in the last stage of the RO membrane system because this is where super-saturation is at maximum and where nucleation and growth of crystals will first take place (Lisdonk, *et al.*, 2000). Figure, 2.24 shows the two stages RO membrane unit.

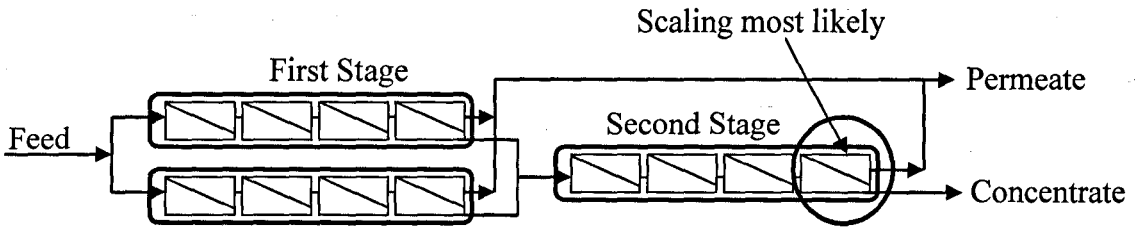

Figure 2.24: Two Stages of RO membrane unit, (Lisdonk, 2000)

The calculation procedures are based on the concentration of ion species in the concentrate stream. These are usually not known but they can be estimated from the ion species concentrations in the feed stream by multiplication with the concentration factor (CF). The concentration factor is derived from the membrane system recovery (R) as shown earlier in equation (2.12) (Boerlage, *et al.*, 2002). The most frequently used indices in the desalination industry are Langelier Saturation Index (LSI) (ASTM-D3739, 1998) and Stiff and Davis stability index (S&DSI) (ASTM-D4582, 2005), and the procedure for calculation of S&DSI is given in Appendix (A. section 3). Generally, scaling can be prevented using physical and chemical prevention methods (Boeralge, *et al.*, 2002; Bonne, *et al.*, 2000). The simplest physical method is to lower system recovery however, lowering recovery is uneconomical where less permeate will be produced and high concentrate will be disposed off (Boeralge, *et al.*, 2002; Hasson, *et al.*, 2001). The second physical method is to minimise the concentration polarisation at the membrane surface by increasing the cross flow velocity and promoting turbulence using membrane feed spacer. However, if the feed water is saturated with the sparingly soluble salts, then this method will have a limited effect. The other physical scaling prevention method is the combination of NF membranes with RO membranes. NF can remove scaling ions, then the NF permeate is fed to the RO membranes (Hilal, *et al.*, 2003). The chemical scaling prevention methods are addition of acids and anti-scalants to the RO feed water. Acid addition (HCL and H_2SO_4) is the common method to prevent alkaline scale. After addition of (HCl and H_2SO_4) to the feed water, the bicarbonate ions (HCO^-_3) are converted to CO_2 as follows:

$$H_2SO_4 + 2HCO^-_3 \rightarrow 2H_2O + CO_2 + SO^{2-}_4 \quad (2.27)$$

$$HCl + HCO^-_3 \rightarrow H_2O + CO_2 + Cl^- \quad (2.28)$$

H_2SO_4 is widely used in SWRO desalination plant because it is less expensive however; the use of H_2SO_4 leads to corrosion problems as well as increases the sulphate ions in the water which increase the potential of sulphate scaling (Boeralge, 2002). Anti-scalants are added to prevent sulphate scaling ($CaSO_4$, $BaSO_4$ and $SrSO_4$). Anti-scalant keeps scalant ions in solution by adsorbing onto the crystal surface preventing further crystal growth (Boerlage, *et al.*, 2002)

2.14.4 Measurement of Biological Activity

Several strategies are currently employed to control biofouling and biofilm formation in RO membrane systems these are: regular inspection of RO plant components (pipes, multimedia filters, cartridge filters and membrane system manifolds), routine collection of feed, permeate and concentrate water samples for culturing processes, identification and enumeration of biological species, disinfection and chemical cleaning (Saad, 1992 and 2002). It is not possible to monitor biofilm by sampling the water phase. Such samples do not give information about the composition of a biofilm. Therefore, a classic example for monitoring biofilm is the so-called "Robbins device" which consists of plugs inserted flush with pipe walls, thereby experiencing the same shear stress as the wall itself. After given periods of time, they are removed and analysed in the laboratory for all biofilm-relevant parameters. The disadvantage of such systems is the time-lag between analysis and result. Unfortunately, there is still no technology available to take biofilm samples non-destructively from an operating membrane assembly. In practice, either a bypass membrane device is used from which membranes can be removed and investigated destructively, or other accessible representative surfaces are sampled, such as cartridge filters (Flemming, *et al.*, 1997).

2.14.5 Normalisation of Operating Parameters

The evaluation of the reverse osmosis membrane systems performance is very important in order to differentiate between fouling and other operational problems. Different theoretical and software standardisation methods are used to evaluate the performance of RO membrane systems. The theoretical standardisation methods are ASTM (D4516) and HSDM, methods, while the software packages are ROSA (DOM FilmTec), RAData (Hydranuatics), CARTON (Toray) and NORMPRO (Koch). These software packages were derived from ASTM (D4516) method.

2.14.5.1 Theoretical Standardisation Methods

2.14.5.1.1 ASTM D 4516 Method

The most widely used method for standardisation of actual operating conditions in RO membrane systems is the ASTM (D 4516) method (Zhao and Taylor, 2005). This was developed by Du Pont, the early leader in membrane manufacture. The mathematical model consists of two main parameters: normalised permeate flow (Eq.2-31) and normalised salt passage (Eq. 2-36) which are both based on the start up (standard condition) condition of the membrane system in terms of feed pressure and osmotic pressure. By using this method, the actual membrane conditions can be compared with standard or reference conditions.

Normalised permeate flow (NFP) is a calculation that allows the comparison of a measured (actual) permeate flow (Q_{pa}) to a standard (or start up) condition. Permeate flow is a function of Net Driving Pressure (NDP) and feed water temperature. A decrease in NPF of 10-15% indicates that membrane cleaning is required.

$$NPF = \frac{NDP_s}{NDP_a}\frac{TCF_s}{TCF_a}Qp_a \qquad (2\text{-}29)$$

Performance of the reverse osmosis membrane system is affected by the net driving pressure (NDP). NDP is a summation of different pressures acting upon the RO membrane during operation. The NDP is calculated by the following equation:

$$NDP = P_f - 0.5\Delta P - P_p - \pi_{fc} + \pi_p) \qquad (2\text{-}30)$$

Where:

NPF – is the normalised permeate flow ($m^3 \cdot h^{-1}$)

Qp_a= actual and standardised permeate flow ($m^3 \cdot h^{-1}$)

P_f - is the feed pressure (bar).

ΔP - is the pressure differential between feed and concentrate streams (bar).

P_c - is the concentrate pressure (bar).

P_p - is the permeate pressure (bar)

π_{fc} - is the osmotic pressure of the feed – concentrate streams (bar).

π_p – is the osmotic pressure of the permeate stream (bar).

Subscripts a = actual operating data

Subscript s = standard operating data

The ASTM (D 4516) method equation of osmotic pressure (π_{fc}) is based on feed – concentrate average concentration (C_{fc}) and feed water temperature (T) and can be calculated using the following equation (Zhao, 2005; Lu, *et al.*, 2006):

$$\pi_{fc} = \frac{0.2654 \times C_{fc} \times (T + 273.15)}{1000 - \frac{C_{fc}}{1000}} \qquad (2.31)$$

Where:

π_{fc} - is the average feed – concentrate osmotic pressure (kpa) (1 bar = 100 kpa)

C_{fc} – is the feed concentration ($mg.L^{-1}$)

T - is the absolute temperature (Kelvin)

Performance of the reverse osmosis membrane is affected by the temperature of the feed water. The effect of temperature must be taken into account before comparing or evaluating the performance of a membrane element or a reverse osmosis system. The higher the feed

water temperature, the more the product flow and salt passage and vice versa. All reverse osmosis membrane elements are rated at 25 °C and a temperature correction factor (TCF) must be applied in order to evaluate the performance of RO membranes to correct the effect of temperature on permeate flux. The simplified ASTM method uses the TCF described in equation (2-32), while membrane manufacturers use equation (2-33).

$$TCF = 1.03^{(25-T)} \tag{2-32}$$

$$TCF = \exp\left(K\left(\frac{1}{T+273} - \frac{1}{298}\right)\right) \tag{2-33}$$

Where:

K- is the membrane temperature coefficient depending on the membrane material and it is around 2700 to 3100.

The normalised salt passage gives an indication of the loss of water quality due to fouling and/or operational problems in the RO membrane system and can be calculated using the following equation:

$$NSP = \frac{NDP_a}{NDP_s}\frac{Cfc_s}{Cfc_a}\frac{Cf_a}{Cf_s}Sp_a \tag{2-34}$$

Where:

NSP – is the normalised salt passage (%)

SP_a – is the actual salt passage (%)

NDP – is the net driving pressure (bar)

TFC – is the temperature correction factor (dimensionless)

C_{fc} – is the average feed and concentrate concentration ($mg.l^{-1}$).

C_f – is the feed concentration ($mg.l^{-1}$).

Subscripts a – is the actual operating data

Subscript s – is the standard operating data

The average feed – concentrate concentration (C_{fc}) is calculated by the following equation:

$$C_{fc} = C_f \frac{\ln\left(\frac{1}{1-Y}\right)}{Y} \qquad (2\text{-}35)$$

Where

Y – is the system recover (%) = $Y = \left(\frac{Q_p}{Q_f}\right) \times 100\,\%$

Q_p – is the permeate water and defined as the purified product water produced by the membrane element (L. h^{-1}).

Q_f – is the rate of feed water introduced to the membrane element (L. h^{-1}).

The ASTM method requires data on all ions to calculate osmotic pressure. In practice a full analysis of the feed water is only available twice a year and only conductivity values for feed, permeate and concentrate are more regularly available. Therefore, the average feed and concentrate osmotic pressure can be calculated by combining the average concentration of the feed and the concentrate and feed water temperature. Any deviation in actual osmotic pressure makes little difference to the normalisation calculations.

2.14.5.1.2 Homogenous Solution Diffusion Method (HSDM)

The HSDM method can be used to standardise permeate flow and salt passage for any RO membrane system. However, it requires various operating parameters such as, permeate flow and permeate concentration, flux, recovery and mass transfer coefficients for water and salt (Zhao and Taylor, 2005).

$$NPF = \frac{(\Delta P_s - \Delta \pi_s) \times TCF_s}{(\Delta P_a - \Delta \pi_a) \times TCF_a} \times Q_{pa} \qquad (2\text{-}36)$$

Where

Q_p – is the permeate water flow ($m^3 \cdot h^{-1}$)

TFC – is the temperature correction factor (dimensionless)

ΔP - is the pressure differential between feed and concentrate streams ($\Delta P = \frac{(P_f + P_c)}{2}$)(bar).

P_f - is the feed pressure (bar).

P_c - is the concentrate pressure (bar).

$\Delta\pi$ - is the Osmotic pressure gradient = (π_{fc} - π_p) (bar)

π_{fc} - is the osmotic pressure of the feed – concentrate streams (bar).

π_p – is the osmotic pressure of the permeate stream (bar) = $0.01 \times \pi_{fc}$.

Subscripts a – is the actual operating data

Subscript s – is the standard operating data

The mass transfer coefficients for water (K_w) can be determined using the following equations:

$$J = K_w \times (\Delta P - \Delta\pi) = \frac{Q_p}{A} \qquad (2\text{-}37)$$

$$K_w = \frac{Q_p}{A(\Delta P - \Delta\pi)} \qquad (2\text{-}38)$$

Where:

J – is the water flux ($l.m^{-2}.h^{-1}$)

K_w – is the mass transfer coefficient for water ($l.m^{-2}.h^{-1}.bar^{-1}$)

Q_p – is the permeate water flow ($m^3 \cdot h^{-1}$).

A – is the membrane surface area (m^2)

The mass transfer coefficients for salt (K_s) can be calculated using the following equations:

$$J_s = K_s \times \Delta C = J \times C_p \qquad (2\text{-}39)$$

$$K_s = \frac{Q_p \times C_p}{A(C_{fc} - C_p)} \quad (2\text{-}40)$$

Where:

J_s – is the salt flux ($m.s^{-1}$)

K_s – is the mass transfer coefficient for salt ($m.s^{-1}$)

A – is the membrane surface area (m^2)

ΔC – is the concentration gradient = (C_{fc}-C_p) ($mg.L^{-1}$)

C_p – is the permeate concentration ($mg.L^{-1}$)

C_f – is the feed concentration ($mg.L^{-1}$)

C_{fc} – is the feed-concentrate concentration ($mg.L^{-1}$)

The salt passage (SP) which is a ratio of diffusion salt flux (Eq. 2-40) divided by diffusion water flux (Eq. 2-38) can be calculated using equation (2-41) (Zhao and Taylor, 2005).

$$SP = \frac{K_s \times C_{fc}}{K_w \times (\Delta P - \Delta \pi) \times C_f} \quad (2\text{-}41)$$

2.14.5.2 Normalisation Software

Normalisation software is usually used to differentiate between fouling and other operational problems and to determine when chemical cleaning should be implemented. The software packages that can be used are ROSA (DOM FilmTec), RAData (Hydranuatics), CARTON (Toray) and NORMPRO (Koch). These software packages were derived from the ASTM (D4516) method. They use the same equations as the ASTM method to calculate the normalised permeate flow and the normalised salt passage but are slightly different in calculating some parameters such as osmotic pressure and temperature correction factors. In order to run the normalization software plant operators input values for flows (feed and permeate), pressure (feed and concentrate or differential pressure) and conductivity (feed and permeate) into an Excel spreadsheet. The software then calculates the normalized permeate flow, salt passage, salt rejection and differential pressure and produces graphs. These graphs are used to monitor the membrane systems performance. Another software system known as

MASAR (Membrane Analysis System and Automated Report) is used to monitor the membrane systems performance of nanofiltration and reverse osmosis desalination plants (Saad, 2004). The difference between the normalization software and MASAR is that the normalization software are used to produce a long-term flux decline performance trend by comparing the normalized permeate quantity and quality to design one under the same conditions. The MASAR is based on detecting fouling and scaling as soon as it starts to develop in the membrane systems in real-time, eliminating the need for long-term analysis. However, there is a lack in scientific publications describing the real benefits of using this software.

Membrane manufacturers report that change of normalised permeate flow, salt passage and differential pressure values during the operation of an RO membrane system are symptoms of formation of fouling or membrane damage. They recommend that RO membrane systems should be cleaned if the normalized permeate flow decreases by 15% and if the normalized salt passage and differential pressure values increase by about 15%. Table 2.8 shows the symptoms of operational problems of RO membrane systems and method of control, while Table 2.9 shows summary of fouling symptoms, causes and corrective measures.

Table 2.8: Symptoms of operational problems in RO membrane systems (Scott, 1998).

Symptoms			**Possible Cause**	**Possible Location**	**Corrective measure**
Permeate flow	**Salt passage**	**Differential pressure**			
Increasing	Increasing	Not changing or reducing	Membrane oxidation (Cl_2, Ozone, $KMnO_4$)	First RO pass	-Replace new RO element
Increasing	Increasing	Not changing or reducing	Glue leaks, abrasion, permeate backpressure	All RO passes	-Replace new RO element
Increasing	Increasing	Not changing or reducing	O-ring leak	All RO passes	-Replace O-ring
Increasing	Increasing	Not changing or reducing	Leaking product tube	All RO passes	-Replace element
Decreasing	Increasing	Not changing	High recovery	All RO passes	-Adjust recovery
Decreasing	Decreasing	Not change	Compaction/ water hummer	All RO passes	-Control feed pressure

Table 2.9: Symptoms, causes and corrective measures of membrane fouling (Hutting, *et al.*, 2001).

Fouling Symptoms			Possible Cause	Possible location	Corrective measure
Permeate flow	**Salt passage**	**Differential pressure**			
Decreasing	Increasing	Increasing	Scaling	Second pass	-Scale control -Cleaning
Decreasing	Increasing	Increasing	Colloidal fouling	First pass	-Cleaning, Improve pre-treatment
Decreasing	Increasing	Increasing	Metal oxide fouling	First pass	-Cleaning, Improve pre-treatment
Decreasing	Increasing	Increasing	Biofouling	Any RO passes	-Cleaning, Disifection, - Improve pre-treatment
Decreasing	Not changing	Not changing	Organic fouling	All RO passes	-Cleaning, Improve pre-treatment

2.15 Identification of RO Membrane Fouling by Autopsy

The indirect evaluation of performance of RO membrane system gives an indication of fouling and when chemical cleaning should be implemented. However, the cleaning process required is strongly dependent on the type of fouling. The only reliable method of determining the true identity of the foulant is by membrane autopsy (Darton and Faxell, 2001). The term autopsy is used to describe a series of visual practices and scientific tests made on a used RO membrane element. Membrane autopsy is a destructive study used to identify the cause of fouling of an RO membrane. In the literature, direct examination of fouled RO membranes is rather limited and the published papers relating to membrane autopsy have only recently started to appear (Butt, *et al.*, 1997). Carrying out membrane autopsy and obtaining reliable results requires skilled and trained personnel, and selection of the appropriate membrane element and equipment for analysis, such as scanning electron microscopy (SEM), Atomic Force Microscopy (AFM), X-ray Photoelectron Spectrometry (XPS), and Fourier Transform Infrared Spectroscopy (FTIR) (Vrouwenvelder *et al.*, 2001). Moreover, precautions must be taken during the autopsy process to preserve the original biomass composition, activity, spatial distribution and density, as present under operational conditions in the membrane element. These precautions are: coverage of the end caps of the elements after removal from the pressure vessel to prevent any contamination (Figure 2.24), storage of the membrane element on crushed ice (4°C) until analysis which should preferably be within 24 hours of removal of the membrane.

Figure 2.25: Removal of membrane element, (Darton and Faxell, 2001).

The autopsy includes several steps; visual inspection for damage (telescoping or fractures of the end caps and casing), weighing, opening the element lengthwise, visual inspection of membrane envelops and feed spacers, scraping of foulant material from the membrane surface for determining biomass and organic and inorganic elements (Figure 2.26).

Figure 2.26: Scraping of fouling material, (Darton and Faxell, 2001).

A statistical review of 150 membrane autopsies was carried out by Darton and Faxell, (2001) and showed the following:

- Every membrane has a biofilm on its surface
- It is a seldom problem when bacteria on the membrane surface present at less than 10^4 cfu.cm^{-2}.
- Most biofilms contain similar bacteria such as the slime-forming genus

Pseudamonas.

- Problematic biofouling occurs with bacteria counts more than 10^5 cfu.cm^{-2}.
- 34% of membranes had bacteria count more than10^5 cfu.cm^{-2}.
- With bacteria levels above 10^7 cfu.cm^{-2}, it is not possible to completely remove biofouling.
- Organic fouling and biological fouling has no geographic boundaries.
- 67% of membranes have deposits containing more than 40% organic content.

Table 2.10 summarise analytical results of membrane autopsy from different desalination plants.

Table 2.10: Summary results of membrane autopsies from different desalination plants (Baker and Dudley, 1998; Boubakri and Bouguecha, 2008).

Plant Location	**Size ($m^3.hr^{-1}$)**	**Water Source**	**Major foulants**	**Foulant Moisture Content**
Netherlands	18	Brackish	44% Organic, 30% Fe,10% SiO_2	89%
Canary Islands	63	Seawater	63% Organic, 4.7% $MgCO_3$, 10% $CaSO_4$	92%
Spain	12	Brackish	66% Organic, 14% Alumina, 3.4% SiO_2	94%
Italy	36	Brackish	26% Organic, 36% Fe,13% SiO_2	85%
Argentina	160	Brackish	44% Organic, 5% Fe, 37% SiO_2	93%
Germany	22	Brackish	76% Organic, 7.1% Fe, 5.1% $CaPO_4$	85%
Spain	1000	Brackish	67% Organic, 4.5% Alumina, 13% SiO_2	90%
Egypt	200	Brackish	50% Organic, 39% Fe, 2.9% $CaSO_4$	92%
Tunisia	625	Brackish	41% Organic, 28% Fe, 3.8% SiO_2, 3.6%$Ca_3(PO_4)_2$	
UK	105	Brackish	59% Organic, 18% Fe, 7%SiO_2, 1.7 Al.	94%

Baker and Dudley, (1998) carried out viable counts of microorganisms from biofouled spiral wound RO membranes. They found that several species of bacteria, fungi and yeasts were

present in the majority of biofilms investigated. These types of microorganisms are found on the membrane surface, plastic feed spacer, and permeate spacer. The numbers and common micro-organisms identified from the membrane biofilm are shown in Table 2.11 and Table 2.12.

Table 2.11: Typical microbiological activity in biofouled spiral wound RO membrane, (Baker and Dudley, 1998)

	Rang of viable bacteria count cfu.cm^{-2}	**Range of fungal counts cfu.cm^{-2}**
Fouled Membrane	$1 \times 10^2 - 1 \times 10^8$	$0 - 1 \times 10^3$
Plastic feed spacer	$4 \times 10^2 - 5 \times 10^6$	$0 - 1 \times 10^3$
Permeate spacer	$< 10^2 - 1 \times 10^6$	None

Table 2.12: Common microorganisms in RO membrane biofilm, (Baker and Dudley, 1998).

Type of microorganism	The name of microorganism
Bacteria	Pseudomonas, Bacillus, Artrobacter, Flavobacterium, Aeromonas, Corynebacterium
Fungai	Penicillium, Trichoderma, mucor, Fusarium, Aspergillus

2.16 Fouling Prevention Methods

RO membrane technology is simple to design and operate and can be combined with different treatment processes to prevent fouling including conventional pre-treatment and membrane separation techniques (Vedavyasan, 2007). Developments in pre-treatment technology include using of automatic self-cleaning filters for reducing of membrane fouling (Ovadia, 2008; Komlenic, 2007). The Amiad AMF^2 filter uses fibre thread technology which trap the particles as fine as 2 microns. These filters have high efficiency in removing of total suspended solids (TSS), silt density index (SDI) and can reduce Transparent Exopolymer particles (TEP) and biofouling. They can be used as pre-treatment for MF, UF and RO membrane systems (Ovadia, 2008). Hu, *et al.* (2005) used biofiltration as possible pre-treatment to reduce biofouling in RO membrane. The biofilter was constructed of acrylic

material with an inner diametr of 15.6 cm. He found that the operational time could be prolonged for five times with biofiltration pre-treatment. However, this filter can remove only about 50% of assimilable organic carbon (AOC), which indicates that the risk of biofouling still high. AOC is a low molecular weight dissolved organic carbon that can easily be utilised by bacteria and leading to growth. In order to prevent re-growth of microorganisms, AOC level must be less than 10 -20 $\mu g.l^{-1}$ (van der Kooil, 1992; LeChevallier, *et al.*, 1993).

The promising pre-treatment technique that has capability to eliminate membrane fouling is the nano-alumina depth filter (Disruptor ^{TM}). Disruptor^{TM} is depth filter made of nano-alumina fibres and is an alternative to MF and UF membranes. The nano-alumina fibre is 2nm in diameter and 200-300 nm in length. It has a dense electropositive charge, a very large surface area (500 $cm^2. g^{-1}$,) and 2 micron pore size which allowing a high flow rate and low pressure drop. It can remove nano-sized particles including bacteria, viruses, colloids and dissolved metals from water (Komlenic, 2007). The non-woven media is pleated and sold as cartridges with a diameter up to 2.5″ (6.4 cm) and as long as 40″ (102 cm). Figure 2.27 shows the retention efficiency of Disruptor^{TM}.

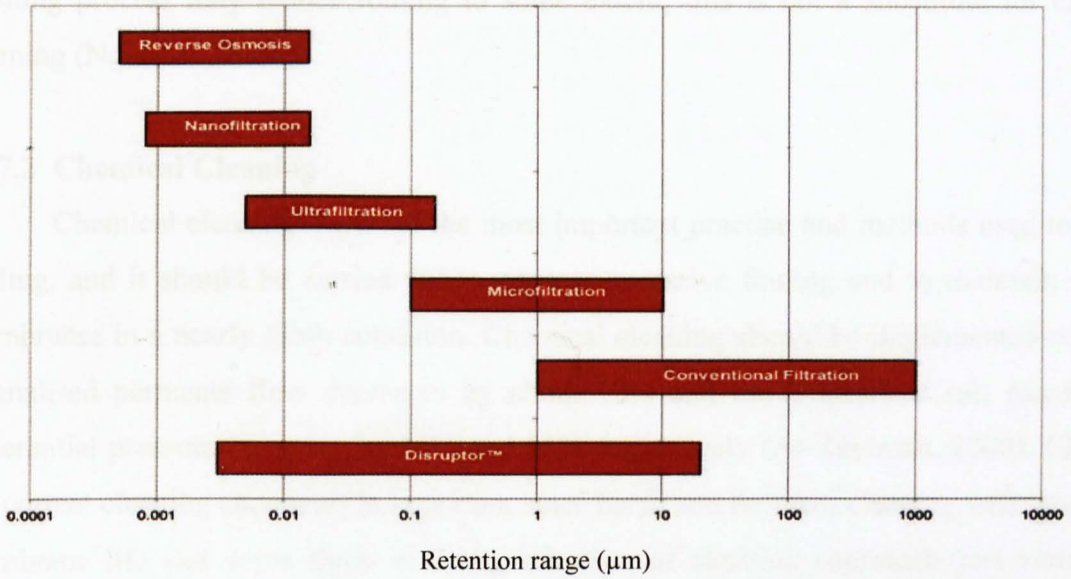

Figure 2.27: Filtration spectrum of disruptor (Reproduced from Komlenic, 2007).

Combining of ultrafiltration membranes and/or automatic self-cleaning filters and Disruptor^{TM} would be the best solution for prevention of membrane fouling and reduction of operation and maintenance costs. The limitations of DisruptorTM are narrow pH rang (4 – 9) and can not be regenerated as it gets blocked it should be replaced.

2.17 Membrane Cleaning

Membrane cleaning technology has been of great importance to restore the performance of the membrane systems. Although all cleaning techniques can only reduce fouling to some extent, cleaning methods will always be employed in practice. The frequency with which membranes need to be cleaned can be estimated from the normalization of RO membrane systems performance. The choice of the cleaning method mainly depends on the type of membrane and type of foulant deposited on the membrane surface, the module configuration and the chemical resistance of the membrane.

2.17.1 Hydraulic Cleaning

Seawater is flushed through the RO membrane systems with low pressure (2 bar) to remove the rejected contaminants that accumulate on the membrane surface. While the flushing process may reduce fouling to some extent; this is not a substitute for chemical cleaning (Ng, *et al.*, 2008).

2.17.2 Chemical Cleaning

Chemical cleaning is one of the most important practice and methods used to reduce fouling, and it should be carried out to prevent excessive fouling and to maintain the RO membranes in a nearly clean condition. Chemical cleaning should be implemented when the normalised permeate flow decreases by about 10% and the normalised salt passage and differential pressure increases by 10% and 15% respectively (Al-Rammah, 2000). Choosing the correct cleaning chemicals is important since harsh and frequent cleaning will shorten the membrane life and some times a wrong selection of cleaning chemicals can worsen the fouling situation. Therefore, the type of foulants should be determined before implementing of chemical cleaning process. Effective cleaning is evaluated by the return of the normalised parameters to their initial "start up" values. It is very important to clean RO membranes

when they are lightly fouled, and not heavily fouled. Heavy fouling can impair the effectiveness of the cleaning chemical by impeding the penetration of the chemical into the fouling layer. If normalised membrane performance drops by 30% to 50%, it may be impossible to fully restore the performance of the membranes back to the initial condition. Typically chemical cleaning starts with a high pH cleaning to remove biological matter, colloids and organic matter followed by a low pH cleaning to remove mineral scaling and metal oxides. However, depending on the type of fouling some times only one cleaning solution is used or the order of high and low pH cleaning is reversed. The most common chemicals used in membrane cleaning are shown in Table 2.13.

Table 2.13: Cleaning chemicals for RO membranes, (FilmTec Technical Manual, 2002).

Foulant	**Cleaning Chemical**	**Comments**
Inorganic salts ($CaCO_3$, $CaSO_4$, $BaSO_4$)	- 0.1% Hydrochloric Acid - 0.5% Phosphoric Acid - 2% Cirtic Acid	Best OK OK
Metal Oxides (Iron)	- 0.5% phosphoric Acid - 1.0% Sodium Hydrosulfite	Good Good
Biological Fouling (Biofilm)	- 0.1% Sodium Hydroxide, 30°C - 1.0% Sodium Ethylene Diamine Tetra Acitic Acid (Na_4EDTA) and 0.1% NAHO, at 30°C - 1.0% (W) Sodium Triphosphate - 1.0% (W) Sodium Triphosphate, 1.0% Sodium Ethylene Diamine Tetra Acitic Acid (Na_4EDTA)	Best Best when biofilm contains scaling Good Good
Organics	- 0.1% Sodium Dodecylsulfate/ 0.1% NaOH, 30° - 0.1% Sodium Triphosphate/ 1% Na_4EDTA	Good OK
Silica	- 0.1% Sodium Hydroxide, 30°C - 1.0% Sodium Ethylene Diamine Tetra Acitic Acid (Na_4EDTA) and 0.1% NAHO, at 30°C	OK OK

2.18 Summary

Based on the literature reviewed on the application of RO technology in the desalination of seawater and brackish waters, several conclusions can be drawn:

(a) Reverse osmosis (RO) membrane technology is being increasingly used in the desalination of brackish water and seawater in many countries. Following improvements in RO membrane performance and reduction in capital and operation costs, it is now considered the most attractive desalination technique. Consequently many large-scale SWRO desalination plants have been constructed in various parts of the world that suffer from shortage of fresh water due to the continuing growth in domestic and industrial needs.

(b) Membrane fouling and degradation is the most frequent problem in most seawater RO membrane systems, particularly when raw feed water is drawn from an open sea intake. Extensive research has been carried out on fouling control in RO membrane systems through the application of different pre-treatment methods upstream to RO membranes, improvement of membrane materials and feed spacer design, as well as through improvement of anti-scalant performance.

(c) Different pre-treatment processes have been applied in SWRO desalination plants. These include conventional pre-treatment (disinfection, coagulation/flocculation, multimedia filters followed by cartridge filters) and membrane separation (microfiltration and ultrafiltration). However, conventional pre-treatment produces variable feed water quality and quantity, and has to be optimised and developed for the particular water source and feed water quality requirements. Microfiltration (MF) and ultrafiltration (UF) require frequent backwashing and chemical cleaning due to blockage of membrane channels by foulants, and they have limitations in the removal of small molecular weight organic molecules. Despite the high removal efficiency of such membranes, fouling is still considered as a serious problem in RO membrane systems.

(d) Biofouling is the most difficult type of fouling to control in RO membrane systems, due to the fast growth, multiplication and relocation of micro-organisms.

In addition to the bacteria there are their products including transparent exopolymer particles (TEP). Little research has been carried out to investigate the role of transparent exopolymer particles TEP in biofilm formation and development on RO membranes. The conventional pre-treatment methods available in the commercial SWRO desalination plants have been unable to remove TEP adequately from RO feed water.

(e) Monitoring RO plant performance is essential in order to recognise when membranes are becoming fouled. Indirect observation methods of membrane fouling such as *in-situ* fouling monitoring methods (e. g. turbidity, SDI, theoretical and software standardisation calculations) have limitations and the true identity of fouling can only be determined by carrying out a destructive study "autopsy" on RO membrane element.

(f) Considerable work has been carried out to study the mechanism of the development of single types of fouling formation in sea and brackish water RO desalination plants. However, little research has been carried out to study the effect of composite fouling. In this study, the accuracy of conventional *in-situ* fouling monitoring methods and RO standardisation methods in predicting the type of fouling has been investigated. The identity of the foulants causing the deterioration of plant performance has been investigated by carrying out destructive "autopsy" and laboratory investigations on two types of RO membranes. The Tajoura SWRO desalination plant in Libya was selected as model for this study. Finally, a novel fouling prevention technique has been investigated for its ability to reduce membrane fouling and improve the operational performance of SWRO desalination plants.

CHAPTER 3

MATERIALS AND METHODS

3.1 Performance Evaluation of the Tajoura SWRO Desalination Plant.

3.1.1 *In-Situ* Fouling Monitoring Methods

3.1.1.1 Silt-Density Index (SDI) Measurements.

The SDI test was used to predict the potential of particulate and colloidal fouling in raw and pre-treated seawater. The SDI analytical protocol was standardised for the ASTM (D 4189-95) method and was recognised by membrane suppliers and the desalination community for estimating the quantity of matter in feed water that may foul the RO membranes. The SDI test unit (Figure 3.1) was connected into the sample point and then a filter was inserted into the filter holder using tweezers to avoid membrane damage. The test unit was tightly closed and the air bubbles were completely removed.

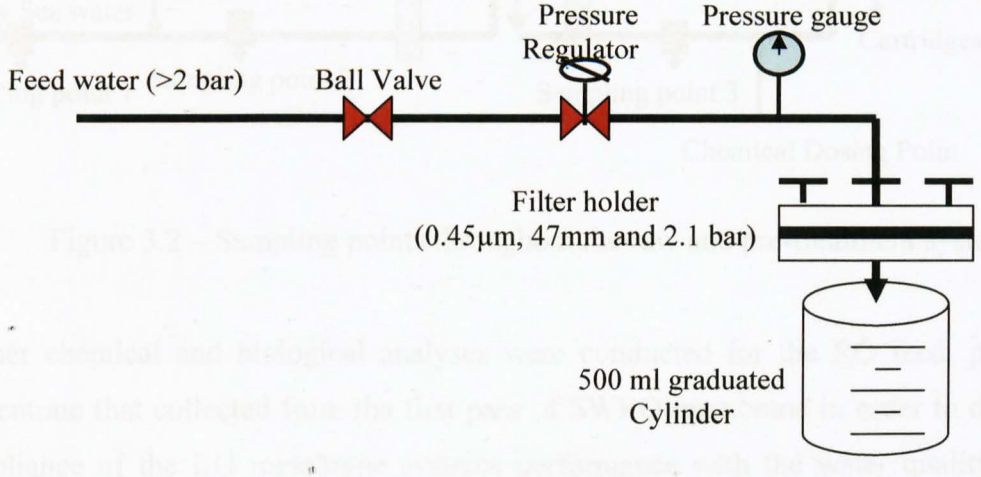

Figure 3.1 Silt density index (SDI) measuring unit.

The SDI test was performed by timing the hydraulic flow through a 0.45 µm membrane filter at a constant pressure of 2.1 bars. The time required for 500 ml of the feed water to pass through the membrane filter was measured when the test is first initiated, and again after 15 minutes of the start of the test. The value of the SDI was calculated using equation 2.24.

3.1.1.2 Biological Growth Measurements

Raw seawater and pre-treated seawater were collected from the Tajoura desalination plant in pre-sterilised plastic bottles for chemical and biological analysis. The standard procedures for collection and storage of water samples applied by The American Public Health Association (APHA) and American Water Works Association (AWWA) were applied. The raw seawater was collected upstream the chemical injection points (sampling point 1), while the pre-treated seawater samples were collected down stream the cartridge filters (sampling point 4) (Figure 3.2).

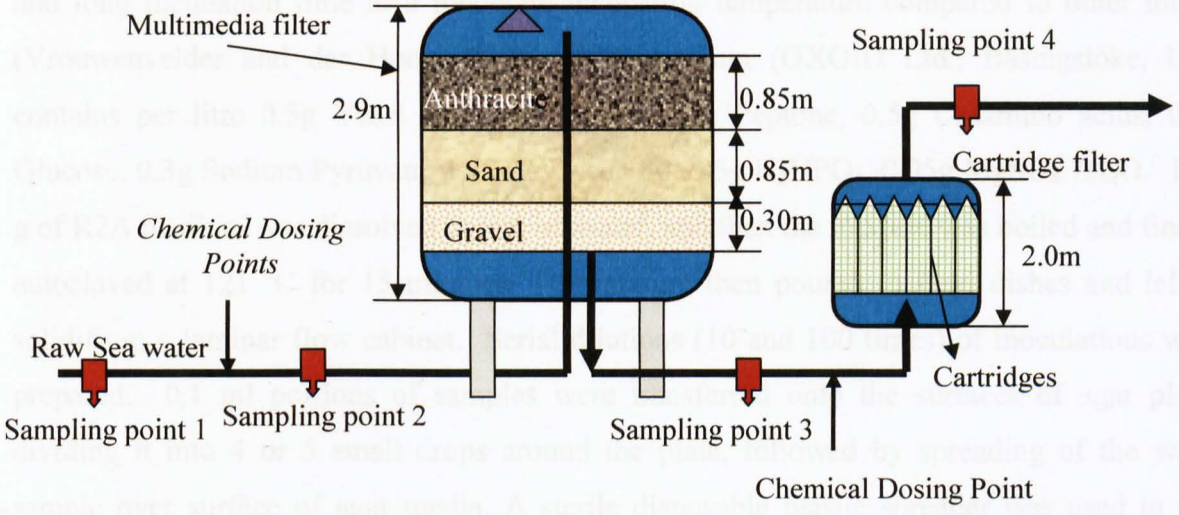

Figure 3.2 – Sampling points throughout the raw and pre-treatment systems.

Further chemical and biological analyses were conducted for the RO feed, permeate and concentrate that collected from the first pass of SWRO membrane in order to determine the compliance of the RO membrane systems performance with the water quality parameters recommended by the membrane manufacturer.

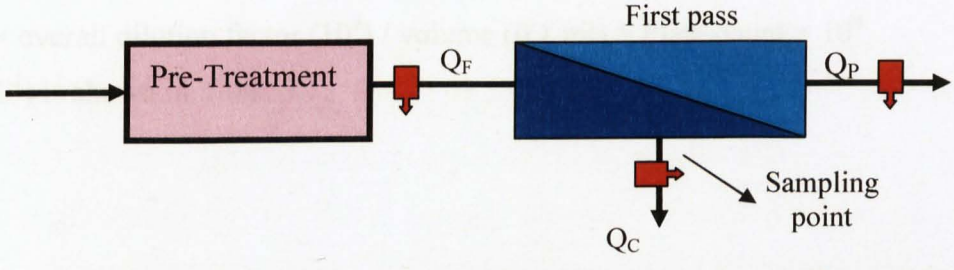

Figure 3.3: RO feed (Q_F), permeate (Q_P) and concentrate (Q_C) sampling collection points.

3.1.1.3 Colony Forming Units

The plate count method was used to measure the number of living culturable microorganisms present in water samples and in fouling materials. The microbiological analysis was carried out according to the method of Schneider, *et al.* (2005) and Vrouwenvelder and van der Hooij, (2001). The fouling material was swabbed from a known area (5x5cm) of membrane and transferred into a 100 ml test tube containing autoclaved raw seawater and then vortexed. The used raw sea water contains the following elements in $mg.l^{-1}$: 430 Ca^{2+}, 1370 Mg^{2+}, 12100 Na^{+}, 500 K^{+}, 139 HCO^{-}_{3}, 3120 SO^{2-}_{4} and 20900 Cl^{-}. R2A agar medium was selected and used for this experiment because of its low nutrients concentration and long incubation time at a moderate incubation temperature compared to other media (Vrouwenvelder and der Hooij, 2001). R2A medium (OXOID Ltd., Basingstoke, UK) contains per litre 0.5g Yeast Extract, 0.5g Protease Peptone, 0.5g Casamino acids, 0.5g Glucose, 0.3g Sodium Pyruvate, 1.12ml Tween 80, 0.3g K_2HPO_4, 0.05g $MgSO_4.7H_2O$. 18.9 g of R2A medium was dissolved in raw seawater, and then the mixture was boiled and finally autoclaved at 121 °C for 15 minutes. The mixture then poured in Petri dishes and left to solidify in a laminar flow cabinet. Serial dilutions (10 and 100 times) of inoculations were prepared. 0.1 ml portions of samples were transferred onto the surfaces of agar plates dividing it into 4 or 5 small drops around the plate, followed by spreading of the water sample over surface of agar media. A sterile disposable plastic spreader was used in this experiment, in order to obtain between 30 and 300 colonies per plate, which is statistically valid. The plates were finely sealed with "parafilm", to prevent contamination and drying, and were placed in an inverted position in an incubator preset at 28 °C for 7 days.

To calculate the total colony forming units (CFU) per ml of sample, the average of the triplicate plate count was multiplied by the dilution factor of the sample and by the volume added to the plate. Example of concentration calculation from plate counts (Average plate count × overall dilution factor (10^3) / volume (0.1 ml) = Plate count × 10^4 ($cfu.ml^{-1}$) is shown in Table 3.1.

Table 3.1. Average plate count calculation expressed in (cfu.ml^{-1}).

Plate Count (CFU)	Dilution Factor	Volume added to plate (ml)	Overall dilution factor	Sample concentration (CFU.ml^{-1})
132	10^2	0.1	10^3	$1.32x10^5$

3.1.1.4 Prediction of Scaling Potential

Calcium carbonate ($CaCO_3$) and calcium sulphate ($CaSO_4$) scaling potential were calculated according to the calculation procedure described by Waly *et al.* (2008), Sheikholeslami (2005) and Dow Technical Manual (2002). $CaCO_3$ scaling potential was calculated in terms of Stiff and Davis Stability Index (S&DSI) (Equation 3.1), while $CaSO_4$ was determined in terms of ionic strength and solubility product.

$$S\,\&\,DSI = pH - pH_s \qquad (3.1)$$

Where:

pH – is the pH of feed water.

pH_s – is the pH at which the concentrate stream is saturated with $CaCO_3$

Some values were determined from the graphs according to the procedure described in DOW Technical Manual (2002) and ASTM D4562-05 (See Appendix A, Section 3).

3.1.2 Analytical Methods

3.1.2.1 Inductively Coupled Plasma Mass Spectroscopy (ICP-MS)

Inductively Coupled Plasma (ICP) Spectroscopy (PerklinElmer - Canada) was used to detect trace metals concentration of both of the collected water samples and the digested fouling materials. The main elements in the water samples that were measured by ICP were iron zinc, aluminium and copper. The raw seawater, pre-treated seawater (RO feed) and RO concentrate were first diluted to 10,000 times and then 5 ml of each sample was placed in special ICP tubes. Standard solution from MERCK (ISP-Meher element VI) was used to prepare serial dilutions with different concentrations of the elements to be analysed. For each element, six standard solutions of different concentration were prepared. Depending on the

element to be analysed, different concentrations were prepared. For Al, and Cu the following standard concentrations (1.0, 2.0, 5.0, 10, 25, and 50 ppb) were prepared, while for Fe the following concentration were prepared (10.0, 20.0, 50.0, 100.0, 250.0 and 500.0 ppb). The instrument was calibrated prior to every analysis.

3.1.2.2 Ion Chromatography (IC)

Ion chromatography (IC) (Dionex - DX120 –UK) was used to determine the concentration of cations and anions in water samples. The collected samples from raw seawater, pre-treated seawater (RO feed), RO concentrate and RO permeate were firstly diluted to proper dilutions prior to analysis. Instrument calibration for each element was conducted using external standard solutions of 1000 ppm obtained from Fisher Chemicals Supplier, UK. The standard solutions were prepared by diluting each stock standard with de-ionised water at various concentrations (0.1, 1.0, 5.0, 10.0, and 20.0 ppm). Calibration curves were used to determine the relationship between peak heights and/or areas found for each component and their concentrations in the water samples.

3.1.2.3 pH measurement

The pH measurements were carried out using a pH meter (Model- HI 8424, Hanna Instruments). The pH meter was calibrated using pH 4.0, 7.0 and 10.0 standard buffer solutions (Fisher Scientific) for most of the measurements which were in the range of pH 2 – 11 (See Appendix H, Section 1).

3.1.2.4 Conductivity and Total Dissolved Solids (TDS) Measurements

Conductivity meter is commonly used to monitor the overall ionic purity of water. However, this instrument should regularly be calibrated (Spitzer, *et al.*, 2005). The conductivity/ TDS meter ((Model CON 410, OAKTON- Eutech Instruments) was used for measuring the conductivity ($\mu S.cm^{-1}$), TDS ($mg.l^{-1}$) and temperature (^{o}C) of water samples during all experimental runs. The conductivity meter was firstly calibrated with the sodium chloride solutions (80, 12,300 and 80,000 $\mu S.cm^{-1}$) (Fisher Scientific) prior to each measurement (See Appendix H, Section 2). The conductivity, TDS and temperature of both raw and pre-filtered seawater samples were measured by dipping a previously rinsed by DI

water electrode in the water sample. The electrode was shacked few times, left for few minutes to stabilise and then the values of conductivity, TDS and temperature were recorded.

3.2 Actual and Standardised Operating Data.

Actual operating data for a period of 360 days from the Tajoura plant were collected. These data included RO feed and permeate conductivity, RO feed pressure, differential pressure, RO feed flow and RO permeate flow and feed water temperature. The actual operating data of Fluid Systems membrane unit are presented in Appendix B, Section 1, while the actual operating data of Toray membrane unit are presented in Appendix C, Section 1. The actual and calculated operating data in terms of permeate flow and salt passage were standardised using theoretical (ASTM and HSDM) and computer software packages (ROSA and ROData) standardisation methods (See Appendix B and Appendix C). The equations described in Appendixes B and C were used for standardisation of the actual operating parameters and for the evaluation of the performance of RO membrane systems of the Tajoura plant.

3.3 Filtration Unit and Reverse Osmosis Test Unit

The laboratory-scale filtration test unit used in this experiment consists of water tank volume of 60 L, transfer pump, and two filter casings containing 1μm cartridge filter and Disruptor^{TM}, in sequence. The reverse osmosis (RO) unit consists of feed water tank volume of 60 L, a high pressure RO cell, hydra-cell positive displacement industrial pressure pump (Model DO3-991-2400A, manufactured by Wanner Engineering), pressure regulator for increasing feed pressure, flow meter (0 – 10 L.min^{-1}), pressure gauges (0 – 100 bar) from (Ascroft-USA) for measuring feed and concentrate pressure. The high pressure pump is fitted with a variable speed drive motor, which is capable to generate high pressure up to (100 bar). The transmembrane pressure was controlled by a installed on the concentrate outlet of the RO membrane unit. The flow rates were measured by digital flow meters (Cole-Parmer Instrument Company Ltd., England). All the piping, fitting, and test cell were manufactured from stainless steel to prevent corrosion. The dimensions of the rectangular, cross flow, channel membrane unit were 15 cm × 15 cm with a channel height of 2 mm (Figure 3.4).

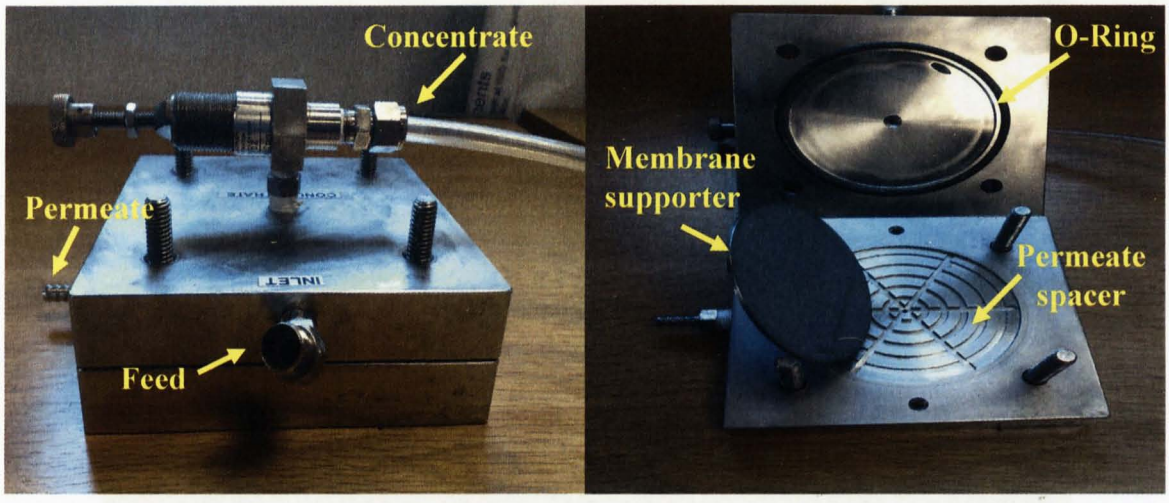

Figure 3.4: Laboratory scale cross flow reverse osmosis unit.

The schematic diagram and a photograph of the filtration unit and the RO test unit are shown in Figures 3.5 and 3.6 respectively. The RO unit can be operated by either full recycling mode to study the concentration polarisation phenomenon, or by partial recycling mode to investigate the permeate flux change due to fouling. The RO cell has a working membrane area of 81cm^2.

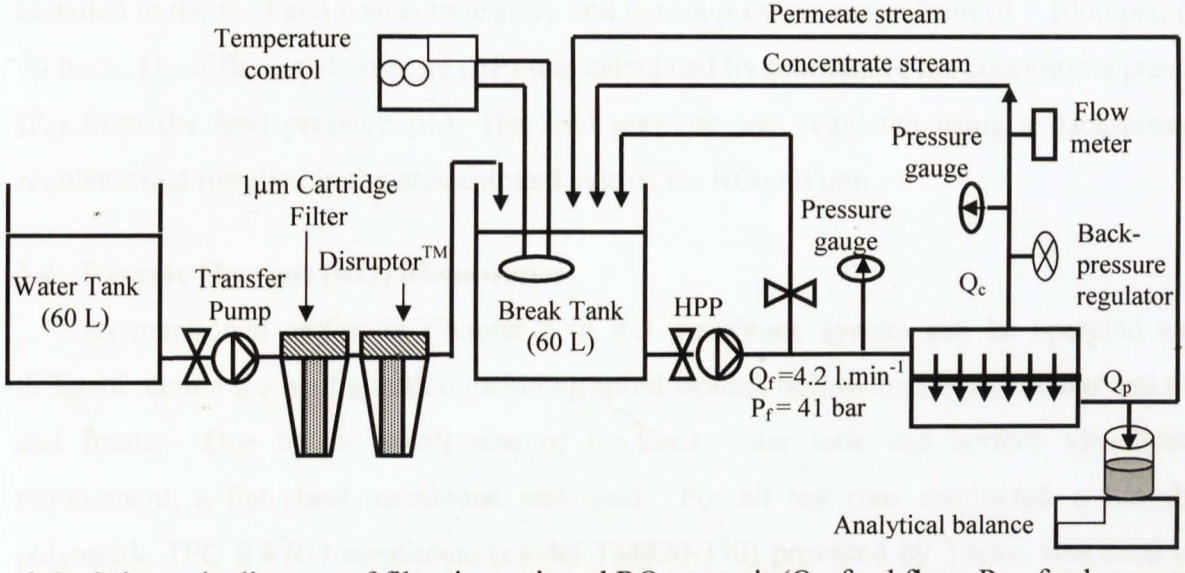

3.5: Schematic diagram of filtration unit and RO test unit (Q_f- feed flow, P_f – feed pressure, Q_c – concentrate flow and Q_p – permeate flow).

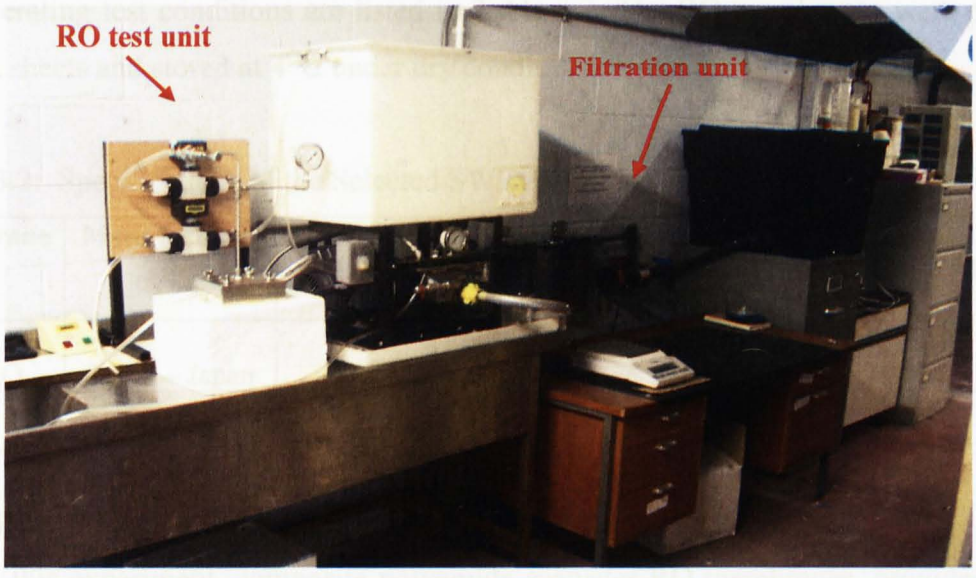

Figure 3.6: A Photograph of filtration unit and RO test unit.

The concentrate flow was measured using battery – powered digital flow meter model CZ-32555-04 (Cole-Parmer). The flow range of the flow meter is 0.8 – 8 GPM (3–30 $L.min^{-1}$) with an accuracy of ± 2%. The flow meter can be used at high temperature (up to 93 °C) and at high pressure (up to 21 bar). Pressure gauges model KH-68022-07 (Cole-Parmer) were installed in the feed and concentrate sides and have a pressure range from (0 – 1000 psi) (0 – 70 bar). The differential pressure (ΔP) was calculated by subtracting the concentrate pressure (P_c) from the feed pressure (P_f). The feed pressure was regulated using a back-pressure regulator that installed in the concentrated side of the RO cell unit.

3.4 Reverse Osmosis (RO) Membranes

As mentioned earlier in Chapter 2, a RO membrane system can be operated using different membrane configuration including spiral wound, hollow fine fibre, tubular and plate and frame. Due to the small size of the feed water tank and surface visualisation requirement, a flat sheet membrane was used. For all test runs conducted, a flat sheet polyamide TFC SWRO membrane (model TM820-370) provided by Toray, was used as a model membrane for this study. This membrane is commonly used in the desalination process of seawater and commercially available as flat sheets. The membrane specifications

and operating test conditions are listed in Table 3.2. The RO membranes were provided as A4 flat sheets and stored at 4^{O}C under dry conditions.

Table 3.2: Specifications of the Selected SWRO Membrane.

Membrane	Manufacturer	Operating pressure (bar)	Operating pH	Operating Temperature (^{O}C)	Salt rejection (%)	Flux (l.m^{-2}.h^{-1})
SWRO	Toray – Japan	55.2	2 – 11	4 - 45	99.75	9.58

3.5 Membrane Conditioning

In this experiment, composite polyamide seawater RO membranes, provided by Toray were used. The required size was cut from the membrane sheet and soaked in DI water for 24 h. Then, the membranes were installed into the test cell and were cleaned by high quality RO permeate for 30 min at 100 psi feed pressure. The preconditioning of new RO membranes was essential in order to eliminate the effect of membrane compaction and to stabilise the permeate flux. Therefore, prior to each experimental run, the selected membrane was installed into the test cell and conditioned by high grade RO permeate for 6 h in full recycling mode according to the method used by (Ng and Elimelch, 2004; Liu *et al.*, 2006). The operating pressure was increased gradually from 100 up to 600 psi (6.9 – 41 bar) using back-pressure regulator. The membrane was conditioned by filtering high quality RO permeate (permeate wasted and concentrate recycled) for 6 h under constant feed pressure (41 bar), stable feed flow rate (4.2 L.min^{-1}) and temperature (25 ± 2 °C). The temperature of the feed was controlled using a water cooling chiller (Model 6100, Cole-Parmer Instrument Company Ltd., England). The permeate flow, concentrate flow, feed pressure, concentrate pressure, feed and permeate TDS were measured and recorded. The operation of RO unit was maintained at test pressure of 41 bar until the permeate flux became stable. Permeate flux was measured by weighing the permeate collected in a preweighed beaker using digital weight balance.

3.6 Filtration Scenarios

Four filtration scenarios were carried out in this study. In the first filtration scenario untreated seawater from the Mediterranean Sea and the North Sea were pumped directly to the RO membrane, in order to investigate the effect of composite fouling on the permeate flux and salt passage. In the second filtration scenario both seawater samples were filtered through a Disruptor^{TM} alone. However, in the third, the North Sea raw seawater was filtered through a 1 μm filter alone and through a 5 μm alone in two separate experiments. Whilst, the fourth filtration scenario investigated the long term performance of the Disruptor^{TM}. The North Sea raw seawater was filtered through a 1 μm filter followed by the Disruptor^{TM}. After each filtration test, the per-filtered seawater was pumped into the RO test cell unit and the permeate flux and concentration were measured over time, using digital weight balance model (Model, XB-1600C, Precica Instruments – Switzerland) and conductivity / TDS meter (Model CON 410, OAKTON-Eutech Instruments).

3.7 Test Conditions

All tests were conducted under pre-defined hydrodynamic conditions. The major dynamic conditions that were used in the test runs with high quality RO permeate, raw, pre-filtered sea waters are presented in Table 3.3.

Table 3.3: Dynamic Test Conditions

Parameters	**High quality RO permeate**	**Raw Seawater**	**Pre-filtered Seawater**
Membrane manufacturer	Toray	Toray	Toray
Solution Volume (l)	30	30	30
Feed pressure (bar)	41	41	41
Mode of operation	Concentrate recycle	Concentrate recycle	Concentrate recycle
Temperature (^{o}C)	25 ± 2	25 ± 2	25 ± 2
pH	6.5	8.3	8.2
Feed TDS (mg.l^{-1})	2.5	37,000$^{(1)}$; 25,500$^{(2)}$	37000 ; 25,500

(1) The Mediterranean Sea; $^{(2)}$ The North Sea.

3.8 Chemical Cleaning of Filtration Units

After each fouling experiment, the filtration units were cleaned to remove fouling materials that remined in the system according to the procedure described by Ng and Elimelech, 2004). The cleaning procedure was carried out as following:

- The feed water tanks were empited and cleaned by ID water.
- The filtration units were firstly cleaned by recirculating DI water for 30 min.
- DI water adjusted with pH = 11 was recirculated for 1 h at temperature of 30 °C and applied pressure of 6.8 bar.
- The feed water was replaced with ID water (pH = 7) and reciculated for 30 min at room temperature and applied pressure of 6.8 bar.
- DI water adjusted with pH = 2 was recirculated for 1 h at temperature room and applied pressure of 6.8 bar.
- The feed water was placed with ID water (pH = 7) and recirculated for 30 min at room temperature and applied pressure of 6.8 bar.

3.9 Microscopic Techniques

3.9.1 Contact Angle

The contact angles of both the examined new and the fouled RO membranes from Koch and Toray membrane companies were measured using sessile drop method. Both the clean and the fouled RO membrane coupons were transferred into clean Petri dishes, and dried in a laminar flow cabinet prior to SEM investigation according to the method used by Vrijenhoek, *et al.* (2001). The contact angle values of the clean and the fouled membranes were measured using contact angle meter (KRUSS - DSA100) (Figure 3.7). The sessile drop method was used, in which a small piece of membrane (e.g. 2 x 2 cm^2) was cut from the membrane sheet and mounted on the sample holder using double sided tape. The contact angle was measured by depositing a 5 µl droplet of ultra pure water onto dried membrane surface using a micro-syringe. The contact angle values were calculated by taking averages of 5 replicates of 5 droplets.

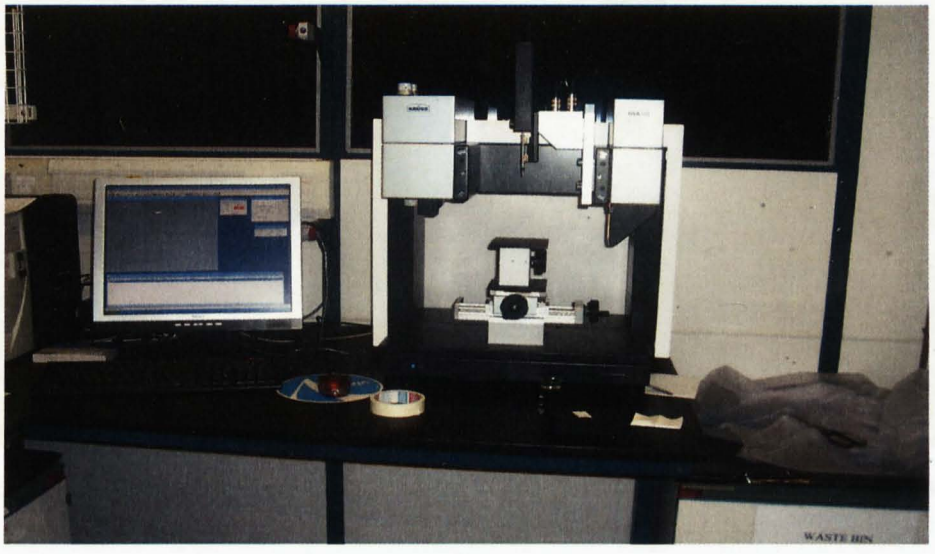

Figure 3.7: A photograph of contact angle measuring equipment (Kruss-DSA100).

3.9.2 Atomic Force Microscope (AFM)

A Nanoscope III atomic force microscope (Digital Instruments, USA) (Figure 3.8) was used to investigate the surface morphology of the clean and the fouled RO membrane samples. Membrane coupons were cut from clean and fouled flat sheet composite polyamide membranes as well as from the fouled Fluid Systems and Toray SWRO membranes collected earlier from the Tajoura plant. The clean membrane coupons were soaked in distilled water for 30 minutes at room temperature and then loaded into the test cell and flushed by distilled water for another 30 minutes at low pressure. Standard Nanoprobe Silicon (Si) cantilevers (OMCL-AC160TS-E - Olympus SPM-Probes) were used. The cantilever has a spring constant of 42 $N.m^{-1}$, resonance frequency of 300 kHz and length of 160 μm, while the tip has radius of 7nm. A tapping mode in the dry state was used due to the sensitivity of fouling material. The membrane coupons were dried prior to AFM investigation following similar procedure mentioned in Section 3.3.1. To prepare membrane samples for AFM analysis, 1 cm^2 membrane samples were cut out from the air dried membrane samples and placed on a stainless steel disc with double – sided tape and investigated by AFM.

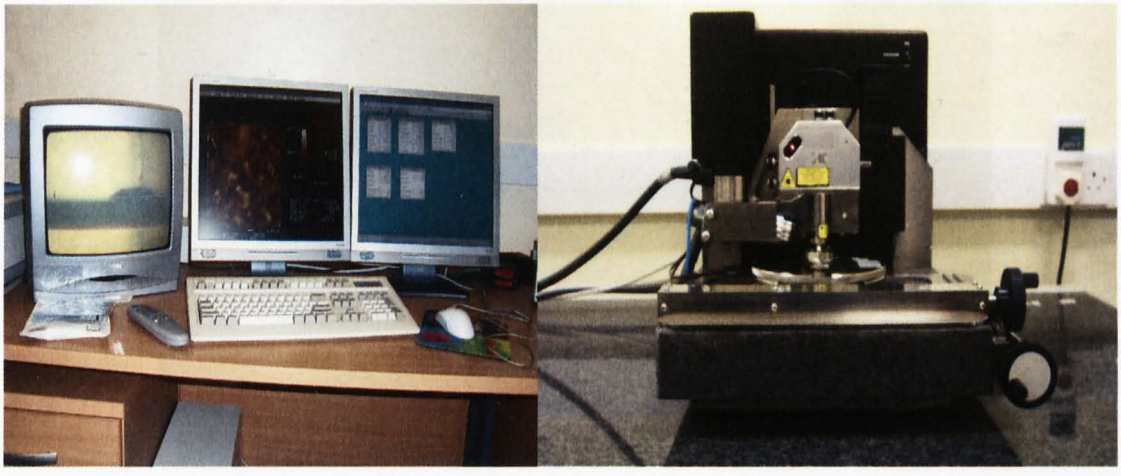

Figure. 3.8: A photograph of a Nanoscope III atomic force microscope used in this study

3.9.3 Scanning Electron Microscope (SEM)

A scanning electron microscope (SEM) (Model InspectF, FEI Instruments) (Figure 3.9) equipped with energy dispersive X-ray spectrometer (Oxford) was used for imaging (SEM) and elemental analysis (EDX) of fouling material formed on the membrane surface during the filtration experiments. InspectF SEM was selected because of its high-brightness and high-resolution imaging. It is equipped with a Schottky Field Emission source which, provide clear, sharp and noise-free imaging. The membrane coupons were dried prior to SEM investigation following similar procedures mentioned earlier in Section 3.3.1. A membrane samples (1 cm^2) were cut from clean and fouled Disruptor^{TM} filter and RO membranes, and were then mounted on the test disc and were finally coated with gold powder. The coating process of the membrane samples were left to dry and were tested for the images of fouling morphology and elemental analysis. For both SEM and EDS investigations, a fixed accelerating voltage of 500 Kev was set and the magnification of the images was between 4000x and 25000x.

Figure. 3.9: A photograph of scanning electron microscope (InspectF).

3.9.4 Attenuated Total Reflection - Fourier Transformation Infrared (ATR- FTIR) Spectrophotometer.

Attenuated total reflection – Fourier Transformation Infrared (ATR-FTIR) spectroscopy is a very useful tool for determining the chemical composition of RO membranes and fouling material. Attenuated total reflection (ATR) offers the possibility to investigate the chemical composition of smooth surfaces such as RO membranes without any sample preparation, and thus in the undisturbed state. The IR beam can penetrate through the membrane or fouling layer and gives a spectrum of the average composition of this layer. In this experiment, ATR-FTIR (Figure 3.10) was used to investigate the functional group of both the clean and the fouled thin film composite SWRO membrane samples. Small samples (3 × 3 cm) of both the clean and the membranes were cut from membrane sheets and transferred into clean Petri dishes for drying. The membrane coupons were dried prior to FTIR investigation following similar procedures mentioned earlier in Section 3.3.1. The membrane coupons were dried prior to FTIR investigation following similar procedures mentioned earlier in Section 3.3.1. FTIR analysis was conducted using a PerkinElmer FTIR spectroscope with membrane samples pressed against each side of a germanium (GE) reflection element (6 mm, 45°). All spectra (100 scan at 4 cm^{-1} resolution) were recorded at 25 °C.

Figure 3.10: A photograph of PerkinElmer FTIR spectroscope

3.9.5 X-Ray Diffraction (XRD)

The crystalline phases of fouling material deposited on the surface of both SWRO membranes (Fluid Systems and Toray) were analysed by XRD. The XRD was carried out to determine the chemical nature of the scales deposited on the surface of RO membranes and to determine if the $CaCO_3$ scale is present as calcite, aragonite or as a mixture of both. The membrane coupons were dried prior to XRD investigation conducting similar procedures mentioned earlier in Section 3.3.1. A (2×2 cm^2) section of each membrane sample was cut out from the dried membrane samples and placed on glass slide with double – sided tape and investigated by XRD. A Philips X-Ray Diffract meter was used to scan clean and fouled RO membranes samples over the range of 5 – 80 degree at scan speed of 1 degree /min and a step size of 0.02 degree.

3.9.6 Light Microscope

Light microscope ((Zeiss Axioplan 2 – Zeiss Instruments) (Figure 3.11) was used to determine the concentration of transparent exopolymers particles (TEPs), while epifluorescent microscope was used to determine the bacterial cells present in both the raw and the pre-filtered North Sea seawater samples. TEPs concentrations were measured according to the method described by Bar-Zeev, *et al.* (2008). 500 ml of the raw and the pre-filtered North Sea seawater samples were placed in sterile glass beakers. Sterile glass microscope slides were suspended in the water in each glass beaker. The glass beakers were

then incubated at 25°C and gently shacked at 100 rpm. Slides in each beaker were removed after 48, 72 and 168 h and transferred into sterile Petri dishes, stained with 0.02% Alcian blue for 7 min, and rinsed twice by DI water to remove access dye. The slides were covered with cover slips and viewed under the light microscope. TEPs were counted in 20 images at a magnification of 20×. In order to quantify the attached bacteria, other slides of the same treatment were stained with 10 µl of 4',6-diamidino-2-phenylindole (DAPI, concentration 3µg ml^{-1}) for 7 min in the dark. A drop of immersion oil (Olympus, Fisher) was placed onto a glass slide and flattened by placing a cover slip on the top of the slide and then viewed under epifluorescence microscope. DAPI stained bacteria were counted in 20 sets of images taken from each slide.

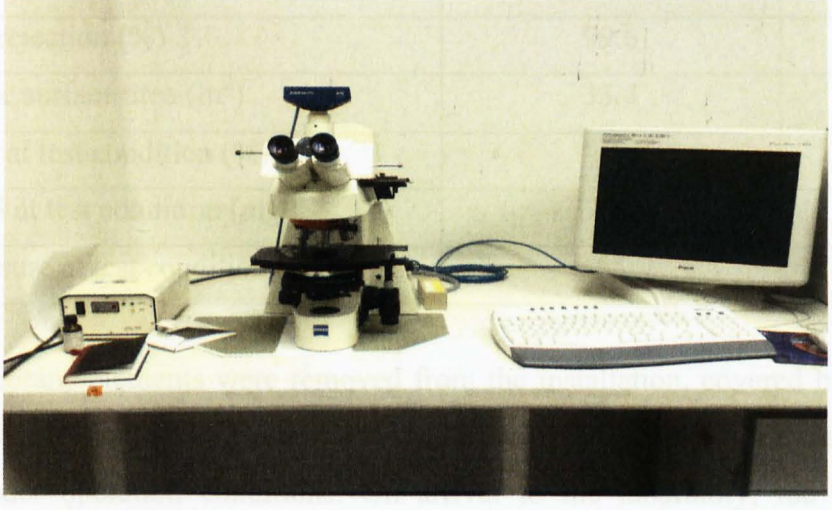

Figure 3.11: A photograph of Zeiss light microscope used in this study.

3.10 Membrane Autopsy and Visualisation

Seawater reverse osmosis (SWRO) membranes manufactured by Fluid Systems and Toray, were collected from the Tajoura SWRO desalination plant – Libya on 8/10/2007 and 16/02/2008 respectively. Both membranes have been in operation for 6 years and 4 years, respectively. The specifications of both membranes are present in Table 3.4.

Table 3.4: Specifications of Fluid Systems and Toray SWRO membrane elements collected from the Tajoura SWRO desalination plant.

Parameter	Specifications	
Membrane type	Polyamide thin film composite	Polyamide thin film composite
Manufacturer	Fluid Systems	Toray
Membrane model	TFC 2822SS-360	TM320-370
Serial Number	0619032	020210560
Membrane dry weight (kg)	20	16
Permeate flow (m^3/d)	22.7	23
Chloride rejection (%)	99.6	99.75
Membrane surface area (m^2)	33.4	34
Recovery at test condition (%)	7	8
Feed TDS at test condition (mg/l)	32000	32000
Feed pressure at test condition (bar)	55	55.2

Both membrane elements were removed from the installation, covered by sterilised plastic bags and finally stored at 4°C until analysis to preserve the original biomass composition as present under operation conditions. On arrival to the laboratory, the feed sides of the collected membrane elements were determined before removing the end caps by putting a sign on the permeate water tube. The end caps and outer plastic casing of the membrane elements were visually inspected and removed by using wood mallet and chisel. The membrane type and serial number were recorded. The membrane elements were then unrolled and the membrane envelopes and feed and permeate spacers were visually inspected conducting the standard autopsy procedures (Gossen, *et. al.,* 2004, Dudely, *et. al.,* 1997; Darton, *et. al.,* 2004; and Lopez, *et. al.,* 2005).

3.10.1 Acid Digestion

Acid digestion was carried out according to the standard method described by Tran, *et al.* (2007). Membrane coupons areas of 4 cm^2 were cut from the feed, the centre and the

concentrate sides of both Fluid Systems and Toray SWRO membranes. The membrane coupons were accurately weighed and transferred into clean 100 ml test tubes (Table 3.5).

Table 3.5: Area and weight of both membrane samples that used for acid digestion experiments.

Membrane sample	Weight (g)
Fluid Systems RO membrane (Clean)	0.157
Fluid Systems RO membrane (Fouled)	0.381
Toray RO membrane (Clean)	0.151
Toray RO membrane (Fouled)	3.43

Duplicate tubes were prepared and 10 ml of nitric acid (HNO_3) was added into 90 ml of water to prepare 10% v/v nitric acid solution. 10 ml of diluted HNO_3 was added into each test tube and then the test tubes were covered by glass marbles. The tubes were heated to 100 °C for 12 hours. After the acid digestion, the samples were filtered through a 0.2 μm filter type MILLEX@GP (Millipore – USA) and then the concentrations of trace metals were measured using ICP-MS (See Section 3.1.4.1). A blank of 10% v/v HNO_3 was used in the same manners as for the membrane samples.

3.10.2 Loss on Ignition Test

Loss on ignition test was used in order to determine the relative percentage by weight of organic content to inorganic content in the fouling materials according to the method described by Heiri, *et al.* (2001). Crucibles volume of 10 ml were cleaned, placed in the oven and heated for 2 h at 550 °C. The crucibles were then removed from the oven using tongs to prevent any contaminations and placed in a desiccator until they cooled down to room temperature and then weighed. Foulants were carefully scrapped from the surfaces of both Fluid Systems and Toray SWRO membranes using sterile glass slides (Figure 3.12).

Figure 3.12: Photographs of scraping of fouling material from the surfaces of Fluid Systems (a) and Toray (b) SWRO membranes

1.0 g portions of each fouling material were transferred to empty crucibles and the wet weight was recorded (Table 3.6).

Table 3.6: Samples and crucibles weights before and after heating processes.

Membrane sample	**Sample weight (g)**	**Empty Crucible (g)**	**Crucible and sample (g)**	**110 (°C)**	**550 (°C)**
Fluid System membrane	1.14	14.68	15.82	14.95	14.85
Fluid System membrane	1.11	13.95	15.06	14.15	14.7
Toray membrane	1.10	13.84	14.89	14.00	13.93
Toray membrane	1.10	14.23	15.33	14.23	14.32

The crucibles with fouling material were dried at 110 °C for 2 hours and then removed from the oven and placed in a desiccator and weighed after cooling. The dried fouling material was in the crucibles were placed in the oven and heated at 550°C for 2 hours, then removed from the oven and placed in a desiccator and left to cool to room temperature then weighed. The percentage of the dry weight lost on ignition of foulants was calculated using the following formula (Konen, *et al,*. 2002) (See Appendix D, Section 2):

$$\%LOI = \frac{(W_{T1} - W_{T2})}{(W_{T1} - W_0)} \times 100\% \qquad (3.2)$$

Where:

W_0 – is the weight of empty crucible

W_{T1} – is the weight of crucible and sample heated at 100 °C.

W_{T2} – is the weight of crucible and sample heated at 550 °C.

3.10.3 Chemical Cleaning of Fouled SWRO Membranes

Fouled Fluid Systems and Toray SWRO membranes coupons were chemically cleaned according to the cleaning protocol recommended by each membrane manufacturer. A laboratory scale RO test unit, described in Section 3.3, was used to perform the chemical cleaning practices. Membrane coupon area of 81 cm^2 was cut from each membrane envelopes of the membranes and was placed in the RO cell unit. The feed water tank was initially filled with an appropriate volume of high grade RO permeate and the membrane coupon was flushed for 15 minutes. The chemical agents that were used for cleaning of both fouled membranes are hydrochloric acid (HCl), sodium hydroxide (NaOH) and Sodium Ethylene Diamine Tetra Acitic Acid (Na_4EDTA). In the first cleaning cycle the RO permeate was heated to 30 °C and the high pH cleaning solution was prepared by adding 10 mg w/v of NaOH (0.1%) and 10 mg w/v of Na_4EDTA (0.1%) and pH adjusted to 11. The temperature of cleaning solution increased to 35 °C in order to increase the solubility of chemical species. The cleaning solution was recirculated for 30 min and soaked for another 30 minutes before draining. Followed by flushing the membrane coupons by fresh RO permeate for 15 min. In the second cleaning cycle low pH cleaning solution was prepared by adding 10 ml v/v of HCl (0.1%) into RO permeate and pH was adjusted to 2. The cleaning solution was recirculated for 30 min and soaked for another 30 minutes and then drained. The chemically cleaned membrane coupons were transferred into clean Petri dishes and dried in a laminar flow cabinet prior to the investigations by atomic force microscopy (AFM), scanning electron microscopy (SEM) and Fourier Transformation Infrared (FTIR) Spectrophotometer and X-ray diffraction analyses.

3.10.4 Membrane Performance Testing

In order to evaluate the efficiency of chemical cleaning, pure water flux of fouled and chemically cleaned Fluid Systems and Toray SWRO membranes were preformed in duplicate using laboratory scale RO test cell. Membrane coupons with area of 81 cm^2 were cut from the new flat sheets and from the fouled membrane envelopes of both membranes. Each membrane coupons was loaded into the test cell and flushed by RO permeate for 15 minutes. Feed pressure was measured at starting pressure of 100 psi and then increased gradually to 600 psi. The water flux of fouled and chemically cleaned membrane coupons was determined at constant feed pressure and constant temperature (e.g. 600 psi and 25 ± 2 °C respectively) (Appendix D, Section 4). Conductivity and pH of feed and permeate waters were measured every 30 min using conductivity meter (Model CON 410 Series, OAKTON-waterproof) and pH meter (Model- HI 8424, Hanna Instruments).

3.11 Experimental Design and Statistical Analysis

Experimental design and the experimental runs that have been conducted in this study are shown in Table 3. 7. Statistical analyses were performed on all data from three and two replications using mathematical functions within Excel (Version 2003). For the bacterial growth experiments (Chapter 4 and Chapter 6), the experimental runs were conducted in triplicate. In the water flux and fouling monitoring study (Chapter 6, Chapter 7) duplicate experimental runs were conducted due to large quantities of raw and pre-filtered seawaters were required for each run, time needed and the high cost of measuring techniques such as AFM and SEM.

Table 3.7: Experimental design and sampling frequency at various research stages.

Scope	Parameter	Number of replications	Sampling Frequency	Reproducibility
In – Situ water sampling	Water sampling	2	2	90 – 95%
	Physical/chemical analysis	2	2	95%
Bacterial culturing and growth	CFU	3	2	95%
fouling monitoring	Temperature	2	Every 30 min	90 – 95%
	Permeate flow		Every 30 min	90 – 95%
	Concentrate flow		Every 30 min	90 – 95%
	Feed pressure		Every 30 min	90 – 95%
	Concentrate pressure		Every 30 min	90 – 95%
	Feed conductivity		Every 30 min	90 – 95%
	Permeate conductivity		Every 30 min	90 – 95%
	pH		Every 30 min	90 – 95%
Chemical cleaning	Permeate flow	2	Every 30 min	90 – 95%
	Concentrate flow		Every 30 min	90 – 95%
	Temperature		Every 30 min	90 – 95%
	Feed pressure		Every 30 min	90 – 95%
	concentrate pressure		Every 30 min	90 – 95%
	Feed conductivity		Every 30 min	90 – 95%
	Permeate conductivity		Every 30 min	90 – 95%
	pH		Every 30 min	90 – 95%

Statistical analysis was executed using Microsoft Excel 5 and preformed using a confidence interval of 95% ($P<0.05$). Experimental tests reproducibility was determined based on the average value and relative standard deviation obtained for all samples collected during each experimental run.

CHAPTER 4

EVALUATION OF THE PERFORMANCE OF THE TAJOURA SWRO DESALINATION PLANT

4.1 Introduction

Fouling can be monitored by measuring silt density index (SDI) and biological activity in both raw and pre-treated seawater as well as by analysis of the operating data such as permeate flow, salt passage, and differential pressure (Saad, 2004). However, as the values of operating parameters fluctuate, it is generally recommended that these are standardised. Standardisation the operating data enables changes in product water quality and quantity to be related to fouling, damage to the membranes or merely due to changing in the operation conditions (Song, *et al.,* 2003; Wilf and Klinko, 1994; Al-Ahmmed, *et al,* 2000; Huiting, *et al.*, 2001).

Changes in these parameters simply indicate that a problem in the desalination plant has developed but by applying a correct standardisation process, it becomes possible to detect when and where the problem arose. The widely applied standardisation methods for spiral wound reverse osmosis membranes are the FilmTec method (Safar, *et al.,* 1998), the American Standard for Testing Materials (ASTM) method (Darwish, *et al.*, 1989; Al-Bastaki and Abbas, 2004) and the Homogenous Solution Diffusion (HSD) method (Zhao, and Taylor, 2005). However, these methods can not be used to evaluate actual permeate flow and salt passage unless standard values, such as net driving pressure, average concentration of feed and concentrate, average feed – concentrate osmotic pressure and water and salt permeability coefficients are known (Zhao and Taylor, 2005). Wilf and Klinko, (1994); Al-bastaki and Abbas, (2004) and Fujiwara *et al.* (1999) reported that the permeability coefficients for water and salt can be used for performance evaluation of SWRO membrane systems. In addition to theoretical standardisation methods there are different types of standardisation software that are available to evaluate the performance of RO membranes. These are based on the ASTM D 4516 method and represent the membrane manufacturer's view of membrane performance

in terms of permeate flow and salt passage based on testing synthetic feed water under laboratory conditions and do not represent actual conditions (Saad, 2004). The software packages were developed by various membranes manufactures, such as FilmTec (ROSA software), Toray (CARTON), Hydrunatics (ROdata) and Koch (NORMPRO). The purpose of such software is to analyse actual operating data of a particular RO system and to compare this with initial performance.

In this chapter, the performance of applied pre-treatment and RO membrane systems of the Tajoura SWRO desalination plant (Tripoli - Libya) were evaluated using in-situ fouling monitoring methods, theoretical standardisation methods and software packages. Silt density index (SDI), biological activity and scaling potential were measured. Actual operating data was analysed and permeate flow and salt passage values were standardised over a period of 360 days using ASTM, HSDM, ROSA and ROdata normalisation software. The use and accuracy of these methods in performance evaluation and prediction of fouling types are presented and compared.

4.2 Materials and Methods

4.2.1 Performance Evaluation of Pre-treatment Systems

4.2.1.1 Silt-Density Index (SDI)

The SDI values of raw and pre-treated sea water were measured according to the protocol described in Section 3.1. SDI values of raw and pre-treated seawater are presented in Section 1, Appendix A.

4.2.1.2 Colony Forming Units

Bacterial colony forming units (CFU) were measured in water samples and single bacterial colonies with various morphologies were determined according to the procedures described in Section 3.1.1.2. Triplicate measurements were carried out and the average and standard deviations were calculated (See Section 2, Appendix A).

4.2.1.3 Chemical Analysis of Water Samples

The compositions of raw seawater, RO feed, RO permeate and RO concentrate were determined using Inductively Coupled Plasma Spectroscopy (ICP) and Ion Chromatography (IC) according to the procedures described in Sections 3.1.2.1 and 3.1.2.2, respectively.

4.2.1.4 Calculation of Scaling Potential

Calcium carbonate ($CaCO_3$) and calcium sulphate $CaSO_4$ scaling potentials were calculated (See Section 3.1.1.4). The equations used are described in section 4.4.4. The Stiff and Davis Stability Index (S&DSI) was calculated using Equation 3.2 (Chapter 3). Graphs from Dow Technical Manual (2002) were used (See Section 6, Appendix A).

4.3 Performance Evaluation of the Reverse Osmosis Membrane Systems

The performance of the reverse osmosis membrane systems were evaluated by normalising the permeate flow and salt passage using ASTM and HSDM theoretical standardisation methods and FilmTec and Hydranautics normalisation software packages (See Appendix B and Appendix C).

4.3.1 The ASTM Standardisation Method

The ASTM (D 4516) method consists of two main parameters: normalised permeate flow and normalised salt passage (Equations 2-28, and 2-40, Chapter 2).

4.3.2 Homogenous Solution Diffusion Method (HSDM)

The HSDM method was applied to standardise permeate flow and salt passage. The normalised permeate flow was calculated using equation 2-35 (Chapter 2), while the normalized salt passage was calculated using equation 2-38 (Chapter2).

4.3.3 FilmTec Normalisation Software Package (ROSA)

ROSA normalisation software uses the same equation described in the ASTM Method (Equation 2-28 and 2-33, Chapter 2). However, in this method the average feed – concentrate osmotic pressure and permeate osmotic pressure, temperature correction factors are calculated using the following equations:

- Average feed – concentrate osmotic pressure:

$$\pi_{fc} = \frac{(0.0117 \times C_{fc}) - 34}{14.23} \times \frac{T + 320}{345} \quad (4\text{-}1)$$

- Permeate osmotic pressure:

$$\pi_p = 0.01 \pi_{fc} \quad (4\text{-}2)$$

- Temperature correction factor:

$$TCF = \exp\left(K\left(\frac{1}{273+T} - \frac{1}{298}\right)\right) \quad (4\text{-}3)$$

Where K is a constant depends on the membrane material. (K=2600 for T > 25 °C and 3480 for T < 25 °C)

4.3.4 Hydranautics Normalisation Software package (ROdata-XL414)

The ROdata – XL 414 software was used to evaluate membrane performance using equation 2-28 (Chapter 2) for normalisation of permeate flow. The average feed – concentrate osmotic pressure and permeate osmotic pressure and temperature correction factor are calculated using the following equations:

- Average feed – concentrate osmotic pressure:

$$\pi_{fc} = \frac{11.8 \times C_{fc} \times (T + 273)}{298 \times 1000} \quad (4\text{-}4)$$

- Permeate osmotic pressure:

$$\pi_{fc} = \frac{11.8 \times C_p \times (T + 273)}{298 \times 1000} \qquad (4\text{-}5)$$

- Temperature correction factor:

$$TCF = \exp\left(K\left(\frac{1}{273+T} - \frac{1}{298}\right)\right) \qquad (4\text{-}6)$$

Where K is a constant depends on the membrane material (K=2700)

The salt passage (SP) which is the ratio of concentration of salt on the permeate (C_p) side of the membrane is normalised using the following equation:

$$NSP = S_{Pa} \times \frac{Q_{pa}}{Q_{ps}} \times \frac{TCF_s}{TCF_a} \qquad (4\text{-}7)$$

Where:

NSP – is the normalised salt passage (%)

SP_a- is the actual salt passage (%)

Q_P is the permeate flow ($m^3.h^{-1}$).

TFC – is the temperature correction factor (dimensionless)

C_{fc} – is the average feed - concentrate concentration ($mg.l^{-1}$).

C_f – is the feed concentration ($mg.l^{-1}$).

Subscripts a –is the actual operating data

Subscript s – is the standard operating data

4.4 Results and Discussion

4.4.1 Measuring Colloidal Fouling Potential

Particulate and colloidal fouling potentials in raw and pre-treated seawater at the Tajoura SWRO desalination plant were investigated using the SDI standard method during February 2005 and the results show unstable SDI values (Figure 4.1) (data in Section 1, Appendix A).

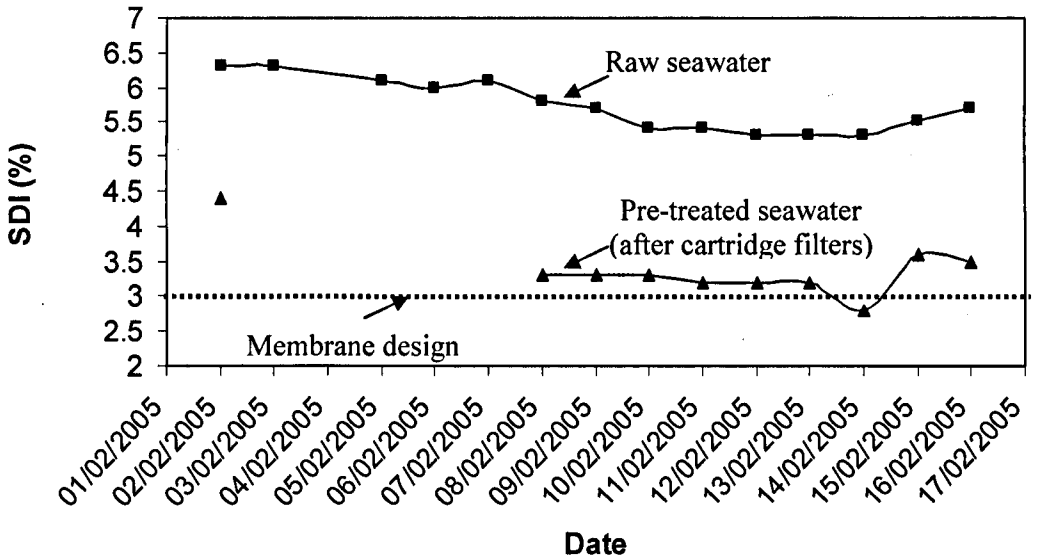

Figure 4.1: SDI values for raw and pre-treated seawater at the Tajoura SWRO desalination plant.

High SDI values were observed (6.5%) between the 3rd and 8th of February 2005 possibly due to the high load of silt which were brought into the intake basin and it is near to the maximum SDI value (6.7%).

In order to avoid rapid blocking of filters and increasing colloidal fouling in the RO membranes, the raw seawater with high SDI values is discharged back to the sea and the plant shut down in this period. When the SDI value of the pre-treated seawater dropped to acceptable values as recommended by the membrane manufacturer (less than 4) the pre-treated seawater was again passed to the RO membrane system.

Figure 4.2 shows a photograph of clean and fouled SDI filters by raw and pre-treated water from the Mediterranean Sea. The average SDI value in pre-treated seawater was 3.4, which is acceptable according to the membrane manufacturer's recommendations (e.g. SDI<4). However, fouling will still occur in the membrane systems despite the low SDI values.

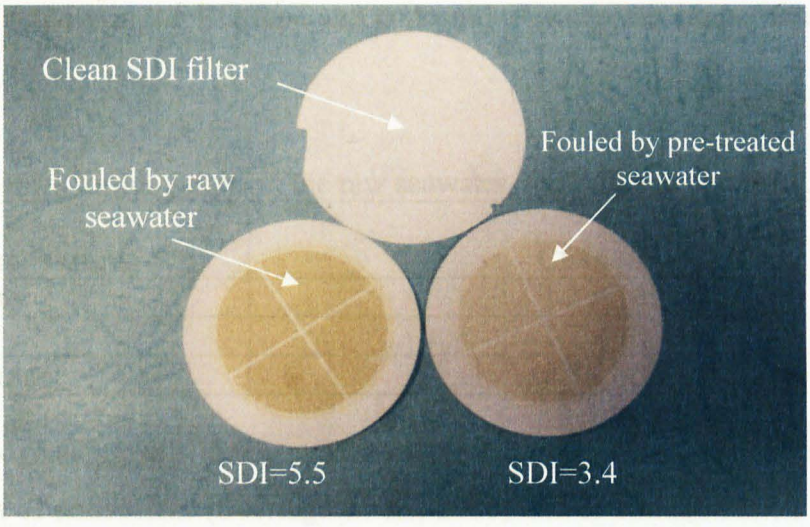

Figure 4.2: A photograph of clean and fouled SDI filters by raw and pretreated Mediterranean Sea seawater.

Despite the importance of SDI for the design and operation of RO membrane processes (Mosset *et al.*, 2008), some researchers (Coules *et al.*, 2008; Boerlage *et al.*, 2002) point out that SDI does not provide information regarding the nature of the foulants passing through a 0.45 μm filter and the potential of biofouling as fouling can occur even with very low SDI values. Boerlage *et al.* (2003) recommend a modified fouling index (MFI-UF) as an alternative to SDI as particles smaller than 0.45 μm in size can not be captured by the 0.45μm membrane, whereas in the MFI experiment, membranes with a pore size of 0.05μm are used. However, the MFI-UF method has limitations in predicting fouling because RO membrane systems are operated in a cross flow mode while the MFI-UF is a dead-end filtration test (Rodriguez *et al.*, 2009). Moreover, the characteristics of the cake layer that forms on the RO membrane is different from that which forms in the dead-end filtration mode. This is why, in the majority of large scale RO desalination plants, operators still use the SDI test as an indicator for particulate fouling.

4.4.2 Measuring Biofouling Potential

The biological activities in raw, RO feed and RO concentrate waters were measured by spreading 0.1 ml of the water sample on the surface of R2A agar medium in Petri dishes. After 7 days of incubation at 28 °C, colony forming units were counted. It was observed that the biological activity in the RO feed and concentrate water was higher than in the raw sea water (Table 4.1).

Table 4.1: Colonies forming units in the raw seawater, the RO feed and the RO concentrate.

Water sample	CFU.ml^{-1}
Raw seawater	1.2×10^3
RO feed	1.7×10^3
RO concentrate	1.8×10^4

The high biological growth down stream to the cartridge filters can be attributed to the biodegradation of antiscalent (Boerlage *et. al.*, 2000) and/or contamination of the pipes and fittings (Huiting and Bosklopper, 2001).

Kurihara *et al.* (2001) evaluated the performance of SWRO desalination plant in Japan and found the biological growth after cartridge filters to be much higher than in the raw seawater (Figure 4.3).

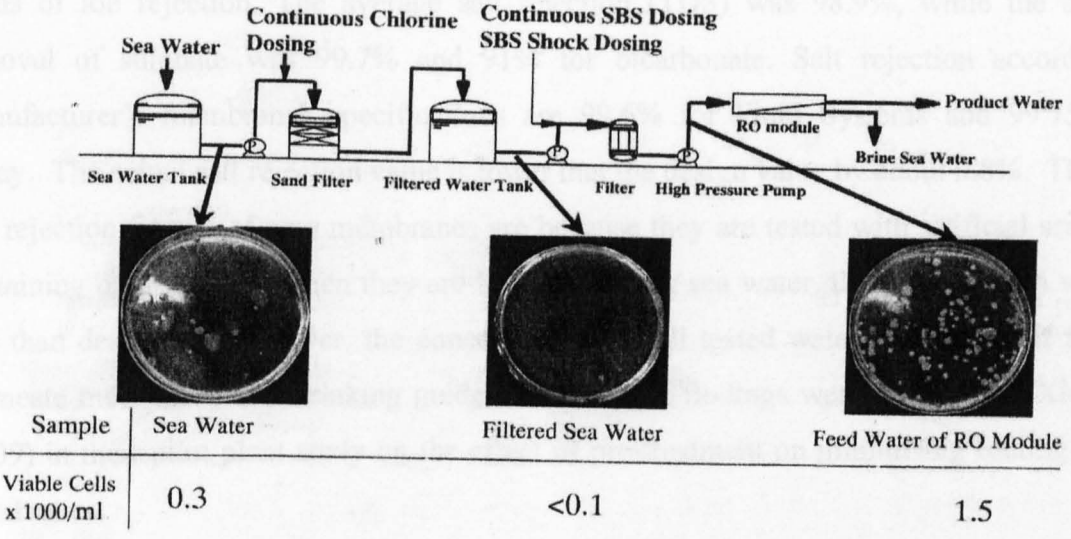

Figure 4.3: High biological growth after cartridge filters (pre-treated seawater).
Ref., Kurihara *et al.* (2001)

The morphological characteristics of the colonies are presented in Table 4.2.

Table 4.2: Morphological characteristics of bacterial colonies from the raw seawater, the RO feed and the RO concentrate.

Water sample	Colony colour	Colony size
Raw seawater	-Yellowish with brown centre	~ 4 mm circular shape.
	- Milky-white round	~ 2 mm irregular shape.
	- Cream-colored	~ 3 mm irregular shape.
	- White round	~10 mm irregular shape.
RO feed water	- Yellow round	~1 mm irregular shape.
	- Light yellow	~10 mm irregular shape.
	- Orange round	~ 3 mm irregular shape
RO concentrate water	- Light yellow	~1 mm circular shape.
	- Translucent	~10 mm irregular shape.
	- Cream-white with slight yellow.	~ 3 mm irregular shape

4.4.3 Characteristics of Water Quality

Water samples were chemically analysed for a range of parameters (Table 4.3). According to the results of water analysis the RO membranes would have functioned well in terms of ion rejection. The average salt rejection (TDS) was 98.9%, while the average removal of sulphate was 99.7% and 91% for bicarbonate. Salt rejection according to manufacturer's membranes specifications are 99.6% for Fluid Systems and 99.75% for Toray. The actual salt rejection value is lower that the design value by about 0.8%. The high salt rejection figures of new membranes are because they are tested with artificial sea water containing only (NaCl). When they are tested with raw sea water, the salt rejection value is less than designed. However, the concentrations of all tested water parameters of the RO permeate meet the WHO drinking guidelines. Similar findings were reported by Xie *et al.* (2009) in their pilot plant study on the effect of pre-treatment on minimising fouling of RO membranes.

Table 4.3: Composition of raw seawater, RO feed, RO permeate and RO concentrate

Element	Raw seawater (mg. L^{-1})	RO feed (mg. L^{-1})	RO permeate (mg. L^{-1})	RO concentrate (mg. L^{-1})
Calcium	540 ± 14.14	522 ± 3.54	6.1 ± 0.071	855 ± 7.1
Magnesium	1427 ± 5. 66	1412.5 ± 3. 54	5.9 ± 0.14	2237.6 ± 3.39
Sodium	11630 ± 42.93	11247.5 ± 3.54	144.5 ± 0.71	12625 ± 35.36
Potassium	464.5 ± 64.35	425 ± 7.07	6.95 ± 0.071	507.5 ± 3.54
Chlorine	21018.5 ± 44.6	21055 ± 7.07	212.9 ± 1.63	30377.2 ± 32.31
Sulfate	2962.5 ± 64.35	3455 ± 7.071	9.5 ± 0.42	4639.7 ± 0.41
Bicarbonate	139.5 ± 4.95	142.5 ± 3.54	12.35 ± 0.12	233.4 ± 2.26
Barium	0.27 ± 0.12	0.28 ± 0.001	0.001 ± 0	0.38 ± 0.028
Strontium	8.6 ± 0.57	8.25 ± 0.07	0.006 ± 0	9.35 ± 0.11
Fluoride	1.25 ± 0.07	1.20 ± 0	0.28 ± 0.04	0.93 ± 0.03
Copper	0.013 ± 0.004	0.19 ± 0.14	0.001 ± 0	0.299 ± 0.002
Manganese	0.15 ± 0.03	0.15 ± 0.03	0.011 ± 0.001	0.34 ± 0.021
Aluminium	0.20 ± 0.01	0.20 ± 0.01	0.001± 0	1.73 ± 2.0
Iron	0.032 ± 0.003	0.063 ± 0.004	0.001 ± 0	0.32 ± 0.021
Zinc	0.012 ± 0.003	0.01 ± 0.003	0.01 ± 0	0.023 ± 0
TDS	38750 ± 14.14	38189.8 ± 1.77	398.2 ± 2.62	51028.3 ± 2.4
pH	8.25 ± 0.071	7.1 ± 0.07	6.65 ± 0.21	7.25 ± 0.071

4.4.4 Measurement of Scaling Potential.

Scaling calculations were carried in order to determine whether $CaCO_3$ and $CaSO_4$ have created a potential scaling problem in the RO membrane units. Scaling calculations were carried out according to the ASTM D4582-86 for both the calculations and adjustments of the Stiff and Davis Stability Index for reverse osmosis membranes. The ionic products of $CaCO_3$ and $CaSO_4$ in the RO concentrate were compared with the solubility products (Ks) for both salts. The major anions and cations that are used in the calculations are given in Table 4.4. The ion concentrations were converted from $mg.l^{-1}$ to molal concentration using Equation 4.10.

$$m_i = \frac{C_i}{1000 \times MW_i} \quad (4.8)$$

Table 4.4: The major cations and anions present in the Mediterranean Sea.

Cations	Concentration		Anions	Concentration	
	mg. l^{-1}	mol. l^{-1}		mg. l^{-1}	mol. l^{-1}
Ca^{2+}	455	11.4×10^{-3}	HCO^{-}_3	136	2.23×10^{-3}
Mg^{++}	1427	58.7×10^{-3}	SO^{2-}_4	2915	30.4×10^{-3}
Na^{+}	11600	504.4×10^{-3}	Cl^{-}	20987	591×10^{-3}
K+	419	10.7×10^{-3}			

The ionic strength in the raw seawater was calculated using Equation 4.11.

$$I_f = \frac{1}{2}\sum m_i \times Z_i^2 \quad (4.9)$$

Where, m_i is the molal concentration of ion (mol kg^{-1}); C_i is the concentration of ion (mg l^{-1}), the MW_i is molecular weight of ion and Z_i is the ionic charge.

$$I_f = \frac{1}{2}\sum\{(11.4+58.7+30.4)\times 2^2 \times 10^{-3} + (504.4+10.7+2.23+591)\times 10^{-3}\} = 0.8 \text{ mol.l}^{-1} \quad (4.10)$$

The ionic strength in the concentrate water was calculated by multiplying the ionic strength of seawater by the concentration factor which is a function of recovery using Equation 4.13.

$$I_c = I_f \times \left(\frac{1}{1-Y}\right) \quad (4.11)$$

$$Y = \frac{Q_p}{Q_f} \times 100\ \% \quad (4\text{-}12)$$

Where,

I_f – is the ionic strength of feed water

Y – is the recovery rate which is the ratio of the product flow rate to the feed flow rate.

Q_p – is the permeate flow rate ($m^3.h^{-1}$)

Q_f - is the feed flow rate ($m^3.h^{-1}$)

$$I_c = 0.8 \times \left(\frac{1}{1-0.35} \right) = 1.23 \qquad (4.12)$$

The concentration of calcium and alkalinity in the concentrate can be calculated by multiplying the calcium and alkalinity concentration in the feed water by the concentration factor (Assuming 100% rejection).

$$(Ca^{2+})_c = (Ca^{2+})_f \frac{1}{1-Y} \qquad (4.13)$$

$$(Ca^{2+})_c = 455 \times \left(\frac{1}{1-0.35} \right) = 700 \ mg.l^{-1} \qquad (4.14)$$

$$(Alkalinity)_c = (Alkalinity)_f \frac{1}{1-Y} \qquad (4.15)$$

$$(Alkalinity)_c = 136 \times \left(\frac{1}{1-0.35} \right) = 209.4 \ mg.l^{-1} \qquad (4.16)$$

The pH at which the concentrate stream is saturated with $CaCO_3$ can be calculated using Equation 4.17.

$$pH_s = p[Ca^{2+}] + p[HCO^-_3] + K \qquad (4.17)$$

The constant "K" as a function of concentrate ionic strength and temperature was calculated according to the equation (4.18) (derived by Al-Shammiri *et al.*, 2005).

A similar value was obtained from the graph (Figure 1, Appendix B, Section 6).

$$K = \left[\left(-0.7083\ I_c^{\,2}\right) + \left(1.8798\ I_c\right) + 2.1727\right] = 3.4 \quad (4.18)$$

Where:

I_c – is the concentrate ionic strength = 1.23

The calculated and obtained values of $p[Ca^{2+}]$ and $p[HCO^{-}_3]$ and "K" are presented in Table 4.5.

Table 4.5: The calculated and the obtained values of $p[Ca^{2+}]$, $p[HCO^{-}_3]$ and "K" from the graph.

Parameter	Calculated ASTM method	Calculated (Al-Shammairi, *et al.*, 2006)	Obtained from graph value (Appendix A, Section 6, Figure 3)
$p[Ca^{2+}]$	1.4	1.4	2.8
$p[HCO^{-}_3]$	2.6	2.6	2.5
"K"	3.4	3.4	3.4

The free carbon dioxide (CO_2) content in the concentrate stream can be calculated by assuming that the CO_2 concentration in the concentrate stream is equal to the CO_2 in the feed: $(CO_2)_f = (CO_2)_c$. The concentration of free CO_2 in the feed as a function of alkalinity and pH of the feed water was determined from the graph (Appendix A, Section 6, Figure 3). The measured RO feed water pH is 7.0 and the ratio of alkalinity to CO_2 concentration was determined from the graph (See Appendix A, Section 6, Figure 2) and found to be 5. The free CO_2 content in the feed water at pH 7.0 and alkalinity concentration of 136 $mg.l^{-1}$ was calculated.

$$CO_2 = \frac{136 mg.l^{-1}}{5} = 27.2 \qquad (4.19)$$

The ratio of alkalinity to CO_2 content in the concentrate stream was calculated.

$$\frac{209.4 mg.l^{-1}}{27.2} = 7.7 \qquad (4.20)$$

The pH of the concentrate stream at alkalinity / CO_2 ratio of 7.7 was determined from the graph (See Appendix A, Section 6, Figure 4) and found to be 7.2. As the concentration of CO_2 will not change in the concentrate or permeate streams (Alhadidi *et al.* 2009), and concentration of Ca^{2+} and HCO_3^- and the pH of the concentrate stream can be calculated based on recovery of the plant (35%) and membrane rejection (99.8%). This keeps the concentration factor (CF) value close to 1.54 for a recovery of 35%. The pH of concentrate stream can be calculated using Eq. 4.21.

$$pH_c = \log\ CF + pH_{actual} = 0.19 + 7 = 7.19 \qquad (4.21)$$

The pH_s and S&DSI values were calculated using Equations 4.19 and 4.22 as well as the Hydranautics software (ICM Design Version 2009) (See Appendix A, Section 6) and the results are presented in Table 4.6.

$$S\ \&\ DSI = pH_c - pH_s \qquad (4.22)$$

Table 4.6: The calculated values for pH_s and S&DSI values respectively.

Parameter	Calculated (Al-Shammairi, *et al.*, 2006)	Obtained from graph value (ASTM Method)	ISM Design Software (Hydranautics)
pH_c	7.19	7.2	7.2
pH_s	7.4	7.7	7.8
S&DSI	-0.21	-0.5	-0.6

Negative S&DSI values indicate that no $CaCO_3$ scale forms because the water is in equilibrium with $CaCO_3$. Waly *et al.* (2008) reported that the induction time of concentrate water of SWRO plants operating at 30% recovery and a pH 8.3 was about 100 min. which suggests that $CaCO_3$ scaling will not occur in SWRO systems, since the residence time is just a couple of minutes. However, addition of acid (H_2SO_4) in the pre-treatment further reduces the potential of $CaCO_3$ scaling. Normally acid (H_2SO_4 and/or HCl) is added to the feed water to reduce pH and convert HCO^-_3 ions to CO_2 as follows:

$$H_2SO_4 + 2HCO^-_3 \rightarrow 2H_2O + CO_2 + SO_4^{2-} \qquad (4.23)$$

Sulphuric acid is more commonly used as it is the least expensive acid available, however the use of H_2SO_4 leads to corrosion problems and its addition provides a source of SO_4^{2-} ions, which will increase the potential of sulphate scaling precipitation.

The calcium sulphate ($CaSO_4$) scaling potential was determined by calculating the ion product (IPc) for CaSO4 in the concentrate stream using Equation 4.24.

$$IP_c = \left[\left(Ca^{2+}\right)_f \times \frac{1}{1-R}\right] \times \left[\left(SO_4^{2-}\right)_f \times \frac{1}{1-R}\right] \qquad (4.24)$$

$$IP_c = \left[\left(17.6\times10^{-3}\right)\times\left(46.82\times10^{-3}\right)\right] = 8.24\times10^{-3} \qquad (4.25)$$

The solubility product for the $CaSO_4$ at an ionic strength of 1.23 was determined from the graph (See Appendix- A, Section 6, Figure 5) and found to be $K_{sp} = 2\times10^{-3}$. The ion product (IP_c) of $CaSO_4$ in the concentrate stream was compared with this solubility product. It was found that the $IP_c = 0.24K_{sp}$ and $CaSO_4$ scaling is predicted not to occur. As $CaSO_4$ scaling will only occur if the $IP_c > 0.8\ K_{sp}$. This approach to calculate the scaling potential in RO membrane systems is widely used, however in some studies (Wally, *et al.*, 2008; Sheikholeslami, 2005; Borlage, *et al.*, 2002) it is reported that the most common used indices to estimate $CaSO_4$ scaling potential have limitations due to the use of simplified relationships.

4.5 Analysis of Actual Operating Data

The performance evaluation, of two commercial seawater reverse osmosis (SWRO) membrane units at the Tajoura SWRO desalination plant was studied. Detailed information on plant design, operating data and various water quality analyses was gathered over a period of 360 days. The operating data included RO feed and permeate conductivity, RO feed pressure, differential pressure, RO feed flow and permeate flow and feed water temperature averaged over 30 day periods (See Appendix B and C). Data on permeate flow, permeate concentration, and differential pressure was analysed in order to study the membrane system performance. These data were standardised in order to distinguish between fouling and other operational problems.

4.5.1 Actual Permeate Flow (Q_p)

Figure (4.4) represents the actual permeate flow rate over time for two RO membrane units compared to the design permeate flow. The results show stable productivity of 138 $m^3.h^{-1}$ over 360 days of operation. Stability of permeate flow does not indicate that the performance of the membrane system was stable. Changes in net driven pressure and feed water temperature can change membrane performance even when there is no change in the actual permeates flow.

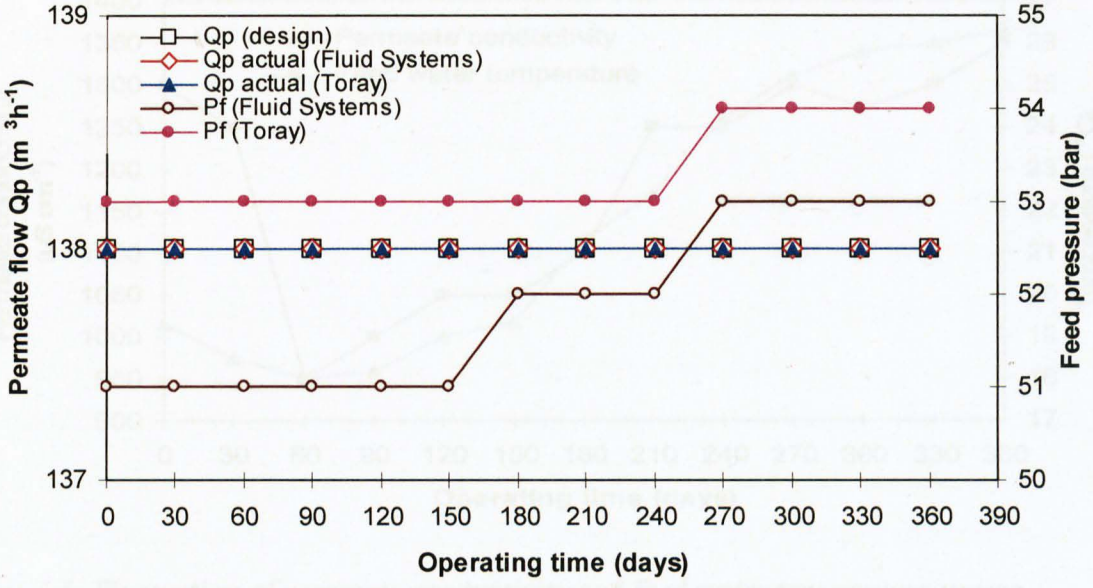

Figure 4.4: Permeate flow verses operating time for the SWRO membrane units.

Since both membrane units were operated at constant permeate flow and recovery rates (e.g. 35%), no decline in productivity was observed. However, the feed pressure had to be increased to keep constant productivity, especially during the last four months of operation. Increasing feed pressure and differential pressure values indicated fouling was forming in both membrane units.

4.5.2 Actual Permeate Conductivity

Increased permeate conductivity over time may occur due to operational and/or mechanical problems including fouling, increasing feed water temperature, system recovery, membrane degradation, damaged O-rings and glue lines (Lomax, 2008). Figures 4.5 and 4.6 illustrate the relationship between permeate conductivity and feed water temperature for each membrane unit. The permeate conductivity of Fluid Systems membrane unit is higher than the permeate conductivity of Toray membrane unit due to differences in the salt rejection (99.6% and 99.75%, respectively).

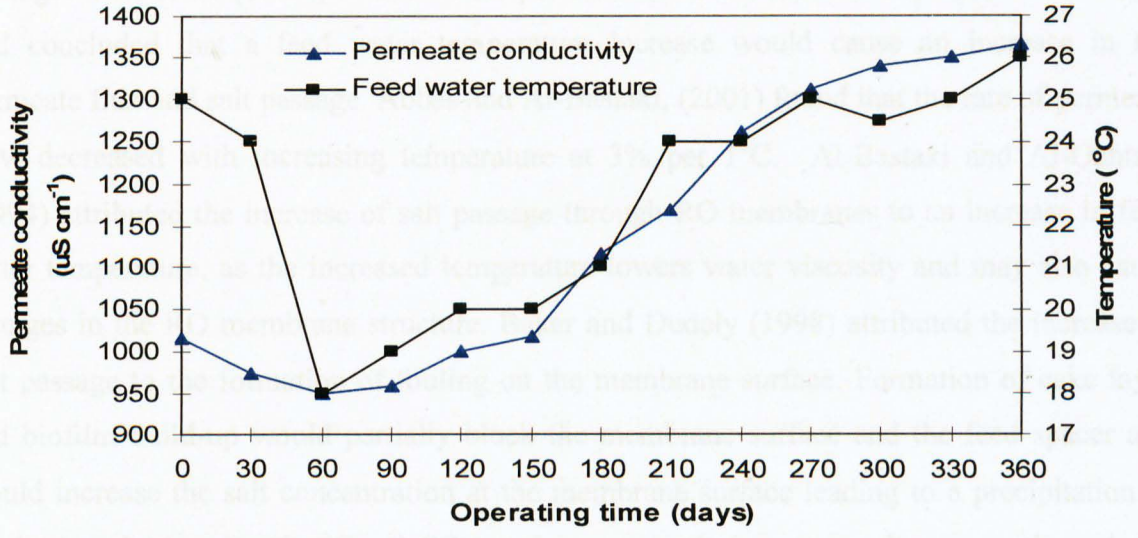

Figure 4.5: Fluctuation of permeate conductivity and feed water temperature verses operating time for the Fluid Systems RO membranes.

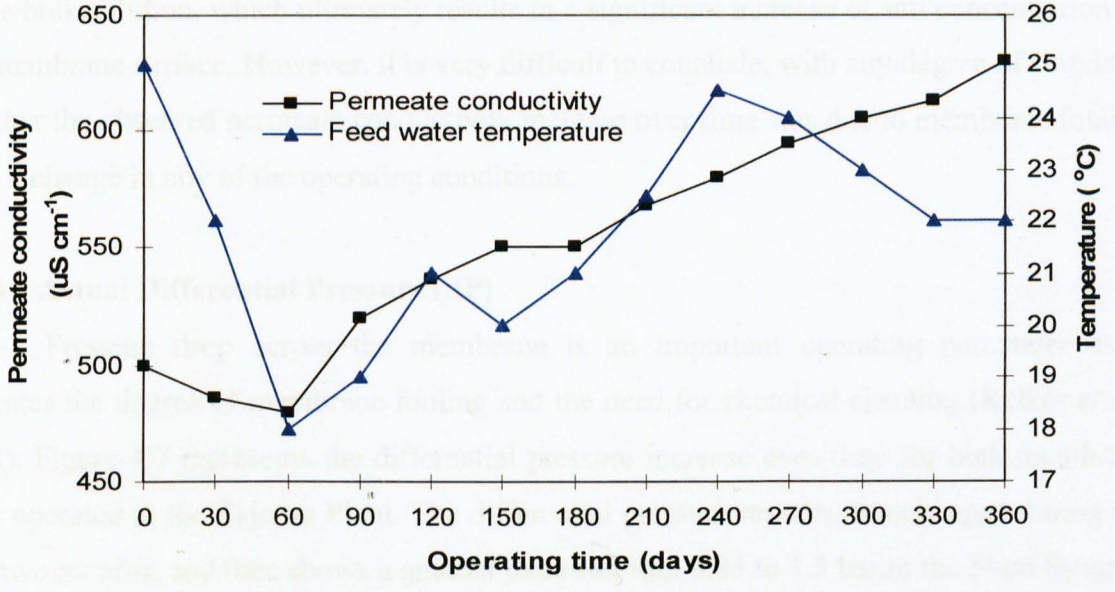

Figure 4.6: Fluctuation of permeate conductivity and feed water temperature verses operating time for the Toray RO membranes.

The results show a slight decrease in the permeate conductivity for both membrane units during the first two months of operation, then a gradual increase by about 21% after 360 days of operation. Variations in permeate conductivity could be attributed to the variation of feed

water temperature and/or a formation of fouling as both will cause an increase in salt passage. Pais *et al.* (2007), evaluated the performance of an industrial RO plant in Portugal and concluded that a feed water temperature increase would cause an increase in the permeate flux and salt passage. Abbas and Al-Bastaki, (2001) found that the rate of permeate flow decreased with increasing temperature at 3% per 1°C. Al-Bastaki and Al-Qahtani (1994) attributed the increase of salt passage through RO membranes to an increase in feed water temperature, as the increased temperature lowers water viscosity and may also cause changes in the RO membrane structure. Baker and Dudely (1998) attributed the increase in salt passage to the formation of fouling on the membrane surface. Formation of cake layer and biofilm build-up would partially block the membrane surface and the feed spacer and would increase the salt concentration at the membrane surface leading to a precipitation of sparingly soluble salts ($CaCO_3$, $CaSO_4$) and consequently increases salt passage through the membrane. On the other hand, Hoek *et al.* (2002) and Elimelech *et al.* (1997) found that the formation of a fouling layer on the membrane surface would limit back diffusion of salt ions to the bulk solution, which ultimately results in a significant increase of salt concentration on the membrane surface. However, it is very difficult to conclude, with any degree of certainty, whether the observed permeate conductivity increase over time was due to membrane fouling or to a change in any of the operating conditions.

4.5.3 Actual Differential Pressure (ΔP)

Pressure drop across the membrane is an important operating parameter as it indicates the degree of membrane fouling and the need for chemical cleaning (Kelkar *et al.*, 2003). Figure 4.7 represents the differential pressure increase over time for both membrane units operated at the Tajoura Plant. The differential pressure remained unchanged during the first two months, and then shows a gradual increase from 0.85 to 1.5 bar in the Fluid Systems membrane unit and from 0.7 to 1 bar in the Toray membrane unit. Subsequently, slight increments in the feed pressure were introduced for both membrane units in order to maintain a constant permeate flow.

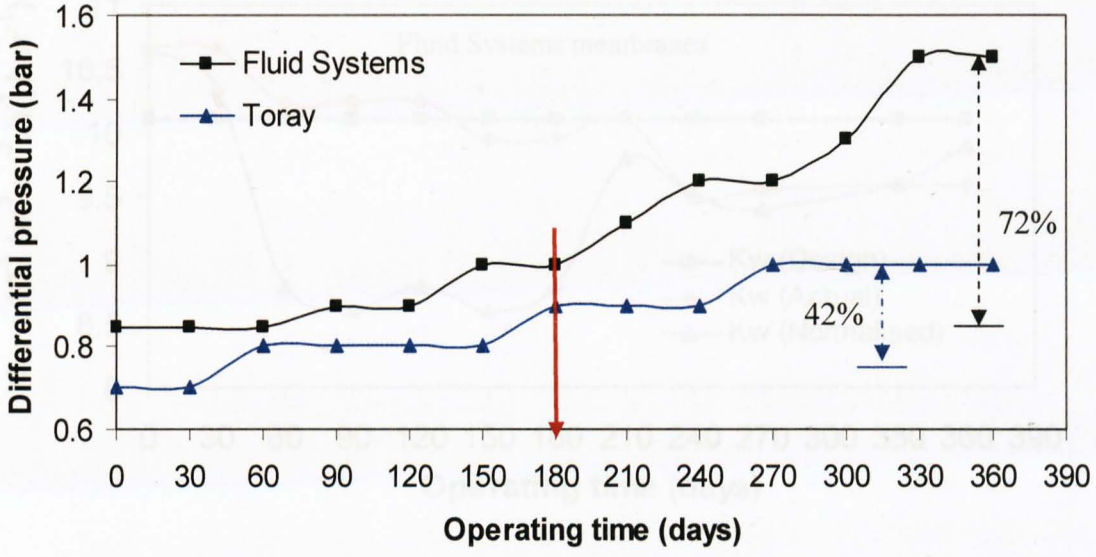

Figure 4.7: Differential pressure verses operating time for membrane units.

The gradual increase in the differential pressure in both units, particularly after six months operation, was possibly due to the blocking of feed channels and spaces of both membrane elements by fouling (particulate, metal and/or biofouling). This resulted in differential pressure increases in both units at the end of the operating period of 72% for Fluid Systems and 42% for Toray membranes.

These observations can be explained by the formation of severe fouling on the membrane surfaces and feed spacers of both membrane units. Similar studies (Gulamhusein *et al.*, 2008; Leparc *et al.*, 2007 and Delkar *et al.*, 2002) have reported that increasing differential pressure is an indication of fouling. Chemical cleaning should be implemented in such systems after 6 months because ΔP increased by 15%. Ignoring chemical cleaning caused the severity of fouling in both RO membrane units in this case.

4.5.4 Water and Salt Permeability Coefficient

It is useful to express water flux and salt passage in terms of water and salt permeability coefficients (K_w and K_s). The water permeability coefficient (K_w) was calculated using equation (2.40), while the salt permeability coefficient (K_s) was calculated using equations (2.42). The values of K_w of both membrane units are shown in Figures 4.8.

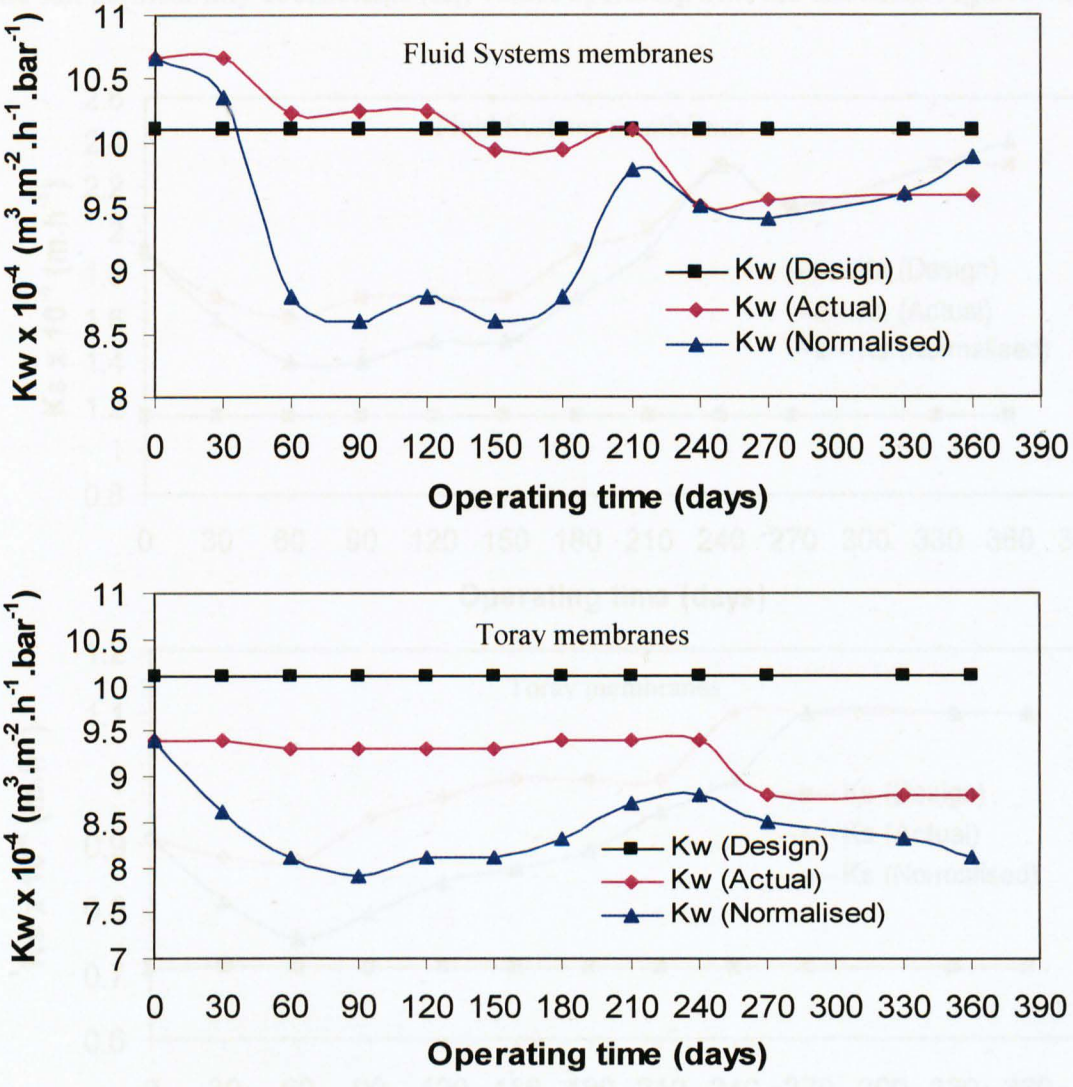

Figure 4.8: Design, actual and normalised water permeability coefficient verses time for SWRO membranes (Fluid Systems SWRO membranes).

From Figure 4.8 it can be seen that the normalised water permeability coefficients of Fluid Systems membranes unit was slightly higher than the design criteria in the first two months, possibly due to operational problem. The normalised water permeability coefficient of both membrane units rapidly declined in the first two months of operation and then increased gradually due to increasing of feed pressure. Increasing water flux requires higher pressure which in turn increases the energy consumption as well as the fouling rate. After 360 days the actual and normalised water permeability coefficients of both units had decreased by about 12% and 14%, respectively due to fouling.

The salt permeability coefficients (K_s) verses operating time are shown in Figures 4.9.

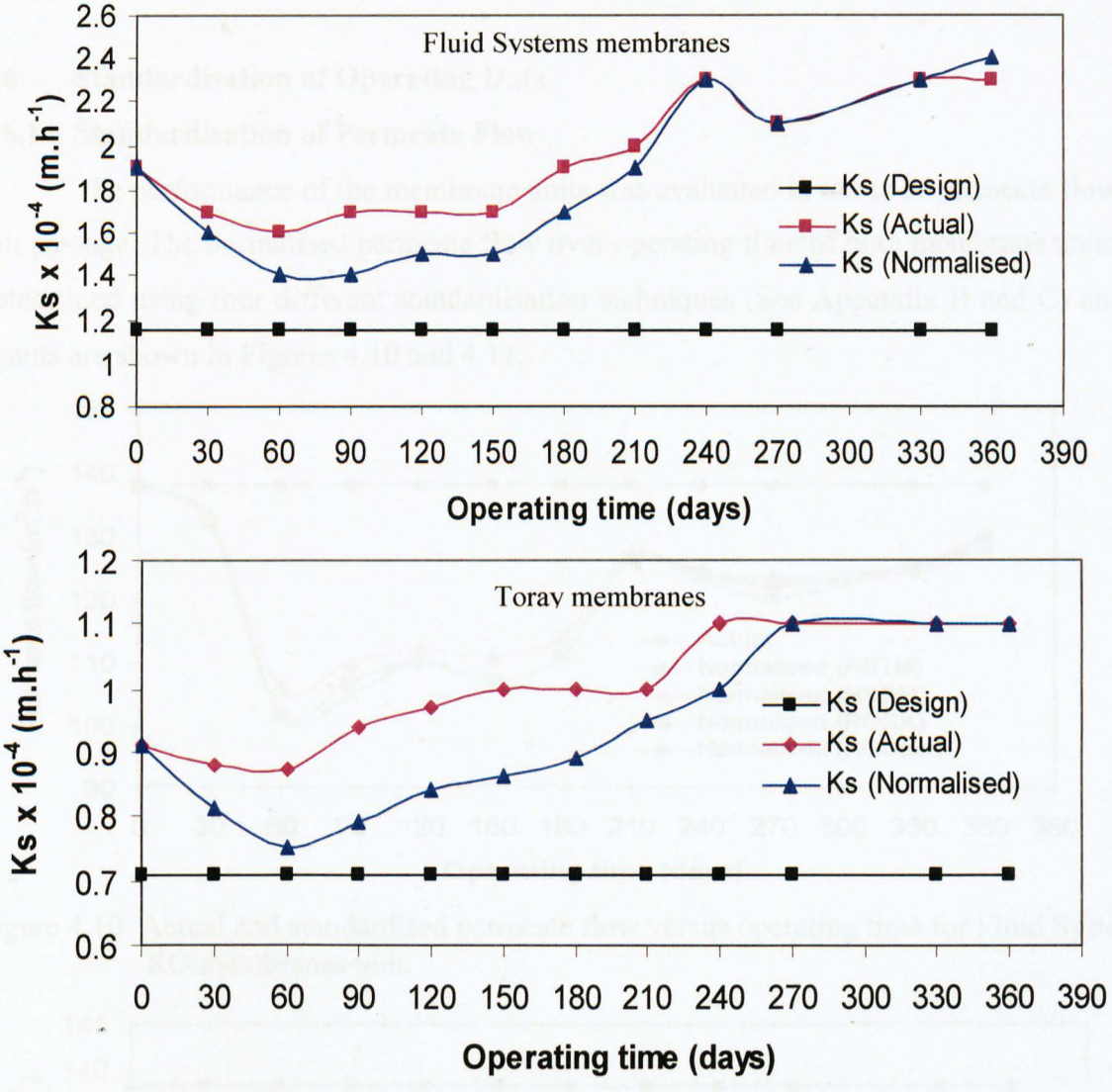

Figure 4.9: Design, actual and normalised salt permeability coefficient verses operating time for Fluid Systems and Toray SWRO membrane units.

Figures 4.9, shows that the normalised salt permeability coefficients of both membrane units were higher than the design criteria. However, they decreased in the first three months of operation and then gradual increased again and after 360 days had increased by 21% and 17%, respectively. The increase in salt permeability coefficients can be attributed to the formation of fouling, or possibly slight damage in the O-rings and/or membrane envelope glue lines. In their studies on a medium-scale industrial water RO desalination plant in

Bahrain, Al-Bstaki and Abbas (2004) found that the permeability coefficients for water and salts declined by about 39% and 60% due to fouling.

4.6 Standardisation of Operating Data

4.6.1 Standardisation of Permeate Flow

The performance of the membrane units was evaluated in terms of permeate flow and salt passage. The normalised permeate flow over operating time of both membrane units was determined using four different standardisation techniques (See Appendix B and C) and the results are shown in Figures 4.10 and 4.11.

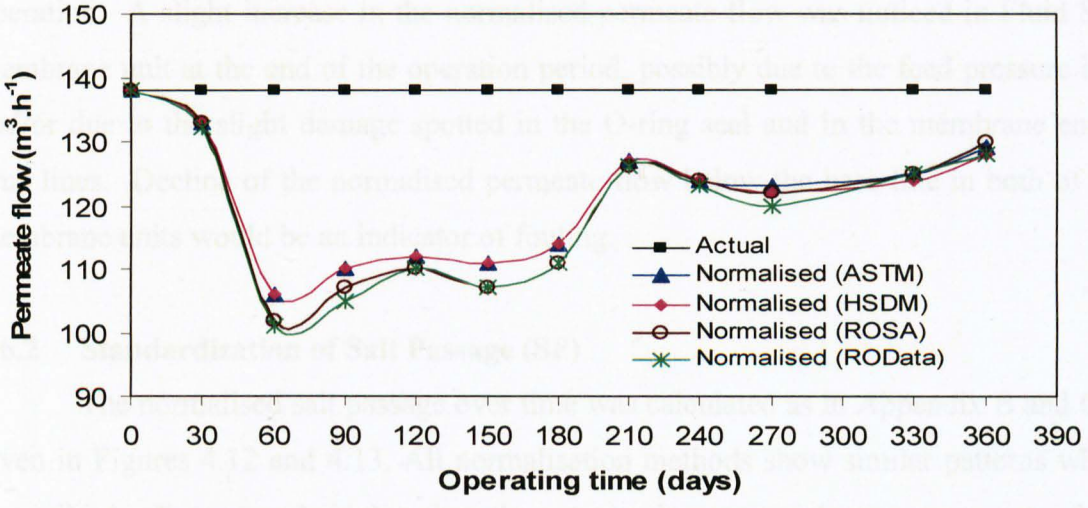

Figure 4.10: Actual and standardised permeate flow versus operating time for Fluid Systems RO membranes unit.

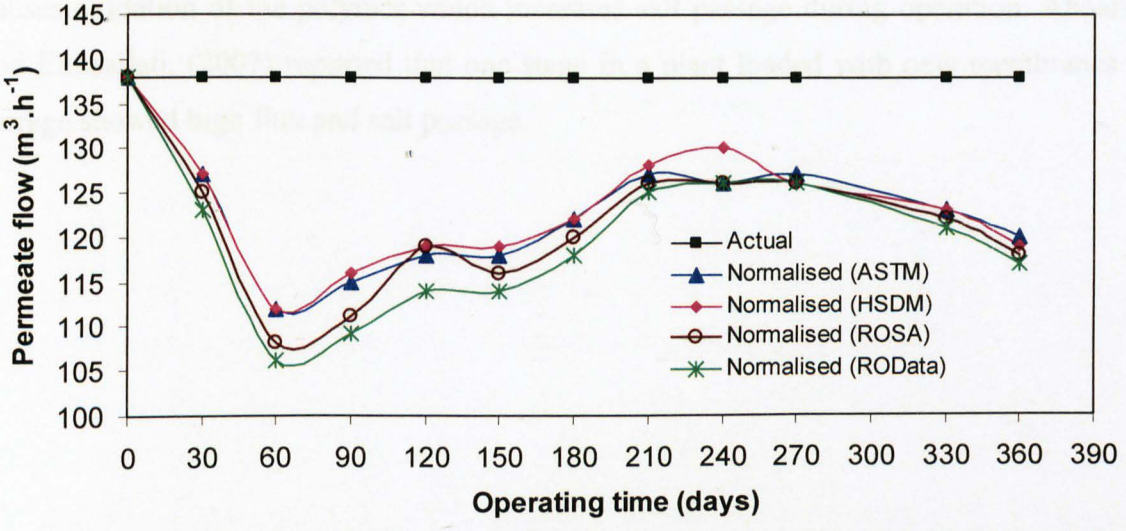

Figure 4.11: Actual and standardised permeate flow versus operating time for Toray RO membranes unit.

From Figures 4.10 and 4.11 it can be seen that the mathematical and software standardisation methods exhibited similar patterns. A significant decline (20% and 17%) in the normalised permeate flow was observed after 3 months operation due to fouling followed by a gradual increase due to increasing feed pressure. Similar findings were reported by Syed *et al.* (2007) and Safar *et al.* (1998).

RO operating guidelines recommend that chemical cleaning should be implemented when a normalised permeate flow decreases by about 15%, in order to prevent irreversible fouling. These results indicate that chemical cleaning should be implemented after 3 months of operation. A slight increase in the normalised permeate flow was noticed in Fluid Systems membrane unit at the end of the operation period, possibly due to the feed pressure increase and/or due to the slight damage spotted in the O-ring seal and in the membrane envelopes glue lines. Decline of the normalised permeate flow below the base line in both of the RO membrane units would be an indicator of fouling.

4.6.2 Standardisation of Salt Passage (SP)

The normalised salt passage over time was calculated as in Appendix B and C and is given in Figures 4.12 and 4.13. All normalisation methods show similar patterns where the normalised salt passage is higher than the actual salt passage. Improper storage of the RO membrane can cause serious damage because mold can grow on the membrane surface and causes oxidation of the polymer which increases salt passage during operation. Aboabboud and Elmsallati, (2007) reported that one stage in a plant loaded with new membranes from storage showed high flux and salt passage.

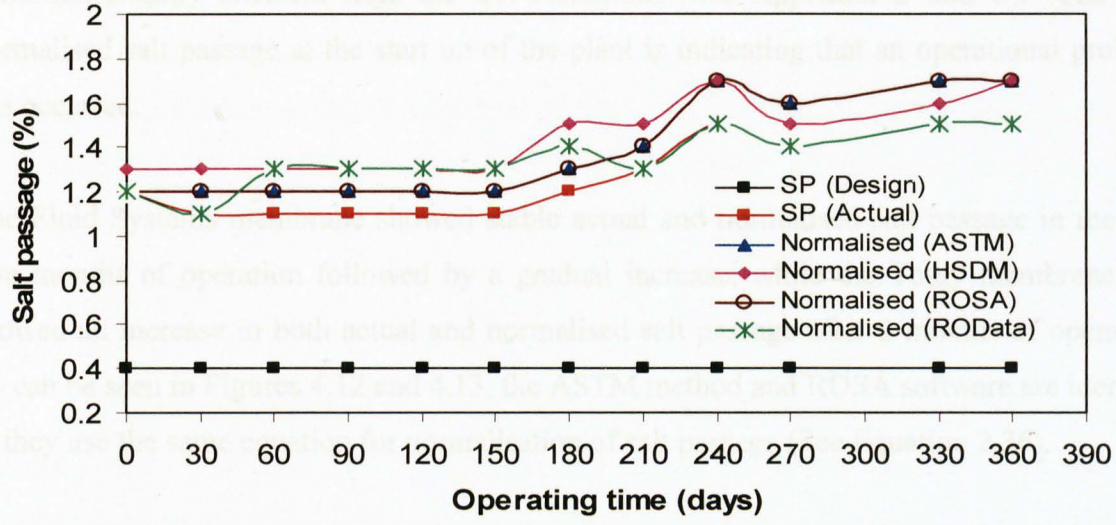

Figure 4.12: Design, actual and standardised salt passage verses operating time for Fluid Systems RO membranes unit.

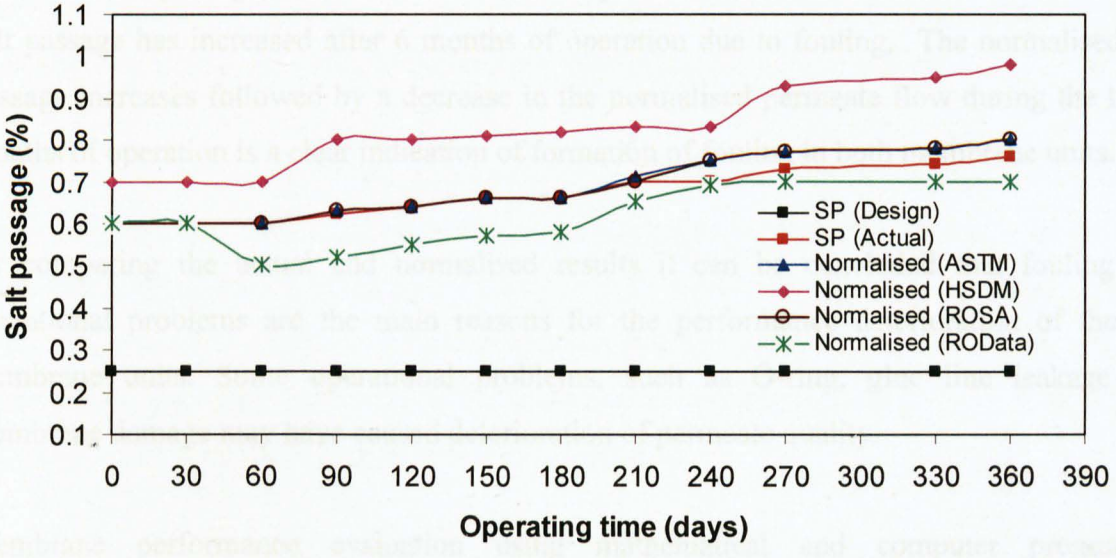

Figure 4.13: Actual and standardised salt passage verses operating time for Toray RO membranes unit.

The values of actual and normalised salt passage in both membrane units were 3 times higher than the design values. According to the membrane manufacturers both RO membranes have high salt rejection (99.6% and 99.75% respectively). However, in real operation this high salt rejection can not be achieved possibly, due to the presence of different types of contaminants in the raw seawater as well as differences in operation conditions. According to the operating data collected from the plant, both membrane units were operated at a

condition slightly different from the test conditions (See Appendix B and C). The high normalised salt passage at the start up of the plant is indicating that an operational problem has occurred.

The Fluid Systems membrane showed stable actual and normalised salt passage in the first five months of operation followed by a gradual increase, while the Toray membrane unit showed an increase in both actual and normalised salt passage after 2 months of operation. As can be seen in Figures 4.12 and 4.13, the ASTM method and ROSA software are identical as they use the same equation for normalisation of salt passage (See Equation 2.36).

The normalised salt passage increased in both membrane units by about 15% after 6 months of operation. Safar *et al.* (1998) used ASTM and FilmTec normalisation methods to normalise salt passage in the Doha desalination plant in Kuwait and noticed that normalised salt passage has increased after 6 months of operation due to fouling. The normalised salt passage increases followed by a decrease in the normalised permeate flow during the last 6 months of operation is a clear indication of formation of fouling in both membrane units.

By comparing the actual and normalised results it can be concluded that fouling and operational problems are the main reasons for the performance deterioration of the RO membrane units. Some operational problems, such as O-ring, glue line leakage and membrane damage may have caused deterioration of permeate quality.

Membrane performance evaluation using mathematical and computer programme standardisation methods have some limitations in determining the true identity and causes of fouling. They are essentially used to determine best time for chemical cleaning application for RO membranes in order to prevent irreversible fouling. Most membrane manufacturers recommend that when the normalised permeate flow decreases by 15%, and normalised salt passage and differential pressure increases by 15% chemical cleaning should be applied (Huiting and Bosklopper, 2001). However, it is difficult to detect early development of fouling and to predict its type even through long – term monitoring, because fouling is cumulative and builds up with operating time (Saad, 2004).

The causes of the fouling symptoms and corrective measures to be taken are presented in Table 2.3, Chapter 2. However, some of these symptoms are similar for different types of fouling which make the prediction difficult. Therefore, membrane autopsy is the only reliable method for determining the true identity of membrane fouling and is discussed in more detail in Chapter 5.

4.7 Summary

The pre-treatment systems of the Tajoura SWRO desalination plant were evaluated based on the measurement of SDI and biological growth in the raw and pre-treated seawater. Results show an average SDI value of 3.4 which is acceptable according to the membrane manufacturer recommendations. However, with this SDI value colloidal fouling would occur if $FeCl_3$ is not dosed. Scaling calculations show that S&DSI is negative and $CaCO_3$ scaling should not occur in the membrane systems. Biological growth was higher in the pre-treated seawater than in raw seawater, indicating that biofouling is likely to occur.

A comparative evaluation of two spiral wound SWRO membrane units were carried out for a period of 360 days. The actual permeate concentration and differential pressure values show a noticeable deterioration in the performance of both membrane systems after four months of operation, while the permeate flow and recovery were maintained constant. Water and salt permeability coefficients show a slight decrease in water permeability and a significant increase in salt permeability after 360 days of operation.

ASTM and HSDM standardisation methods and standardisation software are useful tools for the evaluation of RO membrane performance. Mathematical and the software standardisation methods show a similar pattern, in which the normalised permeate flow was less than the designed values in the first five months of operation due to fouling, followed by a gradual increase due to increasing of feed pressure.

The ASTM and ROSA normalisation software show identical results, in which the normalised salt passage gradually increases over operating time. The HSD method and ROdata normalisation software show higher normalised salt passage in the first 6 months

compared to the ASTM and ROSA software. This can be attributed to the normalisation methodology that are used by both methods which slightly differ from the ASTM method and ROSA software.

The normalisation methods exhibit some limitations, possibly due to the effect of temperature on salt passage. It can be concluded that the standardisation methods have limitations in determining the identity of fouling, which can only be achieved by conducting a membrane autopsy as discussed later in Chapter 5.

CHAPTER 5

FOULING CHARACTERISATION OF TWO COMMERCIAL SEAWATER REVERSE OSMOSIS MEMBRANES: A CASE STUDY

5.1 Introduction

The mechanism of membrane fouling can be understood and its identity determined by the destructive study "autopsy" of the membrane (Vrouwenvelder *et. al.,* 2001; Tran *et al.,* 2007; Huiting *et. al.,* 2001). A "membrane autopsy" combines different fouling examination techniques capable of revealing information about the nature of deposits on the membrane surface, including Fourier transform infrared spectroscopy (FITR), scanning electron microscopy (SEM), atomic force microscope (AFM) and inductively coupled plasma (ICP) spectroscopy (Beverly *et al.*, 2000; Darton *et al.,* 2004; Lopez *et al.,* 2005; Schneider *et al.*, 2005; Shon *et al.*, 2009).

In this chapter two sets of 8 inch commercial SWRO membrane elements were subjected to autopsy, in order to identify the causes of membrane failure. Standard procedures for membrane autopsy for RO membranes were used (Gossen *et. al.,* 2004; Dudely and Darton, 1996; Darton *et. al.,* 2004; Lopez *et. al.,* 2005).

5.2 Materials and Methods

5.2.1 Membrane Autopsy

To investigate the causes of deterioration of plant performance and to determine the true identity of fouling, two sets of commercial SWRO membrane elements were collected from the Tajoura SWRO desalination plant. The two membrane elements are referred as membrane number one based on their position in the pressure vessel (Figure 5.1).

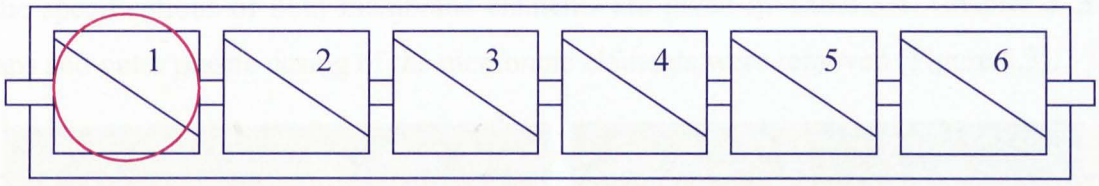

Figure 5.1 Schematic diagram of membrane arrangement in the pressure vessel.

The membrane elements were removed from their pressure vessels and were positioned vertically to drain the excess water (Figure 5.2). They were visually inspected for telescoping and fibre case damage, then both ends were covered by sterilised plastic bags to prevent excessive drying and contamination. In order to preserve the original biomass composition present during operational conditions, the membrane elements were stored at 4 ^{o}C until analysis.

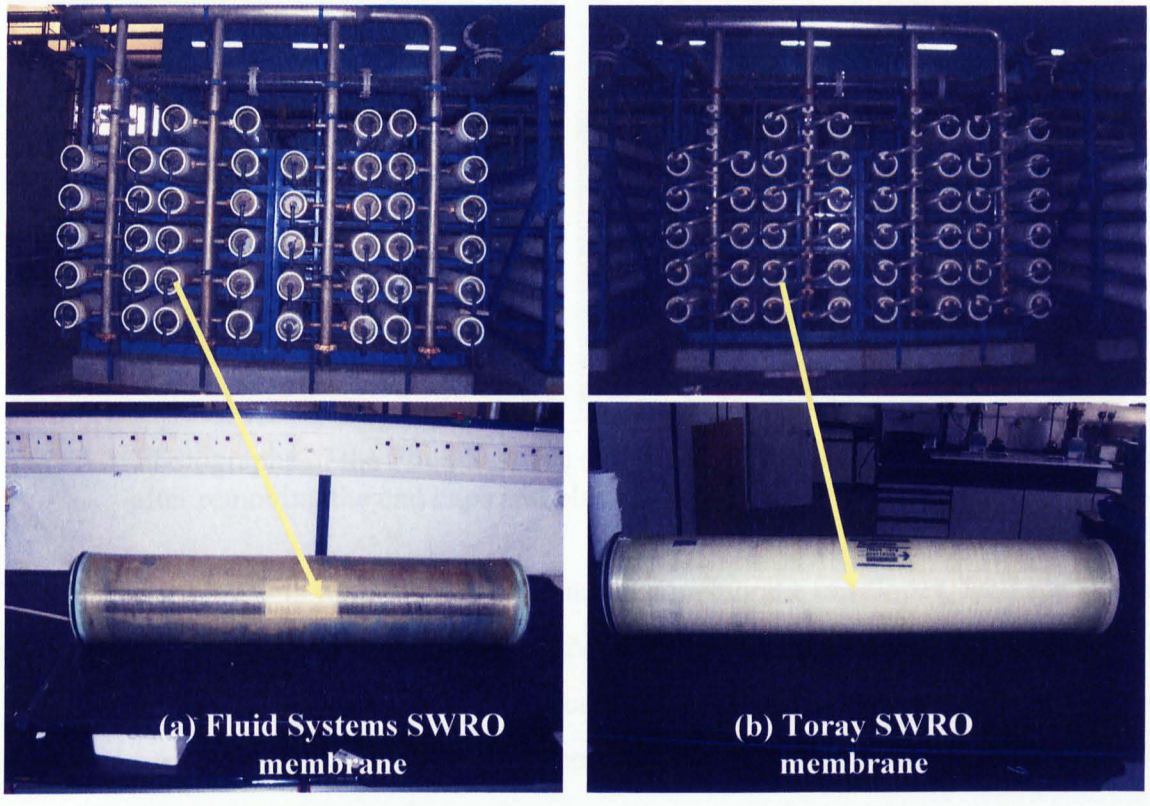

Figure 5.2: Photographs of the membrane trains and 8 x 40 Inch (20 x 100cm) Fluid Systems and Toray SWRO membrane elements

The specifications of both membrane elements are given in Table 3.4, Chapter 3. The end caps and outer plastic casing of the membrane elements were removed (Figure 5.3).

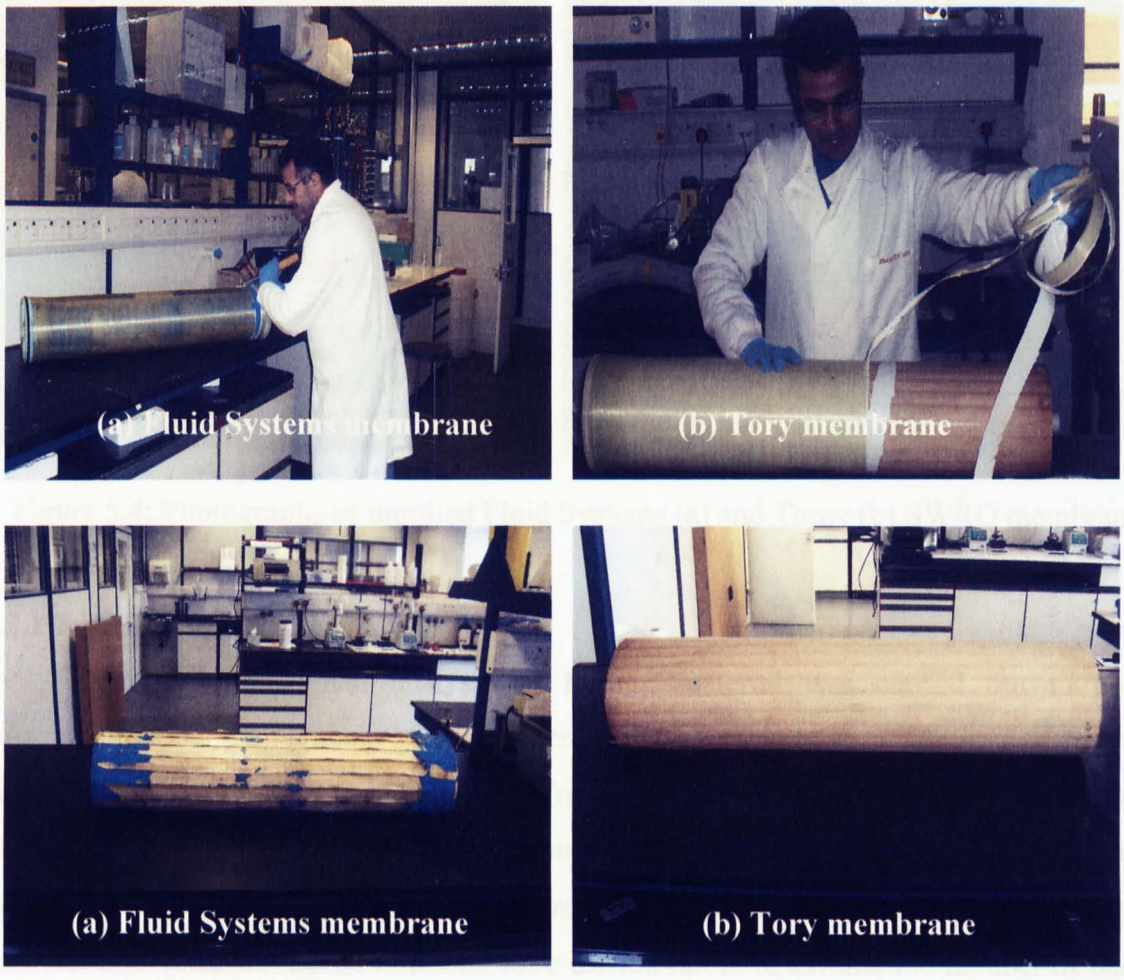

Figure 5.3; Photographs of the Fluid Systems (a) and Toray (b) SWRO membrane before and after removing the end cups and plastic casing.

The membrane elements were then unrolled and the membrane envelopes, feed and permeate spacers were visually inspected following the standard autopsy procedures (Darton *et. al.*, 2004; Lopez *et. al.*, 2005). The membrane surfaces and feed spacers were visually inspected for colour, odour, presence of particles, mucous material and for special phenomena such as presence of bladders and creep (Figure 5.4).

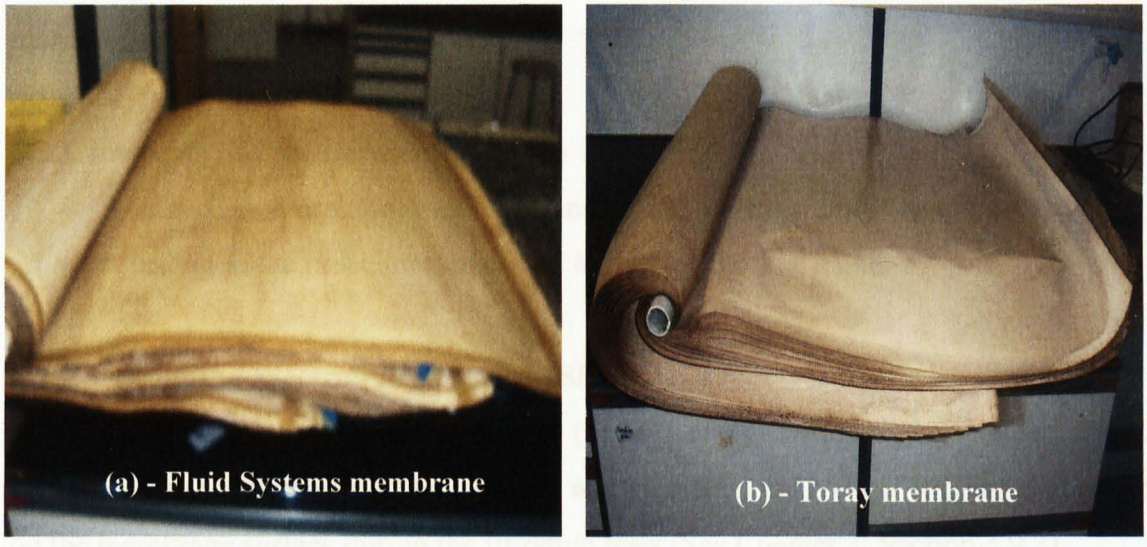

Figure 5.4: Photographs of unrolled Fluid Systems (a) and Toray (b) SWRO membranes.

5.2.1.1 Culturable Plate Count

The microbiological analysis of fouling material was carried out to provide information about the numbers of living micro-organisms that have capability to grow on the medium according to the method used by Vrouwenvelder and van der Kooij D., (2001) (See Section 3.1.1.3, Chapter 3). Fouled membrane samples of known area (5x5cm) were cut off from both membrane sheets and transferred into test tubes containing 10ml of sterile seawater and vortexed. Serial dilutions were carried out to determine the number of bacteria (expressed in colony forming units per area ($cfu.cm^{-2}$) on R2A agar medium.

5.2.1.2 Loss on Ignition Test

Loss on ignition test was used as a rough estimate for determining the relative percentage by weight of organic content to inorganic content in the foulant deposits according to the method described by Heiri *et al.* (2001) (See Section 3.10.2, Chapter 3).

5.2.1.3 Acid Digestion

The acid digestion experiment was carried out in order to dissolve metals that are present in the fouling material according to the ASTM D5198 (See Chapter 3, Section

3.10.1). The concentration of trace metals in fouling materials of both membrane samples as measured using ICP-MS (Section 3.1.2.1).

5.2.1.4 Atomic Force Microscopy (AFM)

The surface morphology of clean and fouled RO membranes were investigated using AFM according to the procedure described in Section 3.9.2, Chapter 3.

5.2.1.5 Scanning Electron Microscopy (SEM)

Scanning electron microscopy (SEM) along with energy dispersive X-ray spectrometer (EDX) was used for imaging and elemental analysis of fouling material formed on the membrane surface during the filtration tests (See Chapter 3, Section 3.9.3).

5.2.1.6 ATR-FTIR

Attenuated total reflection-Fourier transform infrared spectroscopy (ATR-FTIR) (PerklinElmer- USA) was used to determine the functional groups of clean and fouled membranes (See Section 3.9.4, Chapter 3). Clean and fouled membrane coupons were prepared by the procedure given in Section 3.9.1.

5.2.1.7 XRD of Membrane Samples

The crystalline phases of fouling material deposited on the surface of both SWRO membranes were analysed by XRD (See Chapter 3, Section 3.9.5).

5.2.1.8 Chemical Cleaning of Fouled SWRO Membranes

The chemical cleaning tests were carried out according to the procedures described in Section 3.10.3.

5.3 Results and Discussion

5.3.1 External and Internal Inspection of SWRO Membranes

The performance evaluation of both membrane units (Section 4.6.1 and 4.6.2) show declining normalised permeate flow and increasing normalised salt passage and differential pressure due to fouling. Membrane autopsies were carried out to investigate this. The

external visual inspection of both membranes indicated that no physical damage (e. g. telescoping and/or damaging of outer casing). However, large deposits had accumulated on the feed side of the elements. Moreover, the feed and the concentrate sides of both membranes were reddish – brownish in color indicating iron rich deposits (Figure 5.5). Farooque *et al.*, 2009 carried an autopsy on NF membrane elements collected from the Ummlujj SWRO plant and found similar observations. This could be originated from the excess dose of coagulant ($FeCl_3$) not being removed by dual media filters and/or due to the corrosion of the stainless steel pipes in the high pressure facilities. Darton *et al.*, (2004); Butt *et al.*, (1997) and Farooque *et al.*, (1997) conducted similar membrane autopsies on different RO membranes and reported similar results.

Figure 5.5: Photos of feed and concentrate sides of Fluid Systems (a) and Toray (b) membrane elements.

Visual inspection of unrolled Fluid Systems membrane elements showed a creep alongside the glue lines (Figure 5.6). The presence of creep along the glue lines of this membrane is most likely due to the high differential pressures across the membrane unit, water hammering and/or a manufacturing fault.

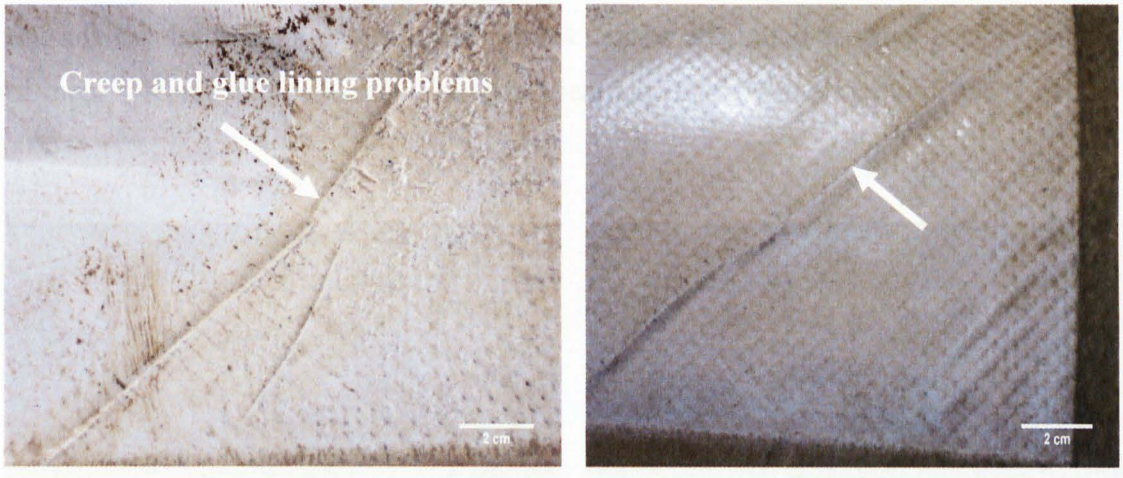

Figure 5.6: Photographs of creep near the glue lines of Fluid Systems membrane element. (Scale bar 2cm).

Creep was not observed in the Toray membrane, however there was a small piece of membrane (2×3 cm) stuck on the surface of one the membrane envelopes to cover a hole or scratch (Figure 5.7).

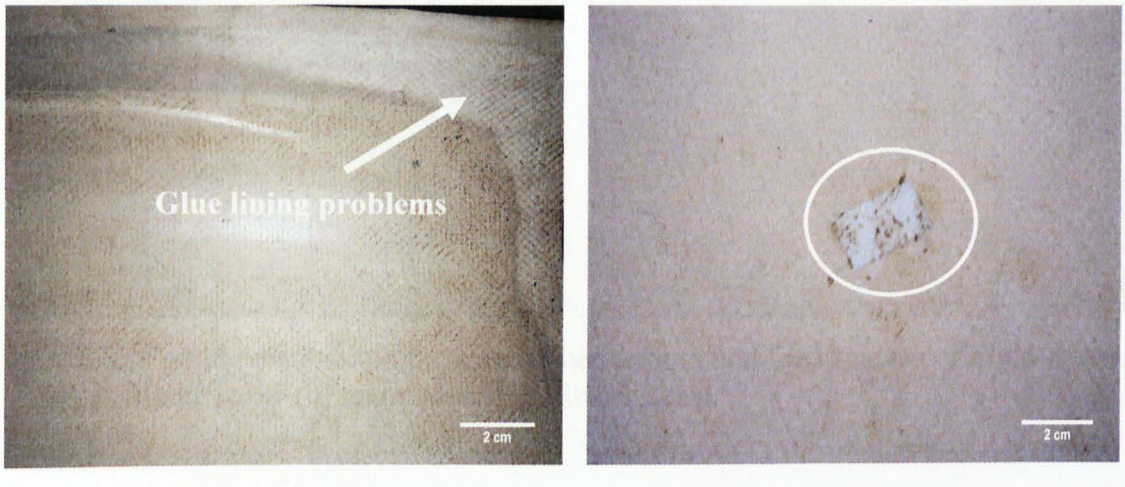

Figure 5.7: Photo shows manufacturer problems in a spiral wound Toray membranes. (Scale bar 2cm).

Both membranes had similar glue line problems, where glue was spread inside the membrane envelopes and reduced the membrane surface area. The surfaces and feed spacers of both membranes have experienced serious fouling and were covered in reddish brown deposits (Figure 5.8). Similar findings were reported by Butt *et al.*, (1997) and Al-Moudi and Farooque (2005) and Farooque *et al.*, (2009). The accumulation of large amount of fouling materials on the surface of both membranes can be attributed to poor performance of pre-treatment systems and/or lack of chemical cleaning (Dudely and Darton 1996; Karime *et al.*, 2008).

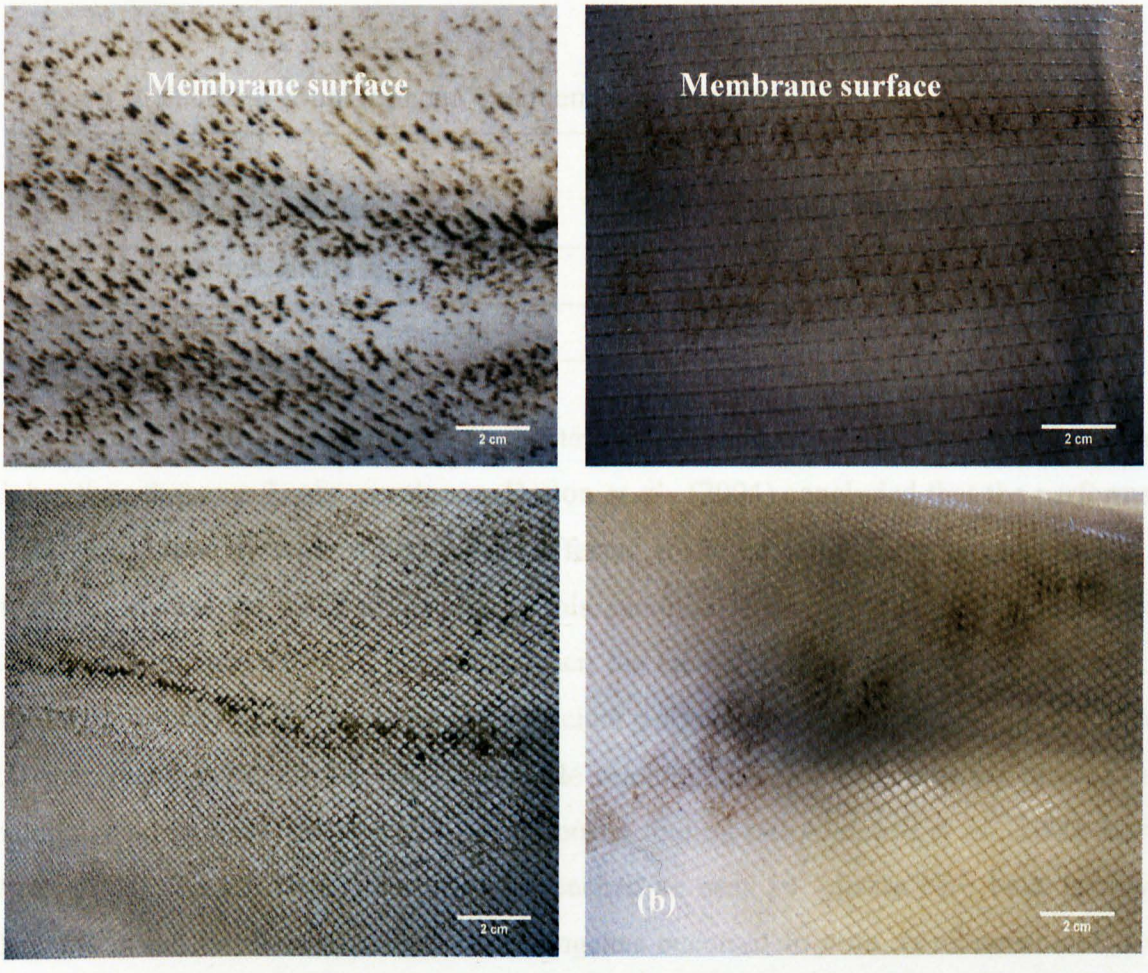

Figure 5.8: Fouling material on the membrane surfaces and feed spacers of Fluid Systems (a) and Toray (b) membranes. (Scale bar 2cm).

Deposits on the surfaces of both membranes were soft and amorphous (non-crystalline) and could be easily removed from the membrane surface by swabbing and scraping. Similar studies (Howe *et. al,* 2002; Butt *et al.*, 1997) also found an amorphous brown fouling layer.

5.3.2 Microbiological Enumeration Results

Microbiological analyses were carried out on known areas (5x5cm) of the membrane surfaces using the plate count method on R2A agar medium. The number of microorganisms that were present is expressed as colony forming units per area ($cfu.cm^{-2}$) (Table 5.1).

Table 5.1: Bacterial count ($cfu.cm^{-2}$) of membrane samples

Membrane samples	**Fouling material ($cfu.cm^{-2}$)**
Fluid Systems membrane	11×10^4
Toray membrane	6.2×10^4

From Table 5.1 it can be seen that the bacterial counts on the Fulid Systems membrane is higher than those on Toray membrane. Darton *et al.,* (2004) concluded that the performance of RO membrane systems would not be affected if the bacterial count remains below 10^4 $cfu.cm^{-2}$, because the biofilm is stable in this condition and many plants work satisfactory with such a biofilm thikness. However, when the bacterial count exceeds 10^5 $cfu.cm^{-2}$, the biofilm is considered to be producing sufficient polysaccharides to become problematic in RO membrane systems. The polysaccharide material can act as a trap for other fouling materials and increase the potential of composite fouling (Al-Ahmmed *et al.*, 2000; Karime *et al.*, 2008). As the bacterial count has reached or near 10^5 $cfu.cm^{-2}$ for both membrane elements it can be concluded that biofouling has occurred in both membranes and it was potentially one of the operational problems in the plant.

5.3.3 Loss on Ignition Results

The scrapped deposits from the surfaces of both membranes were sludge like material. Loss on ignition results showed that the fouling material collected from both RO membranes contains organic matter of about 61.5 ± 2.1% and 58.2 ± 2.7%, respectively (Table 5.2).

Table 5.2: The percentage of inorganic to organic content of fouled Fluid Systems and Toray membrane elements.

Membrane type	Inorganic content (%)	Organic content (%)
Fluid Systems	38.5 ± 2.12	61.5 ± 2.12
Toray	41.9 ± 2.69	58.1 ± 2.69

From Table 5.2 it can be seen that the organic content is higher than the inorganic content. Similar results were reported by Dudely and Darton (1996) and Yang *et al.*, (2008). To identify the inorganic compounds and organic matter present in the fouling material of both RO membranes, acid digestion, ICP-MS EDX and ATR-FTIR investigations were used in this study. Results of the findings are presented in the following sections.

5.3.4 Acid Digestion Results

According to visual inspection, iron fouling possibly occurred in both RO membrane systems. Therefore, the concentration of trace metals present in the fouling materials of both membranes was determined. After acid digestion (Section 3.10.1) the samples were filtered though 0.2 micron filters and analysed using ICP-MS. The actual concentration of Aluminum (Al), Iron (Fe), Copper (Cu) and Zinc (Zn) were measured (Table 5.3).

Table 5.3: The concentration of metals in fouling material deposited on the surface of Fluid Systems and Toray membrane elements.

Element	Fluid System membrane	Toray membrane
Aluminum (mg l^{-1})	6.67 ± 0.25	0.94 ± 0.25
Iron (mg l^{-1})	9.37 ± 0.25	3.47 ± 0.25
Copper (mg l^{-1})	2.45 ± 0.25	0.26 ± 0.25
Zinc(mg l^{-1})	0.67 ± 0.25	0.047 ± 0.25

Results show that high concentrations of iron were present in the fouling materials indicating the possibility of iron fouling due to the residual ferric chloride (particulate fouling by small flocks that not removed by dual filters and fine micron filters) present in RO feed water and/or as a result of corrosion of metal pipes and pumps. Precipitation of coagulant residuals on the membrane surface can negatively affect the RO membrane performance process. Iron hydroxide fouling can be formed at iron concentrations of < 0.3 mg l^{-1} (Gabelich *et al.*, 2002; Zhu X., and Elimelech, 1997; Darton *et al.*, 2004; Glater *et al.*, 1994).

Gabelich *et al.* (2002) tested three different RO membranes at three different RO plants in southern California using aluminum sulfate and ferric chloride as coagulants. They have reported that the collected foulants on the membrane surfaces contain aluminum hydroxide, aluminum silicate and iron hydroxide due to coagulant residuals present in RO feed water. Both foulants can cause decline in water flux and an increase in salt passage. They attributed decreasing water flux and salt rejection to the formation of a thick fouling layer on the membrane surface, which eventually caused a reduction in the Donnan potential. In this experiment it can be concluded that the precipitation of iron hydroxide and aluminum silicate on the surfaces of RO membranes are one of the problems that cause deterioration of the permeate quality and quantity in desalination plants.

5.3.5 Atomic Force Microscope Results

The surface morphology and membrane roughness of the clean and fouled membrane samples collected from the Tajoura plant was investigated using AFM. The obtained results showed that the clean RO membrane samples of both membrane types (Fluid Systems and

Toray) have shown relatively rougher surfaces, with peak-and-valley structures, compared to those for fouled membranes (Figure 5.9). Several studies (Kim *et al.*, 1999; Knoell *et al.*, 1999; Kwak *et al.*, 1997) have shown that there is a linear relationship between the membrane surface roughness and permeate flux in which permeability increased with increasing surface roughness. Hirose *et al.*, (1996) and Veijenhoek *et al.*, (2001) attributed this linear relationship to surface unevenness of the RO membrane skin layer, which resulted in enlargement of the effective membrane area. However, this structure could trap fouling materials, which may enhance fouling.

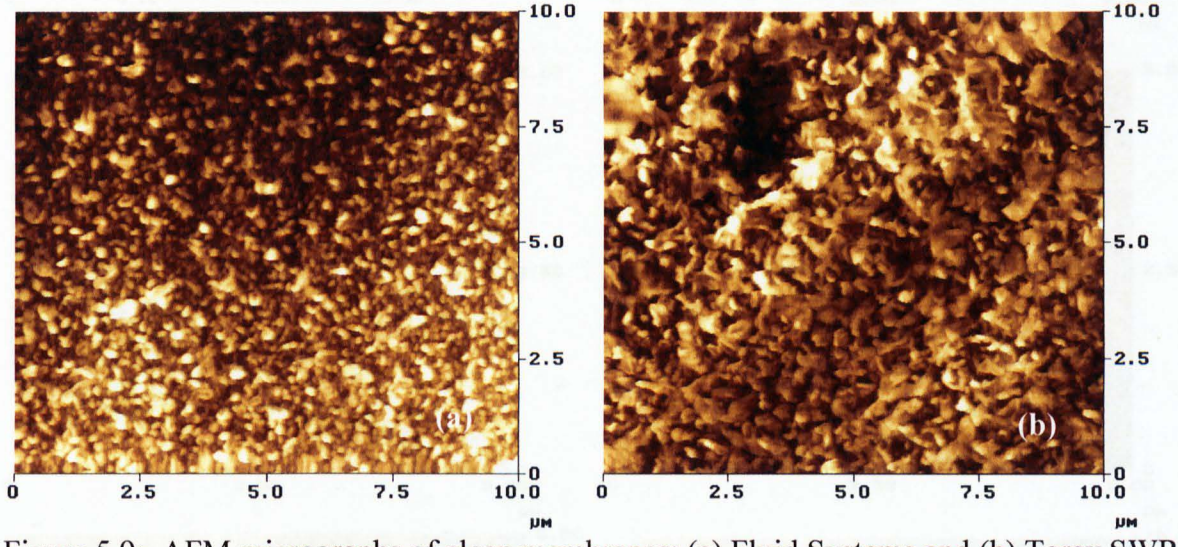

Figure 5.9: AFM micrographs of clean membranes: (a) Fluid Systems and (b) Toray SWRO membranes.

The AFM images of the fouled membranes are markedly different from their identical clean membranes (Figure 5.10). It was found that both of the fouled membranes contain similar fouling materials. Despite the amorphous nature of deposits, crystalline substances were found on the surfaces of both membranes when magnification was increased.

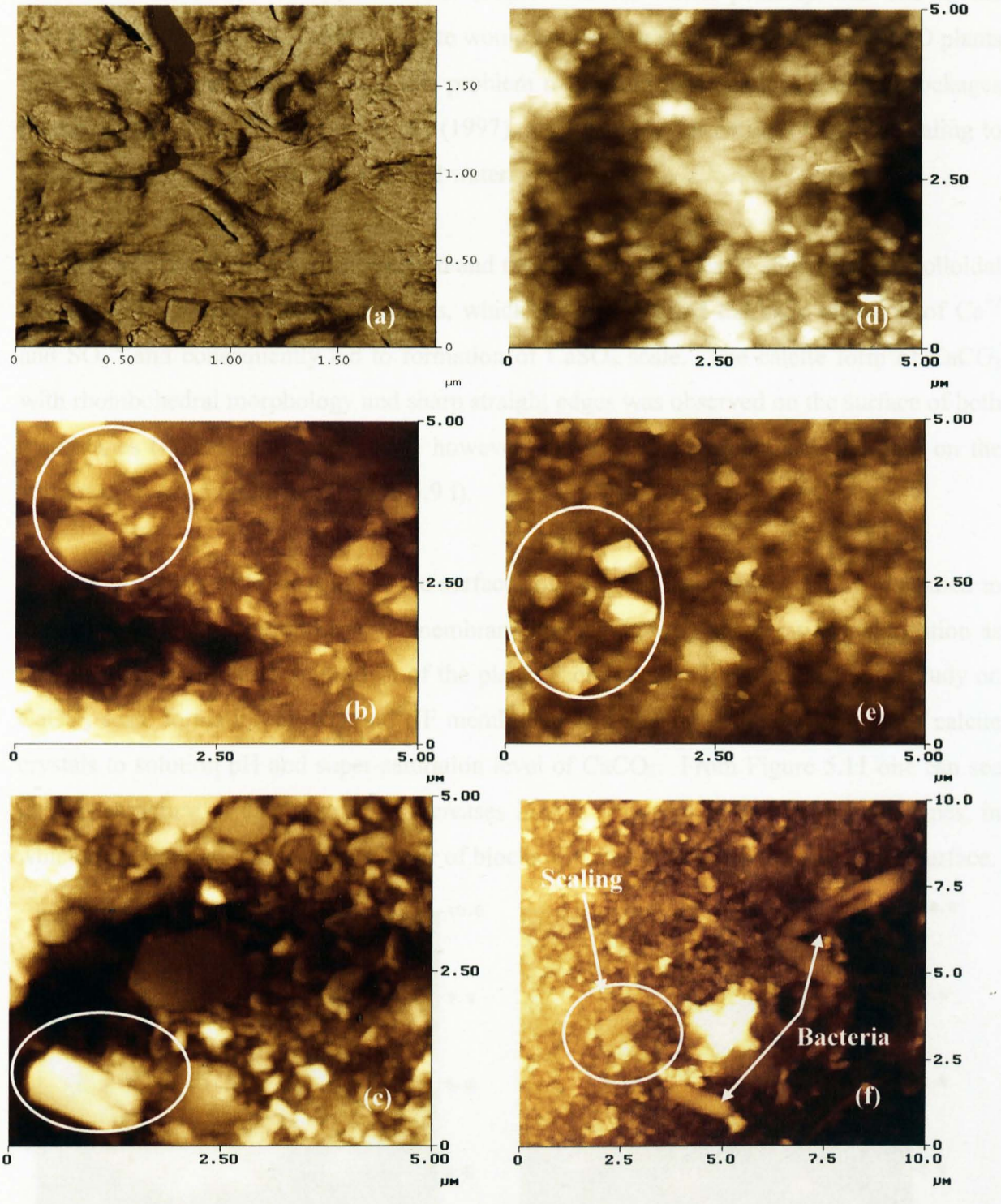

Figure 5.10: AFM images of fouled Fluid Systems (a, b and c) and Toray (d, e and f) SWRO membranes.

From Figure 5.10, (images a and d), it can be seen that both membrane surfaces are completely covered by fouling materials. Long needles of crystals were observed on the

surface of the fouled Toray membrane (Figure 6.9 d), which possibly was due to the precipitation of $CaSO_4$. Calcium sulphate would not cause a scaling problem at SWRO plants operated at low recovery however, this problem may occur as a result of biofilm blockages (Baker and Dudley, 1998). Butt *et al.*, (1997), attributed the formation of $CaSO_4$ scaling to the presence of Ca and SO_4^{2-} in RO feed water.

In the present case, the visual inspection and the AFM results clearly show that the colloidal fouling was severe on both membranes, which possibly limited the back diffusion of Ca^{+2} and SO_4^{-2} and consequently led to formation of $CaSO_4$ scale. The calcite form of $CaCO_3$ with rhombohedral morphology and sharp straight edges was observed on the surface of both membranes (Figures 8 b, c, d and f) however, rod-shaped microbes were detected on the surface of Toray membranes (Figure 5.9 f).

The presence of $CaCO_3$ scaling on the surfaces of both RO membranes can be attributed to the high salt concentration near the membrane surface due to concentration polarisation as well as due to long term shut down of the plant. Tzotzi *et al.*, (2007) carried out a study on $CaCO_3$ scale formation on RO and NF membranes and attributed the domination of calcite crystals to solution pH and super-saturation level of $CaCO_3$. From Figure 5.11 one can see that the structure of calcite crystals increases in size with regular and deformed shapes, in which they agglomerate forming a layer of blocks and plates blocking the membrane surface.

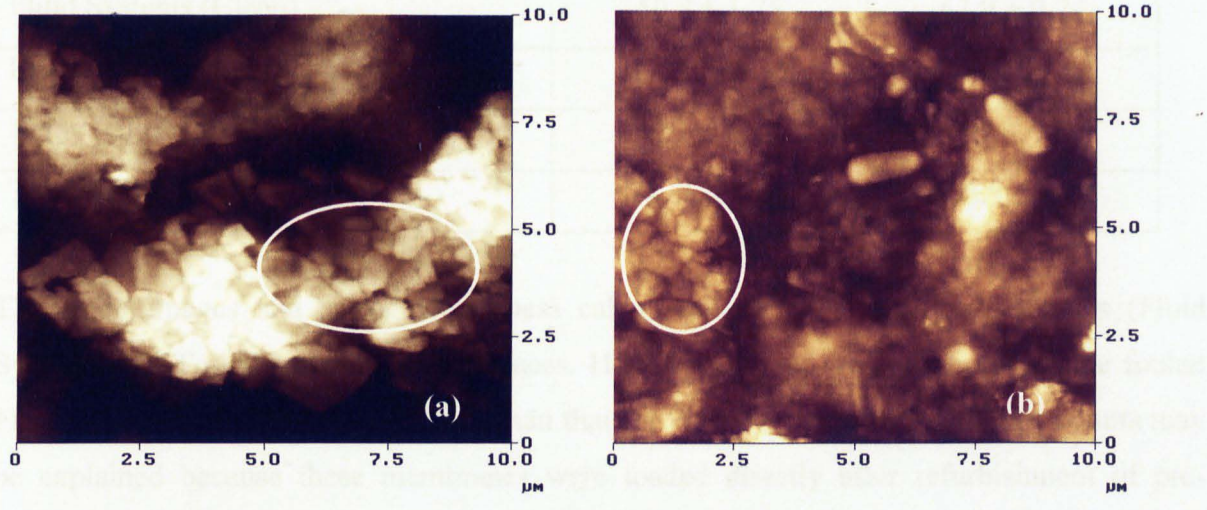

Figure. 5.11. AFM images of blocking layer of calcite crystals on the surface of Fluid Systems (a) and Toray (b) membranes.

The Mg^{2+} ion is more hydrated compared to Ca^{2+} ion and is strongly adsorbed onto surface of growing calcite crystals depending on the magnesium/calcium ratio in solution, calcite precipitation (low Mg^{2+}) and aragonite precipitation (high Mg^{2+}) may occur (Loste *et al.*, 2003). Chen *et al.*, (2005), investigated the effect of Mg^{2+} on $CaCO_3$ formation and found that, with increasing Mg^{2+} concentration the formation of calcite crystals with distorted edges is increased and the cubical and/or rhombohedral structure of crystals has changed. He observed that at 0% concentration of Mg^{2+} in solution all calcite crystals are perfect in structure. With increasing Mg^{2+}, however the structure distorted due to Mg^{2+} ions being adsorbed on the surface of the calcite crystal and forming crystals with rough surfaces. Similar results are observed on the surface of SWRO membranes in this work which can be attributed to the high concentration of Mg^{2+} in the RO feed water (*e.g.* 1427 $mg.l^{-1}$) which acts as an inhibitor of calcite scaling.

The AFM allows measurement of the arithmetic (R_a) and the geometric mean (R_{ms}) of surface roughness (Bachmann *et al.*, 2006). Table 5.4 presents the R_a and R_{ms} values for clean and fouled membranes.

Table 5.4 – Surface roughness of clean and fouled Fluid Systems and Toray membranes.

Membrane type	**R_a (nm)**	**R_{ms} (nm)**
Fluid Systems (Clean)	50.8 ± 1.75	63.9 ± 0.74
Fluid Systems (Fouled)	112.3 ± 1.32	144.1 ± 2.04
Toray (Clean)	58.6 ± 6.54	77.3 ± 9.82
Toray (Fouled)	78.68 ± 4.03	103.9 ± 1.21

The AFM images and surface roughness calculation show that both membranes (Fluid Systems and Toray) have rougher surfaces. However, the surface roughness of the fouled Fluid Systems membranes was higher than that for the Toray membranes. These results may be explained because these membranes were loaded directly after refurbishment of pre-treatment systems at the plant. The AFM images and the surface roughness calculations

show that the fouling potential in the plant was still high even after the refurbishment of pre-treatment systems.

5.3.6 SEM and EDX Results

Figure 5.12 and Figure 5.13 illustrate SEM micrographs and the EDX analysis of the fouled membranes. The SEM results show that both of the membranes are completely covered with a thick fouling layer in conformity with the visual inspection and the AFM results. The EDX spectra of both fouled membranes were also in conformity with the obtained chemical analysis. The deposits on the surfaces of both membranes were similar in composition consisting mainly of aluminium silicates (clay), iron (residual coagulant) and calcium in addition to carbon and oxygen.

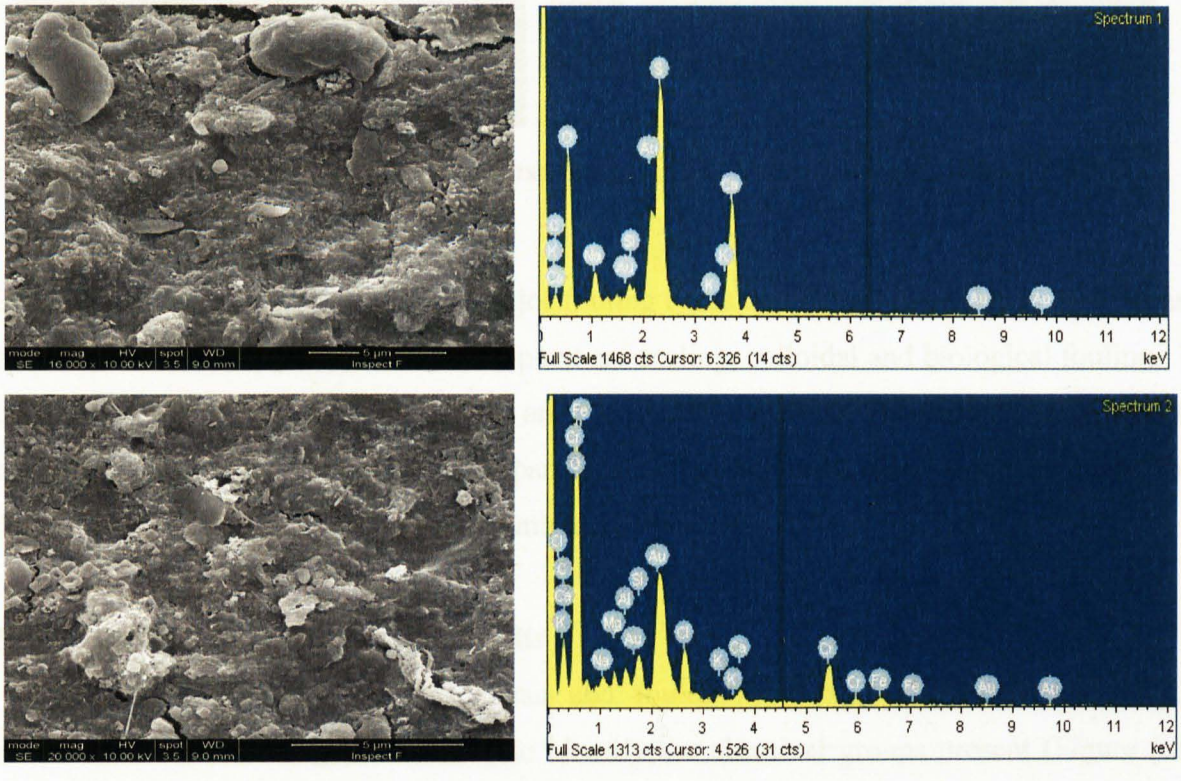

Figure 5.12: SEM micrographs and corresponding EDX spectra of fouled Fluid Systems SWRO membrane.

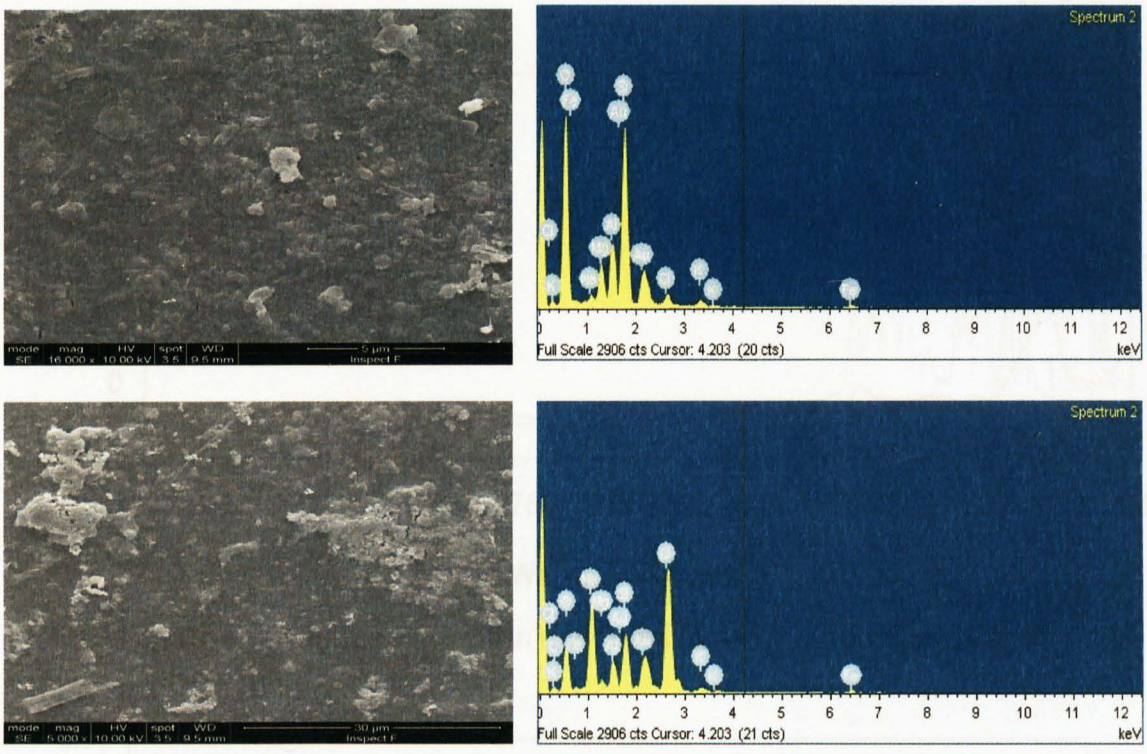

Figure 5.13: SEM micrographs and corresponding EDX spectra of fouled Toray SWRO membrane.

SEM and EDX results show that the major fouling types that deteriorated the RO membrane performance at the Tajoura desalination plant are scaling, colloidal and biological fouling. In their studies, Dudely and Darton (1996) and Schneider *et al.*, (2005) reported similar results, in which biofouling, colloidal and particulate fouling were the major foulants that deteriorated the performances of RO membrane systems.

5.3.7 ATR-FTIR Spectroscopy Results

The FTIR spectra of both clean and fouled Fluid Systems and Toray SWRO membranes were investigated in order to identify the chemical groups present (Figure 5.14 and 5.15).

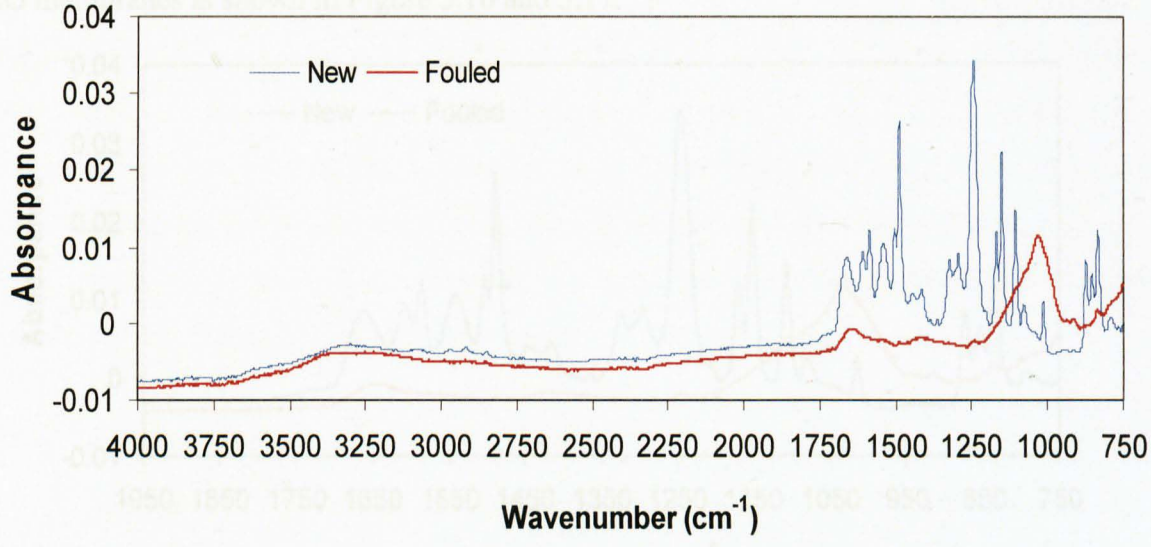

Figure 5.14: ATR-FTIR spectrum of clean (new) and fouled Fluid Systems SWRO membrane.

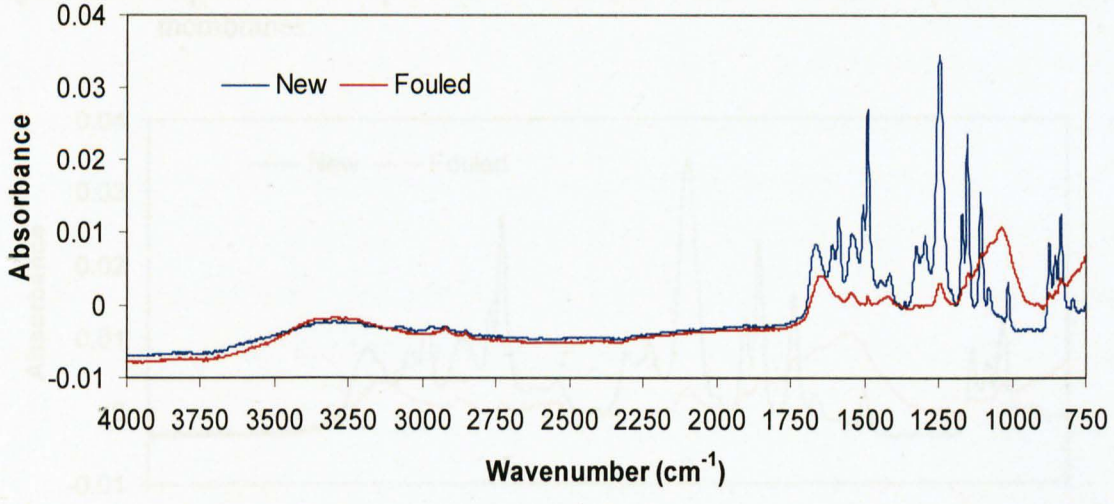

Figure 5.15: ATR-FTIR spectrum of clean (new) and fouled Toray SWRO membrane.

Both clean SWRO membranes have similar spectra where the majority of peaks are located in the amide and carbohydrates regions (1750 and 750 cm^{-1}). These peaks are not present in the spectra of fouled membranes. It indicates that the fouled layer is possibly more than 1 μm thick, which is the maximum depth that the infrared light can penetrate.

An expanded region of the FTIR spectra between 1950 and 750 cm^{-1} for the clean and fouled RO membranes is shown in Figure 5.16 and 5.17.

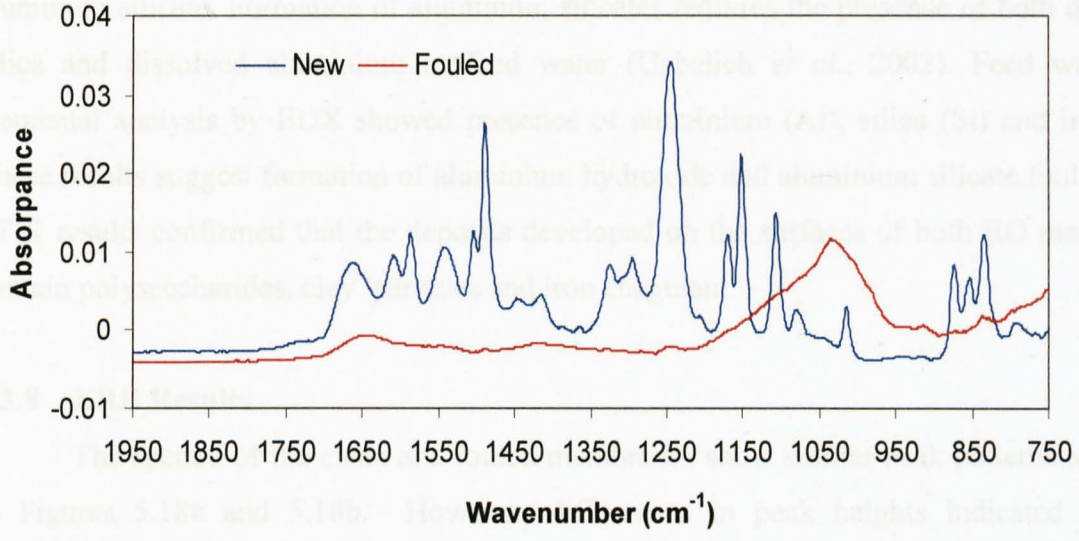

Figure 5.16: Expanded FTIR spectrum of clean (new) and fouled Fluid Systems SWRO membranes.

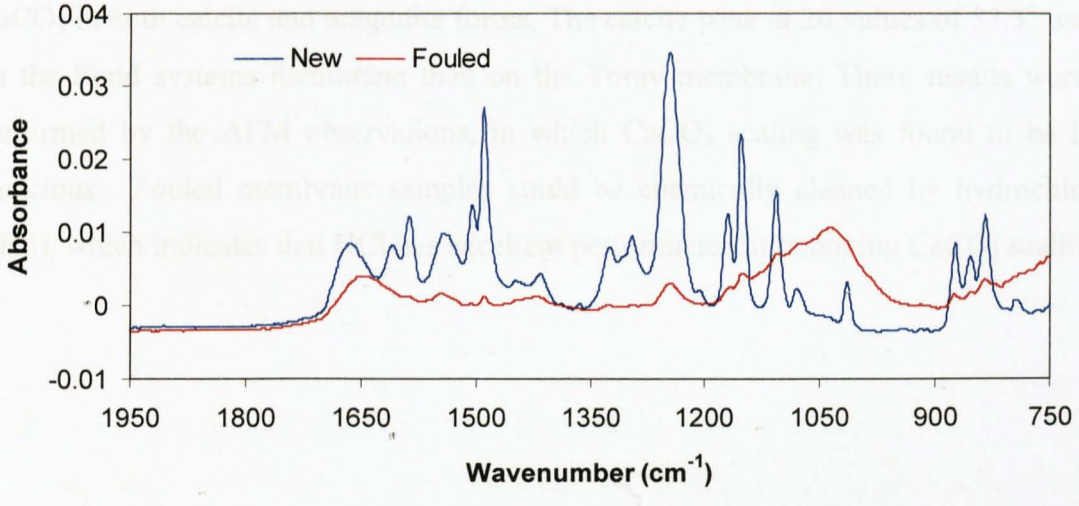

Figure 5.17: Expanded FTIR spectrum of clean (new) and fouled Toray SWRO membranes.

The peaks appear in the spectra of the fouled membranes indicate that the fouling materials consist of polysaccharides, hematite and/or aluminum silicate (1038 and 930 cm^{-1}) and proteins (1570 – 1640 m^{-1}) (Yang *et el.,* 2008; Schmitt *et al.,* 1998). In a similar study Cho *et al.*, (1998) attributed the FTIR absorption in this region to the presence of polysaccharides,

while Howe *et al.* (2002) referred it to the absorption to silicate impurities. Xu *et al,*, (2006), attributes absorption in the carbohydrate region was due to the polysaccharides and aluminum silicate. Formation of aluminium silicates requires the presence of both dissolved silica and dissolved aluminium in feed water (Gabelich *et al.*, 2002). Feed water and elemental analysis by EDX showed presence of aluminium (Al), silica (Si) and iron (Fe). These results suggest formation of aluminium hydroxide and aluminium silicate fouling. The FTIR results confirmed that the deposits developed on the surfaces of both RO membranes contain polysaccharides, clay particles and iron coagulant.

5.3.8 XRD Results

The spectra of the clean and fouled membranes show similar peak patterns as shown in Figures 5.18a and 5.18b. However, differences in peak heights indicated that the concentration of $CaCO_3$ scale was higher in Fluid Systems membrane than that for Toray membranes. The X-Ray patterns of the fouled membranes were found to contain several crystalline peaks at 2θ values of 33.3°, 46.3° and 66.5°. These crystalline peaks represent $CaCO_3$ in both calcite and aragonite forms. The calcite peak at 2θ values of 33.3° was higher on the Fluid systems membrane than on the Toray membrane. These results were further confirmed by the AFM observations, in which $CaCO_3$ scaling was found to be hard and tenacious. Fouled membrane samples could be chemically cleaned by hydrochloric acid (HCl), which indicates that HCl has excellent performance in removing $CaCO_3$ scaling.

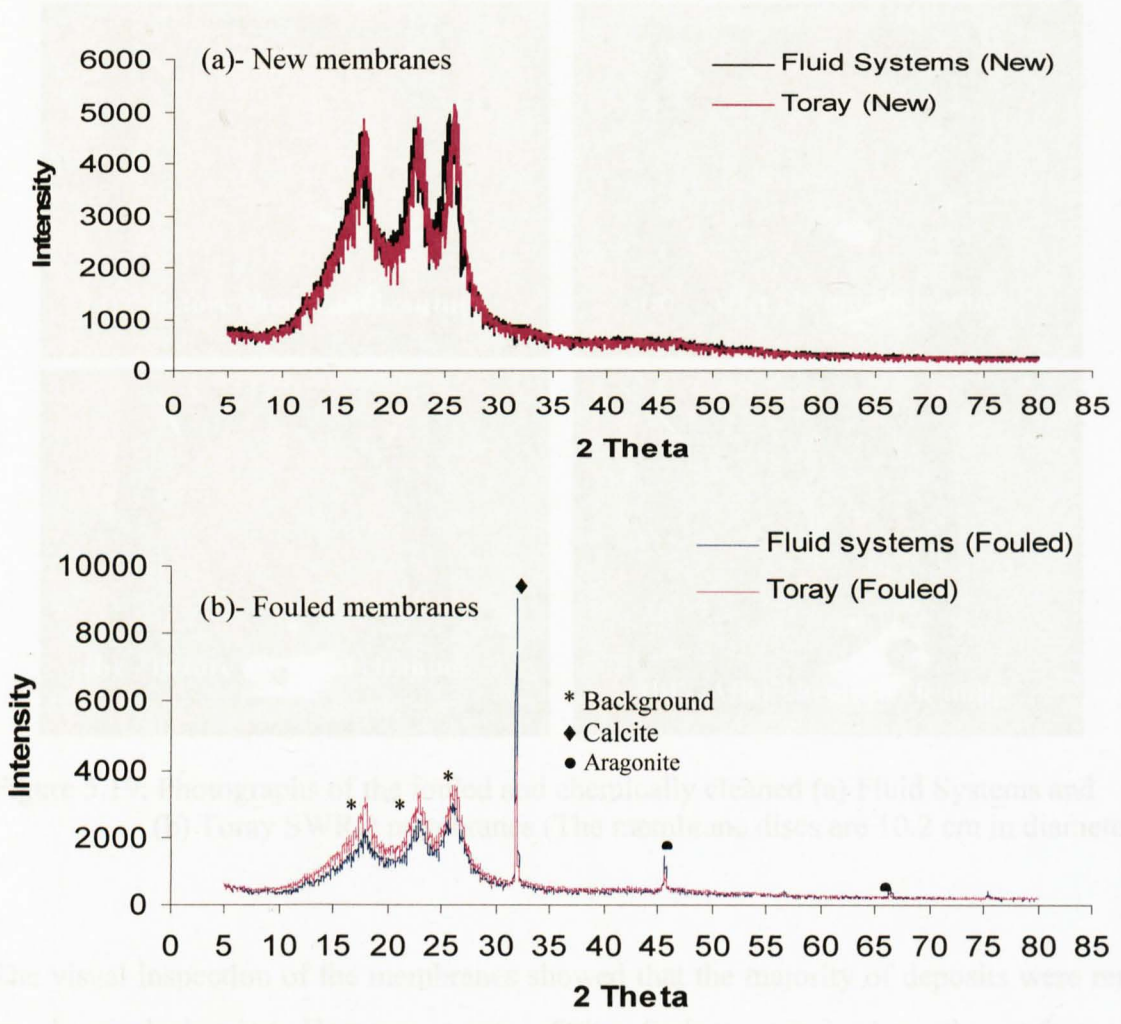

Figure. 5.18. XRD spectra of Fluid Systems and Toray membranes (a) clean membranes and (b) fouled membranes.

5.3.9 Chemical Cleaning of the Fouled Membranes

Caustic (NaOH) cleaning was applied in order to remove organic fouling and biofouling, while acid (HCl) was used to remove scaling and metal oxide fouling from the membranes. Figure 5.19 shows the photographs of the fouled and chemically cleaned SWRO membranes.

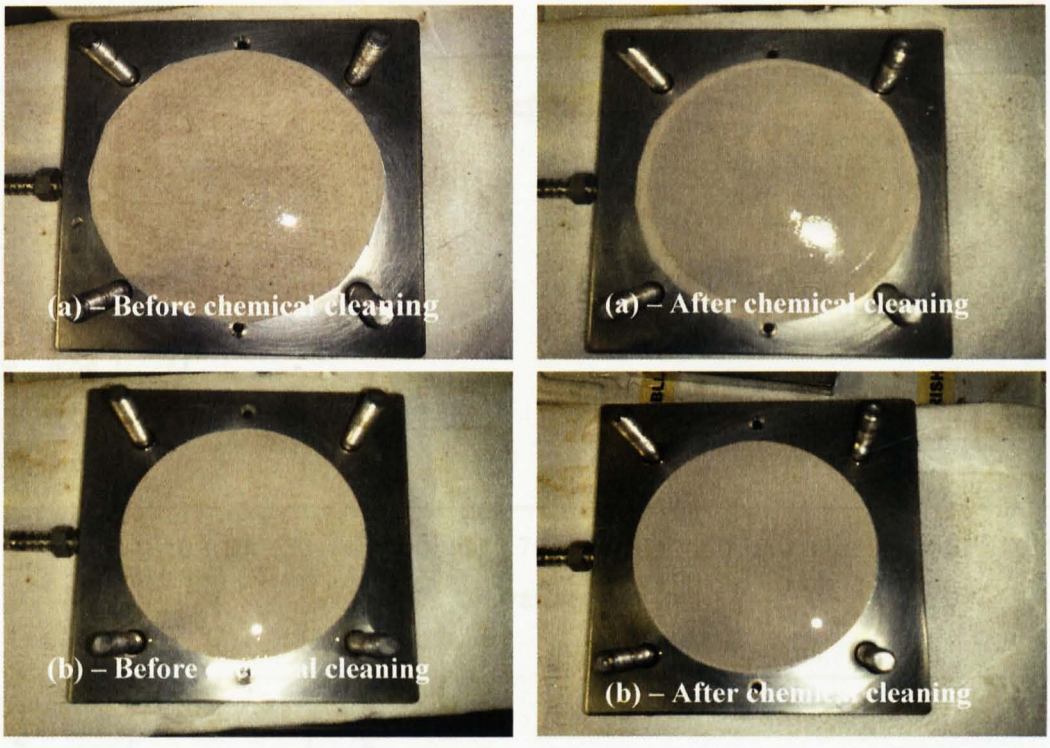

Figure 5.19: Photographs of the fouled and chemically cleaned (a) Fluid Systems and (b) Toray SWRO membranes (The membrane discs are 10.2 cm in diameter).

The visual inspection of the membranes showed that the majority of deposits were removed by chemical cleaning. However, traces of tiny foulants remained on the surface of both membranes.

5.3.10 Permeate Flux

Chemical cleaning was carried out on fouled Fluid Systems and Toray membrane samples. Since the two membranes were fouled by similar foulants, the same chemicals and chemical cleaning protocols were applied as recommended by the membrane manufacturers. After chemical cleaning, membrane samples were rinsed with distilled water and then the permeate flux was determined (Appendix D, Section 4). Feed temperature and pressure were maintained constant (600 psi and 25 ± 2 ^{o}C) during permeate flux measurements. The obtained results (Figure 5.20a and 5.20b) show that there are no improvements to permeate flux in either membrane.

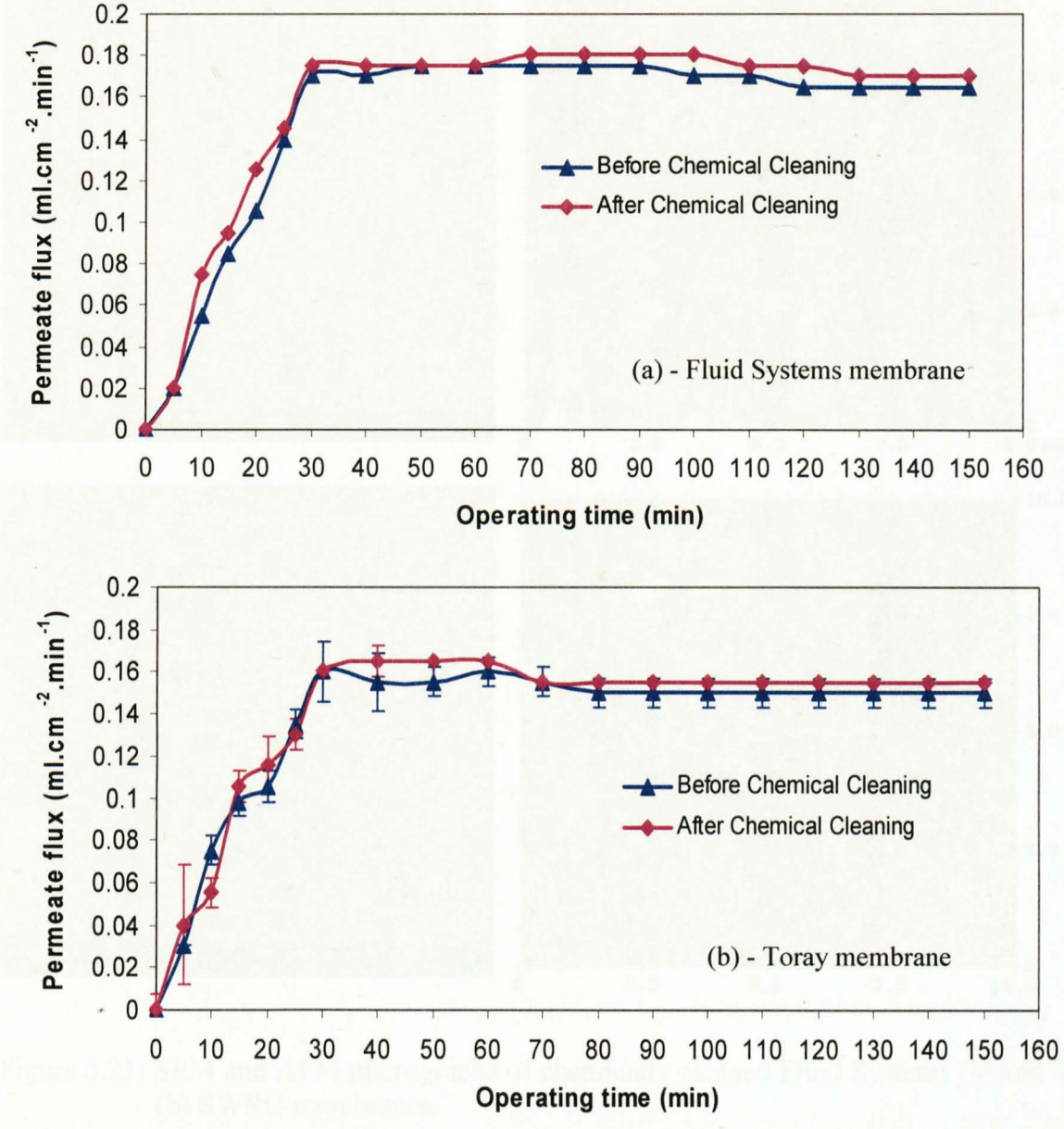

Figure 5.20: Water flux verses operating time after implementing of chemical cleaning: (a) Fluid Systems and (b) Toary SWRO membranes.

In order to evaluate the performance of the chemical cleaning process removing foulants from the membrane surfaces, a combination of the SEM, AFM, ATR-FTIR and XRD techniques were used. The SEM results show less foulants on the surface of both membranes after acidic and caustic chemical cleaning compare to fouled membranes (Figure 5.21).

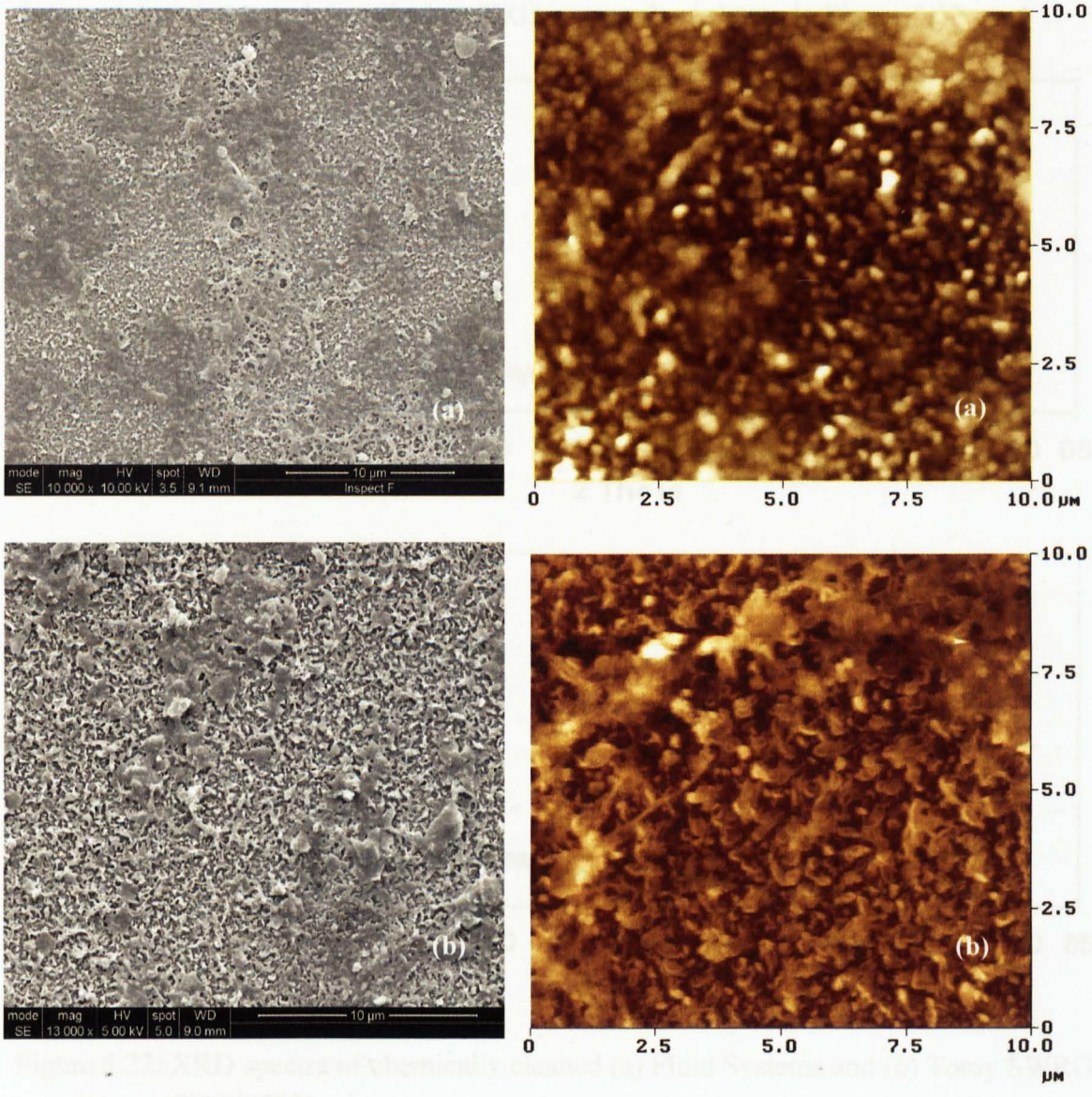

Figure 5.21: SEM and AFM micrographs of chemically cleaned Fluid Systems (a) and Toray (b) SWRO membranes.

No crystal peaks were detected when XRD was used, as shown in Figure 5.22.

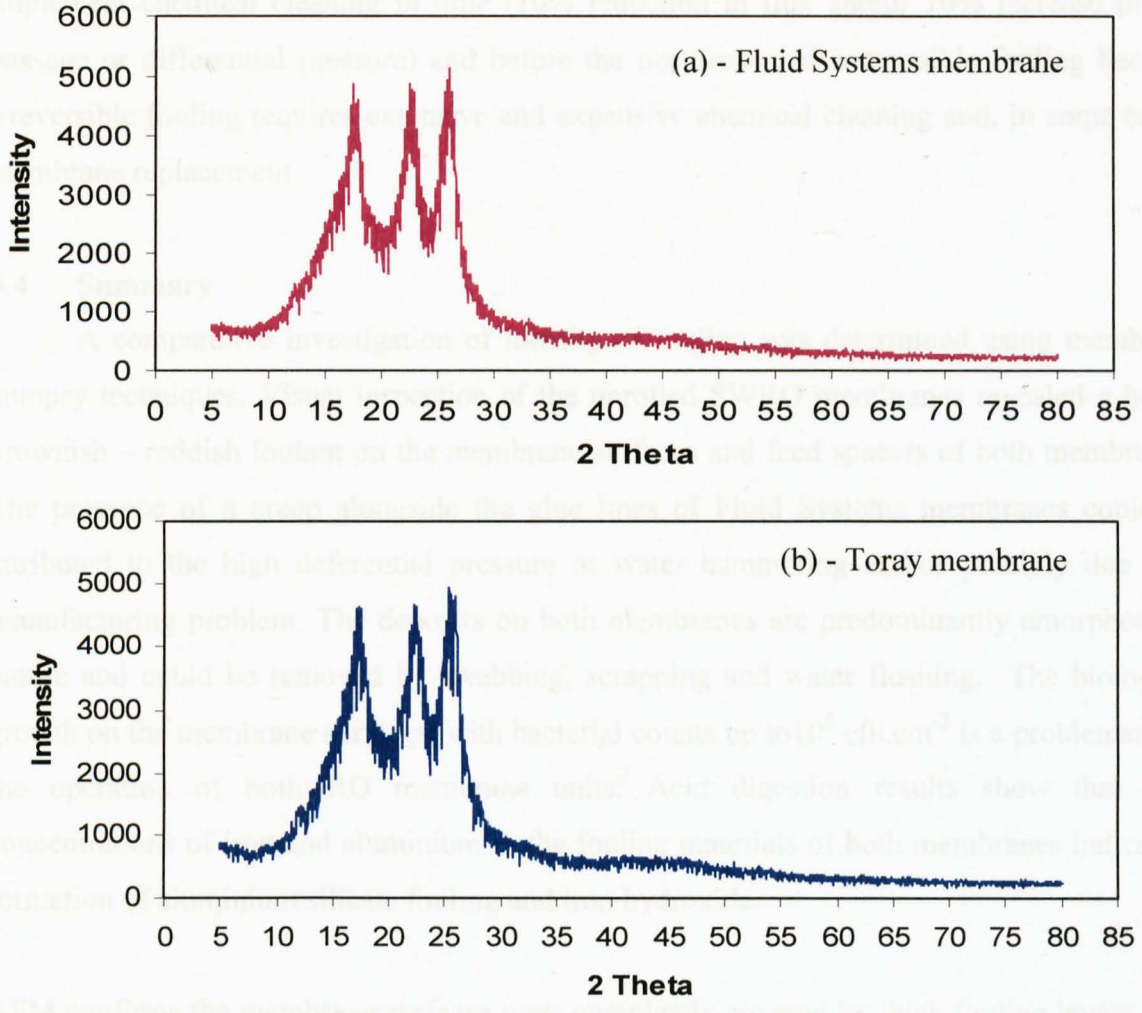

Figure 5.22: XRD spectra of chemically cleaned (a) Fluid Systems and (b) Toray SWRO membranes.

Due to severity of the fouling and the delay in applying chemical cleaning in the plant, the initial water flux could not be restored after applying chemical cleaning using RO test rig. The results obtained using SEM, AFM and XRD show that the use of NaOH, Na-EDTA and HCl as cleaning agents was effective and can be used to remove scaling, metal fouling and biofouling. Possibly an extensive chemical cleaning is required to remove small colloids and to restore membranes performance. Sadhwani and Vezal (2001) carried out membrane cleaning at a large seawater desalination plant (Las Palmas III, Gran Canary), and reported that membrane performance can be improved using acid cleaning (HCl) with detergent (Ultrasil P-75) and caustic cleaning (NaOH) with detergent (Ulstril P-10). However, it

depends on the degree of fouling on the membrane surface. Therefore, it is very important to implement chemical cleaning in time (10% reduction in flux and/or 10% increase in salt passage or differential pressure) and before the occurrence of irreversible fouling because irreversible fouling requires extensive and expensive chemical cleaning and, in some cases, membrane replacement.

5.4 Summary

A comparative investigation of identity of fouling was determined using membrane autopsy techniques. Visual inspection of the unrolled SWRO membranes revealed a heavy brownish – reddish foulant on the membrane surfaces and feed spacers of both membranes. The presence of a creep alongside the glue lines of Fluid Systems membranes could be attributed to the high deferential pressure or water hammering and/or possibly due to a manufacturing problem. The deposits on both membranes are predominantly amorphous in nature and could be removed by swabbing, scrapping and water flushing. The biological growth on the membrane surfaces, with bacterial counts up to10^5 cfu.cm^{-2} is a problematic to the operation of both RO membrane units. Acid digestion results show that high concentrations of iron and aluminium in the fouling materials of both membranes indicating formation of aluminium silicate fouling and iron hydroxide.

AFM confirms the membrane surfaces were completely covered by thick fouling layers. The SEM and EDX results indicate that scaling, colloidal fouling and biofouling severely deteriorate the performance of membrane units in the plant. The ATR-FTIR spectra showed peaks at 1038 and 930 cm^{-1} in the fouled RO membrane corresponding to polysaccharides, hematite and aluminium silicate. Similarly, the XRD results suggest that $CaCO_3$ crystals were formed on the surfaces in the form of calcite and aragonite. The AFM, SEM, EDX, ATR-FTIR and XRD examinations also provide valuable information about fouling that cause the membrane failure. It can also be concluded that NaOH, Na-EDTA and HCl were used effectively to remove scale, colloids and biofouling with limitation to restore the flux back to the baseline conditions when membranes experienced severe fouling.

CHAPTER 6

EFFECT OF COMPOSITE FOULING ON THE PERFORMANCE OF SEAWATER REVERSE OSMOSIS MEMBRANES

6.1 Introduction

Fouling and scaling are major problems that deteriorate the RO membrane performance (Xu *et al.*, 2006). Huiting *et al.* (2001) reported that biofouling is the most common fouling in RO desalination plants followed by scaling, colloids and organic fouling. It is very important to monitor and control fouling in the RO membrane systems because it may cause a decline in permeate flux as well as increases of energy consumption and operational costs (Zularisam *et al.*, 2006; Bonne *et al.*, 2000; Abbas and Al-bastaki, 2001). Membrane fouling in seawater desalination can be caused by deposition of materials present in raw water such as colloids, organics and microorganisms, while scaling is caused by precipitation of sparingly soluble salts such as $CaCO_3$, $CaSO_4$, $BaSO_4$ (Sheikholeslami and Ong, 2003).

Accumulation of these materials on the membrane surface leads to a formation of concentration polarization, where the membrane surface is exposed to a concentration of salt greater than the bulk concentration (Lisdonk *et al.*, 2001; Bhattacharya and Hwang 1997). Increasing salt concentration on the membrane surface decreases the permeate flux through the membrane because of decreasing pressure driving force due to the osmotic pressure increases (Wilf and Klinko, 1994; Goosen *et al.*, 2002). Therefore, the economical operation of any SWRO plant is strongly dependent upon the life of the membranes and fouling control.

Numerous studies in literature (Lisdonk *et al.*, 2000; Hong and Elimelech, 1997; Darto *et al.*, 2004; Lopez *et al.*, 2005) deal with various types of fouling in isolation because of the complexity of composite fouling process. In practice several types of fouling may occur

simultaneously. However, limited information is available regarding the effect of composite fouling on RO membrane systems performance using raw seawater.

In this chapter the effect of composite fouling on membrane performance is studied. To achieve this aim, fouling experiments were carried out with raw seawater from the Mediterranean Sea and the North Sea. The most common way to study fouling and its effect on RO membrane performance, permeate flux and permeate concentration were measured with time. Surface morphology and type of foulant were investigated using different analytical techniques in order to develop an effective fouling prevention technique.

6.2 Materials and Methods

6.2.1 Raw Seawater

Raw seawater was collected from the North Sea and the Mediterranean Sea. The samples were collected at 3 m of seashore and at depth of about 1 m in clean 30 L plastic tanks, transported to the University of Sheffield and stored at 4 °C in a dark refrigerator before the examinations. The characteristics of North Sea and Mediterranean Sea water in terms of conductivity and pH were 39230, 59600 ($\mu S.cm^{-1}$), 8.1 and 8.3, respectively.

6.2.2 Preparation of Reverse Osmosis Membrane

Seawater reverse osmosis (SWRO) polyamide thin film composite membrane (Toray, Japan) was used in all fouling experiments (Table 6.1). The Toray membrane was selected because of its high salt rejection and cost.

Table 6.1: Specifications of the selected SWRO membrane

Membrane	Manufacturer	Material	Surface charge at pH 7	Salt rejection (%)	Feed Pressure (bar)	Flux ($ml.cm^{-2}.min^{-1}$)
SWRO	Toray – Japan	Polyamide	Negative	99.75	55	0.016

The clean RO membrane was cleaned and conditioned according to the procedure described in section 3.5.

6.2.3 Cross-Flow Membrane Filtration Unit

Fouling tests were carried out using a laboratory scale plate and frame cross-flow RO test unit. The cross-flow RO test unit is a commercially available stainless steel unit (Osmonics, Desal, USA). The system consists of a feed water tank, high pressure pump, and two test cells with pressure gauges and regulators (Figure 6.1 and 6.2). The unit can be operated with feed pressure up to 60 bar and provides an effective membrane surface area of 81 cm^2. The feed pressure can be increased and decreased using a needle valve. Fouling tests were conducted in a recycling mode where both permeate and concentrate were recycled back to the feed water tank. Each filtration experiment was conducted over a period of 6 h.

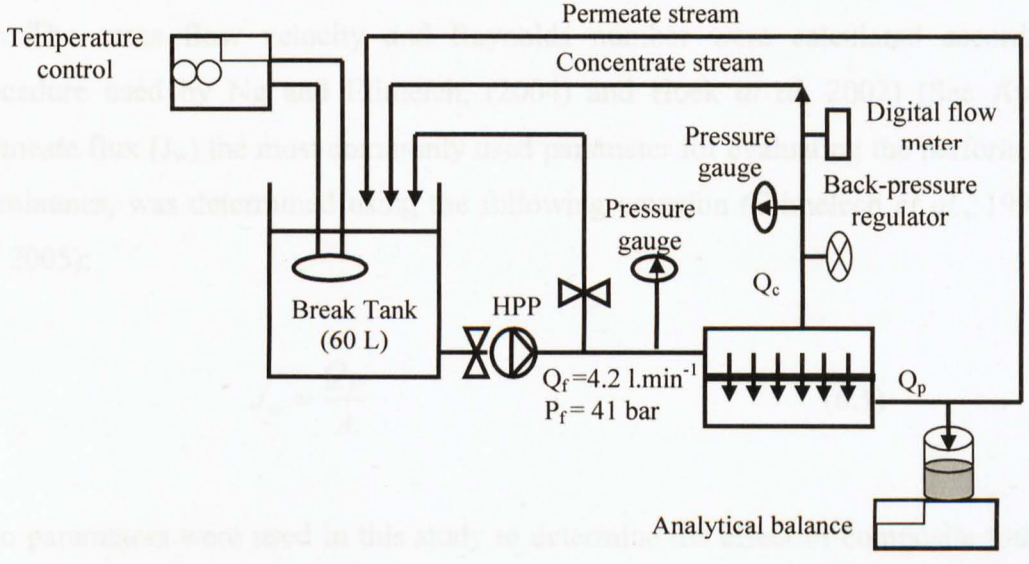

Figure 6.1 Schematic diagrams of bench scales cross – flow RO membrane filtration unit.

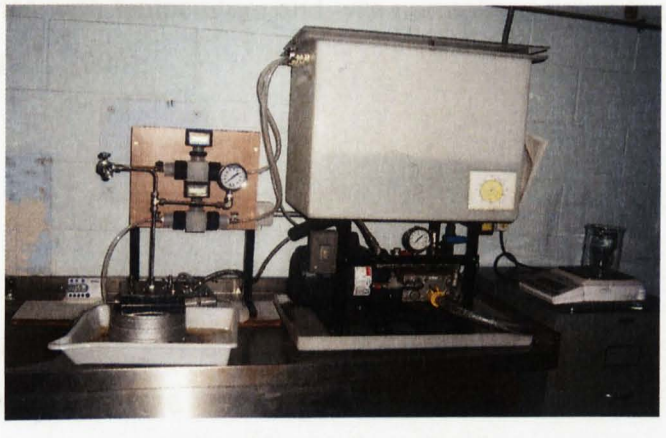

Figure 6.2 A photograph of bench scales cross – flow RO membrane filtration unit.

6.2.4 Membrane Fouling Study

For the composite fouling study, the water tank was filled with raw seawater. The high pressure pump was started with a low operating pressure of 6.8 bar and the first few litres of seawater were drained through the by pass line to avoid dilution of the seawater in the water tank by the high quality permeate that was used for rinsing the filtration unit. Then, the feed pressure was gradually increased and permeate flow and permeate conductivity measured using a digital scale, and an electrical conductivity meter (Model CON 410, OAKTON- Eutech Instruments). The pH of feed water was controlled using microcomputer pH meter (HI 8424-HANNA Instruments). The volume of feed water was 30L and the feed flow was set at 4.2 ($l.min^{-1}$) by adjusting the applied pressure, which was 41 bar. The cross flow velocity and Reynolds number were calculated according to the procedure used by Ng and Elimelch, (2004) and Hoek *at al.* 2002) (See Appendix E). Permeate flux (J_w) the most commonly used parameter for evaluating the performance of RO membranes, was determined using the following equation (Elimelech *et al.*, 1997; Chen *et al.*, 2005):

$$J_w = \frac{Q_p}{A} \qquad (6.1)$$

Two parameters were used in this study to determine the effect of composite fouling on the performance of the RO membrane; normalised permeate flux and permeatre concentration. Permeate flux varies with temperature and was normalised using the following equation (Xu *et al.*, 2006; Liu *et al.*, 2006):

$$J_N = \frac{J_a}{J_0} \qquad (6.2)$$

Where:

$J_{N,}$ - Ratio of permeate flux

J_0 - initial permeate flux ($ml.cm^{-2}.min^{-1}$).

J_a - actual permeate flux ($ml.cm^{-2}.min^{-1}$).

Measured and calculated parameters including permeate flow operating pressure, and permeate flux are presented in Appendix F. At the end of each fouling experiment, the feed tank was emptied and cleaned and the cross-flow RO unit was cleaned according to the procedure described in Section 3.8, Chapter 3.

6.2.5 Membrane Autopsy and Visualisation

Atomic force microscope (AFM) (Digital instruments, USA), Scanning electron microscope (SEM) (FEI Instruments), and a attenuated total reflection-Fourier transform infrared spectroscopy (ATR-FTIR) (PerkinElmer FTIR spectroscope - Canada) were used for investigation of surface morphology and functional groups of clean and fouled RO membranes (See Sections 3.9.2, 3.9.3 and 3.9.4, respectively).

6.3 Results and Discussion

6.3.1 Permeate Flux of Pure Water (J_w)

Duplicate test runs were conducted for each experiment at similar operating conditions. The permeate flux of pure water (high grade RO permeate) was determined for the Toray SWRO membrane. This high grade RO permeate was produced using a RO unit in the laboratory. The permeate flux of pure water as a function of feed pressure was measured (Figure 6.3). It was observed that, as would be expected permeate flux increases with increasing feed pressure. The highest permeate flux of pure water, 0.55 $ml.cm^{-2}.min^{-1}$, was obtained at an operating pressure of 41bar.

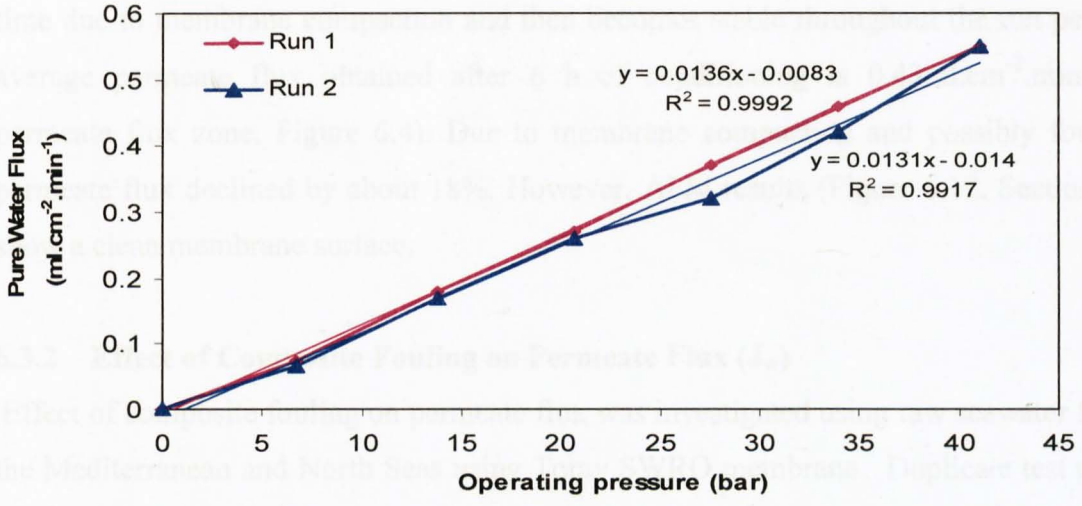

Figure 6.3: Increasing pure water permeate flux with increasing of operating pressure

For seawater applications it is important to distinguish between the effects of fouling and compaction on permeate and salt fluxes (Wilf and Klinko, 1994). In order to differentiate between the effect of membrane compaction and membrane fouling on permeate flux, the clean membrane was conditioned for 6 hrs at constant feed pressure (41 bar) and a constant water temperature (25 ± 2 °C). The water temperature was maintained using a cooling chiller and ice bags. The stability of permeate flux of pure water was measured before performing any fouling tests (Figure 6.4).

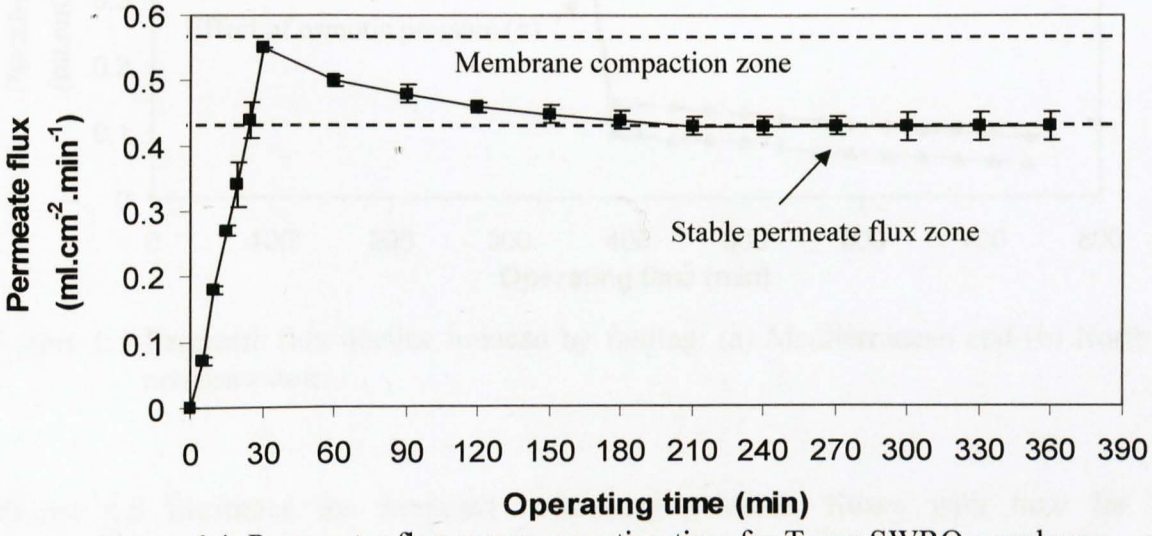

Figure 6.4: Pure water flux verses operating time for Toray SWRO membrane

From Figure 6.4 it can be seen that the permeate flux of pure water decreases gradually with time due to membrane compaction and then becomes stable throughout the run period. The average permeate flux obtained after 6 h of conditioning is 0.43ml.cm^{-2}.min^{-1} (stable permeate flux zone, Figure 6.4). Due to membrane compaction and possibly fouling, the permeate flux declined by about 18%. However, AFM results (Figure 6.12, Section 6.3.8.1) show a clean membrane surface.

6.3.2 Effect of Composite Fouling on Permeate Flux (J_w)

Effect of composite fouling on permeate flux was investigated using raw seawater from both the Mediterranean and North Seas using Toray SWRO membrane. Duplicate test runs were conducted under the same operating conditions. The stable permeate flux of the clean membrane was 0.43 ml.cm^{-2}.min^{-1}, however as raw seawater was added into the feed tank, the permeate flux declined dramatically due to osmotic pressure and then gradually decreased due to fouling. The osmotic pressure of both seawaters was about 30 and 20 bar, respectively. The Mediterranean and the North Sea water samples exhibited initial permeate fluxes of 0.10 and 0.14 ml.cm^{-2}.min^{-1}, respectively (Figure 6.5).

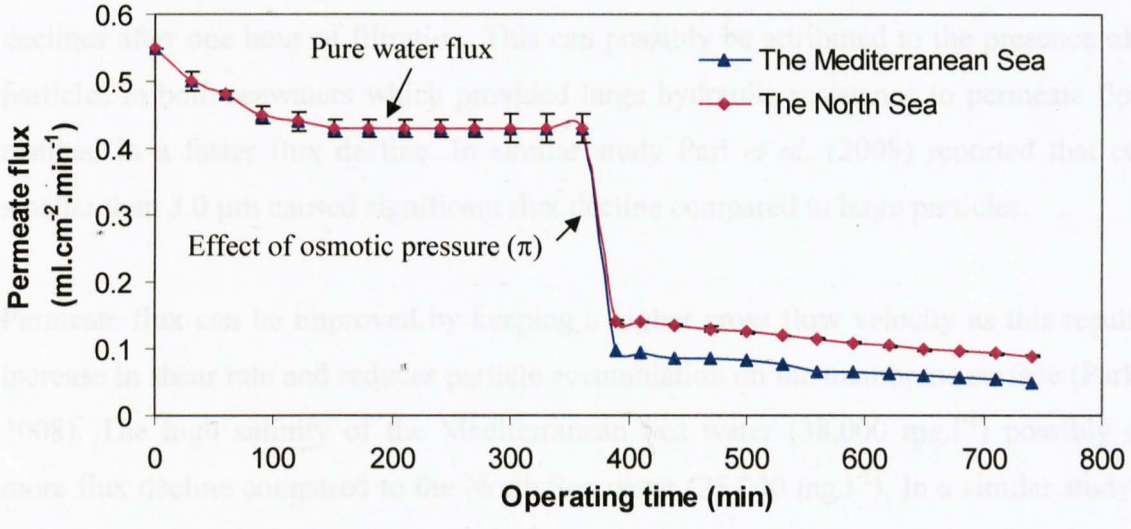

Figure 6.5 Permeate flux decline induced by fouling: (a) Mediterranean and (b) North Sea raw seawaters.

Figure 6.6 illustrates the averaged normalised permeate fluxes with time for both Mediterranean Sea and North Sea raw seawaters.

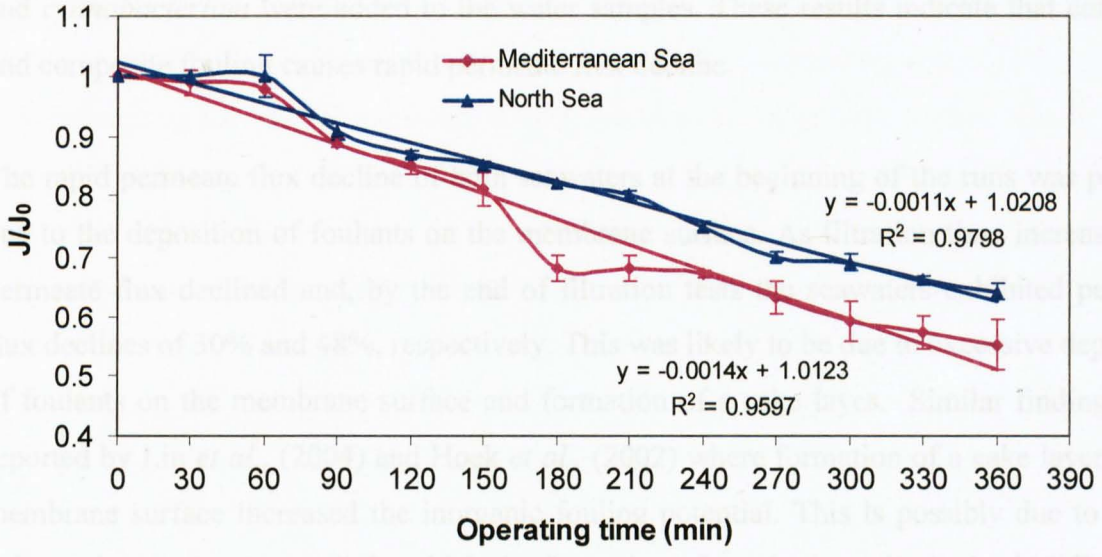

Figure 6.6 Effect of composite fouling on permeate flux of both Mediterranean (a) and North Sea (b) raw seawaters. Test conditions employed were: initial flux (J_0) = 0.097 and 0.11 ml.cm^{-2},min^{-1}, respectively), feed pressure (P_f) = 41 bar, crossflow velocity (V_{xf} =0.34 cm.s^{-1}, T = 25 ± 2.0 and pH=8.2 ± 0.2

It can be seen from Figure 6.6 that the normalised permeate flux of both raw seawaters declines after one hour of filtration. This can possibly be attributed to the presence of small particles in both seawaters which provided large hydraulic resistance to permeate flow and resulted in a faster flux decline. In similar study Parl *et al.* (2008) reported that colloids smaller than 3.0 μm caused significant flux decline compared to large particles.

Permeate flux can be improved by keeping a higher cross flow velocity as this result in an increase in shear rate and reduces particle accumulation on the membrane surface (Park *et al.* 2008). The high salinity of the Mediterranean Sea water (38,000 mg.l^{-1}) possibly caused more flux decline compared to the North Sea water (25,000 mg.l^{-1}). In a similar study Hong and Elimelech (1997) found that flux declined by 50% after 70 h of filtration due to high ionic strength and the presence of calcium. They attributed this to a reduction in electrostatic repulsion between foulants and membranes. Ashhuby, (2007) in similar study used two different artificial water salinities (30,000 mg.l^{-1} and 60,000 mg.l^{-1}) and found that permeate flux decreased markedly at the high salinity (i.e. 60,000 mg.l^{-1}) by an average of 16%. This

author also, found that permeate flux declined by about 35% when cultures of a *halobcturium* and *cyanobacterium* were added to the water samples. These results indicate that combined and composite fouling causes rapid permeate flux decline.

The rapid permeate flux decline of both seawaters at the beginning of the runs was possibly due to the deposition of foulants on the membrane surface. As filtration time increased, the permeate flux declined and, by the end of filtration tests the seawaters exhibited permeate flux declines of 30% and 48%, respectively. This was likely to be due to excessive deposition of foulants on the membrane surface and formation of a cake layer. Similar findings were reported by Lin *et al.*, (2004) and Hoek *et al.,* (2002) where formation of a cake layer on the membrane surface increased the inorganic fouling potential. This is possibly due to "cake-enhanced osmotic pressure", in which the formation of a cake layer limits back diffusion of salt ions from the membrane surface to the bulk solution.

As untreated seawaters were used in these testes, these foulants may contain a combination of scaling, colloids and microorganisms. The increase in the thickness of cake layer with filtration time might have caused a change in the membrane surface characteristics such as roughness, surface charge and/or hydrophobicity/hydrophilicty. These changes would affect the rejection and permeability properties of the membranes (Cho *et al.,* 2000; Xu *et al.*, 2006). Similar finding were reported by Mulder, (2003); Mustafa, (2007) and Wang, (2005), in which the permeate flux has rapidly declined due to a concentration polarisation phenomenon and a formation of cake layer on the membrane surface.

6.3.3 Effect of Concentration Polarisation (CP)

Concentration polrarisation (CP) is an undesirable phenomenon in RO membranes because it increases salt concentration near the membrane and osmotic pressure. This leads to decreased permeate flux due a reduction in the net driving pressure (NDP). The concentration polarisation of both seawaters was calculated according to the calculation procedure described by Sutzkover *et al*, (2000) (See Appendix G). The results are shown in Figure 6.7. The mass transfer coefficient (K) was calculated using equation (2.26). The pure water flux (J_{H2O}) was measured using high grade RO permeate, while the permeate flux of

saline solution (J_{salt}) was measured using seawater from the Mediterranean Sea and the North Sea. Results show a gradual increase in concentration polarisation near the membrane surface. Increasing concentration polarisation causes a significant reduction in the permeate flux through an increase of the solute concentration at the membrane surface which, in turn, induces a high osmotic pressure gradient.

This observation indicates that the concentration polarisation layer develops with operating time and causes reduction in the permeate flux. Similar findings were reported by Song and Yu (1999).

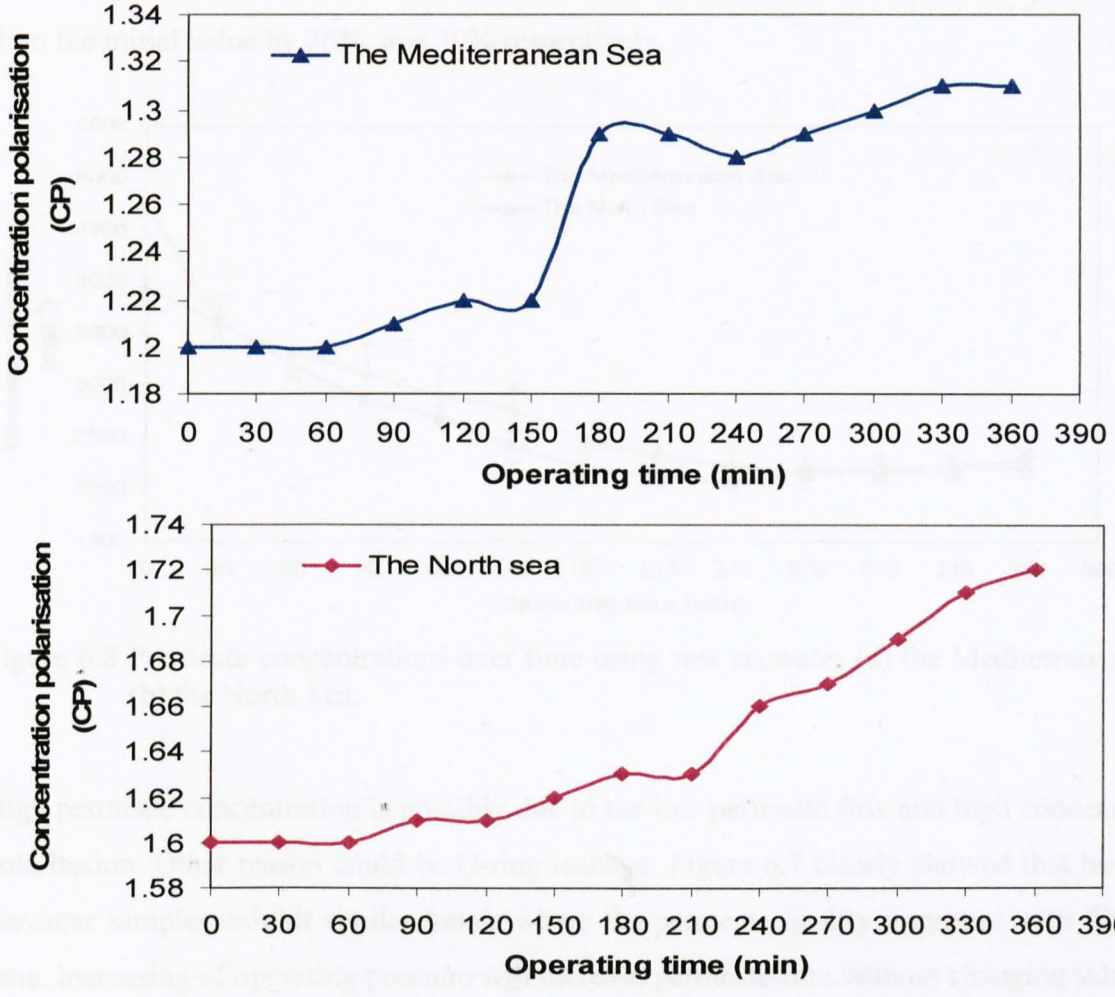

Figure 6.7: Concentration polarisation verse operating time for the Mediterranean Sea and the North Sea.

In Figure 6.7 it can be seen that the concentration polarisation increases with time due to high feed salt concentration. By the end of the filtration tests, the seawaters show an increase in

concentration polarisation of 8% and 7%. It is concluded that the concentration polarisation develops gradually with filtration time as a result of the accumulation of foulants and increasing retained salt ions near the membrane surface.

6.3.4 Permeate Concentration (C_p)

As feed water pressure is increased, the salt passage is increasingly reduced as water is pushed through the membrane at a faster rate than salt can be transported. Figure 6.8 shows the change in permeate concentration over time. In the first hour of filtration the permeate concentrations for the Mediterranean Sea and the North Sea water samples dropped from the initial value by 36%, and 39% respectively.

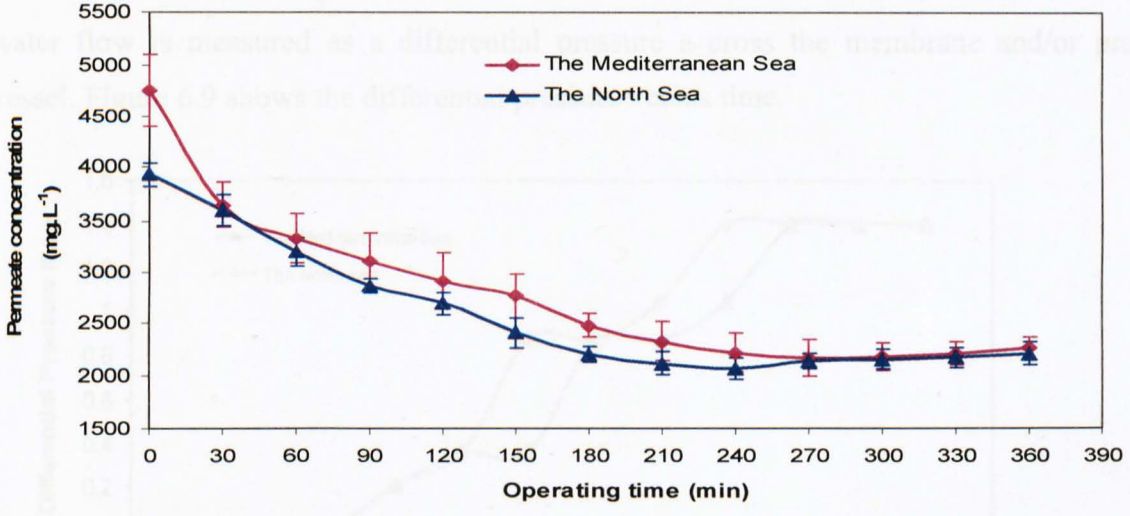

Figure 6.8 Permeate concentrations over time using raw seawater (a) the Mediterranean and (b) the North Sea.

High permeate concentration is possibly due to the low permeate flux and high concentration polarisation. Other reason could be O-ring leakage. Figure 6.7 clearly showed that both raw seawater samples exhibit similar trends where the permeate quality improves with filtration time. Increasing of operating pressure will increase permeate flux without changing salt flow, thus resulting in low permeate concentration. At higher flux rate the salt passage is lower, however the fouling rate increases (Glueckstren *et al.*, 2002). By the end of the filtration run a slight increase in the permeate concentration was observed for the Mediterranean Sea seawater compared to the North Sea raw seawater. This was possibly due to fouling,

concentration polarisation and increasing of temperature. An increasing concentration polarisation means high salt concentration at the membrane surface which increases the rate of cake formation, thus increases the salt passage through the membrane (Liu *et al.*, 2006; Xu *et al.*, 2006).

6.3.5 Differential pressure (ΔP)

Differential pressure is the measure of the resistance of the hydraulic flow of water and it is dependent on the flow rate through the membrane and on temperature. An increase in differential pressure at constant flow rate and feed pressure is usually due to the presence of foulants in RO feed water. As these foulants accumulate on the membrane surface, they increase the differential pressure as well as the resistance to feed_flow. This resistance to water flow is measured as a differential pressure a cross the membrane and/or pressure vessel. Figure 6.9 shows the differential pressure versus time.

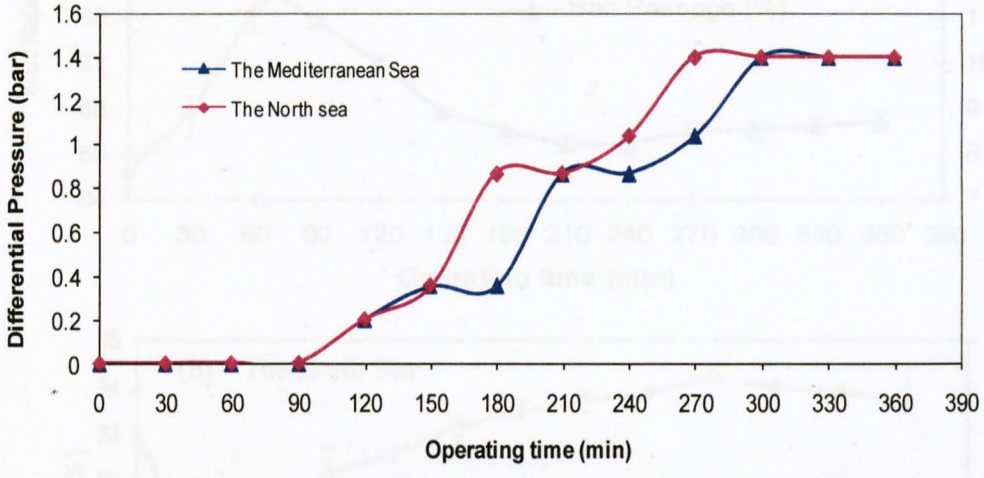

Figure 6.9: Increasing of differential pressure with time using the Mediterranean and the North Sea seawaters.

From Figure 6.9 it can be seen that in the first 90 minutes of the fouling test the differential pressure was stable, indicating that the filtration performance is not affected by fouling, then it gradually increases with time and reaches a stable condition by the end of the experimental run. It is important to maintain permeate and concentrate flow rates as constant as possible in order to monitor membrane plugging that is causing an increase in differential pressure.

6.3.6 Salt Rejection and Salt Passage (%)

Figure 6.10a and 6.10b show the percentage of salt rejection and salt passage with time for both seawaters. Results clearly show similar trends in which salt rejection smoothly increased over time. Furthermore, salt rejection for both samples show a slight improvement with increasing feed pressure and exhibits slight decline by the end of the filtration run, possibly due to excessive fouling. The RO membrane used in this study has a high salt rejection (99.75%), however high salt passage was observed after filtering both seawaters possibly due to leakage (o-ring problem).

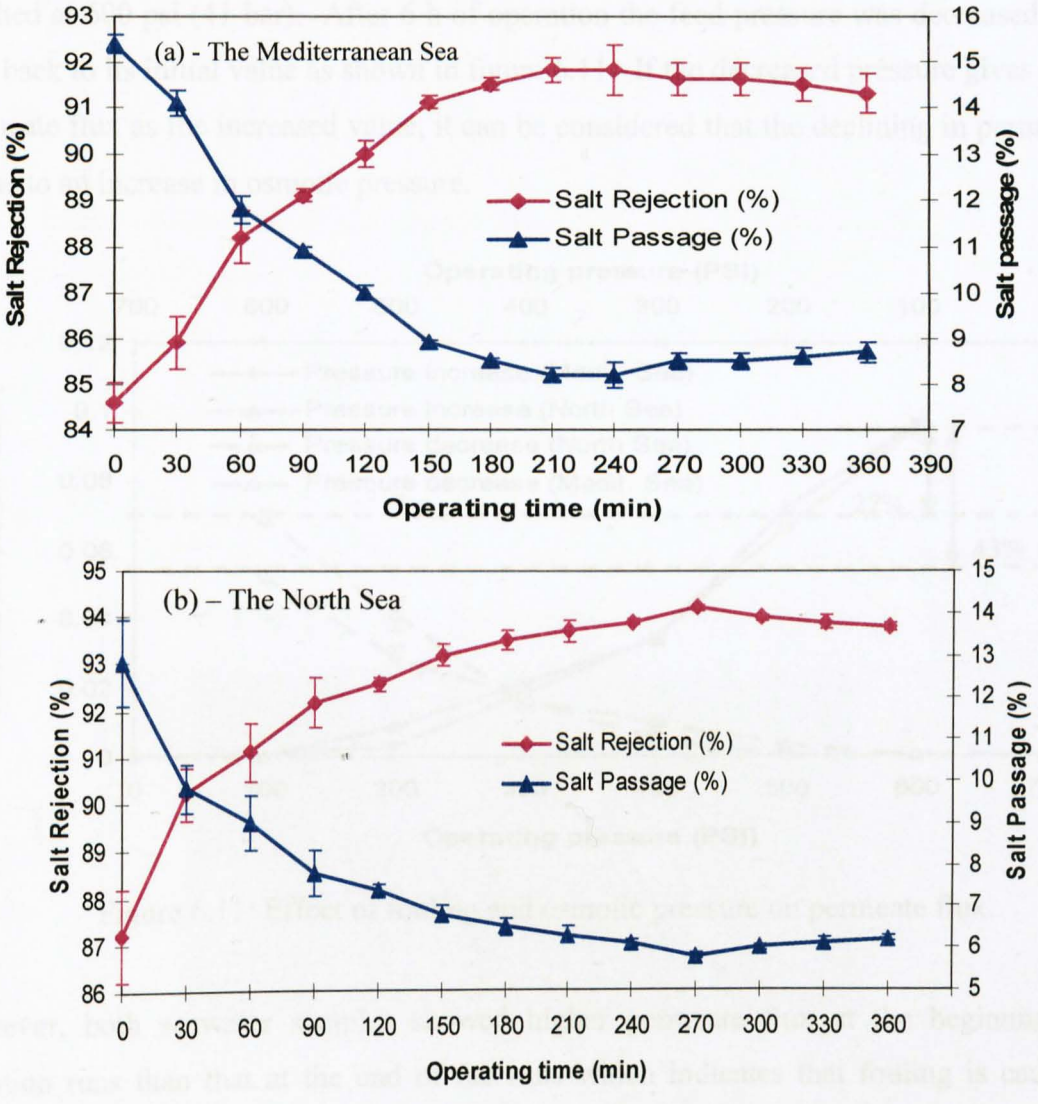

Figure 6.10: Effect of composite fouling on permeate concentration (a) the Mediterranean and (b) the North Sea.

According to the solution diffusion model (Wijmans and Baker, 1995), passing of more salt ions through the membrane will increase the concentration of the permeate water and in turn the chemical potential in permeate side decreases due to increasing in osmotic pressure.

6.3.7 Effect of Fouling and Osmotic Pressure on Permeate Flux

In order to determine whether the decline in permeate flux was due to fouling or due to an increase in the osmotic pressure near the membrane surface, the permeate flux, as a function of operating pressure was, measured at the beginning and at the end of each fouling test. First, the feed pressure is increased step-by-step until maximum permeate flux is reached at 600 psi (41 bar). After 6 h of operation the feed pressure was decreased step-by-step back to its initial value as shown in figure 6.11. If the decreased pressure gives the same permeate flux as the increased value, it can be considered that the declining in permeate flux is due to an increase in osmotic pressure.

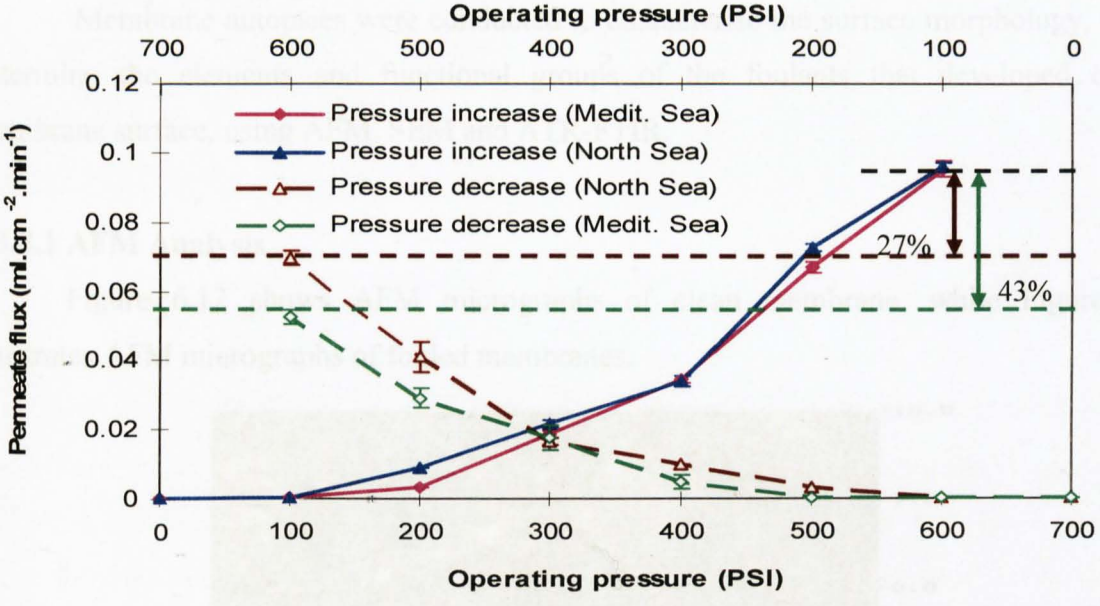

Figure 6.11: Effect of fouling and osmotic pressure on permeate flux.

However, both seawater samples showed higher permeate flux at the beginning of all filtration runs than that at the end of the runs which indicates that fouling is causing the declining of permeate flux. From Figure 6.9 it can be seen that declining in permeate flux at the beginning and the end of filtration run in both seawater samples decreased by about 43%

and 27%, respectively due to fouling. It can be attributed to the formation of packing and/or gel concentration on the membrane surface. In similar study Metsamuuronen *et al.* (2002) reported that difference in permeate flux at the beginning and at the end of fouling test indicates deposition and adsorption of fouling materials on the membrane surface, which in turn caused critical flux decline.

Osmotic pressure may also have an effect due to increasing of concentration polarisation at the membrane surface. The concentration polarisation was calculated for both seawater waters and found to be 1.2 (the Mediterranean Sea) and 1.6 (the North Sea) respectively. Concentration polarisation increases the salt concentration at the membrane surface and hence the resistance to filtration by membrane, which in turn reduces the permeate flux and increases the salt passage (Mulder, 2003).

6.3.8 Membrane Autopsy and Visualisation

Membrane autopsies were conducted to characterise the surface morphology, and to determine the elements and functional groups of the foulants that developed on the membrane surface, using AFM, SEM and ATR-FTIR.

6.3.8.1 AFM Analysis

Figure 6.12 shows AFM micrographs of clean membrane, while Figure 6.13 illustrates AFM micrographs of fouled membranes.

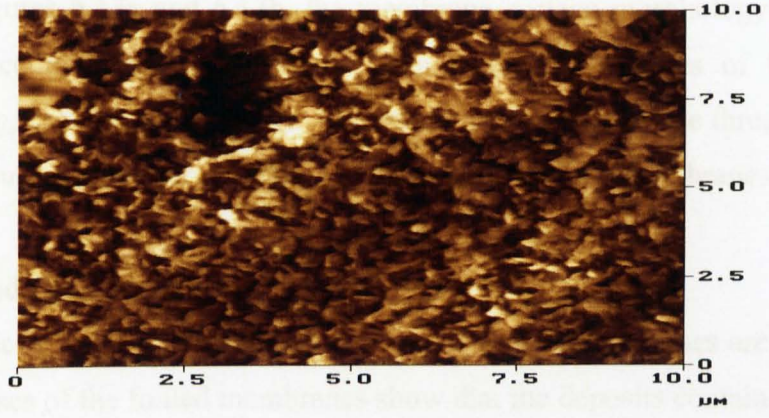

Figure 6.12: AFM micrographs of clean SWRO membrane from Toray.

It can be seen that the clean RO membrane has rough surface with irregular shaped valleys. The rough membrane surface increases the possibility of accumulation of foulants on the membrane surface and the valleys could become quickly clogged by particles and other fouling materials. The hydrophilicity and negative charge of RO membrane should result in less fouling due to higher electrostatic repulsion between the foulants and the membrane surface. However, roughnesses of the membranes surface increased the fouling rate, which in turn increased the resistance to flow and causes a rapid loss on permeate flux. In similar study (Li *et al.*, (2007); Vrijenhoek *et al.*, 2001) found that the rough membrane surfaces increased the fouling rate comparing to smooth membrane surfaces (Li *et al.*, (2007); Vrijenhoek *et al.*, 2001).

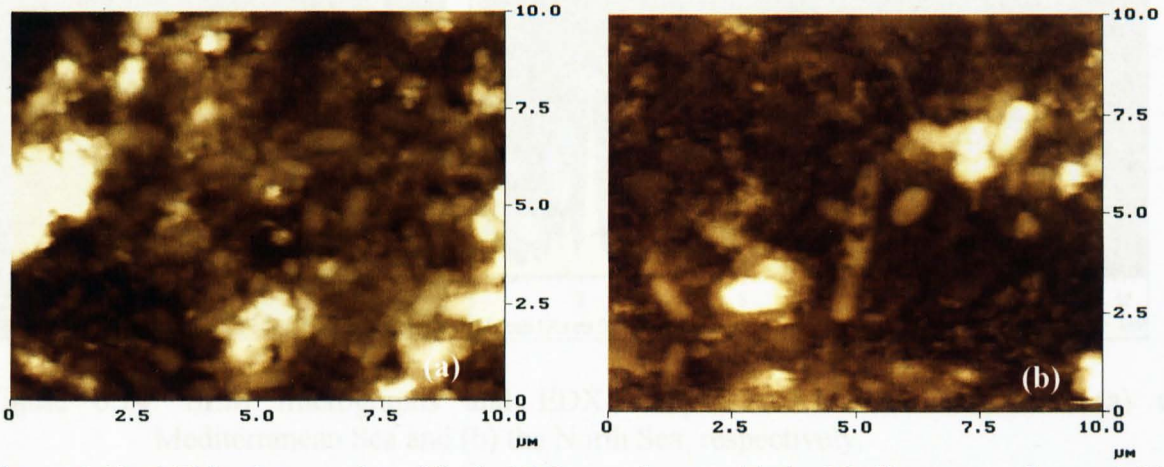

Figure 6.13: AFM micrographs of fouled RO membranes (a) the Mediterranean Sea and (b) the North Sea.

As shown in Figures 6.13a and 6.13b, the membrane surface morphology investigation by AFM showed accumulations of different foulants on the surfaces of both membranes including, scaling, colloids and bacteria. The results indicate that these three types of fouling occur simultaneously and affect the filtration performance of the membranes.

6.3.8.2 SEM and EDX Analysis

SEM micrographs and elemental analysis of fouled membranes are shown in Figure 6.14. EDX analyses of the fouled membranes show that the deposits contain similar elements including; carbon, oxygen, iron, aluminium and silica.

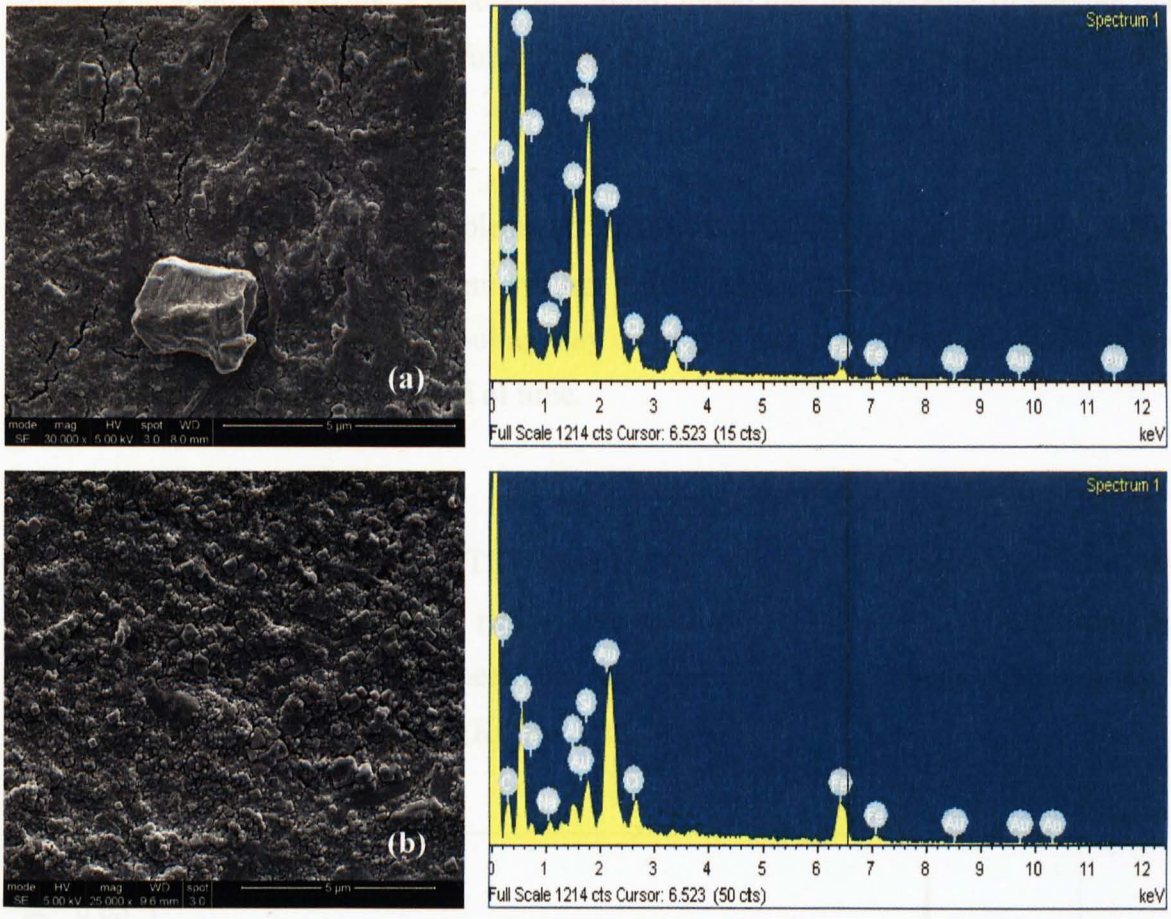

Figure 6.14: SEM micrographs and EDX analysis of fouled membranes (a) the Mediterranean Sea and (b) the North Sea, respectively.

The presence of silica (Si), aluminium (Al), and the presence of iron (Fe) in the foulants indicates that a colloidal fouling types occurring on the membrane surface. The presence of Al and Si suggests formation of aluminium hydroxide and/or aluminium silicate fouling. Gabelich *et al.*, (2002), carried out membrane autopsies and found similar results and attributed the formation of aluminium hydroxide and aluminium silicate fouling on the membrane surface to the presence of Al and Si in the feed water and/or due to the access dose of aluminium sulphate as a coagulant.

Both raw seawaters used contain inorganic, organic and biological matter, and the composition of the foulants is complex, and thus may cause a complex fouling process. During operation of RO membrane systems, once one type of fouling forms, it accelerates and catalyses the formation of other types of fouling, and the fouling process becomes more

severe. Liu *et al.*, (2006) and Kumar *et al.*, (2006) found that the presence of varying matter in the raw water can cause severe fouling and an effective pre-treatment is needed to reduce the composite fouling potential.

The results indicate that the implemented pre-treatment systems should be monitored carefully as when these pre-treatment systems malfunctioned any how in a full scale SWRO desalination plant, the composite fouling may occur and will deteriorates the performance of the RO membranes in a short period of time.

6.3.8.3 ATR-FTIR Analysis

Figure 6.15 shows the FTIR spectrum of a clean RO membrane. The strong absorption peaks are located in the region between 1700 and 700 cm^{-1}. These strong peaks suggested that the used SWRO membrane contains different functional groups including amides, carboxylate and carbonyle (Kumar *et al.*, 2006).

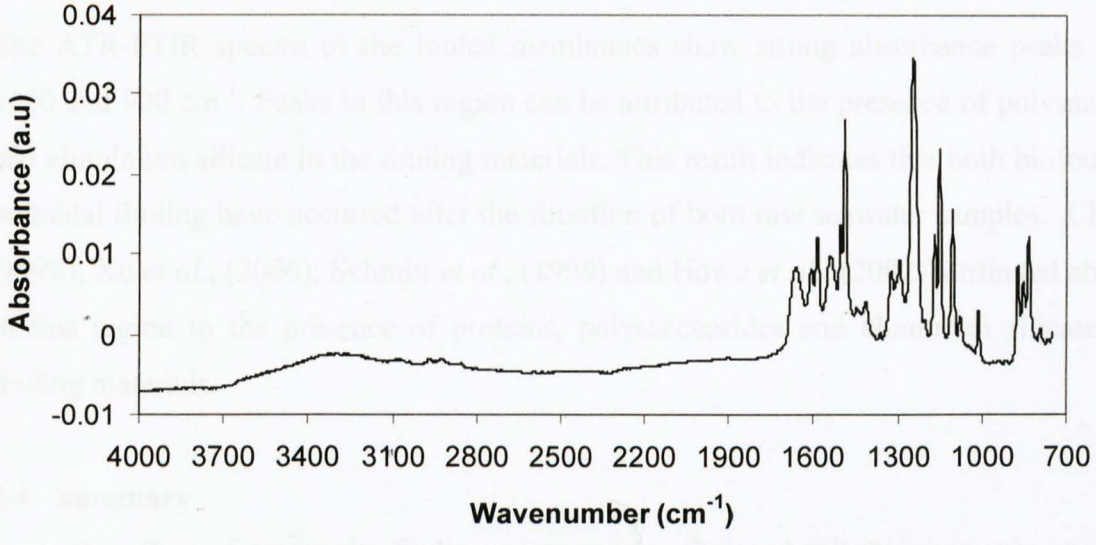

Figure 6.15: FTIR spectrum of clean SWRO membrane

However, these strong peaks were not present in the spectra obtained for similar fouled membranes (Figure 6.16).

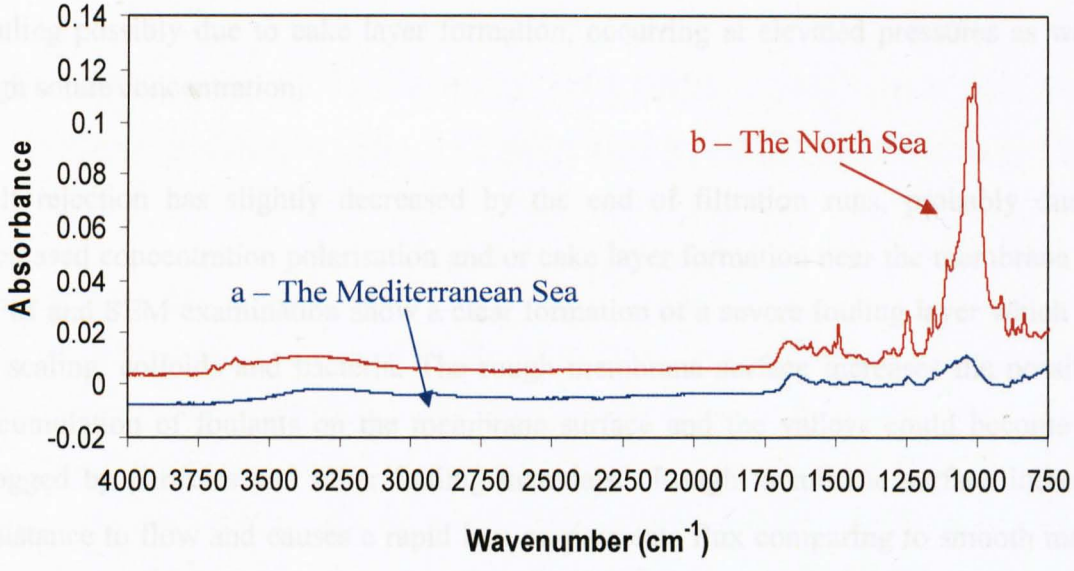

Figure 6.16: FTIR spectra of the fouled RO membranes: (a) the Mediterranean and (b) the North Sea.

The ATR-FTIR spectra of the fouled membranes show strong absorbance peaks between 1100 and 900 cm^{-1}. Peaks in this region can be attributed to the presence of polysaccharides and aluminium silicate in the fouling materials. This result indicates that both biofouling and colloidal fouling have occurred after the filtration of both raw seawater samples. Cho *et al.*, (1998); Xu *et al.*, (2006); Schmitt *et al.*, (1998) and Howe *et al.*, (2002) attributed absorption in this region to the presence of proteins, polysaccharides and aluminum silicates in the fouling materials.

6.4 Summary

The effect of composite fouling on permeates flux and salt rejection was investigated by carrying out a set of laboratory – scale cross flow filtration unit, with raw seawater. In this filtration experiments two types of raw seawater were used (the Mediterranean Sea and the North Sea). The permeate flux and salt passage were measured with time at similar operation conditions. Both seawaters caused a rapid accumulation of foulants on the membrane surfaces, which in turn caused a permeate flux decline of 48% and 30%, respectively. High salinity has a considerable impact on permeate flux and salt passage. However, permeate

flux behaviour of both seawaters represented formation of combined and/or composite fouling possibly due to cake layer formation, occurring at elevated pressures as well as at high solute concentration.

Salt rejection has slightly decreased by the end of filtration runs, probably due to the increased concentration polarisation and/or cake layer formation near the membrane surface. AFM and SEM examination show a clear formation of a severe fouling layer which consists of scaling, colloids and bacteria. The rough membrane surface increases the possibility of accumulation of foulants on the membrane surface and the valleys could become quickly clogged by particles and other fouling materials. Rough membrane surface increases the resistance to flow and causes a rapid loss on permeate flux comparing to smooth membrane surfaces.

EDX results were consistent with ATR-FTIR results as both clearly identified the presence of silica, aluminium and polysaccharides in both seawaters. The presence of excess oxygen indicates the presence of organic fouling. Thus the fouling material of both raw seawaters contains organic, inorganic and biological which eventually leads to composite fouling on the membrane surfaces.

CHAPTER 7

PREVENTION OF SEAWATER REVERSE OSMOSIS MEMBRANE FOULING USING NANO-ALUMIN DEPTH FILTER (DISRUPTOR^{TM})

7.1 Introduction

RO membrane systems can be fouled different types of foulants including inorganic precipitates, particles, precipitated metals, microorganisms and organic matter (Bonnely *et al.*, 2004; Tang *et al.*, 2007). The presence of other components in water sources such as transparent exopolymer particles (TEP) may play a role in conditioning surfaces for biofouling and biofilm development (Breman and Holenberge, 2005). These foulants can be reduced by applying an efficient pre-treatment. The commonly used pre-treatment systems in SWRO desalination plants are the conventional pre-treatment and membrane separation (microfiltration and ultrafiltration) (Vedavyasan *et al.*, 2007). However, conventional pre-treatment must be optimised and developed depending on the variation of feed water quality (Bonnely *et al.*, 2004; Xie *et al.*, 2009). Membrane separation processes such as microfiltration (MF) and ultrafiltration (UF) require frequent backwashing and chemical cleaning (Kumar *et al.*, 2006; van Hoof, *et al.*, 1999).

Recently, automatic backflush filters (Wnuk *et al.*, 2008) and automatic self-cleaning filters (Amiad) (Marcus and Allhands, 2008) have been applied to remove fine sands from untreated water prior to cartridge filters and RO membranes. They offer advantages over traditional multi media filters in terms of capital and installation costs. They can extend the lifetime of the cartridge filter elements and preventing sand from entering the reverse osmosis membranes.

An alternative efficient pre-treatment upstream to RO membranes is required. The use of a depth filter upstream of RO membranes has the potential to significantly reduce membrane fouling, because of its capability to remove the majority of substances that may foul RO membranes. Nano-alumina filter is an electropositive, submicron polishing media that

removes a variety of submicron contaminants through adsorption and mechanical filtration (Tapper and Kaledin, 2007; Komlenic, 2007). Nano-alumina filter can alter the path of particle as it travels through the media until it is adsorbed onto a nanofiber. A typical 2.5"x10" pleated cartridge has more than 10,000 square meters of active surface area with a capability to remove contaminants such as colloids, virus, bacteria and certain metals down to a few nanometers (Komlenic, 2007). Depending on the quality of the untreated water, primary filters may possibly be required to avoid premature surface blinding. Nano-alumina filter media can be used as die cut sheets in plate and frames or as stack disc filters and can be easily pleated for use as cartridge filters.

In this chapter, a study on the nano-alumina filter was made for the novel application of reducing SWRO membrane fouling by controlled bench scale experiments using natural raw seawater from the North Sea and Mediterranean Sea.

7.2 Materials and Methods

7.2.1 Raw Seawater

Natural seawater was collected from the North Sea, transported to the University of Sheffield and stored at 4 °C in a dark refrigerator before the experiments. The characteristics of the North Sea seawaters are; TDS = 25,500 mg/l, pH = 8.1 and T = 17 °C.

7.2.2 Pre-treatment Methods

The cartridge filters selected for this study were 1 μm and 5μm, and nano-alumina filter respectively (Table 8.1). The nano-alumina filter was supplied as a cartridge and as flat sheet. All were supplied by Ahlstrom Filtration LLC, USA and Amazon Filtration Ltd, UK.

Table 7.1: Specifications of the 1 μm, 5μm filters and the nano-alumina filter, respectively.

Filter Type	Material	Pore size	Filter Size	Filtration mechanism
Micron filters	Polypropylene	1μm and 5mμ	2" x 10"	- Sieving
Nano-alumina filter (Disruptor^{TM})	Nano-alumina	2μm	2" x 10"	- Mechanical entrapment - Adsorption

7.2.3 Reverse Osmosis Membrane

Seawater reverse osmosis (SWRO) polyamide thin film composite membrane (Toray, Japan) was used in all fouling experiments. The SWRO membrane samples from Toray were received as flat sheets (A4 size) and stored at 4°C.

7.2.4 Filtration and Cross-Flow Membrane Filtration Unit

Fouling tests were carried out using a laboratory scale filtration unit and plate and frame cross-flow RO test unit (See Figure 3.5, Chapter 3). The filtration unit consists of a feed water tank and two 10 inch cartridge filter casings made of polypropylene (Amozon Filters Ltd-UK). The cross-flow RO test unit is a commercially available stainless steel unit (Osmonics, Desal, USA). It consists of a feed water tank, high pressure pump, and two test cells with pressure gauges and regulators (Figure 7.1). The unit can be operated with feed pressure up to 1000 psi (~ 70 bar) and provides an effective membrane surface area of 81 cm^2. The fouling tests were conducted in recycling mode where both permeate and concentrate flow were recycled back to the feed water tank. Each filtration experiment was conducted over a period of 6 h.

Prior to all tests, the clean RO membrane coupons (area of 81 cm^2) were loaded to the RO filtration unit and rinsed with DI water at 6.8 bar for 30 min in order to remove the impurities attached to the membrane surface. As the membrane coupons to be tested had a small surface area and would be affected by the compaction under high operating pressure, the permeate flux was measured with high quality RO permeate at an operating pressure of 41 bar and temperature (25 ± 2 °C) until a constant flux was achieved. For the fouling tests,

first, the North Sea raw seawater (untreated) was added to the feed tank and pumped directly to the RO test unit containing a previously conditioned flat sheet SWRO membrane in order to investigate the effect of composite fouling on permeate flux. Next, the North Sea raw seawater was filtered through the nano-alumina filter alone, through the 5μm cartridge filter alone and through the 1μm cartridge filter alone in order to investigate the removal efficiency of each filter separately. The pre-filtered seawater from each filter was pumped into the RO test unit containing a conditioned RO membrane each time and the permeate flux was measured over time. In addition, the long-term operation performance of the nano-alumina filter was investigated by filtering the raw seawater thorough the 1 μm filter followed by the nano-alumina filter. For each fouling experimental runs 30L of feed water was used and the feed flow was set at 4.2 ($l.min^{-1}$) at adjusted applied pressure of 41 bar. Pure water flux and fouling filtration tests were preformed in duplicate for each filtration test (See Appendix H).

7.2.5 Membrane Fouling Study

7.2.5.1 Membrane Contact Angle

The clean and fouled RO membrane coupons were dried and contact angle measurements were made using the sessile drop method using a contact angle meter (KRUSS - DSA100), (Section 3.9.1)

7.2.5.2 Atomic Force Microscopy (AFM)

The surface morphology of clean and fouled membranes as well as roughness were analysed using a Nanoscope III atomic force microscope (Digital instruments, USA) (Section 3.9.2).

7.2.5.3 Scanning Electron Microscope (SEM)

Scanning electron microscope (SEM) along with energy dispersive X-ray spectrometer (EDX) were used to investigate the surface structure of the clean and fouled nano-alumina filter and RO membranes (Section 3.9.3).

7.2.5.4 ATR-FTIR Analyses

The clean and fouled nano-alumina filter and RO membranes surfaces were analysed for functional groups using attenuated total reflection-Fourier transform infrared spectroscopy (ATR-FTIR) (PerkinElmer FTIR spectroscope) equipped with an ATR accessory (Section 3.9.4).

7.2.5.5 Transparent Exopolymer Particles (TEP) Measurements.

TEP numbers were measured according to the method described by Bar-Zeev et al., (2009) (Section 3.9.6).

7.2.5.6 Plate Count Experiment

Plate count method was used to measure the number colony forming units in raw and pre-filtered seawater through the nano-alumina filter (section 3.1.1.3).

7.3 Results and Discussion

7.3.1 Filtration of Raw Seawater through the Nano-alumina Filter

Raw seawater from the North Sea was filtered through nano-alumina filter media alone and through nano-alumina filter followed by a 1 μm filter. Visual inspection of the filtered water samples showed that nano-alumina filter removed the majority of contaminants present in water (Figure 7.1).

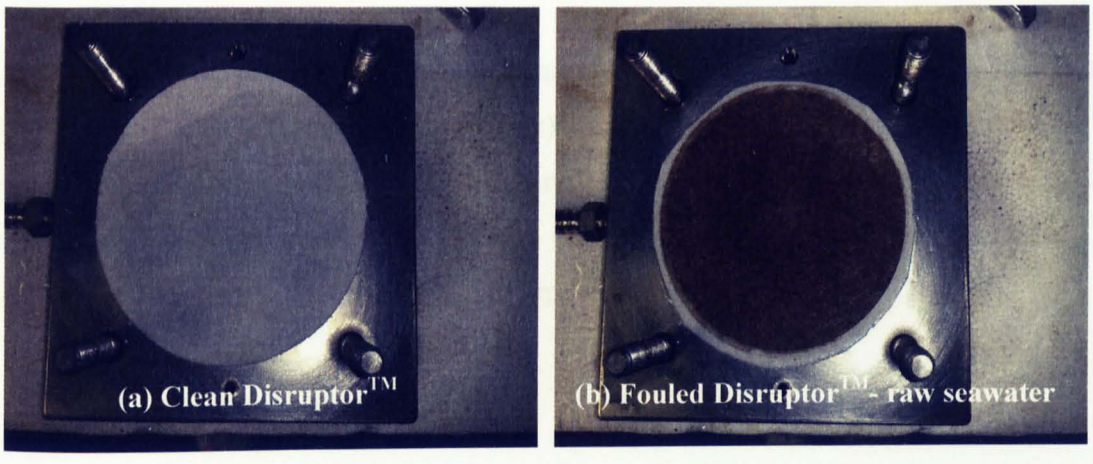

Figure 7.1: Clean (a) and fouled (b) nano-alumina filter by raw North Sea seawater.

The pre-filtered seawater samples were very clean compared to raw water (Figure 7.2). Results indicate that nano-alumina filter has capability to remove the majority of substances that may cause fouling in membrane systems.

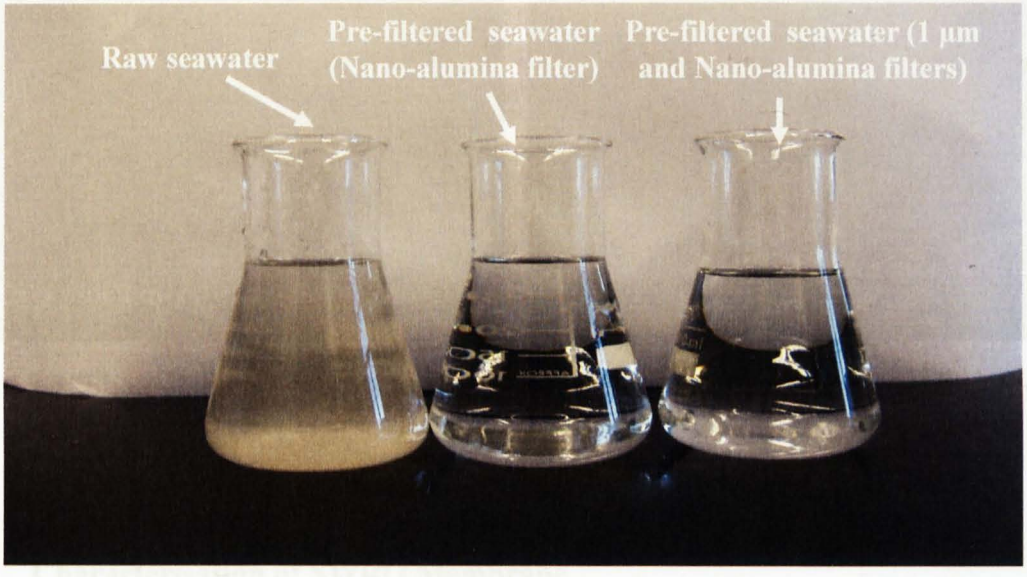

Figure 7.2: Filtration of raw seawater from the North Sea through nano-alumina filter.

From Figure 7.2 it can be seen that, raw seawater has brown colour, indicates the presence of turbidity, particles and NOM (Fan *et al.*, 2001). The presence of particles and microorganisms is found to be the dominant factor causing flux decline in membrane filtration systems (Combe *et al.*, 1999; Kaiya *et al.*, 1996)

Raw and seawater pre-filtered through a nano-alumina filter were pumped to RO test unit containing a SWRO RO membrane (Toray). Visual inspection (Figure 7.3) showed that the surface of membrane receiving pre-filtered seawater through a nano-alumina filter is undistinguishable from a new membrane, while the membrane surface challenged by raw seawater is completely covered by fouling material.

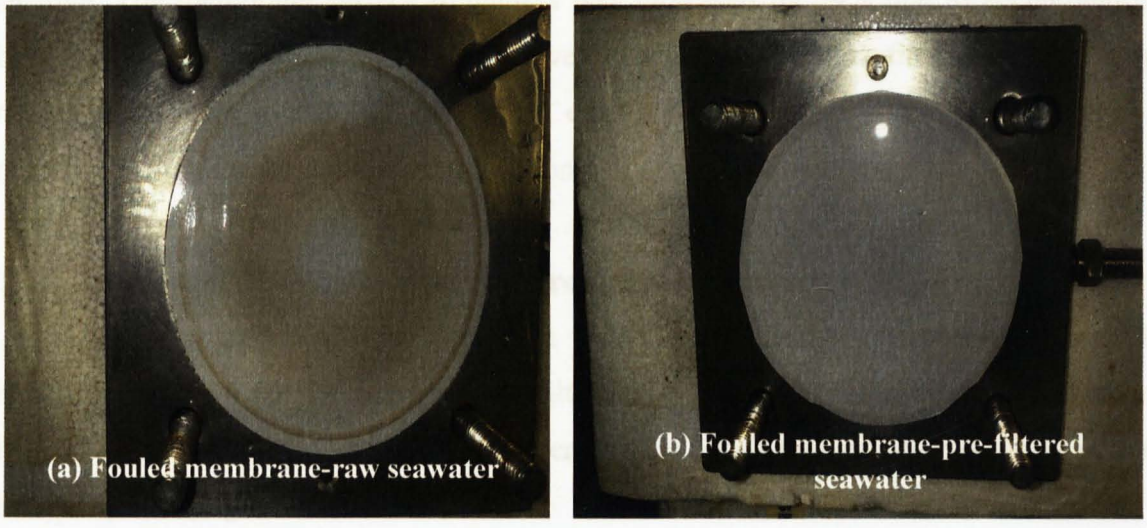

Figure 7.3: Photographs of (a) fouled RO membrane by raw seawater and by (b) pre-filtered seawater through nano-alumina filter, respectively.

7.3.2 Characterisation of SWRO Membrane.

The characteristics of clean and fouled SWRO membrane by raw seawater and seawater pre-filtered through the nano-alumina filter were measured and are summirised in Table 7.2.

Table 7.2: The contact angle and membrane roughness of clean and fouled SWRO membrane by raw and pre-filtered seawater.

Code	New membrane	Fouled membrane (Raw seawater)	Pre-filtered seawater (Nano-alumina filter)
Membrane contact angle	50.4 ± 2.69	41.6 ± 1.19	51.9± 4.17
Membrane roughness (nm)	50.3 ± 1.58	81.7 ± 0.88	63.2 ± 0.001

The clean SWRO membrane exhibits a medium contact angle and a rough surface. After filtration of raw seawater through the RO membrane, the membrane roughness increased while the contact angle decreased. Decreasing of contact angle suggests the hydrophilic nature of fouling materials. Cho *et al.*, (1998) and Park *et al.*, (2006) have reported similar results which included that natural organic components would reduce contact angle by coating negatively charged functional group and making the membrane surface charge less

negative. The membrane surface roughness was increased by 59% due to accumulation of foulants on the membrane surface. However, when nano-alumina filter was used as pre-treatment upstream to the RO membrane, only a slight change in the contact angle and membrane roughness was observed when compared to a new membrane.

7.3.3 Membrane Fouling by Raw and Pre-filtered Seawater

Raw seawater from the North Sea was filtered through different cartridge filters including a 1 μm, a 5μm, a nano-alumina filter and a 1μm filter followed by a nano-alumina filter. The removal efficiency of each filter was investigated through measuring permeate flux verse time (Figure 7.4).

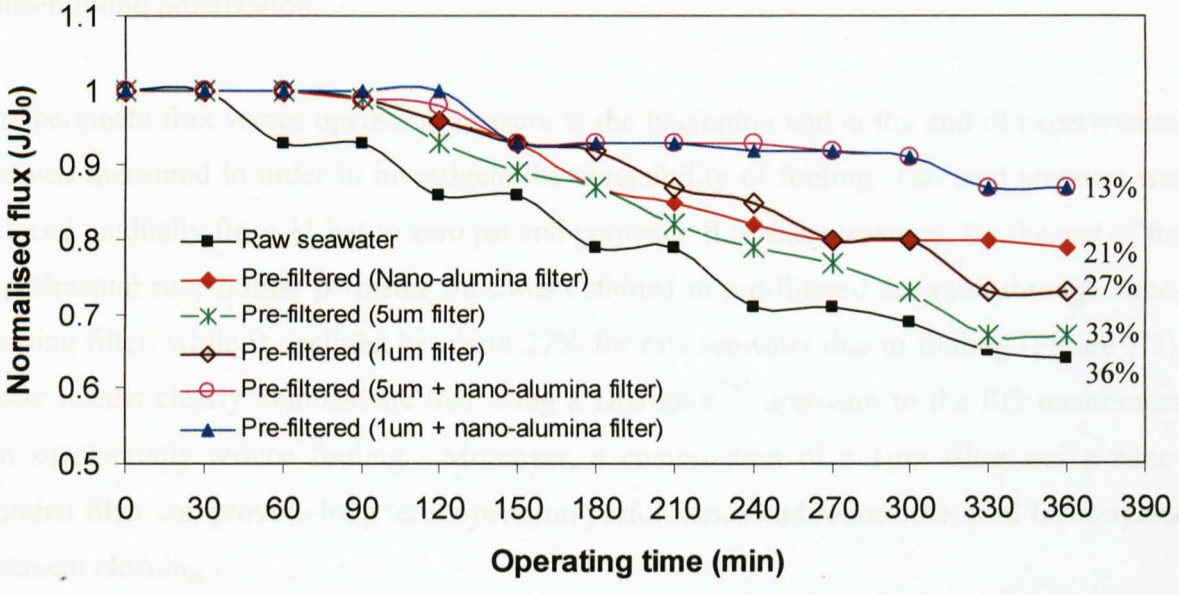

Figure 7.4: Comparative permeate flux decline of untreated seawater and pre filtered through 1 μm filter, 5μm filter, nano-alumina filter and 1 μm filter followed by nano-alumina filter, respectively.

Raw seawater sample exhibited rapid flux decline of 36% over 6 hours due to accumulation of different types of foulants on the membrane surface. Lee *et al.*, (2004) and Bonnely *et al.*, (2004) reported that the accumulation such foulants on the membrane surface causes a large hydraulic resistance to permeate flow and thus results in a rapid permeate flux decline. In similar study (Li *et al.*, 2007) reported that higher flux decline occurred due to high deposition rate of the foulants on the membraner surface, which in turn caused a more

compact fouling layer. The pre-filtered seawater through 1μm, 5μm filters, respectively exhibited similar trends, in which the permeate flux was stable during the first 90 min, followed by a rapid decline, possibly due to accumulation of small colloids and formation of scaling on the membrane surface. In these filtration experiments both the 1 μm and the 5μm filters showed an overall permeate flux decline of about 36 % and 50%, respectively. However, when the nano-alumina filter was used alone and downstream of the 1 μm and 5 μm filters, the resulted showed much less permeate flux decline (25% and 15% respectively). Decrease of the normalised permeate flux of seawater pre-filtered through the nano-alumina filter alone as well as through the micron filters followed by the nano-alumina filter was only noticed after 150 hours of filtration. This decrease is possibly due to the effect of the concentration polarization.

The permeate flux verses operating pressure at the beginning and at the end of experimental run was measured in order to investigate the reversibility of fouling. The feed pressure was reduced gradually from 41 bar to zero psi and permeate flux was measured. By the end of the experimental run, similar permeate flux was obtained in pre-filtered seawater through nano-alumina filter, while it declined by about 27% for raw seawater due to fouling (Figure 7.5). These results clearly demonstrate that using a Disruptor^{TM} upstream to the RO membranes can substantially reduce fouling. Moreover, a combination of a 1μm filter and a nano-alumina filter can provide long term operation performance and reduce the need for frequent chemical cleaning.

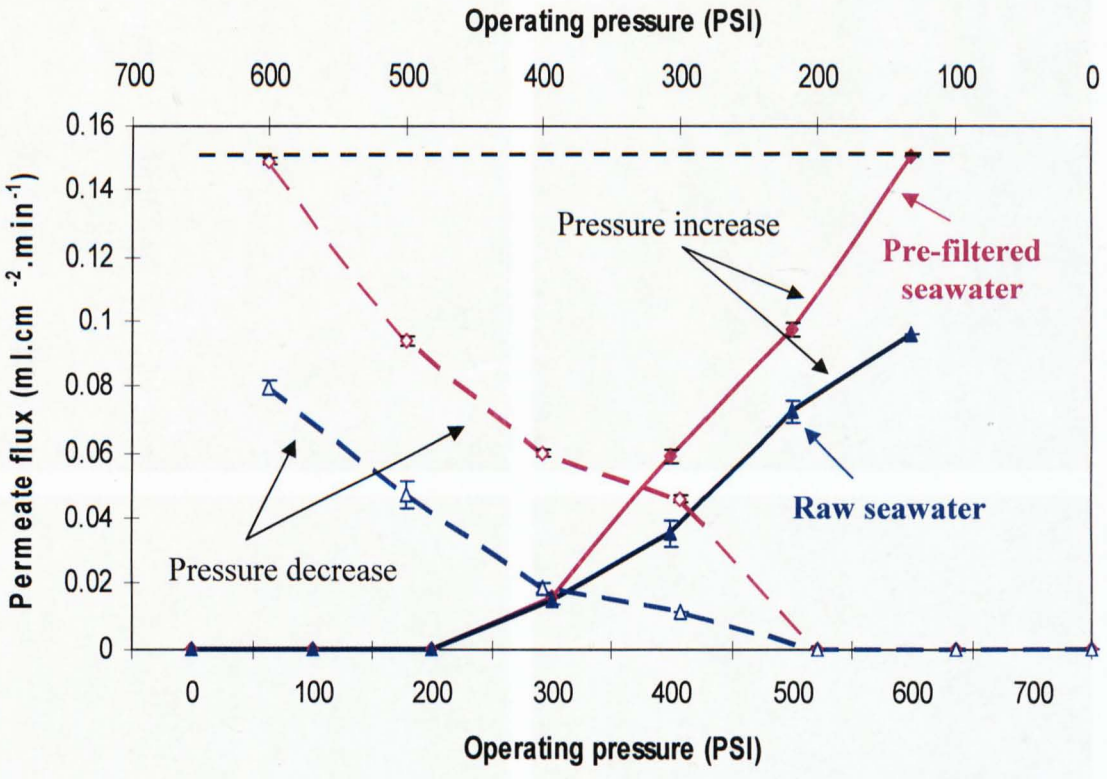

Figure 7.5: Permeate flux verses operating pressure for raw and pre-filtered seawater through nano-alumina filter filter.

7.3.4 Disruptor^{TM} and Membrane Visualisation

7.3.4.1 SEM and EDX Results of Clean and Fouled Nano-alumina Filter.

Figure 7.6 shows the SEM micrographs of clean and fouled nano-alumina filter by raw seawater from the North Sea, while Figure 7.7 illustrates its corresponding EDX spectrum. The SEM results show deposition of a very thick fouling layer on the surface of the nano-alumina filter and that contains scaling, microorganisms, and silica. The EDX spectrum of the fouling layer shows elements including iron, aluminium, silica, calcium and potassium. The silica peak was detected on the shoulder of the strong gold peak. Schneider *et al.*, (2005), analysed a foulant layer of different RO membrane elements and found similar results.

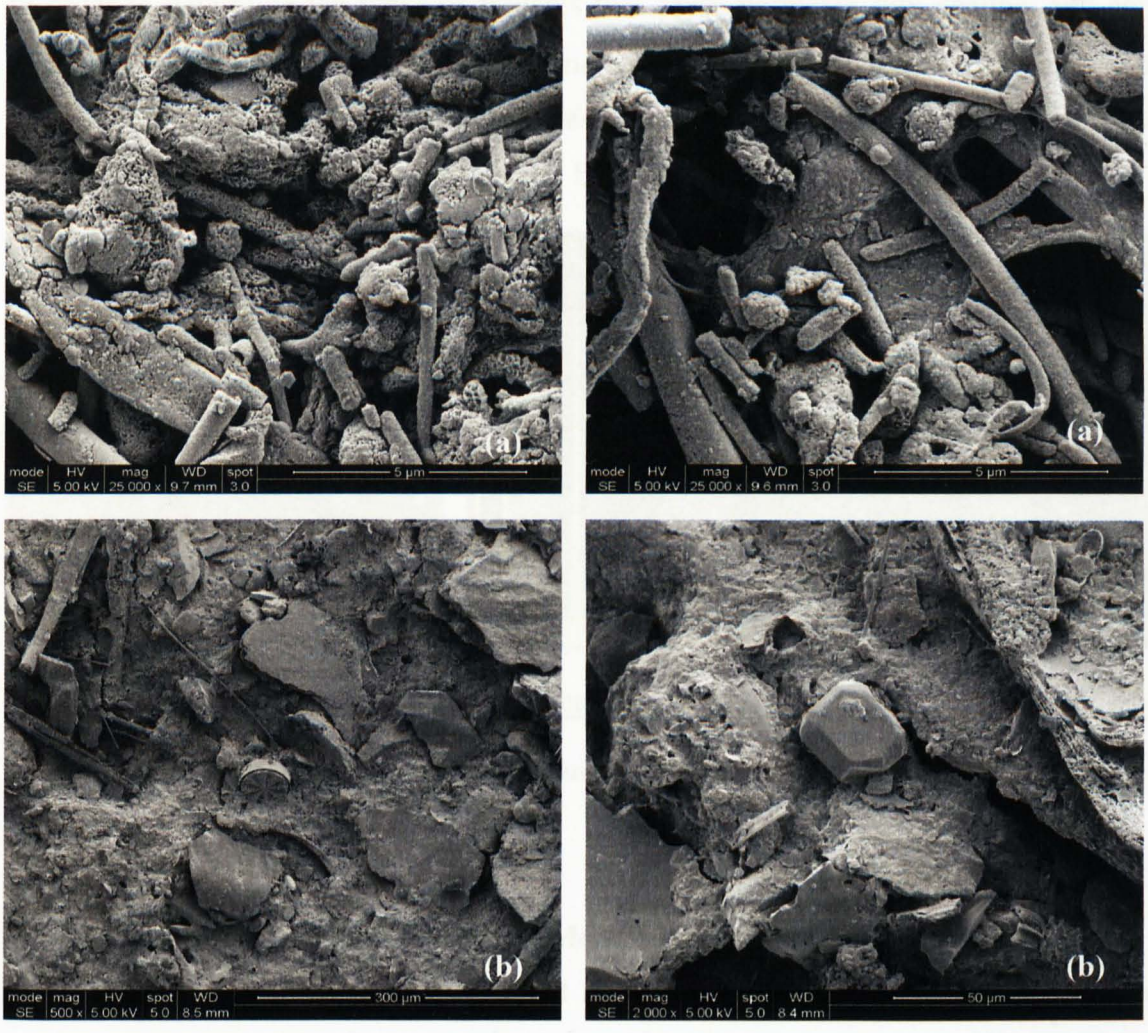

7.6 SEM micrographs of clean and fouled Disruptor^{TM} by the North Sea raw seawater.

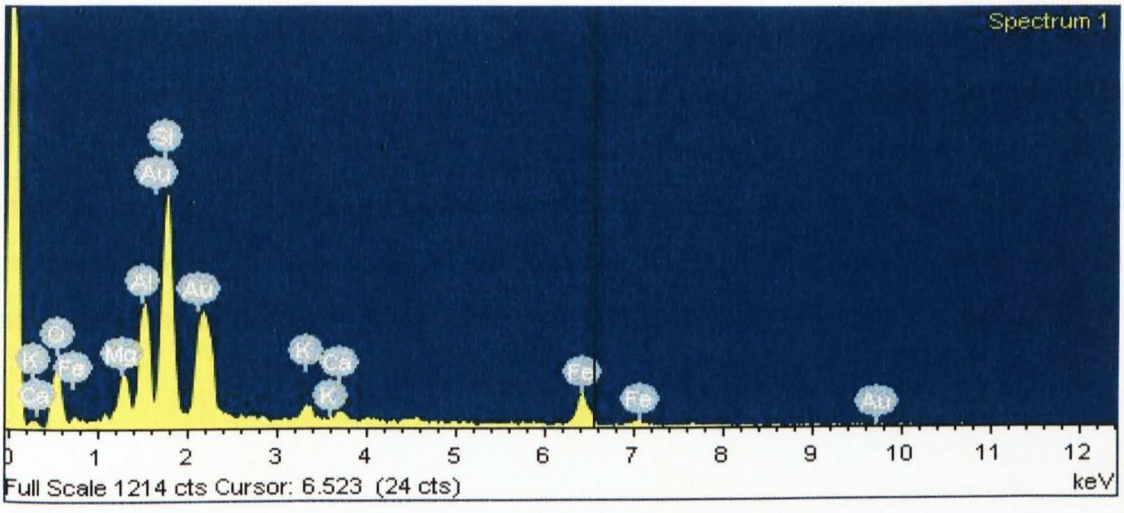

Figure 7.7: EDX spectrum of fouled nano-alumina filter by the North Sea raw seawater.

In order to determine the types of foulants that cause permeate flux decline, and compare them with the foulants retained by the nano-alumina filter media, surface morphologies of clean and fouled RO membranes were investigated using SEM and AFM. Figure 7.8 shows the SEM micrograph and its corresponding EDX spectrum of a fouled RO membrane.

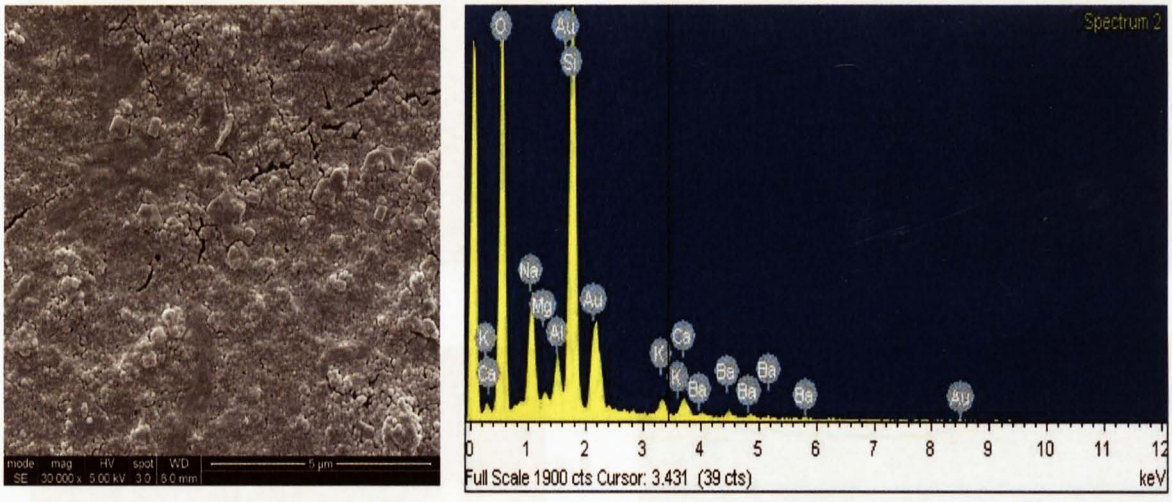

Figure 7.8: SEM micrographs of clean (a) and fouled (b) Toray SWRO membranes and its corresponding EDX spectrum.

7.3.4.2 AFM and SEM Results (RO Membrane)

Figure 7.9 shows the SEM and AFM micrographs of both clean and fouled RO membrane, respectively. The rough surface of the fouled membrane is filled by foulants, which change the membrane surface morphology. Similar studies (Freger *et al.*, 2002; Cho *et al.*, 1998) reported that membrane surface roughness increases membrane fouling by increasing the rate of particle and colloid attachment onto the membrane surface. Vrijenhoek *et al.*, (1991), carried out a study of membrane fouling in a laboratory scale cross flow filtration unit and found that more particles are deposited on rough than on smooth membranes. Also, accumulation of particles on the rough membranes causes fast clogging and severe flux decline.

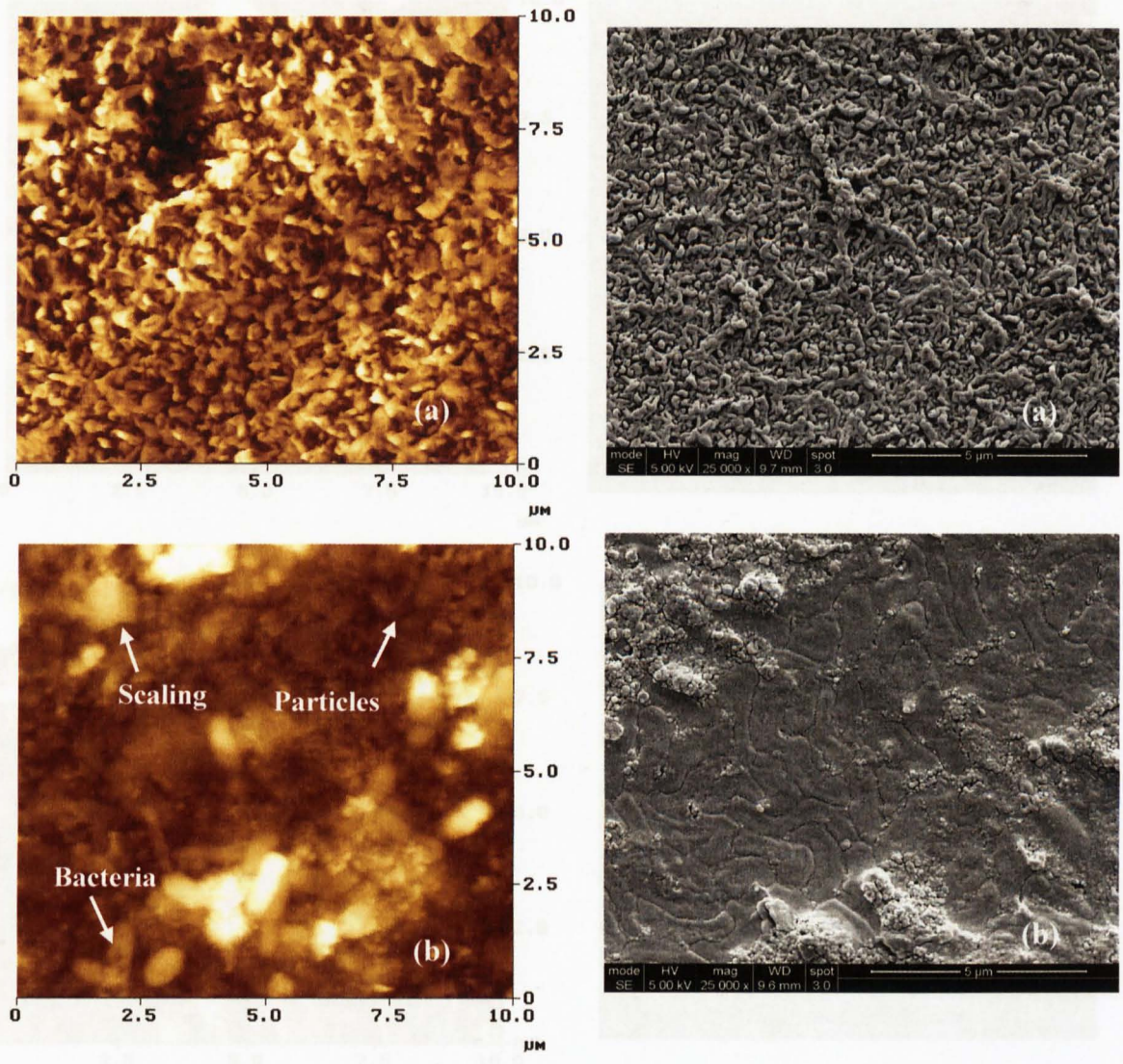

Figure 7.9: AFM and SEM images of clean (a) and fouled (b) RO membranes.

Figure 7.10 shows AFM images of membrane surfaces exposed to seawater filtered through 1μm and 5μm filters. The 5μm filtered seawater (Figure 7.10a) gives deposition of bacteria, clusters of packed particles and/or colloids, while the 1μm filtered seawater (Figure 7.10b) shows deposition of small colloids like materials.

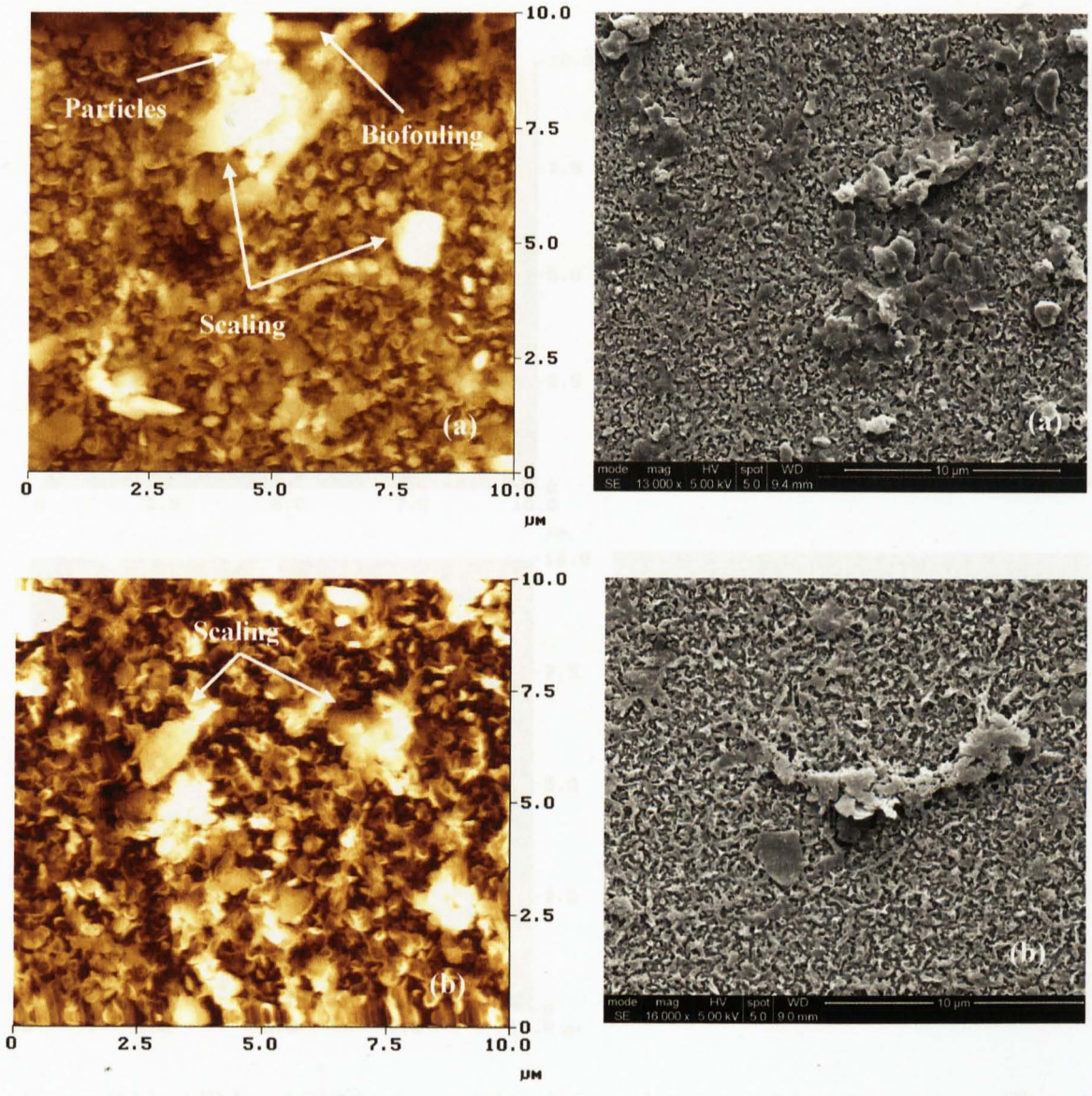

Figure 7.10: AFM and SEM micrographs of seawater pre-filtered through 5μm filter (a) and 1μm filter (b).

However, AFM and SEM images of a membrane receiving seawater pre-filtered through the nano-alumina filter and through 1 μm followed by a nano-alumina filter (Figure 7.11a and b) showed some scaling with a little difference from the new membrane surface.

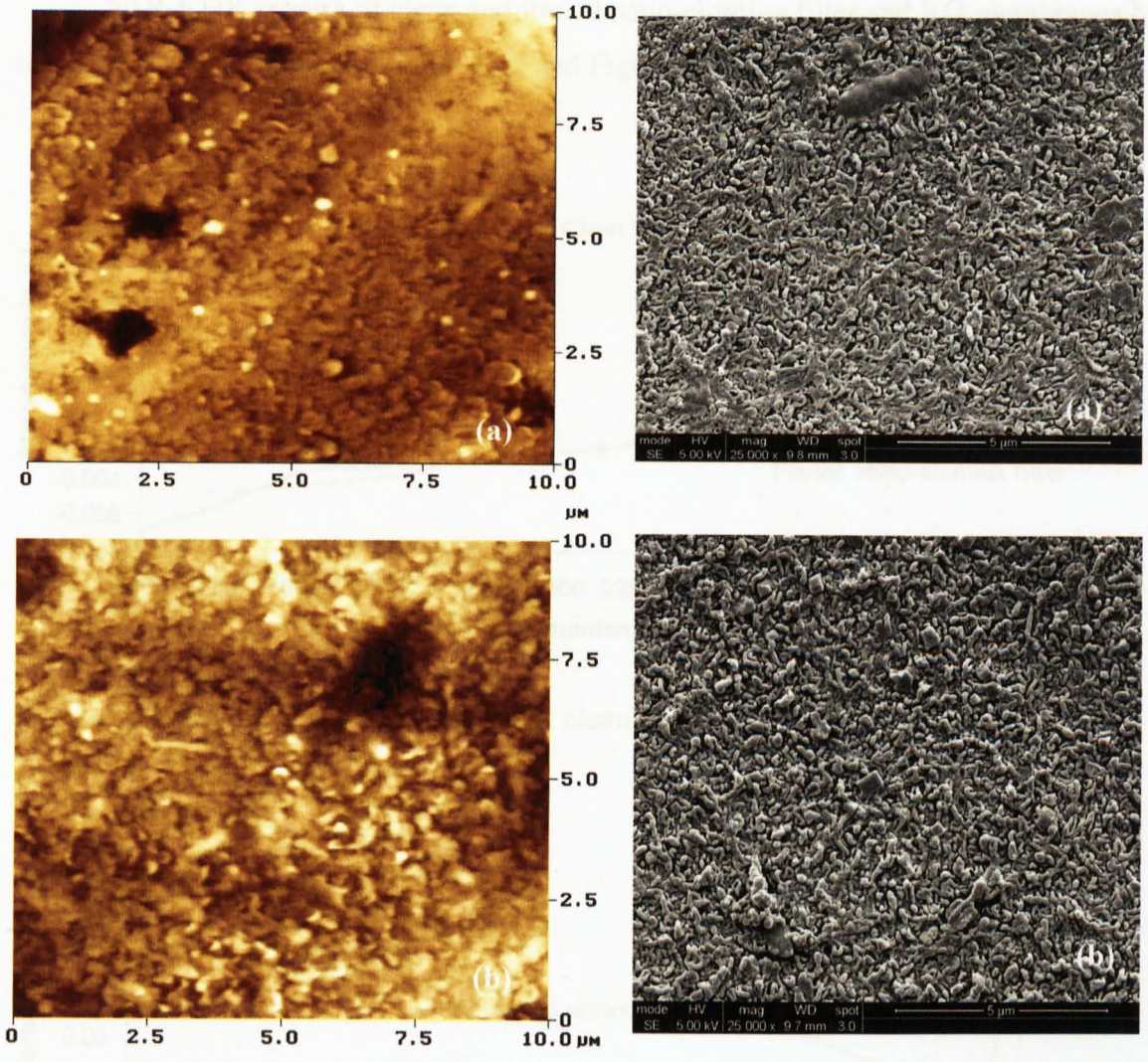

Figure 7.11: AFM and SEM micrographs of a membrane receiving seawater pre-filtered through (a) nano-alumina filter (a) and through (b) 1 μm followed by a nano-alumina filter.

AFM and SEM images clearly demonstrate higher removal efficiency when using a nano-alumina filter compared to 1μm, and 5μm filters. The majority of foulants were obviously removed from the feed water and only scaling was detected. Scaling problems can be prevented by adjustment of the seawater pH using hydrochloric acid (HCl) and/or sulfuric acid (H_2SO_4).

7.3.4 ATR-FTIR Results

ATR-FTIR spectra of clean and fouled nano-alumina filter and RO membranes by raw seawater were investigated (Figure 7.12 and Figure 7.13).

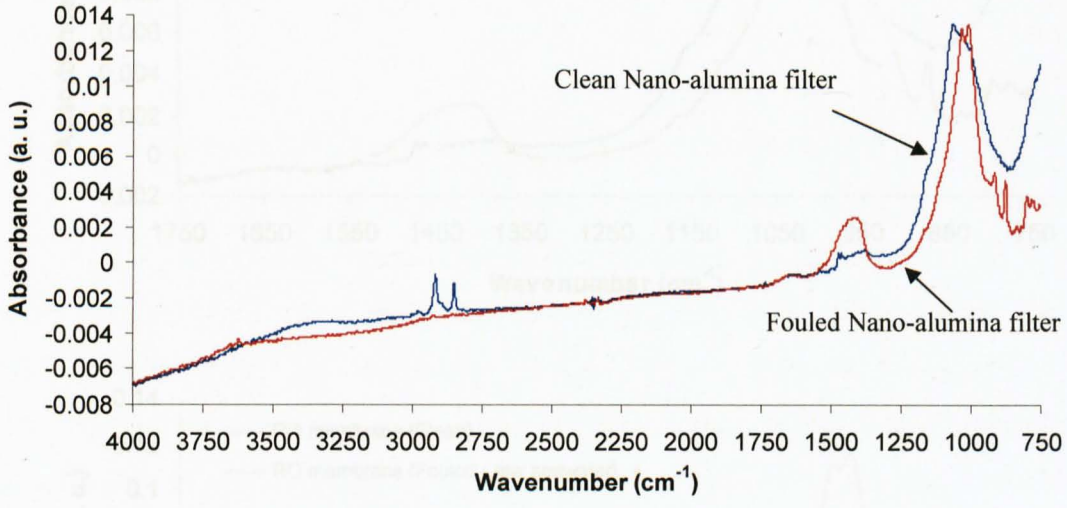

Figure 7.12: FTIR spectra of clean and fouled nano-alumina filter.

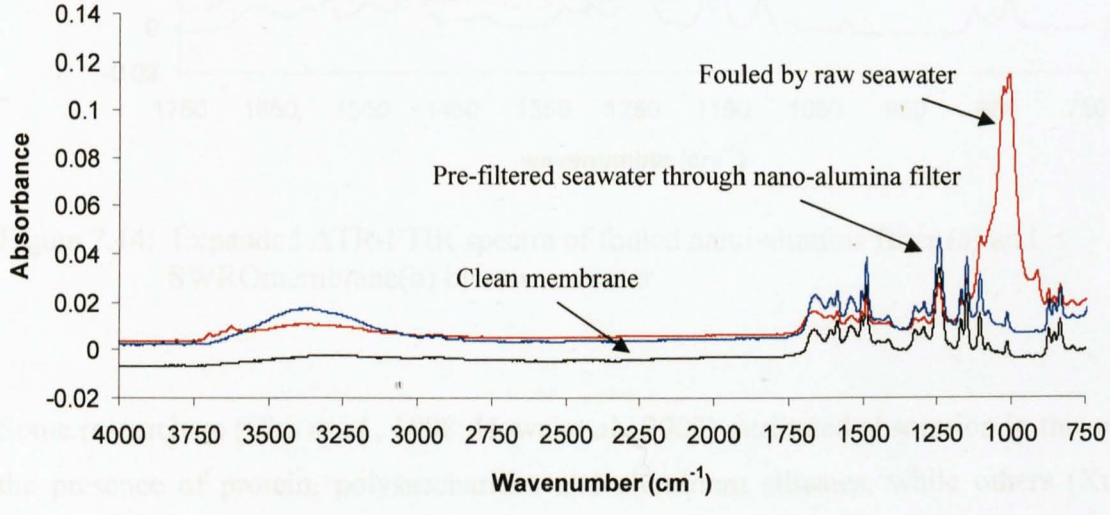

Figure 7.13: FTIR spectra of clean and fouled SWRO membranes

In order to determine the functional groups that are present in the fouling material expanded spectra between 1350 and 750 cm^{-1} were determined (Figure 7.14). Both spectra showed identical absorption bands at 910, 1006 and 1025 cm^{-1}.

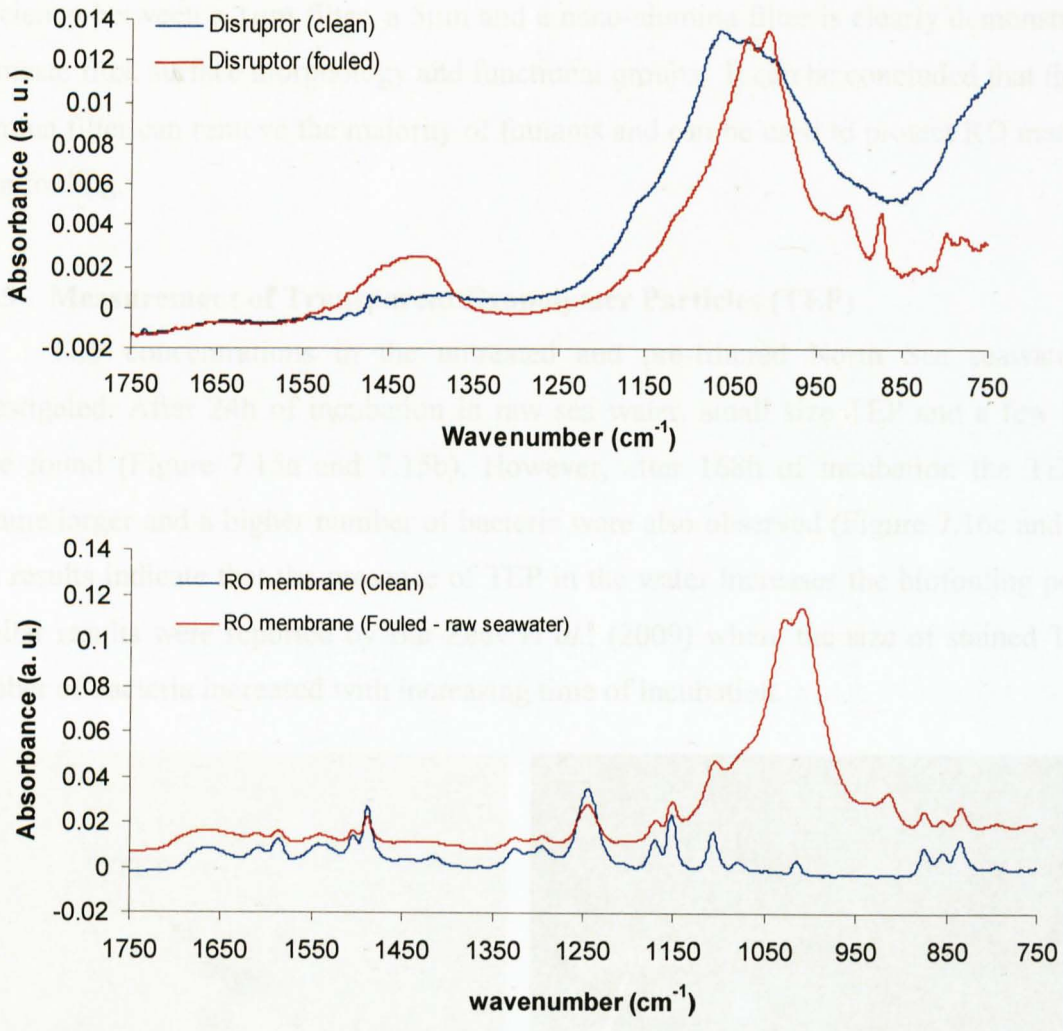

Figure 7.14: Expanded ATR-FTIR spectra of fouled nano-alumina filter (a) and SWROmembrane(b) by raw seawater

Some researchers (Cho *et al.*, 1998; Howe *et al.*, 2002) attributed absorption in this region to the presence of protein, polysaccharides and aluminum silicates, while others (Xu *et al.*, 2006; Schmitt *et al.*, 1998; Amy, 2006) attributed these absorption bands to polysaccharides and silicate colloids. The presence of these absorption bands indicates the colloidal and biofouling nature of fouling material. Cho *et al.*, (1998) reported that presence of polysaccharides or polysaccharides-like substances reduces contact angle and membrane negative charge. AFM, ATR-FTIR and contact angle results strongly support these findings. Fouling materials and absorption band peaks were not seen in the AFM images and spectrum

of seawater pre-filtered through a nano-alumina filter. The substantial difference in removal efficiency between a 1μm filter, a 5μm and a nano-alumina filter is clearly demonstrated by permeate flux, surface morphology and functional groups. It can be concluded that the nano-alumina filter can remove the majority of foulants and can be used to protect RO membranes from fouling.

7.3.5 Measurement of Transparent Exopolymer Particles (TEP)

TEP concentrations in the untreated and pre-filtered North Sea seawater were investigated. After 24h of incubation in raw sea water, small size TEP and a few bacteria were found (Figure 7.15a and 7.15b). However, after 168h of incubation the TEP areas became larger and a higher number of bacteria were also observed (Figure 7.16c and 7.16d). The results indicate that the presence of TEP in the water increases the biofouling potential. Similar results were reported by Bar-Zeev *et al.,* (2009) where the size of stained TEP and number of bacteria increased with increasing time of incubation.

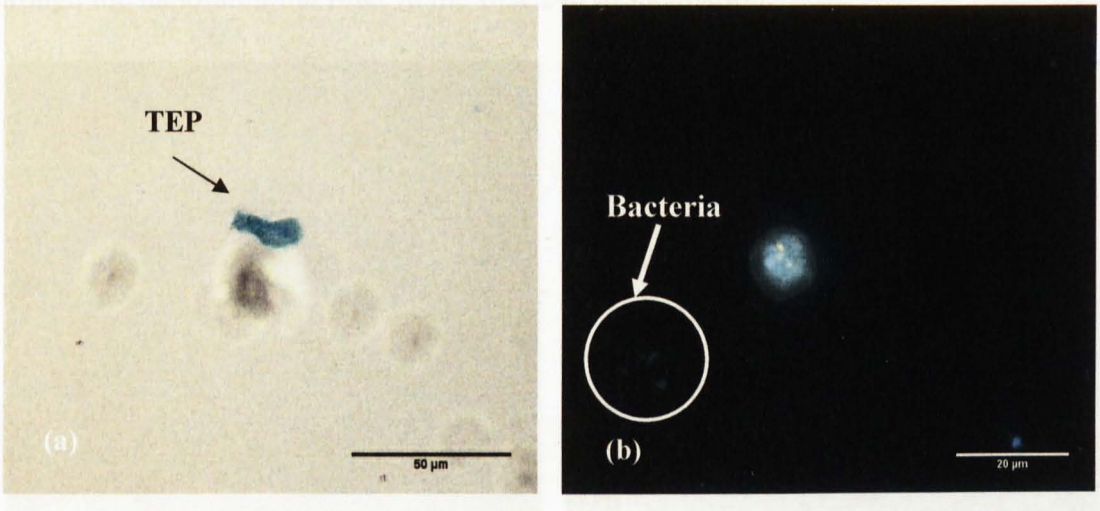

Figure 7.15: TEP and bacterial growth on after 24 h of incubation in North Sea seawater.

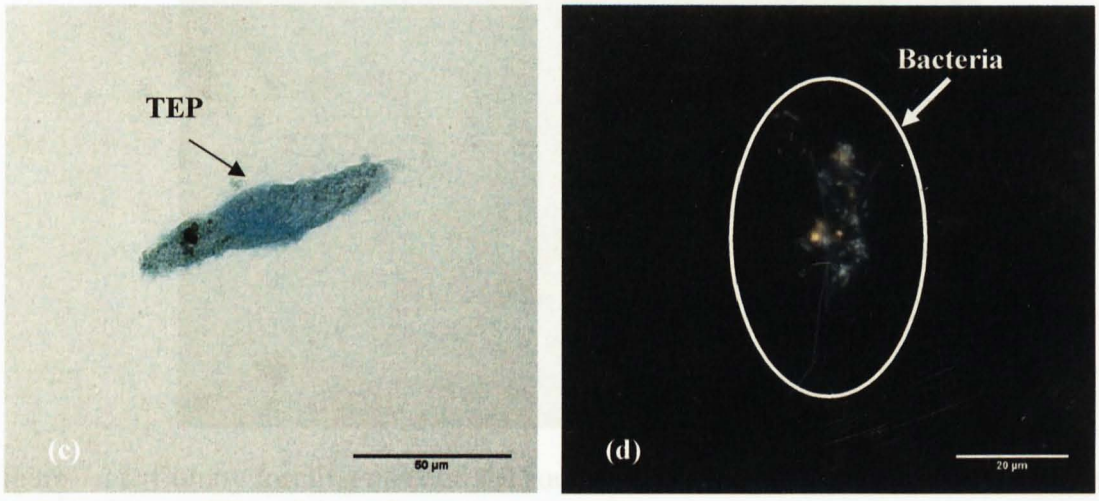

Figure 7.16: TEP and bacterial growth after 168 h of incubation in North Sea seawater.

The results of pre-filtered seawater through the nano-alumina filter showed TEP particles with smaller sizes (Figure 7.17). No bacteria cells were detected in the seawater pre-filtered through the nano-alumina filter in the first 24h of incubation.

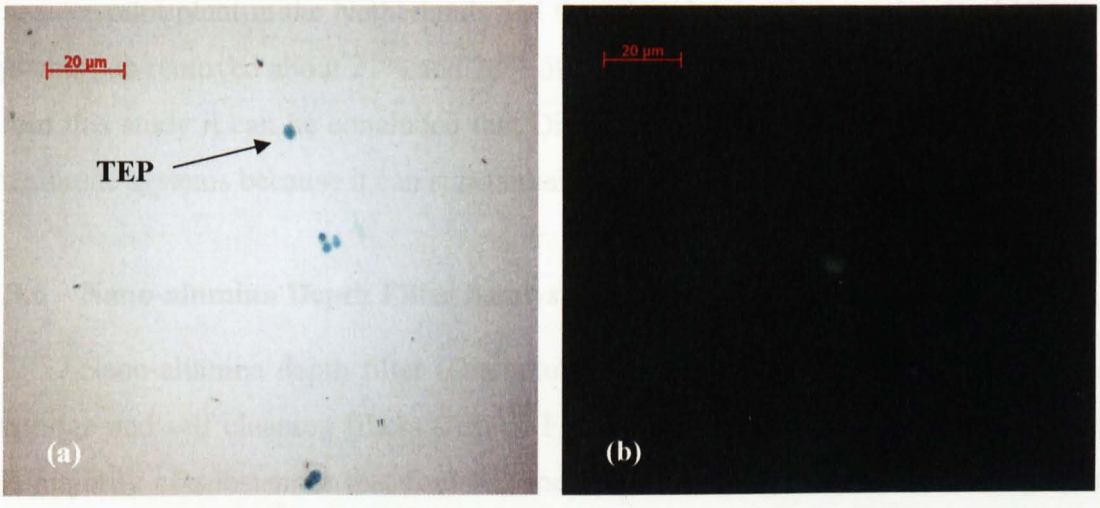

Figure 7.17: TEP after 168 h of incubation in sea seawater pre-filtered through nano-alumina filter.

A few cells were observed on the glass slide after 168h of incubation. The preliminary results showed that the nano-alumina filter has capability to remove up to 80% of TEP particles. Similar results were obtained using the plate count method where a few colonies were observed on the surface of the R2A medium after one week incubation (Figure 7.18).

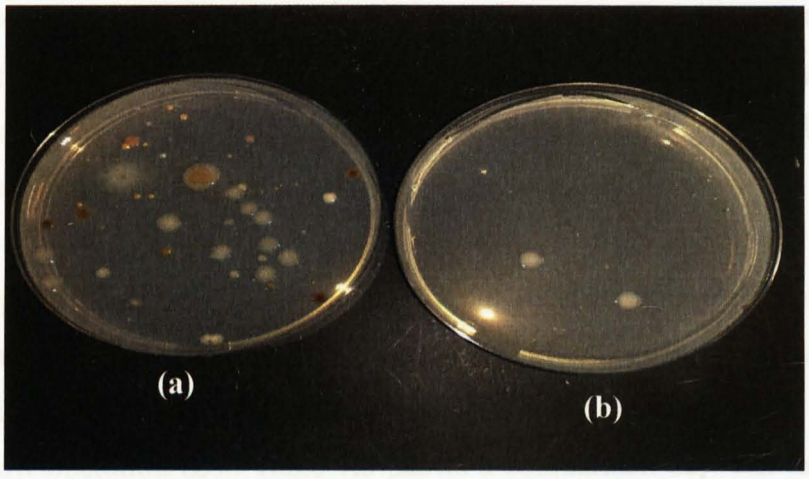

Figure 7.18: Colony forming units on the surface of R2A agar, (a) raw seawater, (b) seawater pre-filtered through nano-alumina filter.

Bar-Zeev *et. al.*, (2009) investigated the removal efficiency of sand filters and 5 micron cartridges filters at Adom Desalination Plant, Ashkelon in removing of TEP from seawater, they found that the concentration of TEP did not decrease after sand filters and cartridge filters, while and Villacorte *et al.*, (2009) monitored the TEP concentration in UF-RO seawater pilot plant in the Netherlands and they found that micro-strainer and UF membrane systems can removed about 21% and 28% of TEP respectively.

From this study it can be concluded that Disruptor™ media is a good pre-treatment for RO membrane systems because it can substantially reduce the severity of fouling.

7.3.6 Nano-alumina Depth Filter Analysis

Nano-alumina depth filter (Disruptor™) can be a more effective pre-treatment than cartridge and self cleaning filters (Amiad Filters) because they have a capability to remove the majority of substances that foul RO membranes. Commonly used cartridge filters can remove particles bigger than 5 μm. Self cleaning filters are used to remove sand and protect cartridge filters from blocking. However, both the cartridge and self cleaning filters have limitations in removing small colloids and dissolved contaminants which are responsible for colloidal and biological fouling.

Microfiltration (MF) and ultrafiltration (UF) membranes are widely used as pre-treatment for RO membranes and their removal efficiency is much better than cartridge and self cleaning

filters. They can remove particles down 0.01 μm, however the will not remove dissolved organics, phosphate and dissolved metals that can foul RO membranes. MF, UF and Self cleaning filters require frequent backwashing and chemical cleaning which both increase the operation and maintenance costs.

The removal performance of fouling materials by the nano-alumina filter is many times better than the cartridge filters and self cleaning filters. Nano-alumina filter provides filtration efficiency similar to MF and UF membranes and can protect RO membrane from fouling with low operation cost. Table 7.3 shows a comparison between the cartridge filter (6.5cm × 100cm), self cleaning filter and nano-alumina filter.

Table 7.3: Comparison between the cartridge filters, self cleaning filters and nano-alumina filter.

Parameter	**Cartridge filters**	**Self cleaning filters**	**Nano-alumina filter**
Flow rate ($L.min^{-1}$)	8.5 ($L.min^{-1}$)	417 $L.min^{-1}$	40 ($L.min^{-1}$)
Operating pressure (bar)	1 – 5	1 – 10	1 – 5
Filtration Size	6.38cm × 102cm	465 cm^2	6.38cm × 102 cm
Maximum working temperature (°C)	82	80	> 100
Pore size (μm)	20 – 1.0	40 – 2.0	2.0
Filtration Mechanism	Sieving	Sieving	Adsorption and mechanical entrapment
Materials	Polypropylene	Polyester	Nano-alumina fibres
SDI	>3	>3	<2
Reducing of fouling	low	low	high
Removal of dissolved metals	No	No	Yes
Regeneration	Disposable	Backwashable	Disposable
Operating cost	low	high	low

7.4 Summary

Nano-alumina filter (Disruptor™) as novel pre-treatment technology was applied in this study. The removal efficiency of nano-alumina filter was investigated using laboratory-scale

fouling experiments. Results showed that the nano-alumina filter media can remove the majority of substances responsible for fouling SWRO membranes. Clean water sample and membrane surface were obtained after using nano-alumina filter media as pre-treatment prior to RO membrane. High and stable permeate flux was observed after filtering untreated seawater through nano-alumina filter media. Contact angle, SEM, AFM and ATR-FTIR results demonstrated that the nano-alumina filter can substantially reduce membrane fouling.

Recent studies show that transparent exopolymer particles (TEP) are abundant in most seawater and fresh water sources and they van initiate and enhance organic and biological fouling in membrane systems. The role of TEP in biofouling and biofilm development was investigated by measuring the TEP concentration in raw and pre-filtered seawater through nano-alumina filter. TEP colonized with high number of bacteria were found on glass slides after 168h incubation in untreated seawater, indicating the involvement of these particles in the development of biofouling. However, it was found that the nano-alumina filter media can remove about 80% of these particles. From this study, it can be concluded that the nano-alumina filter can substantially reduce the severity of fouling and biofilm precursors in SWRO membrane systems. Recent studies showed that conventional pre-treatment as well as UF membranes have limitations in removing TEP particles.

The results of this study show the significant reduction of SWRO membrane fouling on a lab scale. From the obtained results it can be concluded that nano-alumina filter provides an excellent solution to safety filtration prior to RO membranes because of its high removal efficiency and lower cost because it does not need any backwashing or chemical cleaning as MF, UF membranes and backwashable filters. However, pilot plant or full scale testing is necessary to quantify the commercial benefits to be obtained by reducing fouling through the use of nano-alumina filter media. Such benefits would include: reduced energy cost, increased flux rates and reduced chemical and maintenance costs. Large scale testing would also produce membrane life data as an outcome of reduced fouling and cleaning of the RO membranes.

CHAPTER 8
DISCUSSION AND CONCLUSIONS

The previous chapters have answered the objectives proposed in Chapter 1 as follows:

1. To evaluate the performance of the pre-treatment and the SWRO membrane systems at the Tajoura SWRO desalination plant using conventional *in-situ* fouling monitoring methods and theoretical standardisation methods and to relate these methods to the types of fouling. This objective has been covered in Chapter 4.
2. To characterise membrane fouling of the SWRO membrane systems by carrying out a destructive study (membrane autopsy). This has been addressed in Chapter 5.
3. To investigate the effect of the composite fouling on the performance of SWRO membranes and its morphology in the absence of pre-treatment using raw seawater. This has been descried in Chapter 6.
4. To apply a novel pre-treatment method in order to investigate possible improvements of SWRO plant performance. This has been answered through Chapter 6 and Chapter 7.

8.1 Performance Evaluation of Pre-Treatment and Reverse Osmosis Membrane Systems of the Tajoura SWRO Desalination Plant

Monitoring pre-treatment and RO membrane systems for fouling potential is necessary to evaluate their performance. The pre-treatment systems of the Tajoura SWRO desalination plant were evaluated based on the measurement of SDI and biological growth in the raw and pre-treated seawater. Results show that the average SDI value of 3.4 was acceptable according to the membrane manufacturer recommendations. However, with this SDI value a colloidal fouling is expected to occur even with low SDI values (i.e., SDI<1), unless an efficient pre-treatment is used. Despite the importance of SDI for the design and operation of RO membrane processes (Mosset *et al.*, 2008), some researchers (Coules *et al.* 2008; Boerlage *et al.* 2002) pointed out that SDI does not provide any information regarding the nature of the foulants passing through a 0.45 μm filter and the potentials of biofouling occurrence. Boerlage *et al.* (2003) recommended using a modified fouling index with ultrafiltration membrane (MFI-UF) as an alternative to SDI. However, even with their

limitations in predicating type of fouling, turbidity and SDI are still widely used to measure fouling potential in RO desalination plants.

Scaling calculations showed that the S&DSI value was negative and $CaCO_3$ scaling would not occur. Biological growth was higher in the pre-treated seawater than that for raw seawater which indicates that biofouling was most likely has occurred in the RO membrane systems. In similar study Dudely and Darton (1996) found that the bacterial counts were zero in the feed water prior to the cartridge filters but had increased to a significant level just before entering the RO membranes. The biological fouling potential was monitored using the standard plate count. The theory is that the lower the number of viable bacteria in RO feed water, the lower the biofouling potential. In this study the total plate count results indicated that higher biological growth has occurred in the pre-treated seawater compared to the raw seawater. The high biological growth down stream to the cartridge filters can be attributed to various reasons including, biodegradation of anti-scalant (Boerlage *et al.*, 2000) and contamination of the pipeline downstream at the cartridge filters, which may lead to a biofilm development and consequently fouling occurrence in RO membranes (Huiting and Bosklopper, 2001).

A comparative evaluation of two spiral wound SWRO membrane units were carried out. Operating data for a period of 360 days were collected and analysed. The actual permeate concentration and differential pressure values have showed a noticeable deterioration in the performance of both membrane systems after four months of operation, while the permeate flow and recovery were maintained constant. Water and salt permeability results also showed a slight decrease in water permeability and a significant increase in salt permeability after 360 days of operation.

ASTM and HSDM standardisation methods and the normalisation software packages used were useful tools for evaluating RO membrane performance. Manual mathematical calculations and software normalisation methods showed a similar pattern, in which the normalised permeate flow was higher than the designed values in the first five months of

operation, followed by a decrease of about 14% and 7% for Fluid Systems and Toray membrane units, respectively.

The ASTM and HSDM mathematical methods and ROSA normalisation software showed similar results in which the normalised salt passage has gradually increased over operating time. The ROdata software showed a significant decrease in the normalised salt passage during the first six months followed by a gradual increase. This decrease can be explained for that the average feed – concentrate concentration value was not used in the calculation of normalised salt passage.

The ASTM method, ROSA and ROdata software exhibited some limitations, possibly due to the effect of temperature change on salt passage which was not taken in consideration. Therefore, the ASTM method and the normalisation software could not predict the real performance, especially when the RO membrane system was heavely fouled by combined and composite fouling. Whilst, the HSDM method was more accurate in predicting salt passage as it considers parameters that can clearly evaluate membrane performance. In conclusion, all standardisation methods have exhibited limitations in determining the true identity of fouling. These results can be attributed to the normalisation methodology being used was less accurate as well as this practice was only used to know when chemical cleaning should be applied.

Despite the use of these fouling monitoring methods as standard procedures for evaluation of RO plant performance, these methods have limitations in accurately predicating either colloidal or biological fouling. However, to accomplish this purpose, a destructive membrane autopsy had to be conducted.

8.2 Fouling Characterisation of Two Commercial Seawater Reverse Osmosis Membranes: A Case Study

Identifying the causes and types of fouling that deteriorate the performance of RO membranes require a destructive study (autopsy) of one or several RO membrane elements. It is essential to select the appropriate equipment for analysis. In this study, membrane

autopsies were carried out on two commercial SWRO membranes in order to determine the identity of foulants that cause performance deterioration. The autopsy process included visual inspection, lengthways opening, sampling and analysis. Visual inspection of the unrolled SWRO membranes revealed that heavy brownish – reddish foulants on both membrane surfaces and feed spacers is exist. The deposits on both membranes are predominantly amorphous in nature and could easily be removed by swabbing and scrapping. Butt *et al.* (1997), who observed similar phenomena, reported that the fouling material has been deposited on the membrane surface rather than formed by a precipitation mechanism.

There was no evidence that any slimy deposit arises on the surface of either membrane, possibly because the biofilm is stable as the average bacterial count was 10^4 cfu.cm^{-2}. This observation indicated that both membrane elements had biofouling. Darton *et al.* (2004) stated that the performance of RO membrane systems would not be affected if the bacterial count remains below 10^4 cfu.cm^{-2}, because the biofilm has being stable and many plants work satisfactory. However, when bacterial counts exceed 10^5 cfu.cm^{-2}, membranes are considered being biofouled and the biofilm produces sufficient polysaccharides to become problematic to RO membrane operation. This finding was also supported by the amount of organic matter present in the fouling material, since the biofouled membrane organic content exceeds 70% of the total deposit (Al-Amoudi *et al.*, 2005; Baker and Dudely, 1998).

Loss on ignition results showed that the scraped fouling material from both membranes contains organic matter of about 61.5 ± 2.1% and 58.2 ± 2.7%, respectively. Acid digestion revealed high concentrations of iron (Fe), aluminum (Al) and silicon (Si) in the fouling materials of both membranes indicating the formation of aluminum silicate fouling and iron hydroxide. In similar study, Butt *et al.*, (1997) attributed the high concentration of Al, Ca and Si to the presence of complex calcium alumino silicate clays which are too fine to be retained by the 5 μm cartridge filters.

AFM and SEM results showed thick fouling layer and confirmed the formation of scaling, colloidal fouling and biofouling on the surface of both membranes, which deteriorate the performance of RO membrane units in the plant. Similarly, the EDX spectra of both

examined membranes were also in conformity with the chemical analysis. Deposits on the surfaces of both membranes were similar in composition, consisting mainly of aluminum, silica, iron and calcium compounds, in addition to high carbon and oxygen levels. The calcium peak can be attributed to the calcium ions present in seawater, while silica could be originated from the silica silt in the seawater. The presence of iron in the fouling material may have originated from the corrosion of high pressure pumps and stainless steel pipes of RO systems. Al-Amoudi *et al.* (2005); Gabelich *et al.* (2002) and Tran *et al.* (2007) carried out a membrane autopsy and found similar phenomena. They attributed the high level of aluminum and silica to aluminum silicates, which are common foulants in RO operations. The concentration of silica and aluminium was slightly high in RO feed water thus, colloidal aluminium silicates was highly expected to be formed on both membrane surfaces. In a similar study, Gabelich *et al.* (2002) reported that aluminium silicate fouling forms even at low concentrations of silica (~10 $mg.l^{-1}$ as silica) and aluminium (>0.05 $mg.l^{-1}$ aluminium).

The FTIR spectra showed peaks at 1038, 930, 1570 and 1640 cm^{-1} in the examined fouled RO membranes. The obtained results indicated that the fouling materials are mainly consist of polysaccharides, hematite and/or aluminum silicate and proteins. Cho (1998) attributed the FTIR absorption in this region to the presence of polysaccharides, while in another study, Howe *et al.* (2002) referred it to the absorption to silicate impurities. Xu *et al.*, (2006); Yang *et. el.* (2008); Schmitt *et. el.* (1998) reported that the absorption in this region iwas due to the polysaccharides, aluminum silicate and colloids.

The XRD results suggested that $CaCO_3$ crystals were clearly formed on both membranes surfaces in the form of calcite and possibly aragonite. According to the scaling calculations results, it was found that the Stiff & Davis saturation index (S&DSI) was negative and $CaCO_3$ scaling did not occur. However, $CaCO_3$ scaling presence in the form of calcite and aragonite was due to the presence of organic matter and magnesium in the RO feed water. Organic matter and magnesium normally influence much on the calcium carbonate precipitation (Falini, 1994; Loste, 2003; Pavez, 2005). The AFM and SEM results also supported the presence of $CaCO_3$ on the surfaces of both membranes. On the other hand, $CaSO_4$ (Gypsum) scale would not be expected to occur on the first stage RO membranes due

to the low recovery (35%) maintained, as the mechanism of gypsum precipitation is highly depend on the supersaturation. The AFM, SEM, EDX, ATR-FTIR and XRD examinations also provided valuable information about fouling that cause the membrane failure. It can be also concluded that NaOH, Na-EDTA and HCl could be effectively used to remove scale, colloids and biofouling, and within limitations can restore the flux back to baseline conditions.

8.3 Effect of Composite Fouling on the Performance of Seawater Reverse Osmosis Membrane

The effect of composite fouling on permeate flux and salt rejection with the help of AFM, SEM imaging and EDX elemental analysis was investigated by carrying out a set of laboratory – scale cross flow filtration tests using raw seawater. In this experimental work, two types of raw seawater were used (the Mediterranean Sea and the North Sea). Permeate flux and salt passages were measured over time under similar operation conditions. Both seawater samples resulted in a rapid accumulation of foulants on the membrane surfaces, which in turn caused a permeate flux decline of 48% and 30% for the Mediterranean Sea and the North Sea samples, respectively. The permeate flux behaviour of both seawaters samples indicated a formation of a combined and/or a composite fouling, possibly due to cake layer formation, has occurred at elevated pressures, as well as at high solute concentrations. The complexity of the seawater composition and different fouling types and their different formation mechanisms made the characterisation of the resulting fouling more difficult.

Higher salinity has an impact on the permeate flux and the salt passage due to increasing of concentration polarisation and osmotic pressure near the membrane surface. The obtained results showed that the salt rejection values have slightly decreased by the end of the filtration runs, probably due to the increased concentration polarisation and/or cake layer formation near the membrane surface. AFM and SEM examinations clearly showed formation of a severe fouling layer which consists of scaling, colloids and bacteria. The new membrane has a rough surface with valley. This structure increases the accumulation of foulants on the membrane surface and the valleys could become quickly clogged. The higher negative zeta potential and hydrophilicity of RO membrane should result in less fouling due

to higher electrostatic repulsion and lower hydrophobic interaction between the foulants and the membrane surface. However, high fouling rate can be attributed to rough membrane surface, which increases the resistance to flow and causes a rapid loss of permeate flux. Vrijenhoek *et al.* (2001) and Li *et al.* (2007) reported similar findings in which RO membranes with rough surfaces and valleys become rapidly clogged and result in significant losses in permeate fluxes. On the other hand, for the RO membranes with smooth surfaces, they found that no decline on permeate flux was observed before a thick cake layer was formed.

The FTIR spectra showed peaks at 1038, 930, 1570 and 1640 cm^{-1} for the fouled RO membranes examined. Cho (1998) attributed the presence of the FTIR absorption in this region to the presence of polysaccharides within the fouling materials, while Howe *et al.* (2002) referred it to the absorption of the silicate impurities. The EDX obtained results were completely consistent with ATR-FTIR, and both clearly identified the presence of silica, aluminium and polysaccharides in both seawater samples. It also indicates that the fouling materials consist of polysaccharides, hematite and/or aluminum silicate and proteins. In a similar study, Gabelich *et al.* (2002) stated that the presence of Al and Si in the feed water has caused deposition of colloidal aluminium silicates on the membrane surface, even when these elements are present at very low concentrations (~1-$mg.l^{-1}$ as silica and >0.05 $mg.l^{-1}$ aluminium).

The presence of excess oxygen in the fouling materials indicated the presence of organic fouling. Thus the fouling materials of both raw seawater samples contain organic, inorganic and biological materials, which eventually led to composite fouling in both membranes examined.

8.4 Prevention of SWRO Membrane Fouling using Nano-alumina Depth Filter (Disruptor^{TM})

A novel pre-treatment technology was investigated in this study. The removal efficiency of cartridge filter made of nano-alumina was investigated using laboratory-scale fouling

experiments. The obtained results showed that this "Disruptor^{TM}" media has capability to remove the majority of substances responsible for fouling of SWRO membranes. Clean water samples and clean membrane surfaces were observed when this media filter was used as a pre-treatment prior to RO membranes.

A slight decrease in the contact angle was observed in the fouled RO membrane treated by raw seawater. Decrease of contact angle of the fouled membrane indicated the hydrophilic nature of the fouling materials on the membranes examined. The presence of natural organic matter (NOM) in the treated water may decrease (hydrophilic) or increase (hydrophobic) contact angle. Che *et al.* (1998) and Park *et al.* (2006) have reported similar results, which are the hydrophobic organic components caused an increase in the contact angle and reduced the membrane surface charge. Contrarily, the presence of polysaccharides or polysaccharides-like subastances would foul the membrane and reduce contact angle and membrane surface charge. Similar findings were reported by Combe *et al.* (1999), who found that the presence of large molecular weight polysaccharides and proteins in treated water have caused a significant membrane fouling. The ATR-FTIR spectra of the fouled "Disruptor^{TM}" filter and the RO membrane treated by raw seawater samples support these findings. Both obtained spectra showed identical absorption bands at 910, 1006 and 1025 cm^{-1}, indicating the presence of proteins and polysaccharides in the fouling materials.

The pre-filtered raw seawater samples through the RO membranes exhibited gradual flux decline, possibly due to the accumulation of organic, inorganic and microbial materials on the membrane surface. This in turn, caused a large hydraulic resistance to flow and eventually resulted in a rapid flux decline. However, high and stable permeate flux was observed after filtering the untreated seawater samples through the "Disruptor^{TM}" filter media. Also, the permeate flux results showed that using "Disruptor^{TM}" filter as pre-treatment technique has remarkably improved the performance of RO membranes.

The SEM results showed depositions of a thick fouling layer on the surface of the "Disruptor^{TM}" filter containing scaling, colloids and microorganisms. Whilst, the elemental analyses by EDX showed presence of iron (Fe), aluminium (Al), silica (Si), calcium (Ca) and

potassium (K). the obtained results showed that "Disruptor^{TM}" filter media could remove large amounts of foulants which would cause flux decline and performance deterioration of RO membranes. Schneider *et al.*, (2005), analysed a foulant layer of different RO membrane elements and reported that such foulants were responsible for flux decline and low membrane performance. Dudely and Darton (1996) carried out membrane autopsies and stated that colloidal fouling, iron fouling, and biological fouling were the major foulants that deteriorated the performance of RO membranes. Thus, removing these foulants from treated water using "Disruptor^{TM}" filter media, would result in higher removal efficiency of various foulants and producing high quality per-filtered water and to protect RO membranes from fouling.

The types of foulants that cause permeate flux decline of RO membrane were determined by investigating the surface morphologies of both clean and fouled RO membranes using SEM and AFM. It was observed that the clean RO membrane has a rough surface with valley. However, these valleys were filled by foulants and changed the membrane surface morphology. Similar studies (Freger *et al.*, 2002; Cho *et al.*, 1998) reported that membrane surface roughness increases membrane fouling by increasing the rate of particle and colloid attachment onto the membrane surface. In similar study, Vrijenhoek *et al.*, (1991) found that more particles are deposited on rough membrane surfaces than on smooth surfaces and caused fast clogging and severe flux decline.

AFM images of membrane surfaces exposed to seawater filtered through 5μm filter showed clear deposition of scaling, bacteria and clusters of packed particles and/or colloids, while the 1μm filtered samples showed deposition of scaling and colloid like materials. However, AFM and SEM images of a membrane treating seawater pre-filtered through the "Disruptor^{TM}" media and through the 1 μm filter followed by a "Disruptor^{TM}" only show some scaling with a clear surface appearance almost similar to the new membranes surface. Precipitation of $CaCO_3$ scaling on the membrane surface could be attributed to increasing of salt concentration near the membrane surface. The membrane autopsy results showed that the AFM and SEM images clearly demonstrated the high removal efficiency of the "Disruptor^{TM}" media compared to 1μm, and 5μm filters. The majority of foulants were

obviously removed from the feed water and only scaling was detected which could be also avoided by the adjustment of the seawater pH using hydrochloric acid (HCl) and/or sulfuric acid (H_2SO_4).

Recent studies showed that the transparent exopolymer particles (TEPs) are abundant in both seawaters and fresh waters and these materials can initiate and enhance organic and biological fouling in membrane systems. The role of TEP in biofouling and biofilm development was investigated by measuring the TEPs concentration in raw seawater and seawater pre-filtered through "Disruptor^{TM}" media. TEPs, colonised with high numbers of bacteria, were found on glass slides after 168 h incubation in untreated seawater. However, the "Disruptor^{TM}" filter media removed up to 80% of these particles from raw seawater. Recent studies (Bar-Zeev *et. al.*, 2009; Villacorte *et al.*, 2009) showed that conventional pre-treatment, micro-strainers as well as UF membranes could not adequately remove TEPs from seawater.

The results of this study clearly showed that a significant reduction in SWRO membrane fouling could be achieved using "Disruptor^{TM}" filter. Based on obtained results, using of "Disruptor^{TM}" filter as pre-treatment prior to RO membranes would increase flux rate, reduce chemical cleaning and energy consumption. However, pilot plant or full scale tests are required to validate the application of this novel pre-treatment technique.

8.5 Conclusions

Based on the results of this research study, the following conclusions could be drawn:

- The performance of the pre-treatment and RO membrane systems of the Tajoura SWRO desalination plant were evaluated based on the measurement of SDI, biological growth and scaling potentiality in the raw and pre-treated seawater. The obtained results showed that the average SDI value of 3.4 was acceptable according to the membrane manufacturer recommendations. However, with this SDI value, fouling would possibly occur at the Tajoura plant because of cessation of FeCl dosing used as a coagulant. Scaling calculations showed that both S&DSI and IP are negative and $CaCO_3$ scaling wiould not occur in the membrane systems at the Tajoura plant.

The biological growth was higher in the pre-treated seawater than that for the raw seawater, which indicated a possible formation of biofouling in the RO membrane systems. Also, a potential of organic fouling would be occur, despite the hydrophilicity of the natural organic matter present in the RO feed water (low humic content).

- The analysis of the reported operating data for a period of 360 days showed a noticeable deterioration in the performance of both Fluid Systems and Toray membrane systems used at the Tajoura desalination plant after four months of operation under a maintained permeate flow and recovery conditions. Similarly, the calculated water and salt permeability coefficients also showed a slight decrease in water permeability and a significant increase in salt permeability at the end of the operation period (e.g. 360 days).

- The mathematical and the software standardisation methods exhibited identical patterns, in which the normalised permeate flow was slightly higher than the designed values during in the first five months of operation, followed by a decrease by about 14% and 7% for Fluid Systems and Toray membrane units, respectively. The ASTM and HSDM mathematical methods, and ROSA normalisation software also showed similar results in which the normalised salt passage has gradually increased over operating time. The ROdata software clearly showed a significant decrease in the normalised salt passage during the first six months of operation, then it increased gradually.

- The application of the ASTM method, ROSA and ROdata software experienced some limitations, possibly due to the effect of temperature change on salt passage, which was not taken in consideration. Therefore, the ASTM method and the used normalisation software package could not predict the real performance of the plant, especially when the RO membrane system experienced a severe fouling. The applications of HSDM method could be more accurate in the prediction of salt passage as it considers all of the parameters that can clearly influence the membrane

performance. It can also be concluded that the standardisation methods used had limitations in determining the true identity of the fouling developed and this could only be achieved by conducting a destructive membrane autopsy.

- The AFM results revealed the membrane surfaces were covered by a thick fouling layer. ATR-FTIR investigations showed peaks at 1038 and 930 cm^{-1} in the fouled RO membrane corresponding to polysaccharides, hematite and silicate. The XRD results suggested that, the formation of $CaCO_3$ crystals on the surfaces of both membranes studied was in the form of calcite and aragonite.

- Acid digestion results showed high concentrations of iron and aluminium in the fouling materials for both membranes, which indicated a formation of both aluminium silicate and iron hydroxide fouling in both membranes.

- The application of NaOH, Na-EDTA and HCl, as cleaning agents could effectively remove scale, colloids and biofouling, but thses chemicals failed to restore the flux back to the baseline conditions as fouling was quite heavy.

- The removal efficiency of the pre-filter Disruptor™ used to remove substances responsible for fouling SWRO membranes, was investigated. The results showed that the Disruptor™ filter could substantially reduce the RO membrane fouling. A high and stable permeate flux was observed when filtering the raw seawater through the Disruptor™ filter ahead to the RO membrane.

- The contribution of TEPs in biofouling and biofilm development was also investigated. Large sizes of TEPs particles, colonised with high number of bacteria, were found after 168 h of incubation in untreated seawater, indicating the involvement of these particles in the development of biofouling. However, it was found that the Disruptor™ media could efficiently remove up to 80% of TEP materials.

- From this study, it could easily be concluded that the Disruptor^{TM} can substantially reduce the severity of fouling and biofilm formation in SWRO membrane systems.

8.6 Recommendations and Future Work

According to the obtained results, the following recommendations were proposed:

- Regular monitoring of pre-treatment and RO membrane systems in real time operation in order to predict fouling in its early stages.
- More comparative studies should be carried out to validate the accuracy of theoretical and software normalisation methods using real operating data from pilot or full scale RO desalination plants.
- More effective commercial cleaning agents should be applied in the Tajoura plant in order to restore the performance of fouled membranes.
- Continuous addition of $FeCl_3$ would be necessary, in order to reduce SDI values and prevent colloidal fouling in the plant. Addition of $FeCl_3$ in the intake basin could be a good practice to reduce SDI in the Tajoura plant.
- Pilot and full scale studies should be carried out in order to test the removal efficiency and to predict the long term performance of the Disruptor^{TM} filter, as well as to minimise the effect of the experimental error in order to obtain more accurate information.
- Use of back washable filters up stream to Disruptor^{TM} would achieve better long term performance and avoid the rapid membrane blocking.

REFERENCES

1. Abbas, A., and Al-Bastaki, N., (2001), Performance decline in brackish water FilmTec spiral wound RO membranes, *Desalination*, 136, 281-285.
2. Aboabbuod M and Elmasallati S, (2007), Potable water production from seawater by reverse osmosis technique in Libya, *Desalination,* 203, 119-133.
3. Abufayed, A. A, (2003) Performance characteristics of a cyclically operated seawater desalination plant in Tajoura, Libya, *Desalination*, 139, 131 - 132.
4. Al-Ahmmad, M., Abdul Aleem, F. M., Mutiri, A., and Ubaisy, A., (2000), Biofouling in RO membrane systems Part1: Fundamentals and control, *Desalination*,132, 173-179.
5. Al-Amoudi, A. S., and Farooque, A. M., (2005). Performance restoration and autopsy of NF membranes used in seawater pre-treatment, *Desalination,* 178, 261-271
6. Al-Bastaki, N. M. and Abbas, A., (2004), Long-term performance of an industrial water desalination plant, *Chemical Enginering and Processing* 43, 555-558.
7. Al-Bastaki, N. M. and Abbas, A., (1999), Improving the permeate flux by unsteady operation of a reverse osmosis desalination unit *Desalination,* 123, 173-176.
8. Al-Bastaki, N. M., and Al-Qahtani, H. I., (1994), Assessment of thermal effects on the reverse osmosis of salt/water solutions by using a spiral wound polyamide membrane, *Desalination*, 99, 158-168.
9. Alhadidi A., Kennedy M., Diepeveen A., Prummel H., Boorsma M., Shippers J. C., (2009) Scaling potential calculation using different methods, *Desalination and Water treatment,* (2009), 138-143.
10. Alldredge, A. L., Passow, U. and Logan, B. E., (1993). *Deep sea research* (Part I, Oceanographic Research Papers, 40, 1131-1140.
11. Al-Obaidani, S., Macedonio, E. C. F., Di Profio, G., Al-Hinai, H., and Drioli, E.,(2008). Potential of membrane distillation in seawater desalination: Thermal efficency, sensitivity study and cost estimation, Journal of Membrane *Science*, 323, 85-98.
12. Al-Shammiri, M., Salman, A., Al- Shammiri, S., and Ahmad, M., (2005)., Simple program for the estimation of scaling potential in RO systems, *Desalination*, 184,

139-147

13. Amy, G., (2006), Role of soluble microbial products (SMP) in membrane fouling and flux decline, *Environ. Sci. Technol.*, 40, 969 – 974.
14. APHA and AWWA(1998), Standard methods for the examination of water and wastewater. 19th edition, American Public Health Association, Washington DC.
15. Ashhuby, B. A.., (2006) Biofouling studies on reverse osmosis desalination of hypersaline waters, PhD thesis, the Unicersity of Sheffield.
16. Atkins, P. W., (2001) The elements of physics chemistry, 3rd edition, Oxford University Press.
17. Bachmann, R. T., Edyvean, R. G.J., (2006). AFM study of the colonization of stainless steel by A*quabacterium commune*, *International Biodeterioration & Biodegradation*, 58, 112-118.
18. Bahar, R., Hawlader, M. N. A., Ng K. C., and Stanley L. J., (2009). Mmebrane distillation: a potential method of desalination, EDS Conference and exhibition on Desalination for the Environment, 17-20 May 2009, Kongreshaus, Baden-Baden, Germany
19. Bar-Zee E., Frank I. B., Liberman B., Raha E., Passo U. and Berman T., (2009), Transparent exoploymer particles: potential agents for organic fouling and biofilm formation in desalination and water treatment plants, *Desalination and Water Treatment*, 3, 136 – 142.
20. Baker R. W. (2004). Membrane technology and applications, Wiley publication, second edition.
21. Baker, J. S. and Dudley L. Y., (1998), Biofouling in membrane systems-A review", *Desalination,* 118, 81-90.
22. Bartels, C., Franks R., Rybar S., Schierach M., and Wilf M., (2005). The effect of ionic strength on salt passage through reverse osmosis membranes, *Desalination*, 184, 185-195.
23. Berman T. and Holenberge M. (2005), Don't fall foul of biofilm through high TEP levels, *Filtration and Separation*, 42, (4), 30-32.
24. Beverly S., Seal S. and Hong S., (2000) Identification of surface chemical functional groups correlated to failure of reverse osmosis polymeric membranes" *J. Vac. Sci.*

Technol., 18 (4), Jul/Aug. 2000.

25. Bhattacharya, D., and Hwang S. T., (1997), Concentration Polarization, Separation Factor, and Peclet Number in Membrane Processes'' *Journal of Membrane Science* 132, 73 1997.
26. Boerlage S. F. E., Kennedy M., Witkamp G. J., Bremere I., Hoek J. P. V. and Schippers J. C., (2003). Application of the MFI-UF to measure and predict particulate fouling in RO systems, *Journal of Membrane Science*, 220, 97-116.
27. Boerlage S. F. E., Kennedy M., Witkamp G. J., Bremere I., Hoek J. P. V. and Schippers J. C., (2002), The Scaling Potential of $BaSO_4$ Sulphate in Reverse Osmosis Systems" *Journal of Membrane Science*, 197, (2002), 251-268.
28. Boerlage S. F. E., Kennedy M., Bremere I., Witkamp G. J., van der Hoek J. P., and Schippers J. C., (2000), Stable $BaSO_4$ supersaturation in reverse osmosis, *Journal of Membrane Science*, 197, (2002), 47-59.
29. Bonne P. A. C., Hofman J. A. M. H. and Hoek L. P. V., (2000). Scaling control of RO membranes and direct treatment of surface water, Proceedings of the Conference on membrane in Drinking and Industrial Water Production, Paris, France, 3-6 October 2000, Vol. 2, pages140-159.
30. Bruggen van der. B., Carlo Vandecasteele C., , Gestel, van. T. , Wim Doyen, and Roger Leysen (2003), A review of Pressure-Driven Membrane Processes in wastewater Treatment and Drinking Water Production" *Environmental Progress*, 22 No.1, 46-56.
31. Boubakri A. and Bouguecha S., (2008), Diagnostic of membrane autopsy of Djerba Island desalination station, *Desalination*, 220, 403 – 411.
32. Bonnelye V., Guey L. and Castillo J. D., (2008). UF/MF as RO pre-treatment: the real benefit, *Desalination*, 222, 59 – 65.
33. Bonnelye V., Sanx M. A., Durand J. P., Plasse L., Gueguen F., Mazounie P., (2004), Reverse osmosis on open intake seawater: pre-treatment strategy, *Desalination*, 167, 191-200.
34. Bu-Rashid K. A an Czolkoss W., (2007), pilot tests of multibore UF membranes at Addur SWRO desalination plant, Bahrian, *Desalination*, 203, 229 – 242.
35. Butt F. H., Rahman F. and Baduruthamal U., (1995) Identification of Scale Deposits

Through Membrane Autopsy, *Desalination*, 101, 219-230.

36. Butt F. H., Rahman F. and Baduruthamal U. (1997), Hollow fine fiber vs. spiral - wound RO desalination membranes Part 1: pilot plant evaluation, *Desalination*, 101, 67 – 82.
37. Chen K. L., Long L., Ong S. L. and Ng W. J., (2004). The development of membrane fouling in full-scale RO processes, *Journal of Membrane Science*, 232, 63-72.
38. Chen T., Neville A., and Yuan M., (2005). Assessing the effect of Mg^{2+} on $CaCO_3$ scale formation-bulk precipitation and surface deposition, *Journal of Membrane Science*, 275, 1341-1347.
39. Cho J., Amy G., Pellegrino J., and Yoon Y., (1998), Characterisatiom of clean and natural organic matter (NOM) fouled NF and UF membranes, and foulants characterisation, *Desalination*, 118, 101-108.
40. Cho J., Amy G. and Pellegrino J., (2000), Membrane Filtration of NOM: Factors and Mechanisms Affecting Rejection and Flux decline with Charged UF Membrane" *Journal of Membrane Science*, 164, 89-110.
41. Choules P., Schrotter J. C., Leparc J., Gaid K.and Lafon D, (2008), Reverse osmoses improved operation through experience with SWRO plants, *Ultra pure water*, 13 – 21.
42. Combe C., Molise E., Lucas P., Riley R., and Clark M., (1999), The effect of CA membrane properties on adsorptive fouling by humic acid, *Journal of Membrane Science*, 154, 72 – 87.
43. Darton E. G., and Faxell M., (2001), A statistical review of 150 membrane autopsies" Presented at the 62nd Annual International Water Conference, Pittsburg.
44. Darton T., Annunziata U., Vigo Pisano F. V. and Gallego S., (2004) Membrane Autopsy Helps to Provide Solutions to operational Problems" *Desalination*,167, 239-245.
45. Darwish B. A. Q., Abdel-Jawad M., and Alyon G. S., (1989), The standardization of performance data for RO desalination plants, *Desalination*, 74, 125 – 130.
46. Dias C. R., Rosa M J., De Pinho M. N., (1998), Structure of water in asymmetric cellulose ester membranes – an ATR_FTIR study, *Journal of Membrane Science*, 138, 259 – 267.

47. Dudely L. Y. and Darton E. G., (1996), Membrane Autopsy – A Case Study *Desalination*, 105, 135-141.

48. Duarte A. P., Bordado J. C. and Cidade M. T., (2008), Influence of the performance of cellulose acetate reverse osmosis membrane by fibers, *Journal of Applied Polymers Science*, Vol. 109, 2321-2328.

49. El-Azizi I. M. and Omran A. M (2002), Design Criteria of 10,000 m^3/d SWRO Desalination Plant of The Tajoura , Libya" *Desalination*, 153 ,273-279.

50. El-Dessouky H. T. and Ettoueny H. M., (2002) "Fundamentals of Salt Water Desalination", *Elsevier publication.*

51. Elimelech M., Xhu X., Childerss A. E and Hong S., (1997), Role of Membrane Surface Morphology in colloidal Fouling of cellulose Acetate and Composite Aromatic Polyamide Reverse Osmosis membranes, *Journal of Membrane Science,* 127, 101 – 109.

52. El-Saied H., Basta A. H., Barsoum B. N., and Elberry M. M., (2003). Cellulose membrane for reverse osmosis, Part I: RO cellulose acetate membranes including a composite with polypropylene, *Desalination*, 159, 171-181.

53. Faibish R. S., Elimelech M. and Cohen Y., (1998). Effect of interparticle electrostatic double layer interactions on permeate flux decline in crossflow membrane filtration of colloidal suspension: An experimental investigation, *Journal of colloid and interface science*, 204, 77-86.

54. Fan L., Harris J. L., Roddick F. A., and Booker N. A., (2001), Influence of the characteristics of natural organic matter on the fouling of microfiltration membranes, *Water Res.*, 35, 4455 – 4463.

55. Farooque M. A., Green T. N., Mohammed N. K., and Al-Muali F. A., (2009). Autopsy of NF membranes after 5 years of operation at the Ummlujj SWRO plant, *Desalination and water treatment*, 3, 83-90.

56. Feng D., van Devebter J. S. J., and Aldrich C., (2006). Ultrasonic defouing of reverse osmisis membranes used to treat wastewater effluents, *Separation and Purification Technology*, 50, 318-323.

57. Filmtec RO membrane (technical manual) – December – 1991.

58. Flemming H. C., Schaule, G., Griehe, T., Schmitt J., Tamachiarowa A., (1997),

Biofouling- the Achilles heel of membrane processes, *Desalination*, 113, 215 – 225.

59. Flemming H. C. and Tamachkiarow A., (2003), Monitoring of Biofilm in Technical Systems- A Crucial Component of Advanced Ant-Fouling Strategies" *Wat. Sci. Technol.*, 3 (5-6), 199-204.
60. Freger V., Gilron J. and Belfer S., (2002), TFC polyamide membranes modified by grafting of hydrophilic polymers; an FTIR/AFM?TEM study, *Journal of Membrane Science*, 209, 283 – 292.
61. Fujiwara N., Tanaka T., Katsube M., Al-Ghamdi M. A. F., Al-Harthi S. S., Lami H., and Iwahashi H, (1999), Five years operational performance of membrane at 15MGPD Jeddah RO Phase II plant, Proc. San Diego IDA Congress 3 (1999) 89-98.
62. Gabelich C. J., Yun T. I., Coffey B. M., and Suffet I. H., (2002), Effect of aluminum sulfate and ferric chloride coagulant residuals on polyamide membrane performance, *Desalination*, 150, 15-30.
63. Gabelich C. J., Yun T. I., Ishida K. P., Leddy M. B., and Safaril J., (2003), Detection of organic and biological foulants on polyamide membranes during surface water treatment, AWWA membrane technology conference, Atlanta, Georgia.
64. Glater J., Hong S. K. and Flimelech M., (1994), The Research for a Chlorine Resistant Reverse osmosis membrane, *Desalination*, 95, 325 – 341.
65. Glueckstren P., Priel M. and Wilf M., (2002), Field evaluation of capillary UF technology as a pre-treatment for large seawater RO systems, *Desalination*, 147, 55 – 62.
66. Goosen M. F. A., Sabalani S. S., Al-Hinai H., Al-Obeidani S., Al-Belushi R. and Jackson D.,(2004), Fouling of reverese osmosis and ultrafiltration membranr: a critical review, *Separation Science and Technology*, Vol. 39 (10), 2261-2298.
67. Goosen M. F. A., Al-Maskari S. S., Al-Belushi R. H. and Wilf M., (2002), Effect of feed temperature on permeate flux and mass transfer coefficient in spiral - wound reverse osmosis systems, *Desalination*, 144, 367-372.
68. Griebe, T., and Flemming, H. C., (1998), Biocide-free antifouling strategy to protect RO membranes from biofouling, *Desalination*, 113, 153-1.
69. Gulamhusein H. Al Sheikh Khalil A. A. S., Fatah I. A., Boda R. and Rybar S., (2008), IMS SWRO Kindasa-Two years of operational experience, Proceeding of the

Conference on Desalination for Clean Water and Energy, Cooperation among Mediterranean Countries of Europe and the MENA Region, Dead Sea, Jordan, November 9–13.

70. Gustave K., (2004). The largest SWRO plant in the world: Ashkelon 100 million $m^3.d^{-1}$ BOT project, *Desalination*, 166, 467-474.
71. Hanra A. M., Ramachandhran V., (1996), RO performance analysis of cellulose acetate and TFC polyamide membrane systems for separation trace contaminants, *Desalination*, 104, 175-183.
72. Hasson D., Drek A., and Semiat R., (2001). Inception of CaSO4 scaling on RO membranes at various water recovery levels, *Desalination*, 139, 73-81.
73. Herzberg M. and Elimelech M., (2007). Biofouling of reverse osmosis membranes: Role of biofilm-enhanced osmotic pressure, *Journal of Membrane Science*, 295, 11-20.
74. Heiri O., Lotter A., and lemcke G., (2001). Los on ignition as amethod for estimating organic and carbonate content in sediments, *Journal of Paleolimnology*, 25,101-110.
75. Hem J. L., and Efraimsen H., (2001) Assimilable organic carbon in molecular weight fraction of natural organic carbon, *Water Research*, 35(4), 1106-1110.
76. Higa M., Tanokia A. and Kra A., (1998), A novel measurement method of Donnan potential at an interface between a charged membrane and mixed salt solution, *Journal of Membrane Science*, 140.
77. Hilal N., and Mohammed A. W., Atkin A., and Darwish N. A., (2003). Using atomic force microscopy towards improvement in nanofiltration membrane properties for desalination pre-treatment: a review, *Desalination*, 157, 137-144.
78. Hirose M., Ito H., and Kamiyama Y., (1996). Effect of skin layer surface structures on the flux behaviour of RO membranes, *of Membrane Science*, 188, 115-128.
79. Hoek E.M.V., Kim A.S., Elimelech M., (2002), Influence of Cross-flow Membrane Filter Geometry and Share Rate on Colloidal Fouling in RO and NF separation, *Environ. Eng. Soc.* 9, 357-372.
80. Hoek E.M.V. and Elimelech M, (2003) "Cake-Enhanced Concentration polarization: A new fouling mechanism for salt-rejection membranes", *Environ. Eng. Soc.*, 37, (2003), 5581-5588.

81. Hong S., Faibish R. S. and Elimelech M., (1997), Kinetic of Permeate Flux Decline in Cross-flow Membrane Filtration of Colloidal Suspensions" *Journal of Colloidal and Interface Science*, 196, 267-277.
82. Hong S. and Elimelech M., (1997) Chemical and Physical Aspects of NOM Fouling of NF Membranes" *Journal of Membrane Science*,132, 159-181.
83. Howe K., Ishids K.P and Clark M. M., (2002), Use of ATR-FTIR spectrometry to study fouling of microfiltration membranes by batural waters, *Desalination*, 147, 251 – 255.
84. Hu J. Y., Song L. F., Ong S. L., Phua E. T. and Ng W. J.,(2005), Biofiltration pretreatment for reverse osmosis (RO) membrane in a water reclamation system, *Chemosphere*, 59, 127 – 133.
85. Huiting H., Kappelhof J. w. N. M., and Bosklopper T. G. J., (2001), Operation of NF/RO plants: From reactive to protective, *Desalination*, 139, 183 – 189.
86. Jawor A., and Hoek E. M. V., (2009). Effect of feed water temperature on inorganic fouling of brackish water RO membranes, *Dealination*, 235, 44-57.
87. Jones K. L., and O' Melia C. R., (2000), Protein and humic acid adsorption onto hydrophilic membrane surface: effect of pH and ionic strength, *Journal of Membrane Science*, 165, 31 – 46.
88. Kaiya Y., Itoh Y., Fujita K., and Takizawa S., (1996), Study on fouling materials in the membrane treatment process for potable water, *Desalination*, 106, 63 – 76. .
89. Karime M., Bouguecha S. and Hamrouni B., (2008), RO membrane autopsy of Zarzis brackish water desalination plant, *Desalination*, 220, 258-266.
90. Khulbe K. C., Hamad F., Feng C., Matsuura T. and Khayet M., (2004), Study of the surface of the water treated cellulose acetate membrane by atomic force microscopy, *Desalination*, 161, 259-262
91. Kimura S., (1995). Analysis of reverse osmosis membrane behaviours in a long-term verification test, *Desalination*, 100, 77-84.
92. Kim S. and Hoek E. M. V., (2005), Modeling concentration polarisation in reverse osmosis processes, *Desalination*, 186, 111-128.
93. Komlenic R., www.ahlstrom.com/Disruptor
94. Komlenic R., (2007), Water filtration media: Talking about a revolution, *Filtration*

and Separation Publication.

95. Koros, W. J., Ma H. Y., and Shimidzu T., (1996), Terminolgy of membrane and membrane processes, *Journal of Membrane Science*, 120, 149 - 155.
96. Konen M. E., Jacobs P. N., Burras C. L., Talaga B. j., and Mason J. A, (2002). Equation for predicting soil organic carbon using loss-on-ignition for North Central U.S. soils, *Soil Sci. Soc., Am. J.*, 66, 1878-1881.
97. Kumar M., Adham S. S., Pearce W. R., (2006), Investigation of seawater reverse osmosis fouling and its relation to pre-treatment type, *Environ. Sci. Technol*, 40, 2037 – 2044.
98. Kurihara M., Fusaoka Y., Sasaki T., Bairinji R., Uemura T., (1994), Development of cross-linked fully aromatic polyamide ultra-thin composite membranes for sea water desalination, *Desalination*, 96, 133.
99. Kurihara M., Uemura T., Nakagawa Y. and Tonomura T., (1985), The thin film composite low-pressure reverse osmosis membranes, *Desalination,* 54, 75.
100. Lee S., Kim J. and Lee C. H., (1999) Analysis of CaSO4 Scale formation Mechanism in various NF Modules, *Journal of Membrane Science*, 163, 63-74.
101. Lee S., Cho L. and Elimelech M., (2004), Influence of colloidal fouling and feed water recovery on salt rejection of RO and NF membranes, *Desalination*, 160, 1 – 12.
102. Lee S., Ang W. S., and Elimelech M, (2006). Fouling of reverse osmosis membrane by hydrophilic organic matter: implications of water reuse, *Desalination,* 187, 313-321.
103. Leparc J., Rapenne S., Courties C., Lebaron P., Croue J. P., Jacquemet V., and Turner G., (2007). Water quality and performance evaluation at seawater reverse osmosis plants through the use of advanced analytical tolls, *Desalination*, 203, 243-255.
104. Li Q., Xu Z., Pinnau I., (2007) Fouling of reverse osmosis membranes by biopolymers in wastewater secondary effluent: Role of membrane surface properties and intial permeate flux, *Journal of Membrane Science*, 290, 273-282.
105. Lin C., Rao P., and Shirazi S., (2004). Effect of operating parameters on permeate flux decline caused by cake formation – a model study, *Desalination*, 171, 95-105.

106. Lisdonk C. A. C., Paassen J. A. M and Schippers J. C., (2000), Monitoring Scaling in NF and RO membrane Systems" Proceedings of the Conference on membranes in Drinking and industrial Water Production, Desalination, 2 , 141-148.
107. Lisdonk C. A. C, Rietman B. M., Sterk G. R. and Schippers J. C., (2001), The Influence of Concentration Polarization on the Risk of Scaling in spiral Wound Membrane Systems" Proceedings AWWA Membrane Technology Conference San Antonio.
108. Metsamuuronen, s., Howell J., and Nystrom M., (200) Critical flux in ultrafiltration of myoglobin and baker's yeast, *Journal of membrane Science*, 196, 13-25.
109. Liu L. F., Yu S. C., Wu L. G. And Gao C. J., (2006). Study on a novel polyamide-urea reverse osmosis composite membrane (ICIC-MPD), II-Analysis of membrane antifouling performance, *Journal of Membrane Science*, 283, 133-146.
110. Lopez, S. G., Piasno, S. del Vigo., and Munoz J. S., (2005). Membrane autopsies: help to provide solutions to operational problems in reverse osmosis plants, *Water Science and Technology: Water Supply*, Vol, 5, No. 3-4, 129-135.
111. Loste E., Wilson R. M., Seshadri R., and Meldrum F. C., (2003). The role of magnesium in stabilizing amorphous calcium carbonate and controlling calcite morphologies, *Journal of Crystal Growth*, 254, 206-218.
112. Marcus A. N., (2008), Self-cleaning Pre-filtration for RO membrane systems. EuroMed, Desalination for Clean Water and Energy, Cooperation among Mediterranean Countries of Europe and MENA Region, Dead Sea, Jordan, Novemeber, 9-13, 2008.
113. Meindersma, G. W., Guijt, C. M., and de Haan A. B., (2006). Desalination and water recycling by air gap membrane distillation, *Desalination,* 187, 291-301.
114. Mulder M., (2003). Basic Principles of Membrane Technology" Second Edition, Dordrecht, Baston, London: Kluwer Academic Publishers Group.
115. Murphy A. P., Moody C. D., Riley R. L., Lin S. W., Murugavrel B., and Rusin P., (2001). Microbiological damage of cellulose acetate RO membranes, Desalination, 193, 111-121.
116. Mo L. and Huang X., (2003), Fouling Characteristics and Cleaning Strategies in a Coagulation- Microfiltration Combination Process for Water Purification,

Desalination, 159, 1-9.

117. Mosset A., Bonnelye V., Petry M., and Sanz M. A., (2008), The sensitivity of SDI analysis: from RO feed water to raw water, *Desalination*, 222, 17-23.
118. Mustafa G. M., (2007). The study of pretreatment options for composite fouling of reverse osmosis membrane used in water treatment and production, PhD thesis, School of Chemical Science and Engineering, University of New South Wales, Australia.
119. Ning R. Y., Troyer T. L. and Tominello R. S., (2005), Chemical Control of Colloidal Fouling of Reverse Osmosis Systems, Desalination, 172, 1-6.
120. Ng H. N. and Elimelech M., (2004), Influence of Colloidal Fouling on Rejection of trace Organic Contaminants by reverse Osmosis" *Journal of Membrane Science*, 244, pp 215-226.
121. Ng H. Y., Taya K. G., Chuab S. C., Seahb H., (2008), Novel 16-inch spiral-wound RO systems for water reclamation — a quantum leap in water reclamation technology, *Desalination*, 225, 274-287.
122. Ovadia R. B. , "Pre-Treatment upstream of membranes" Proceeding of desalination for clean water and energy conference, EuroMed 2008, Dead Sea, Jordan, 9-13 November 2008.
123. Owen D. M., Amy G. L., Chowdhury,Z. K., Rajendra P., McCoy G. and Viscosil K., (1995), NOM Characteristics and Treatability, *Journal of AWWA*, January, pp 46-63. .
124. Pais J. A. G. C. R., Licinio M. and Ferreira (2007), Performance study of an industrial RO plant fro seawater desalination, *Desalination*, 208, 269-276.
125. Pang C. M., Peiying Hong P., Guo H., and Liu W. T., (2005), Biofilm Formation characteristics of bacterial Isolates retrieved from a RO membrane *Environ. Sci. Technol*, 39, 7541-7550.
126. Park C., Lee Y. H., Lee S. and Hong S., (2008), Effect of cake layer structure on colloidal fouling in reverse osmosis membranes, *Desalination*, 220, 335-344.
127. Park C., Kim H., Hong S., and Choi S., (2006), Variation and prediction of membrane fouling index under various feed water characteristics, *Journal of Membrane Science*, 284, 248-254.

128. Passow U., Shipe R. F., Murry A., Pak D. K., Brzezinski M. A. and Alldredge. A. L., (2001), The origin of transparent exopolymer particles (TEP) and their role in the sedimentation of particulate matter, *Continental Self Research*, 21, 327 – 346.

129. Passow U., and Alldredge A. L., (1995), Adye-binding assay for the spectrophotometric measurement of transparent exopolymer particles, Limnol. Oceaneger, 40 (7), 1326 – 1335.,

130. Peeters J. M. M., Boom J. P., Mulder M. H. V. and HStrathmann H., (1998), Retention measurements of nanofiltration membranes with electrolyte solutions, *Journal of Membrane Science*, 145, 199-209.

131. Pontie M., Rapenne S., Thekkedath A., Duchesne J., Jacquemet V., Leparc J. and Suty H., (2005), tools for membrane autopies and antifouling stratiges in seawater feeds: a review, *Desalination*, 181, 75-90.

132. Ridgway H. F, and Safarik J., (1990), Biofouling of Reverse Osmosis Membranes, Proceeding of the International Workshop on Industrial Biofouling and Biocorrosion, Stutgart, Sep. 13-14, 1991.

133. Rodriguez S. G., Althuluth K., Schurer R., Kennedy M. D., Amy G., and Schippers J.C., (2009), Modified fouling index (MFI-UF) at constant flux for seawater RO applications, Desalination for the Environment, Clean Water and Energy Conference, Baden-Baden, 17-20 May 2009, Germany.

134. Saad M. A., (1992), Biofouling Prevention in RO Polymeric Membrane Systems, Desalination Proceeding of the NWSIA 1992, Biennial Conference, 2, 85-105.

135. Saad M. A., (2002), Effect of dechlorination point location and residual chlorine on biofouling in a seawater reverse osmosis plant, (2002), *Desalination*, 143, 229-235.

136. Saad M. A., (2004), Early discovery of RO membrane fouling and real – time monitoring of plant performance for optimising cost of water, *Desalination*, 183 188– 191.

137. Saaed M. O., Jamaluddin A. T., Tisan I. A., Lawrence D. A., Al-Amri M. M., and Chida K., (2000). Biofouling in a seawater reverse osmosis plant on the Red Sea coast, Saudi Arabia, *Desalination*, 128, 177-190.

138. Safar M., Jafar M., Abdel-Jwad M. and Bou-Hamad S., (1998), Standardisation of RO membrane performance, *Desalination*, 118, 13 – 18.

139. Sadhwani J. J. and Veza J. M., (2001): Cleaning tests for seawater reverse osmosis membranes, *Desalination*, 139, 177-182.

140. Sayed A. B., Ben Boudinar M., Gulamhusein . A. H., Khalil A. A., Rybar S., Saud M., Kaisar A. K., (2007), First Successful Operation of SWRO Plant in Saudi Arabia with UF Pre-treatment, IDA World Congress- Maspalomas, Gran Canaria-Spain October 12-26, 2007.

141. Schneider R. P., Ferreria L. M., Binder P., Bejarano E. M., Goes K. P., Slongo E., Machado C. R., and Rosa G. M. Z., (2005), Dynamics of Organic Carbon and Bacterial Populations in a Conventional Pretreatment Train of a Reverse Osmosis Unit Experiencing Severe Biofouling, *Journal of Membrane Science*, 266, 18-29.

142. Schneider R. P., Ferreria L. M., Binder P., Bejarano E. M., Goes K. P., Slongo E., Machado C. R., and Rosa G. M. Z., (2003), Detection of organic and biological foulants on polyamide membranes during surface water treatment, AWWA Membrane Technology Conference (2003), Atlanta-Gorgia.

143. Schaule G., Griebe T., and Flemming H. C., (1999). Steps in biofilm sampling and characterisation in biofouling cases, Microbially influenced corrosion of industrial materials, Biocorrosion, May, 17-18/1999

144. Shih W. Y., Rahardianto a., Lee R. W. and Cohen Y., (2005), Morphometric Characteriaztion of Calcium Sulphate Dihydrate (gypsum) Scale on Reverse Osmosis Membranes" *Journal of Membrane Science*, 252, 253-263.

145. Seidel A., and Elimelech M., (2002). Coupling between chemical and physical interactions in natural organic matter (NOM) fouling on nanafiltration membranes implications for fouling control, *Journal of Membrane Science,* 203, 245-251.

146. Sheikholeslami, R., (1999). Composite fouling - Inorganic and biological: A review, *Environmental Progress,* Vol. 18, No. 2, 113-122.

147. Sheikholeslami, R., and Ong H. W. K., (2003). Kinetic and thermodynamic of calcium carbonate and calcium sulphate at salinities up to 1.5 M, *Desalination*, 157, 217-234.

148. Sheikholeslami, R., (2005). Scaling potential index (SPI) for CaCO3 Based on Gibbs free energies, *AIChE Journal*, Vol. 51, No.6, 1782-1789.

149. Shon, H. K., Kim, S. H., Vigneswarm, S., Ben Aim, R. Lee, D., and Cho, J., (2009).

Physicochemical pre-treatment of seawater: fouling reduction and membrane characterisation, *Desalination*, 238, 10-21.

150. Singh P. S., Joshi S. V., Trivedi T. J., Devmurari C. V., Rao A. P. and Ghosh P. K., (2006), Probing the structural variations of thin film composite RO membranes obtained by coating polyamide over polysulfone membranes of different pore dimensions, *Journal of Membrane Science*, 278, 19 -25.
151. Spitzer P., Rossi B., Gaignet Y., Mabic S. and Sudmeier U., (2005). New approach to calibrating conductivity meters in the low conductivity range, *Accreditation and Quality Assurance*, 10, 78-81.
152. Schmitt J. and Flemming H. C.,(1998). FTIR spectroscopy in microbial and material analysis, *International Biodeterioration and biodegradation*, 41, 1 – 11.
153. Schippers J. C., Verduw J., (1980). The modified fouling index, a method of determinig the fouling characteristics of water, *Desalination*, 32, 137-148.
154. Scott K., (1996). Handbook of industrial membranes, second edition, Elsevier B. V. publication, The Netherlands.
155. Song L., Hu J. Y., Ong S. L., Ng W. J., Elimelech M., and Wilf M., (2003). Performance limitation of the full-scale reverse osmosis process, *Journal of Membrane Science*, 214, 239-244.
156. Song L. and Yu S. (1999), Concentration polarisation in cross-flow reverse osmosis, *AIChE Journal*, 45, 921-928.
157. Stover R., L., Martin J., and Nelson M., (2007). The 200,000 $m^3.d^{-1}$ Hamma seawater desalination plant-Largest single-Train SWRO capacity in the world and alternative to pressure centre design, IDA world congress – Maspolams, Gran Canaria, October 21-26, 2007 – Spain.
158. Stuzkover I., Hasson D., and Semiat R., (2000). Simple technique for measuring concentration polarisation level in a reverse osmosis system, Proceeding of the conference on membrane in drinking and industrial water production, vol. 1, 167-177, 3-6 October 2000, Paris – France.
159. Taniguchi M. and Kimura Sholi, (2000). Estimation of transport parameters of RO membranes for seawater desalination, *AICHE Journal*, Vol. 46, No. 10, 1967-1973.
160. Tang C. Y., Kwon Y. and Leckie J. O., (2007), Fouling of reverse osmosis and

nanofiltration membranes by humic acid-Effects of solution composition and hydrodynamic conditions, *Journal of Membrane Science*, 290, 86-94.

161. Tansel B., Bao W. Y. and Tansel I. N., (2000), Characterization of Fouling Kinetics in Ultrafiltration Systems by Resistances in Series Model" *Desalination*, 129, 7-14.
162. Tapper F. and Kaledin L., (2007), Non-Woven media incorporating ultra fine or nanosize powders, *US patent application*, 0026041A1.
163. Tenzer B., Adin A., Priel M., (1999), Seawater filtration for fouling prevention under stormy conditions, *Desalination*, 125, 77-88.
164. Teuler A., Glucina K., and Laine J. M., (1999), Assessment of UF pre-treatment prior RO membranes for seawater desalination, *Desalination*, 125, 89 – 96.
165. Tran T., Bolto B., Gary S., Hoang M. and Ostarcevic E., (2007). An autopsy study of a fouled reverse osmosis membrane element used in a brackish water treatment plant, *Water Research*, 41, 3915 – 3923.
166. Tzotzi C., Pahiadaki T., Yiantsios S. G., Karabelas A. J., and Andritsos N., (2007). A study of $CaCO_3$ scale formation and inhibition in RO and NF membrane processes, *Journal of Membrane Science*, 296, 171-184.
167. Van der Bruggen B., Vandcasteele C., van Gestel T., Doyen W., and Leysen R. (2003). A review of pressure – driven membrane processes in waste treatment and drinking water production, *Environmental Progress*, 22, No.1, 46-56.
168. Van der Kooij, (2001) Assimilable organic carbon as indicator of bacterial growth, *Journal of the Ameerican Water Work Association*, 84(2), 57-65.
169. Van Hoof S. J. C., Hashim A. and Kordes A. J., (1999), The effect of ultrafiltration as pre-treatment to reverse osmosis in wastewater reuse and seawater desalination applications, *Desalination*, 124, 231-242.
170. Vedavyasan, C. V., (2007), Pre-treatment trends – an overview, *Desalination*, 203, 296-299.
171. Villacorte L. O., Schurer R., Kennedy M., Amy G. L. and Schippers J. C., (2009). The fate of transparent exopolymer particles (TEP) in seawater UF-RO system: a pilot plant study in Zeeland, The Netherlands, Desalination for the environment, Clean water and energy conference, Baden-Baden, Germany, May 17-20/2009.
172. Vrijenhoek E. M., Hong S. and Elimelech M., (2001), Influence of Membrane

Surface Properties on Initial Rate of Colloidal Fouling of reverse Osmosis and Nanofiltration Membranes" *Journal of Membrane Science*, 188, 115-128.

173. Voros N. G., Maroulis Z. B., and Marinos-Kouris D. (1996), Salt and water permeability in reverse osmosis membranes, *Desalination*, 104, 141-154.
174. Vrouwenvelder J. S. and Van der Kooij D., (2001), Diagnosis, predication and prevention of fouling of NF and RO membrane, *Desalination*, 139, 65-71.
175. Vrouwenvelder J. S. and Van der Kooij D., (2002), Diagnosis of fouling problems of NF and RO membrane installation by a quick scan, *Desalination*, 153, 121-124.
176. Vrouwenvelder J. S. Kappelhof, J. W. N. M., Heijman, S. G. J., Schippers, J. C., and Kooij D. van der, (2003). Tools for fouling diagnosis of NF and RO membranes and assessment of the fouling potential of feed water, *Desalination*, 157, 361-365.
177. Xie R. J., Tanb E. K., Limc S. K., Hawc E., Chiewc C. P., Sivaramanc A., Puahc A. N., Lauc Y. H. and Teo C. P., (2009), Pre-treatment optimization of SWRO membrane desalination under tropical conditions, *Desalination and Water Treatment*, 3, 136 – 142.
178. Xu P., Drewes J. E., Kim T. U., Bellona C.and Amy G., (2006), Effect of membrane fouling on transport of organic contaminanats in NF/RO membrane applications, *Journal of Membrane Science*, 279, 165-175.
179. Waly T., Saleh S., Kennedy M. D., Witkamp G. J., Amy G., Schippers J. C., (2008), Will calcium carbonate really scale in seawater reverse osmosis?, EuroMed, Desalination for Clean Water and Energy, Cooperation among Mediterranean Countries of Europe and MENA Region, Dead Sea, Jordan, Novemeber, 9-13, 2008.
180. Wang Y., (2005). Composite fouling of calcium sulfate and calcium carbonate in a dynamic seawater reverse osmosis unit, PhD thesis, School of Chemical Engineering and Industrial Chemistry, The University of New South Wales, Australia.
181. Winters H., (1997), Twenty years experience in seawater reverse osmosis and how chemicals in pre-treatment affect fouling of membranes, *Desalination*, 110, 93-96.
182. Wijmans J. G., Baker R. W., (1995) The solution – diffusion model: a review,

Journal of Membrane Science, 107, 1-21.

183. Wilf M. and Klinko K., (1994), Performance of commercial seawater membranes, *Desalination*, 96, 465-478.
184. Wilf M. and Schierach M. K., (2001), Improved performance and cost reduction of RO seawater systems using UF pre-treatment, *Desalination*, 135, 61 – 68.
185. Wnuk R., Schlichte B., Mehelm P. and Schnur E., (2008), Extending filter life: using a backwashable filter, *Filtration and Separation Publication*, Vol. 3, 19 – 21.
186. Yang H. L., Huang C. and Pan J. R., (2008), Characterisation of RO foulants in a brackish water desalination plant, *Desalination*, 220, 353 – 358.
187. Yuan W., and Zydeny A. L., (2000). Humic acid fouling during microfiltration, *Environmental Science Technology*, 34, 5043-5050.
188. Zhao Y. and Taylor J. S., (2005), Assessment of ASTM 4516 for evaluation of RO membrane performance, *Desalination*, 180, 231-244.
189. Zhu X., and Elimelech M., (1997). Colloidal fouling of reverse osmosis membranes: measurements and fouling mechanisms, *Environmental Science & Technology*, 31, 3654-3662.
190. Zularisam A. W., Ismail A. F., and Salim R. (2006), Behaviours og NOM in Membrane Filtration for Surface Water Treatment- a Review" *Desalination*,149, 211-231.

APPENDUCES

APPENDIX - A

IN – SITU FOULING MONITORING METHODS

APPENDIX - A

IN – SITU FOULING MONITORING METHODS

1. Silt Density Index (SDI)

The following SDI data were collected from the Tajoura SWRO Desalination Plant in 2005.

Table 1.1: Silt density index values

Date	SDI (Raw Seawater)	SDI (Pre-Treated Seawater)
02/02/2005	4.2	3.8
03/02/2005	4.2	3.8
04/02/2005	6.3	-
05/02/2005	6.1	-
06/02/2005	5.6	-
07/02/2005	6	-
08/02/2005	5.8	3.2
09/02/2005	5.7	3.1
10/02/2005	5.3	3
11/02/2005	5.3	3.5
12/02/2005	5.3	3.4
13/02/2005	5.3	3
14/02/2005	5.3	3
15/02/2005	5.5	3.6
16/02/2005	5.5	3.6
17/02/2005	4.6	3
18/02/2005	4.6	3
19/02/2005	4.6	3.1

2. Culturable Plate Count

$$Concentration\ of\ bacteria\ in\ water\ sample = \frac{Average\ plate\ count \times Overall\ diluution\ factor}{volume\ (0.1\ ml)} = CFU.ml^{-1} \quad (3.1)$$

Table 2.1 - Raw seawater

Time (h)	0	24	48	72	96	144	216	288
P1	0	0	0	6	116	118	130	130
P2	0	0	0	5	118	118	124	124
P3	0	0	0	6	98	98	101	103
Geomean	0	0	0	6	110.9	117.6	118.4	119
Stdev	0	0	0	0.6	11.1	11.6	15.3	14.7

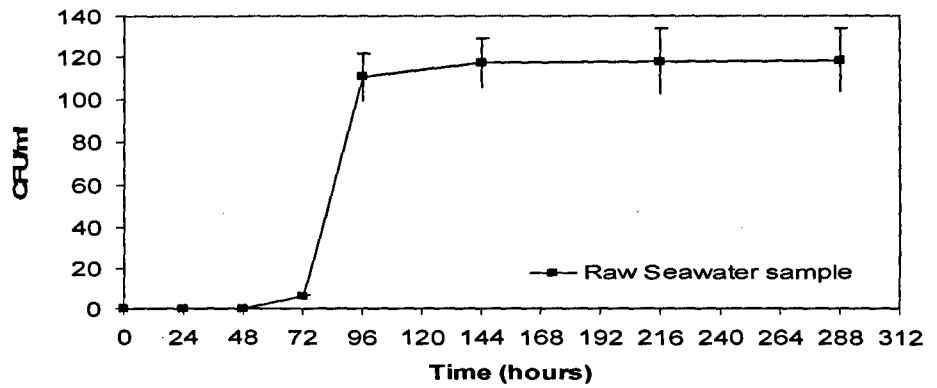

Table 2.2. Pre-treated seawater (RO feed)

Time (h)	0	24	48	72	96	144	216	288
P1	0	0	0	65	185	185	190	190
P2	0	0	0	41	139	139	139	139
P3	0	0	0	99	179	179	189	189
Geomean	0	0	0	64.1	166.4	166.4	170.9	170.9
Stdev	0	0	0	23.9	20.4	20.4	23.8	23.8

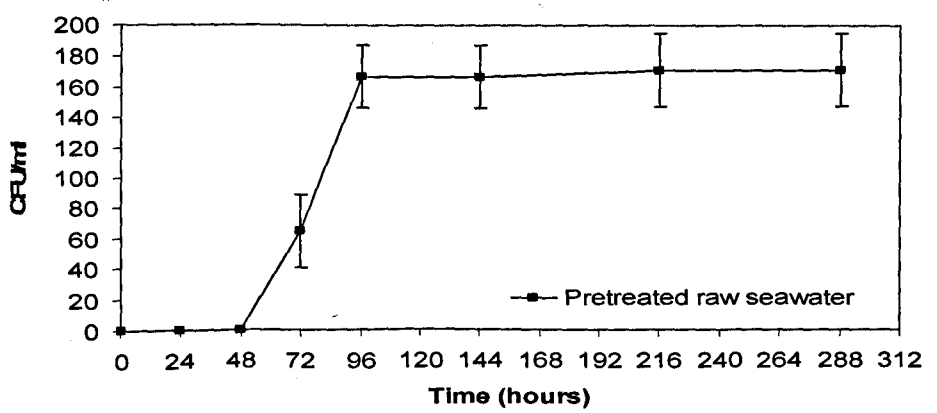

Table 2.3: RO concentrate

	0	24	48	72	96	144	216	288
P1	0	0	0	108	131	132	153	153
P2	0	0	0	139	182	185	188	188
P3	0	0	0	153	186	186	188	188
Geomean	0	0	0	131.9	164.3	165.6	175.5	175.5
Stdev	0	0	0	23	30.7	30.9	20.2	20.2

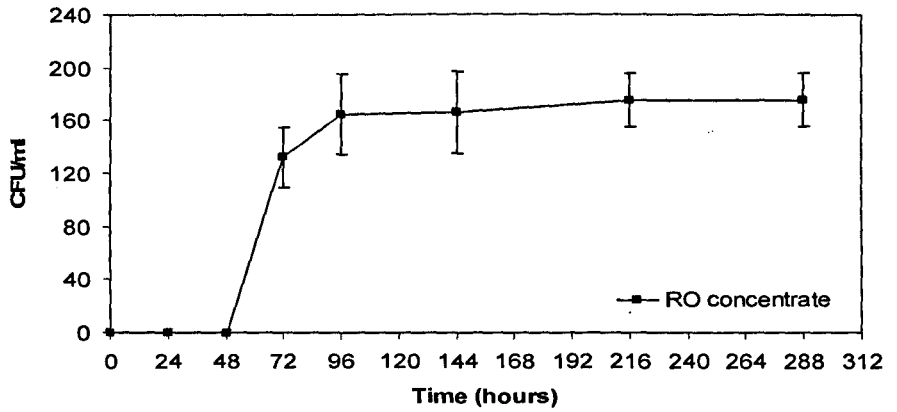

3. Prediction of $CaCO_3$ and $CaSO_4$ Scaling

The scaling potential of calcium carbonate ($CaCO_3$) and calcium sulphate ($CaSO_4$) was calculated based in water analysis (Table 3.1).

Table 3.1: The major anions and cations that present in the Mediterranean Sea seawater.

Anions	Concentration		Cations	Concentration	
	mg. l^{-1}	mol. l^{-1}		mg. l^{-1}	mol. l^{-1}
Ca^{2+}	455	11.4×10^{-3}	HCO^{-}_3	136	2.23×10^{-3}
Mg^{++}	1427	58.7×10^{-3}	SO^{2-}_4	2915	30.4×10^{-3}
Na^{+}	11600	504.4×10^{-3}	Cl^{-}	20987	591×10^{-3}
K+	419	10.7×10^{-3}			

The ionic strength in the raw seawater was calculated using Equation (3.2).

$$I_f = \frac{1}{2}\sum m_i \times Z_i^2 \qquad (3.2)$$

Where, m_i is the molal concentration of ion (mol kg^{-1}); C_i is the concentration of ion (mg. l^{-1}), the MW_i is molecular weight of ion and Z_i is the ionic charge.

$$I_f = \frac{1}{2}\sum\{(11.4+58.7+30.4)\times 4\times 10^{-3} + (504.4+10.7+2.23+591)\times 10^{-3}\} = 0.8 \quad (3.3)$$

The ionic strength in the concentrate water was calculated using Equation (3.4).

$$I_c = I_f \frac{1}{1-R} \quad (3.4)$$

Where, R is systems recovery (dimensionless).

$$I_c = 0.8\times\left(\frac{1}{1-0.35}\right) = 1.23 \quad (3.5)$$

The concentration of calcium and alkalinity as calcium carbonate were determined.

$$(Ca^{2+})_{CaCO_3} = (Ca^{2+})_f \times 2.5 = 11.4\times 10^{-3} = 28.5\times 10^{-3}\ mol\,l^{-1} \quad (3.6)$$

$$(HCO_3^-)_{CaCO_3} = \frac{2.23\times 10^{-3}}{1.22} = 1.83\times 10^{-3}\ mol\,l^{-1} \quad (3.7)$$

The concentration of calcium and alkalinity in the concentrate was calculated by multiplying the calcium and alkalinity concentration in the feed water by the concentration factor.

$$(Ca^{2+})_c = (Ca^{2+})_f \frac{1}{1-R} \quad (3.8)$$

$$(Ca^{2+})_c = 28.5\times 10^{-3}\times\left(\frac{1}{1-0.35}\right) = 43.89\times 10^{-3}\ mol\,l^{-1} \quad (3.9)$$

$$p[Ca^{2+}] = -\log\ [43.89\times 10^{-3}] = 1.4 \quad (3.10)$$

$$(Alkalinity)_c = (Alkalinity)_f \frac{1}{1-R} \quad (3.11)$$

$$(Alkalinity)_c = 1.83\times 10^{-3}\times\left(\frac{1}{1-0.35}\right) = 2.82\times 10^{-3}\ mol\,l^{-1} \quad (3.12)$$

$$p[HCO_3^-] = -\log\ [2.82\times 10^{-3}] = 2.6 \quad (3.13)$$

The p[Ca^{2+}] and p[Alk.] values were determined from graph (Figure 3.1) according to the ASTM D4582-05 and found to be as follows:

$p[Ca^{2+}] = 1.8$ (3.14)

$p[Alk.] = 2.5$ (3.15)

Figure 3.1: Conversion of calcium and alkalinity to $p[Ca^{2+}]$ and p[Alk] (ASTM D4582-05 and FilmTec Technical Manual, (2002).

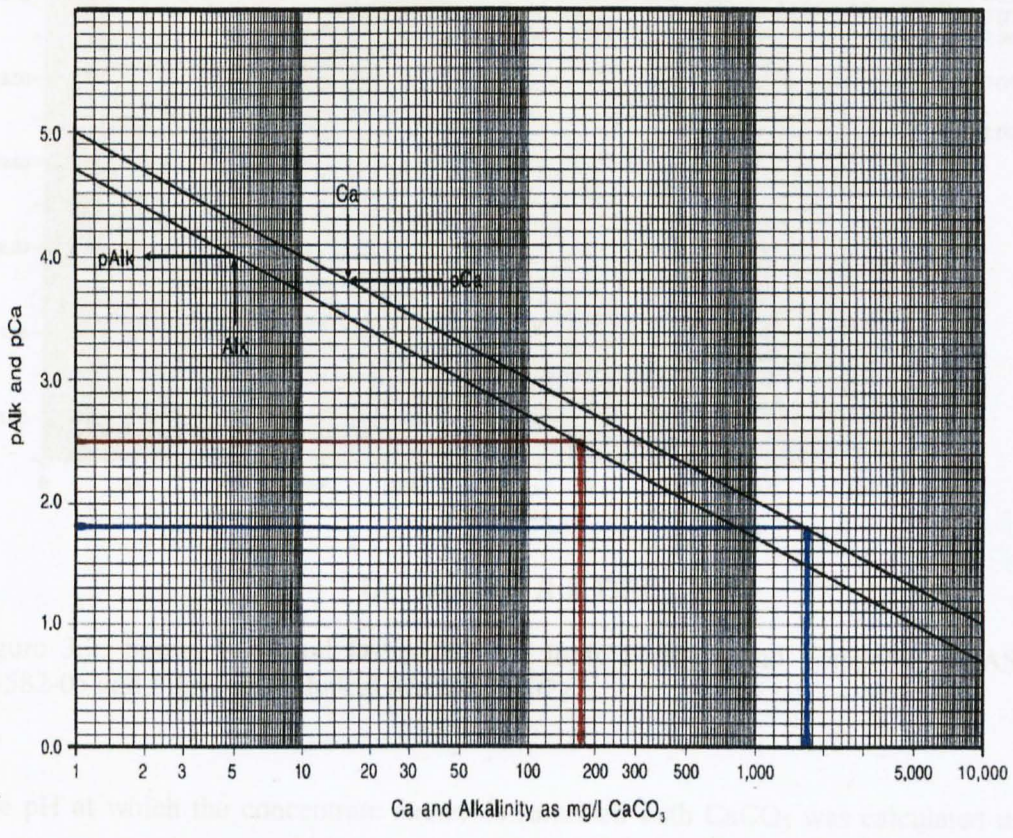

The constant "K" as a function of concentrate ionic strength and temperature was calculated using equation (3.16) (Al-Shammiri *et al.*, 2005) and determined from the graph (Figure 3.2) (ASTM D4582-05).

$$K = (-0.7083\ I_c^{\ 2}) + (1.8798\ I_c) + 2.1727 \quad (3.16)$$

Where: I_c is the ionic strength of concentrate stream.

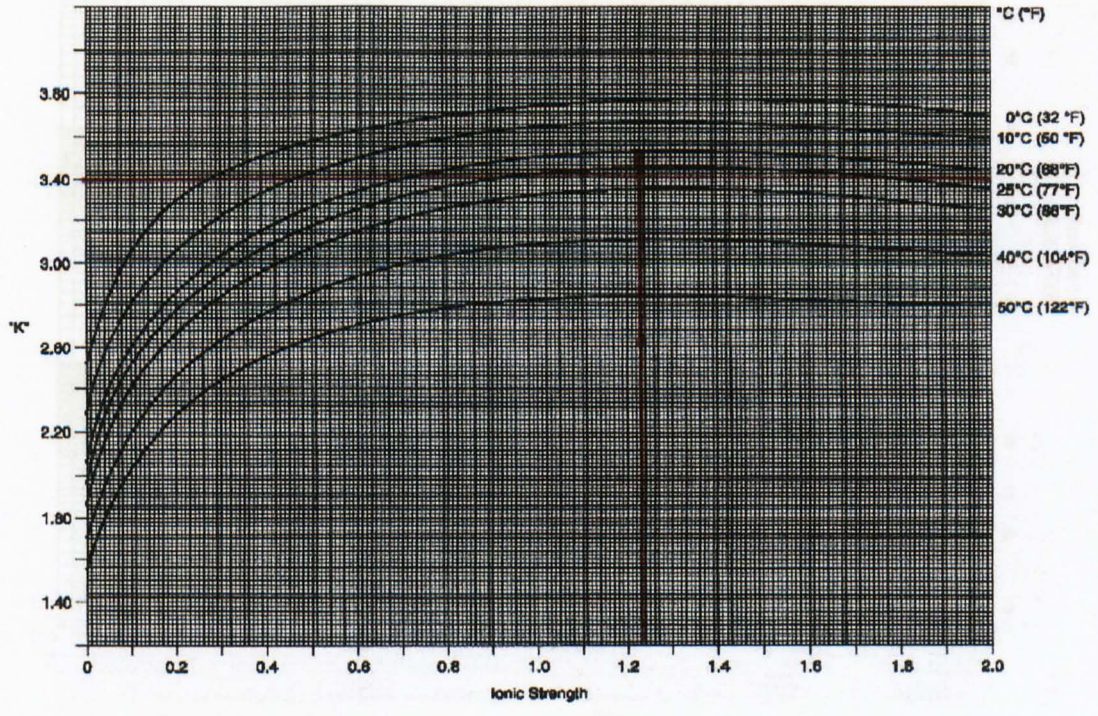

DETERMINING S & DSI

Figure 3.2: Shows Stiff and Davis "K" vs. Ionic Strength and Temperature (ASTM D4582-05 and FilmTec Technical Manual, 2002).

The pH at which the concentrate stream is saturated with $CaCO_3$ was calculated using Equation (3.17).

$$pH_s = p[Ca^{2+}] + p[HCO^-_3] + K \tag{3.17}$$

- From the graphs:

$$pH_s = 1.8 + 2.5 + 3.4 = 7.7 \tag{3.18}$$

- Al-Shammiri *et al.* 2005

$$pH_s = 1.4 + 2.6 + 3.4 = 7.4 \tag{3.19}$$

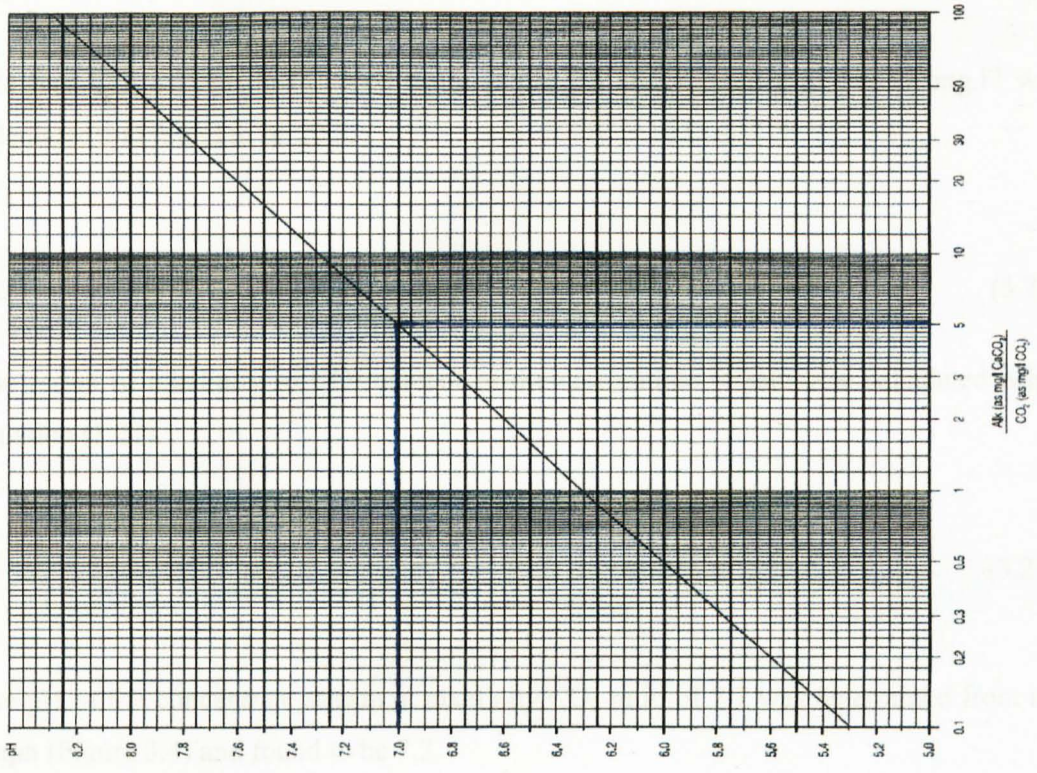

The calculated and the obtained values of $p[Ca^{2+}]$ and $p[HCO^{-}_3]$ and "K" from graphs are presented in Table 3.2.

Table 3.2: The calculated and the obtained values of $p[Ca^{2+}]$, $p[HCO^{-}_3]$ and "K" from the graph.

Parameter	Calculated (Al-Shammairi, *et al.*, 2006)	Obtained from graphs (ASTM D4582-05).
$p[Ca^{2+}]$	1.4	1.8
$p[HCO^{-}_3]$	2.6	2.5
"K"	3.4	3.4
pHs	7.4	7.7

The free carbon dioxide (CO_2) content in the concentrate stream can be determined by assuming that the CO_2 concentration in the concentrate stream is equal to the CO_2 in the feed: $(CO_2)_f = (CO_2)_c$. The measured RO feed water pH is 7.0 and the ratio of alkalinity to CO_2 concentration was determined from the graph (Figure 3.3) and found to be 5.

Figure 3.3: The ratio of alkalinity to CO_2 versus the pH in the feed stream (ASTM D4582-05 and FilmTec Technical Manual, 2002).

The free CO_2 content in the feed water at pH 7.0 and alkalinity of 111.48 $mg.l^{-1}$ was calculated and found to be 22.3

$$CO_2 = \frac{111.48\ mg.l^{-1}}{5} = 22.3\ mg.l^{-1} \tag{3.20}$$

The ration of alkalinity to CO_2 content in the concentrate stream was calculated using equation (3.21).

$$\frac{171.68\ mg.l^{-1}}{22.3} = 7.7\ mg.l^{-1} \tag{3.21}$$

The pH of the concentrate stream at alkalinity/CO_2 ratio of 7.7 was determined from the graph (Figure 3.4) and found to be 7.2.

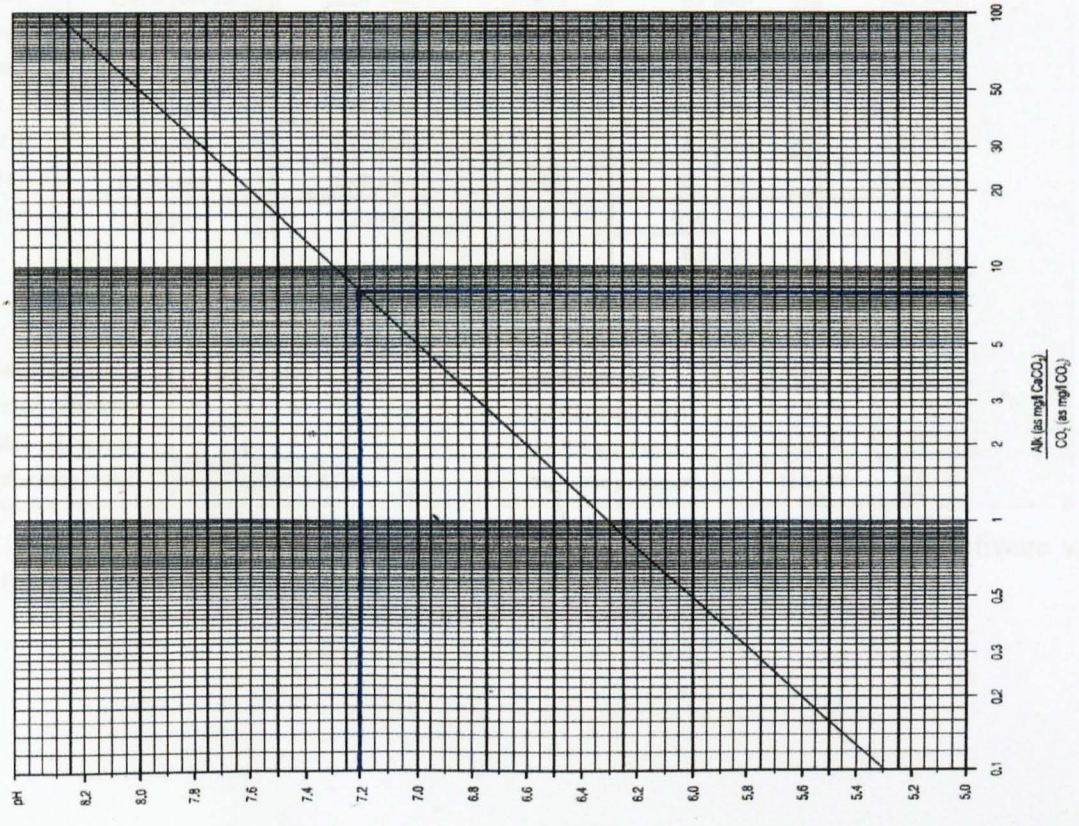

Figure 3.4: The ratio of alkalinity to CO_2 versus the pH in the concentrate stream (ASTM D4582-05 and FilmTec Technical Manual, 2002).

As the concentration of CO_2 will not change in the concentrate or permeate streams (Alhadidi *et al.* 2009). The pH of concentrate stream can be calculated using Eq. (3.22).

$$pH_c = \log\ CF + pH_{actual} = 0.19 + 7 = 7.19 \tag{3.22}$$

The S&DSI values were calculated using Equation 3.23 and determined using Hydranautics Membrane Design Software (Figure 3.5) and the obtained results are presented in Table (Table 3.3).

$$S\ \&\ DSI = pH_c - pH_s \tag{3.23}$$

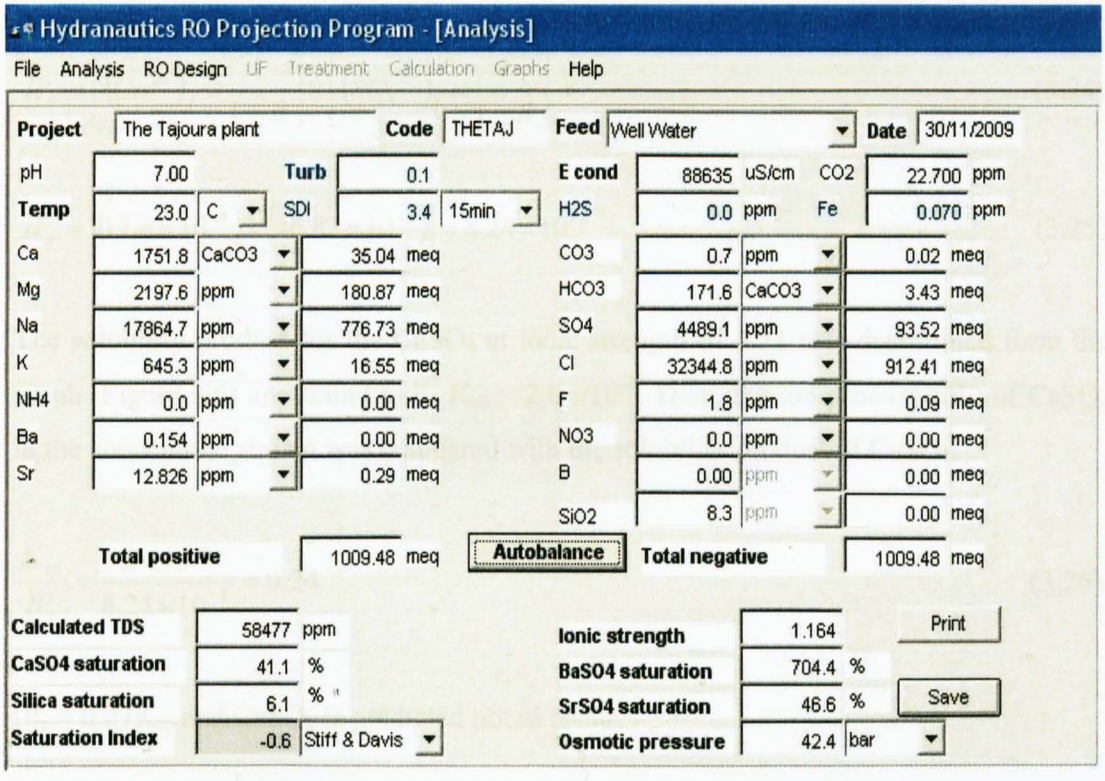

Figure 3.5: Determination of S&DSI using Hydranautics Membrane Design Software v. 2009.

Table 3.3: The calculated values for pH_s and S&DSI values respectively.

Parameter	Determined using Hydranutics Membrane Design Software v. 2009)	Calculated (Al-Shammairi, *et al.*, 2006 and Alhadidi *et al.* 2009)	Obtained from graph value (ASTM D4582-05).
pH_c	-	7.19	7.2
pH_s	-	7.7	7.7
S&DSI	-0.6	-0.51	-0.5

The calcium sulphate ($CaSO_4$) scaling potential was determined by calculating the ion product (IPc) for $CaSO_4$ in the concentrate stream using Equation (3.24).

$$IP_c = \left[\left(Ca^{2+}\right)_f \times \frac{1}{1-R}\right] \times \left[\left(SO_4^{2-}\right)_f \times \frac{1}{1-R}\right] \tag{3.24}$$

$$IP_c = \left[\left(17.6\times10^{-3}\right)\times\left(46.82\times10^{-3}\right)\right] = 8.24\times10^{-3} \tag{3.25}$$

The solubility product for the $CaSO_4$ at ionic strength of 1.23 was determined form the graph (Figure 3.5) and found to be $K_{sp} = 2.0 \times 10^{-3}$. Then, the ion product (IP_c) of $CaSO_4$ in the concentrate stream was compared with the solubility product of $CaSO_4$.

$$\frac{K_{sp}}{IP_c} = \frac{2\times10^{-3}}{8.24\times10^{-3}} = 0.24 \tag{3.26}$$

$IP_c = 0.27K_{sp}$ and $CaSO_4$ is predicted not to occur.

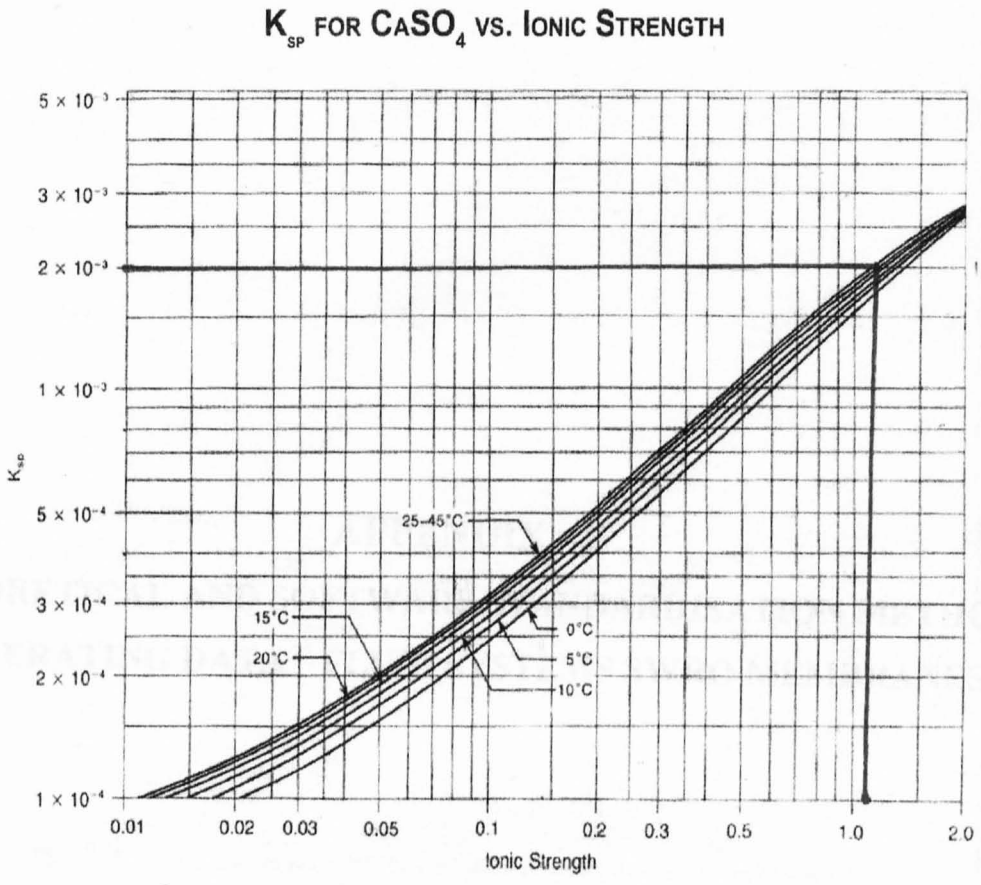

Figure 6.5: K_{sp} for $CaSO_4$ versus ionic strength (FilmTec Technical Manual, 2002).

APPENDIX - B

THEORETICAL AND SOFTWARE STANDARDISATION METHODS

OPERATING DATA – FLUID SYSTEMS SWRO MEMBRANES

APPENDIX - B

OPERATING DATA – FLUID SYSTEMS SWRO MEMBRANES

1 – Fluid Systems SWRO membrane (Specification and Test Condition)

KOCH MEMBRANE SYSTEMS

FLUID SYSTEMS® TFC® - SS 8" ELEMENTS

High Rejection, Seawater, RO Elements

PRODUCT DESCRIPTION

Membrane Chemistry:	Proprietary TFC polyamide
Membrane Type:	TFC-SS membrane
Construction:	Spiral wound with fiberglass outerwrap
Applications:	Seawater desalination, high rejection RO membrane
Options:	40" (1,016 mm) and 60" (1,524 mm) Magnum® length, standard or high area construction

SPECIFICATIONS

Part Numbers	Model	Permeate Flow gpd	Permeate Flow (m^3/d)	Chloride Rejection percent	Membrane Area ft^2	Membrane Area (m^2)
8282200	2822 SS-300	5,000	(18.9)	99.6	300	(27.9)
8282202	2822 SS-360	6,000	(22.7)	99.6	360	(33.4)
8283200	2832 SS-465 Magnum®	7,750	(29.3)	99.6	465	(43.2)
8283201	2832 SS-540 Magnum®	9,000	(34.3)	99.6	540	(50.2)

Test Conditions: 32,800 mg/l NaCl solution (isosmotic to ASTM standard seawater) at 800 psi (5,520 kPa) applied pressure, 7% recovery (11% recovery for Magnum elements), 77°F (25°C) and pH 7.5.

OPERATING & DESIGN INFORMATION

Typical operating pressure:	750-950 psi (5,175 – 6,555 kPa)
Maximum operating pressure:	1,200 psi (8,275 kPa)
Maximum operating temperature:	113°F (45°C)
Maximum cleaning temperature:	113°F (45°C)
Maximum continuous free chlorine:	<0.1 mg/l
Allowable pH – continuous operation:	4 – 11
Allowable pH – short term cleaning:	2.5 – 11
Maximum differential pressure per element:	10/15 psi (69/104 kPa)
Maximum differential pressure per vessel:	60 psi (414 kPa)
Maximum feed turbidity:	1 NTU
Maximum feed SDI (15 minute):	5
Feed spacer thickness:	28/31 mil (0.7/0.8 mm)

PRODUCT DIMENSIONS AND WEIGHT

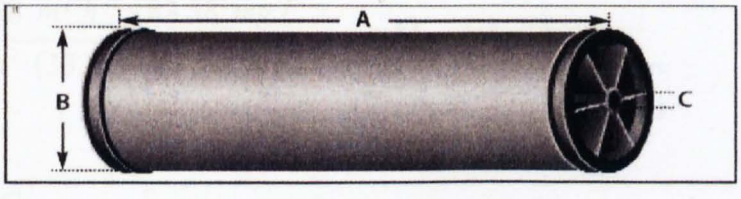

Model	A inches (mm)	B inches (mm)	C inches (mm)	Weight lbs (kg)	Part Numbers Interconnector	O-ring	Brine Seal
2822 SS-300	40 (1,016)	8 (203.2)	1.125 (28.6)	40 (18)	0035260	0035464	0035705
2822 SS-360	40 (1,016)	8 (203.2)	1.125 (28.6)	49 (20)	0035260	0035464	0035705
2832 SS-465 Magnum®	60 (1,524)	8 (203.2)	1.125 (28.6)	58 (26)	0035260	0035464	0035705
2832 SS-540 Magnum®	60 (1,524)	8 (203.2)	1.125 (28.6)	60 (27)	0035260	0035464	0035705

$Q_p = 23\ m^3.d^{-1} = 0.958\ m^3.h^{-1}$

$C_f = 32000\ mg.L^{-1}$

SR = 99.75%

Recovery (Y) = 8%

$$C_{fc} = C_f \frac{\ln\left(\frac{1}{1-Y}\right)}{Y} = 32800 \times \frac{\ln\left(\frac{1}{1-0.08}\right)}{0.08} = 33353 \quad mg.L^{-1}$$

$C_p = C_{fc} \times (1 - SR) = 33353 \times (1\text{-}0.9975) = 83.38\ mg.L^{-1}$

$$\pi_{fc} = \frac{0.8 \times C_{fc}}{1000} = \frac{0.8 \times 33353}{1000} = 26.7 \quad bar$$

$$\pi_p = \frac{0.8 \times C_p}{1000} = \frac{0.8 \times 83.38}{1000} = 0.07 \quad bar$$

$\Delta\pi = \pi_{fc} - \pi_p = 27.29 - 0.07 = 27.22$ bar

Mass transfer Coefficient for Water (K_w)

$$K_w = \frac{Q_p}{A(\Delta P - \Delta\pi)} = \frac{0.958\ m^3.h^{-1}}{34\ m^2\ (55.2 - 27.22)\ bar} = 10.10 \times 10^{-4}\ m^3.m^{-2}.h^{-1}.bar^{-1}$$

Mass transfer Coefficient for Salt (K_s)

$$K_s = \frac{Q_p \times C_p}{A(C_{fc} - C_p)} = \frac{0.958\ m^3.h^{-1} \times 83.38\ mg.L^{-1}}{34\ m^2\ (33353 - 83.38)\ mg.L^{-1}} = 0.71 \times 10^{-4}\ m^3 m^{-2}.h^{-1}$$

$$SP(\%) = \frac{K_s \times C_{fc}}{K_w(\Delta P - \Delta\pi) \times C_f} =$$

$$= \frac{0.71 \times 10^{-4}\ m.h^{-1} \times 33353\ mg.L^{-1}}{10.44 \times 10^{-4}\ m^3.m^{-2}.h^{-1}.bar^{-1} \times 27\ bar \times 32000\ mg.L^{-1}} \times 100 = 0.26\%$$

Recorded and Calculated Operating Data

Table 1: The ASTM Method

Parameter	0	30	60	90	120	150	180	210	240	300	330	360
Q_{Pa} ($m^3.h^{-1}$)	138	138	138	138	138	138	138	138	138	138	138	138
C_p ($m^3.h^{-1}$)	275	267	264	286	295	303	303	312	319	333	337	347
C_{fc} ($mg.L^{-1}$)	45971	45971	45891	45811	45854	45891	45836	45811	45771	45827	45879	45879
C_f ($mg.L^{-1}$)	37375	37375	37310	37245	37280	37310	37265	37245	37213	37258	37300	37300
P_f (bar)	53	53	53	53	53	53	53	53	54	54	54	54
P_c (bar)	52.3	52.3	52.2	52.2	52.2	52.2	52.1	52.1	52.1	53	53	53
ΔP (bar)	0.7	0.7	0.8	0.8	0.8	0.8	0.9	0.9	0.9	1	1	1
T (°C)	25	22	20	19	21	20	21	22.5	24.5	25	23	22
TCF	1	1.09	1.23	1.19	1.13	1.16	1.13	1.08	1.01	1	1.06	1.09
π_{fc} (bar)	36.8	36.8	36.7	36.6	36.7	36.7	36.7	36.6	36.6	36.7	36.7	36.7
π_p (bar)	0.22	0.21	0.21	0.23	0.24	0.24	0.24	0.25	0.26	0.27	0.27	0.28
NDP (bar)	15.6	15.6	15.7	15.8	15.7	15.7	15.6	15.7	16.7	16.5	16.5	16.5
SR(%)	99.4	99.4	99.4	99.38	99.36	99.34	99.34	99.3	99.3	99.27	99.26	99.24
SP (a) (%)	0.6	0.6	0.6	0.62	0.64	0.66	0.66	0.70	0.70	0.73	0.74	0.76
SP (N) (%)	0.6	0.6	0.6	0.63	0.64	0.66	0.66	0.71	0.75	0.77	0.78	0.80
Q_{pN} ($m^3.h^{-1}$)	138	127	112	115	118	118	122	127	126	127	123	120

Table 2: The Homogenous Solution Diffusion Method (HSDM)

Parameter	0	30	60	90	120	150	180	210	240	300	330	360
Q_P ($m^3.h^{-1}$)	138	138	138	138	138	138	138	138	138	138	138	138
C_p ($m^3.h^{-1}$)	275	567	264	286	295	303	303	312	319	333	337	347
C_{fc} ($mg.L^{-1}$)	45971	45971	45891	45811	45854	45891	45836	45811	45771	45827	45879	45879
C_f ($mg.L^{-1}$)	37375	37375	37310	37245	37280	37310	37265	37245	37213	37258	37300	37300
P_f (bar)	53	53	53	53	53	53	53	53	54	54	54	54
P_c (bar)	52.3	52.3	52.2	52.2	52.2	52.2	52.1	52.1	52.1	53	53	53
ΔP (bar)	0.7	0.7	0.8	0.8	0.8	0.8	0.9	0.9	0.9	1	1	1
T (°C)	25	22	20	19	21	20	21	22.5	24.5	25	23	22
TCF	1	1.09	1.23	1.19	1.13	1.16	1.13	1.08	1.01	1	1.06	1.09
π_{fc} (bar)	36.8	36.8	36.7	36.6	36.7	36.7	36.7	36.6	36.6	36.7	36.7	36.7
π_p (bar)	0.22	0.21	0.21	0.23	0.24	0.24	0.24	0.25	0.26	0.27	0.27	0.28
$\Delta P=(p_f+p_c)/2$ (bar)	52.65	52.65	52.6	52.6	52.6	52.6	52.55	52.55	53.05	53.5	53.5	53.5
$(\Delta P-\Delta\pi)$	15.6	15.6	15.7	15.8	15.7	15.7	15.6	15.7	16.2	16.5	16.5	16.5
SR(%)	99.3	99.3	99.3	99.2	99.2	99.2	99.2	99.19	99.10	99.10	99.10	99.10
SP (a) (%)	0.7	0.7	0.7	0.8	0.8	0.8	0.8	0.81	0.9	0.9	0.9	0.9
SP (N) (%)	0.7	0.7	0.7	0.8	0.8	0.81	0.82	0.83	0.93	0.93	0.95	0.98
K_w (a) x 10^{-4}	9.6	9.6	9.6	9.6	9.6	9.6	9.6	9.6	9.3	9.1	9.1	9.1
K_w (N) x 10^{-4}	9.6	8.8	7.8	8.1	8.5	8.3	8.5	8.9	9.0	9.1	8.6	8.3
K_s (a) x 10^{-4}	0.91	0.88	0.87	0.99	0.97	1	1	1	1.1	1.1	1.1	1.1
K_s (N) x 10^{-4}	0.91	0.88	0.75	0.79	0.86	0.86	0.88	0.96	0.99	1	0.98	0.99
Q_{pN} ($m^3.h^{-1}$)	138	127	112	116	119	119	122	128	130	126	123	119

Table 3: ROSA Software (FilmTec Membrane Company)

Parameter	0	30	60	90	120	150	180	210	240	300	330	360
Q_P ($m^3.h^{-1}$)	138	138	138	138	138	138	138	138	138	138	138	138
C_p ($m^3.h^{-1}$)	275	567	264	286	295	303	303	312	319	333	337	347
C_{fc} ($mg.L^{-1}$)	45971	45971	45891	45811	45854	45891	45836	45811	45771	45827	45879	45879
C_f ($mg.L^{-1}$)	37375	37375	37310	37245	37280	37310	37265	37245	37213	37258	37300	37300
P_f (bar)	53	53	53	53	53	53	53	53	54	54	54	54
P_c (bar)	52.3	52.3	52.2	52.2	52.2	52.2	52.1	52.1	52.1	53	53	53
ΔP (bar)	0.7	0.7	0.8	0.8	0.8	0.8	0.9	0.9	0.9	1	1	1
T (°C)	25	22	20	19	21	20	21	22.5	24.5	25	23	22
TCF	1	1.09	1.23	1.19	1.13	1.16	1.13	1.08	1.01	1	1.06	1.09
π_{fc} (bar)	36.8	36.8	36.8	33.5	36.5	36.5	36.5	36.5	36.3	36.4	36.4	36.4
π_p (bar)	0.22	0.21	0.21	0.23	0.24	0.24	0.24	0.25	0.26	0.27	0.27	0.28
NDP (bar)	15.1	15.1	15.1	15.1	15.1	15.1	15.1	15.1	16.3	16.1	16.1	16.1
SR(%)	99.4	99.4	99.4	99.38	99.36	99.34	99.34	99.3	99.3	99.27	99.26	99.24
SP (a) (%)	0.6	0.6	0.6	0.62	0.64	0.66	0.66	0.70	0.70	0.73	0.74	0.76
SP (N) (%)	0.6	0.6	0.6	0.63	0.64	0.66	0.66	0.71	0.75	0.77	0.78	0.80
Q_{pN} ($m^3.h^{-1}$)	138	126	108	111	119	116	120	126	126	126	122	118

Table 4: RAData Software (Hydranautics Membrane Company)

Parameter	0	30	60	90	120	150	180	210	240	300	330	360
Q_P ($m^3.h^{-1}$)	138	138	138	138	138	138	138	138	138	138	138	138
C_p ($m^3.h^{-1}$)	275	567	264	286	295	303	303	312	319	333	337	347
C_{fc} ($mg.L^{-1}$)	45971	45971	45891	45811	45854	45891	45836	45811	45771	45827	45879	45879
C_f ($mg.L^{-1}$)	37375	37375	37310	37245	37280	37310	37265	37245	37213	37258	37300	37300
P_f (bar)	53	53	53	53	53	53	53	53	54	54	54	54
P_c (bar)	52.3	52.3	52.2	52.2	52.2	52.2	52.1	52.1	52.1	53	53	53
ΔP (bar)	0.7	0.7	0.8	0.8	0.8	0.8	0.9	0.9	0.9	1	1	1
T (°C)	25	22	20	19	21	20	21	22.5	24.5	25	23	22
TCF	1	1.09	1.23	1.19	1.13	1.16	1.13	1.08	1.01	1	1.06	1.09
π_{fc} (bar)	30.6	30.6										
π_p (bar)	0.22	0.21	0.21	0.23	0.24	0.24	0.24	0.25	0.26	0.27	0.27	0.28
NDP (bar)	15.1	15.1	15.1	15.1	15.1	15.1	15.1	15.1	16.3	16.1	16.1	16.1
SR(%)	99.4	99.4	99.4	99.38	99.36	99.34	99.34	99.3	99.3	99.27	99.26	99.24
SP (a) (%)	0.6	0.6	0.6	0.62	0.64	0.66	0.66	0.70	0.70	0.73	0.74	0.76
SP (N) (%)	0.7	0.7	0.7	0.8	0.8	0.8	0.8	0.8	0.97	0.96	0.96	0.96
Q_{pN} ($m^3.h^{-1}$)	138	123	106	109	114	114	118	125	126	126	121	117

APPENDIX - C

THEORETICAL AND SOFTWARE STANDARDISATION METHODS

OPERATING DATA – TORAY SWRO MEMBRANES

APPENDIX - C

OPERATING DATA – TORAY SWRO MEMBRANES

2 -Toray SWRO membrane (Specification and Test Condition)

'TORAY'

Seawater RO Elements

TM800

Type	Diameter inch	Membrane Area ft² (m²)	Salt Rejection %	Product Flow Rate gpd (m³/d)
TM810	4"	73 (7)	99.75	1,200 (4.5)
TM820-370	8"	370 (34)	99.75	6,000 (23)
TM820-400	8"	400 (37)	99.75	6,500 (25)

1. Membrane Type		Cross Linked Fully Aromatic Polyamide Composite
2. Test Conditions	Feed Water Pressure	800 psi (5.52 MPa)
	Feed Water Temperature	77 °F (25 °C)
	Feed Water Concentration	32,000 mg/l NaCl
	Recovery Rate	8 %
	Feed Water pH	7
3. Minimum Salt Rejection		99.5 %
4. Minimum Product Flow Rate		1,000 gpd (3.6 m³/d) (TM810) 4,800 gpd (18 m³/d) (TM820-370) 5,200 gpd (20 m³/d) (TM820-400)

Dimensions

All dimensions shown in inches (millimeter).

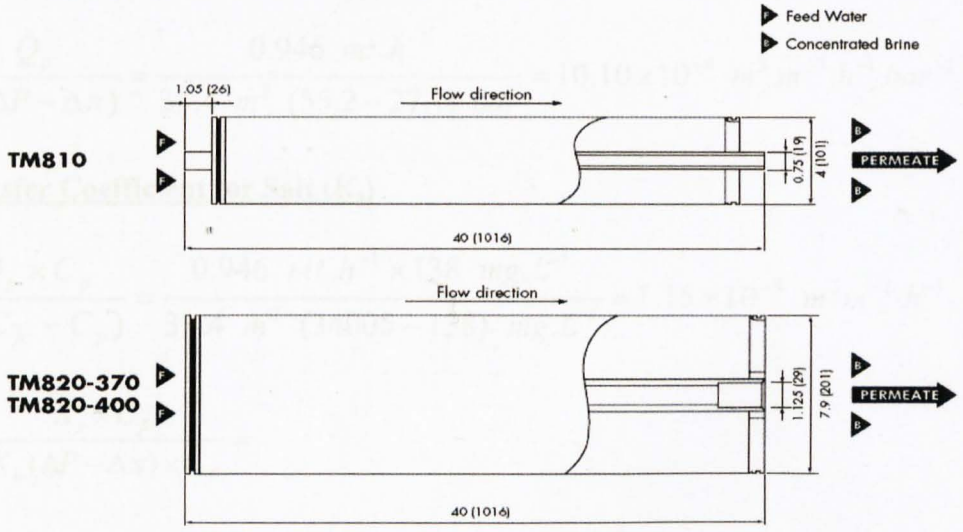

TM800 FEB/2004

$Q_p = 22.7\ m^3.d^{-1} = 0.946\ m^3.h^{-1}$

$C_f = 32800\ mg.L^{-1}$

SR = 99.6%

Recovery (Y) = 7%

$$C_{fc} = C_f \frac{\ln\left(\frac{1}{1-Y}\right)}{Y} = 32800 \times \frac{\ln\left(\frac{1}{1-0.07}\right)}{0.07} = 34005 \quad mg.L^{-1}$$

$C_p = C_{fc} \times (1 - SR) = 34005 \times (1\text{-}0.996) = 136\ mg.L^{-1}$

$$\pi_{fc} = \frac{0.8 \times C_{fc}}{1000} = \frac{0.8 \times 34005}{1000} = 27.2 \quad bar$$

$$\pi_p = \frac{0.8 \times C_p}{1000} = \frac{0.8 \times 136}{1000} = 0.11 \quad bar$$

$\Delta\pi = \pi_{fc} - \pi_p = 27.2 - 0.11 = 27.1$ bar

Mass transfer Coefficient for Water (K_w)

$$K_w = \frac{Q_p}{A(\Delta P - \Delta\pi)} = \frac{0.946\ m^3.h^{-1}}{33.4\ m^2\ (55.2 - 27.1)\ bar} = 10.10 \times 10^{-4}\ m^3.m^{-2}.h^{-1}.bar^{-1}$$

Mass transfer Coefficient for Salt (K_s)

$$K_s = \frac{Q_p \times C_p}{A(C_{fc} - C_p)} = \frac{0.946\ m^3.h^{-1} \times 138\ mg.L^{-1}}{33.4\ m^2\ (34005 - 138)\ mg.L^{-1}} = 1.15 \times 10^{-4}\ m^3 m^{-2}.h^{-1}$$

$$SP(\%) = \frac{K_s \times C_{fc}}{K_w(\Delta P - \Delta\pi) \times C_f} =$$

$$= \frac{1.15 \times 10^{-4}\ m.h^{-1} \times 34005\ mg.L^{-1}}{10.25 \times 10^{-4}\ m^3.m^{-2}.h^{-1}.bar^{-1} \times (27.64)\ bar \times 32800\ mg.L^{-1}} \times 100 = 0.42\%$$

Recorded and Calculated Operating Data

Table 1: The ASTM Method

Parameter	0	30	60	90	120	150	180	210	240	300	330	360
Q_{Pa} ($m^3.h^{-1}$)	138	138	138	138	138	138	138	138	138	138	138	138
C_p ($m^3.h^{-1}$)	558	487	475	479	500	509	558	585	687	633	675	683
C_{fc} ($mg.L^{-1}$)	45766	45766	44914	44927	44802	45715	45731	45953	46025	46089	46097	46097
C_f ($mg.L^{-1}$)	37178	37178	36486	36496	37050	37167	37180	37330	37388	37440	37447	37447
P_f (bar)	51	51	51	51	51	52	52	52	53	53	53	53
P_c (bar)	50.15	50.15	50.15	51.1	51.1	51	51	50.9	51.8	51.8	51.5	51.5
ΔP (bar)	0.85	0.85	0.85	0.9	0.9	1	1	1.1	1.2	1.2	1.5	1.5
T (°C)	25	24	18	19	20	20	21	24	25	24.5	25	26
TCF	1	1.03	1.23	1.19	1.16	1.16	1.13	1.03	1	1.01	1	0.97
π_{fc} (bar)	36.6	36.6	35.9	35.9	35.8	36.6	36.6	36.8	36.9	36.9	36.9	36.9
π_p (bar)	0.45	0.39	0.38	0.38	0.40	0.41	0.45	0.47	0.50	0.51	0.54	0.55
NDP (bar)	13.5	13.5	14.3	14.3	14.4	14.5	14.5	14.2	15	15	14.9	14.9
SR(%)	98.8	98.9	98.9	98.9	98.9	98.9	98.8	98.7	98.5	98.6	98.5	98.5
SP (a) (%)	1.2	1.1	1.1	1.1	1.1	1.1	1.2	1.3	1.5	1.4	1.5	1.5
SP (N) (%)	1.2	1.2	1.2	1.2	1.2	1.2	1.3	1.4	1.7	1.6	1.7	1.7
Q_{PN} ($m^3.h^{-1}$)	138	133	106	110	112	111	114	127	124	123	125	129

Table 2: The Homogenous Solution Diffusion Method (HSDM)

Parameter	0	30	60	90	120	150	180	210	240	300	330	360
Q_P ($m^3.h^{-1}$)	138	138	138	138	138	138	138	138	138	138	138	138
C_p ($m^3.h^{-1}$)	558	487	475	479	500	509	558	585	687	633	675	683
C_{fc} ($mg.L^{-1}$)	45766	45766	44914	44927	44802	45715	45731	45953	46025	46089	46097	46097
C_f ($mg.L^{-1}$)	37178	37178	36486	36496	37050	37167	37180	37330	37388	37440	37447	37447
P_f (bar)	51	51	51	51	51	52	52	52	53	53	53	53
P_c (bar)	50.15	50.15	50.15	51.1	51.1	51	51	50.9	51.8	51.8	51.5	51.5
ΔP (bar)	50.58	50.58	50.58	50.55	50.55	51	51	50.95	51.4	51.4	51.12	51.25
T (°C)	25	24	18	19	20	20	21	24	25	24.5	25	26
TCF	1	1.03	1.23	1.19	1.16	1.16	1.13	1.03	1	1.01	1	0.97
π_{fc} (bar)	36.6	36.6	35.9	35.9	35.8	36.6	36.6	36.8	36.9	36.9	36.9	36.9
π_p (bar)	0.45	0.39	0.38	0.38	0.40	0.41	0.45	0.47	0.50	0.51	0.54	0.55
$\Delta P=(p_f+p_c)/2$ (bar)	50.58	50.58	50.58	50.55	50.55	51.5	51.5	51.45	52.4	52.4	52.25	52.25
$(\Delta P-\Delta\pi)$	14.4	14.4	15	15	15	15.4	15.4	15.2	16.1	16	16	16
98.8	98.7	98.7	98.7	98.7	98.6	98.6	98.5	98.4	98.1	98.3	98.2	98.2
SP (a) (%)	1.3	1.3	1.3	1.3	1.4	1.4	1.5	1.6	1.9	1.7	1.8	1.8
SP (N) (%)	1.3	1.3	1.3	1.3	1.3	1.3	1.5	1.5	1.7	1.5	1.6	1.7
K_w (a) x 10^{-4}	10.65	10.65	10.22	10.24	10.24	9.94	9.94	10.1	9.5	9.6	9.6	9.6
K_w (N) x 10^{-4}	10.65	10.34	8.8	8.6	8.8	8.6	8.8	9.8	9.5	9.4	9.6	9.9
Ks (a) x 10^{-4}	1.89	1.65	1.64	1.65	1.72	1.73	1.89	1.97	2.32	2.13	2.27	2.23
Ks (a) x 10^{-4}	1.89	1.60	1.41	1.39	1.48	1.49	1.67	1.92	2.32	2.10	2.27	2.2.7
Q_{pN} ($m^3.h^{-1}$)	138	133	106	110	112	111	114	127	124	122	124	128

Table 3: ROSA Software (FilmTec Membrane Company)

Parameter	0	30	60	90	120	150	180	210	240	300	330	360
Q_{Pa} ($m^3.h^{-1}$)	138	138	138	138	138	138	138	138	138	138	138	138
C_{pa} ($m^3.h^{-1}$)	558	487	475	479	500	509	558	585	687	633	675	683
C_{fc} ($mg.L^{-1}$)	45766	45766	44914	44927	44802	45715	45731	45953	46025	46089	46097	46097
C_f ($mg.L^{-1}$)	37178	37178	36486	36496	37050	37167	37180	37330	37388	37440	37447	37447
P_f (bar)	51	51	51	51	51	52	52	52	53	53	53	53
P_c (bar)	50.15	50.15	50.15	51.1	51.1	51	51	50.9	51.8	51.8	51.5	51.5
ΔP (bar)	0.85	0.85	0.85	0.9	0.9	1	1	1.1	1.2	1.2	1.5	1.5
T (°C)	25	24	18	19	20	20	21	24	25	24.5	25	26
TCF	1	1.03	1.23	1.19	1.16	1.16	1.13	1.03	1	1.01	1	0.97
π_{fc} (bar)	35.3	35.2	33.8	34	34.1	34.6	34.8	35.3	35.5	35.5	35.5	35.6
π_p (bar)	0.35	0.35	0.34	0.34	0.34	0.35	0.35	0.37	0.36	0.36	0.36	0.36
NDP (bar)	14.9	15	16.4	16.2	16.1	16.6	16.4	15.8	16.5	16.5	16.4	16.3
SR(%)	98.8	98.9	98.9	98.9	98.9	98.9	98.8	98.7	98.5	98.6	98.5	98.5
Sp_a (%)	1.2	1.1	1.1	1.1	1.1	1.1	1.2	1.3	1.5	1.4	1.5	1.5
SP_N (%)	1.2	1.2	1.2	1.2	1.2	1.2	1.3	1.4	1.7	1.6	1.7	1.7
Q_{pN} ($m^3.h^{-1}$)	138	133	102	107	110	107	111	127	124	123	126	130

Table 4: RData Software (Hydranautics Membrane Company)

Parameter	0	30	60	90	120	150	180	210	240	300	330	360
Q_{Pa} ($m^3.h^{-1}$)	138	138	138	138	138	138	138	138	138	138	138	138
C_p ($m^3.h^{-1}$)	558	487	475	479	500	509	558	585	687	633	675	683
C_{fc} ($mg.L^{-1}$)	45766	45766	44914	44927	44802	45715	45731	45953	46025	46089	46097	46097
C_f ($mg.L^{-1}$)	37178	37178	36486	36496	37050	37167	37180	37330	37388	37440	37447	37447
P_f (bar)	51	51	51	51	51	52	52	52	53	53	53	53
P_c (bar)	50.15	50.15	50.15	51.1	51.1	51	51	50.9	51.8	51.8	51.5	51.5
ΔP (bar)	0.85	0.85	0.85	0.9	0.9	1	1	1.1	1.2	1.2	1.5	1.5
T (°C)	25	24	18	19	20	20	21	24	25	24.5	25	26
TCF	1	1.03	1.23	1.19	1.16	1.16	1.13	1.03	1	1.01	1	0.97
π_{fc} (bar)	37.2	37.1	35.7	35.8	35.9	36.5	36.7	37.3	37.5	37.4	37.5	37.6
π_p (bar)	0.45	0.39	0.38	0.38	0.40	0.41	0.45	0.47	0.50	0.51	0.54	0.55
NDP (bar)	12.9	13.1	14.5	14.4	14.3	14.6	14.4	13.7	14.4	14.5	14.2	14.1
SR(%)	98.8	98.9	98.9	98.9	98.9	98.9	98.8	98.7	98.5	98.6	98.5	98.5
SP (a) (%)	1.2	1.1	1.1	1.1	1.1	1.1	1.2	1.3	1.5	1.4	1.5	1.5
SP (N) (%)	1.2	1.1	1.4	1.3	1.3	1.3	1.4	1.3	1.5	1.4	1.5	1.5
Q_{PN} ($m^3.h^{-1}$)	138	132	101	105	110	107	111	126	123	120	125	128

APPENDIX - D

FOULING CHARACTERISATION OF TWO COMMERCIAL SEAWATER REVERSE OSMOSIS MEMBRANES: A CASE STUDY

APPENDIX - D

FOULING CHARACTERISATION OF TWO COMMERCIAL SEAWATER REVERSE OSMOSIS MEMBRANES: A CASE STUDY

1. Culturable Plate Count

The microbiological analysis of fouling material was carried out for determining the numbers of living micro-organisms that have capability to grow on the R2Amedium.

Protocol:

1. Fouled membrane samples of known area (5x5cm) were cut off from both membrane sheets and transferred into test tubes containing 10ml of sterile seawater and vortexed.
2. R2A agar was prepared by dissolving 18.9g of agar medium in 1L of raw seawater.
3. The mixture was autoclaved at 121°C for 15 minutes. Serial dilutions were carried out to determine the number of bacteria (expressed in colony forming units per area (cfu.cm^{-2}) on R2A agar medium.
4. Serial dilutions were prepared and then a 0.1 ml of each tested water sample was spread on sterilised R2A agar medium using sterile disposable plastic spreaders.
5. The plates then were incubated at 25 °C and counted periodically until the number of colonies stabilised.
6. Total colony forming units (CFU) per cm^2 of sample was calculated as follows:

$$Concentraton\ of\ bacteria\ in\ fouling\ material = \frac{Average\ plate\ count \times Overall\ diluution\ factor}{volume\ (0.1\ ml)} = CFU.ml^{-1}$$

Water sample	Plate 1	Plate 2	Plate 3	Average
Fouling material (Fluid System)	26	25	28	26.33 ± 1.53
Fouling material (Toray)	15	14	17	15.66 ± 2.10

- **Fluid Systems Membrane**
  - Membrane area = 25 cm^2
  - Dilution factor = 10000 times

$$CFU = \frac{26.33 \times 10000}{0.1 \times 25} = 11 \times 10^4 cfu.cm^{-2}$$

- **Toray Membrane**
  - Membrane area = 25 cm^2
  - Dilution factor = 10000 times

$$CFU = \frac{15.66 \times 10000}{0.1 \times 25} = 6.3 \times 10^4 cfu.cm^{-2}$$

2. Loss on Ignition

Loss on ignition test was carried out to determine the percentage organic content in the fouling materials of both membranes (Fluid Systems and Toray). The percentage of the dry weight lost on ignition of both foulants was calculated using the following formula:

$$\%LOI = \frac{(W_{T1} - W_{T2})}{(W_{T1} - W_0)} x100\%$$

Where:

W_0 – is the weight of empty crucible

W_{T1} – is the weight of crucible and sample heated at 100 °C.

W_{T2} – is the weight of crucible and sample heated at 550 °C.

Table 2.1: The weight of empty crucibles, after heating to 110 °C and 550 °C respectively.

Weight of fouling material	Weight of empty crucible (W_0)	Weight of crucible after heating (110 °C) (W_{T1})	Weight of crucible after heating (550 °C) (W_{T2})	Inorganic content (%)	Organic content (%)
Fluid Systems SWRO membrane					
1.14g	14.68	14.95	14.85	37	63
1.11g	13.95	14.15	14.07	40	60
Toray SWRO membrane					
1.1g	13.84	14.00	13.93	43.8	56.2
1.10g	14.23	14.38	14.32	40	60

2.1 Calculation Procedure

– Fluid Systems RO membrane

$$\%LOI = \frac{(14.95-14.85)}{(14.95-14.68)} x100\% = 37\%$$

$$\%LOI = \frac{(14.15-14.07)}{(14.15-13.95)} x100\% = 40\%$$

– Toray RO membrane

$$\%LOI = \frac{(14.00-13.93)}{(14.00-13.84)} x100\% = 43.8\%$$

$$\%LOI = \frac{(14.95-14.32)}{(14.95-14.68)} x100\% = 40\%$$

Table 2.2: Percentage of inorganic and organic contents in the fouling material of Fluid Systems and Toray RO membranes.

Membrane	Inorganic content (%)	Organic content (%)
Fluid System	38.5 ± 2.12	61.5 ± 2.12
Toray	41.9 ± 2.69	58.1 ± 2.69

3 Acid Digestions

The acid digestion experiment was carried out in order to dissolve metals that are present in the fouling material according to the ASTM D5198.

Protocol:

1. The digestion glass tubes were cleaned by sitting in 5% v/v nitric acids for 24 h and then rinsed by DI water and dried in laminar flow cabinet.
2. The weights of digestion glass tubes were determined.
3. Membrane coupon areas of 4 cm^2 were cut from the feed, the centre and the concentrate sides of SWRO membranes, weighed and transferred into previously cleaned 100 ml glass tubes.
4. A 10 ml of nitric acid (HNO_3) was added to 90 ml of DI water to prepare a 10% v/v HNO_3 solution and then the glass tubes were covered by glass marble.
5. The hot plate was switched on and left until temperature reached 100 °C.
6. Duplicate tubes were prepared and then placed in a hot plate and heated for 12 hrs at 100 °C.
7. After the acid digestion was done, the samples were filtered through a 0.22 µm type MILLEX@GP (Millipore Express, PES Membrane) to remove particulate matters.
8. The concentration of trace metals (Fe, Cu, Al and Zn) was measured using ICP-MS (PerkinElmer, USA).
9. A blank of 10% v/v HNO_3 was used in the same manner as for the membrane samples.

4 Chemical Cleaning of Fouled RO Membranes

4.1 Fluid Systems SWRO Membrane

4.1.1 Permeate Flux Before Chemical Cleaning

Time (min)	Run 1 Qp ($ml.min^{-1}$)	Run 2 Qp ($ml.min^{-1}$)	$J_w = \frac{Q_p}{A}$ ($ml.cm^{-2}.min^{-1}$)	$J_w = \frac{Q_p}{A}$ ($ml.cm^{-2}.min^{-1}$)	Average flux $ml.cm^{-2}.min^{-1}$)	Standard Deviation
0	0	0	0	0	0	0
5	1.62	1.62	0.02	0.02	0.02	0.007
10	4.05	4.68	0.05	0.06	0.055	0.007
15	6.48	7.29	0.1	0.09	0.085	0.007
20	8.1	8.91	0.13	0.11	0.105	0.014
25	10.35	12.15	0.16	0.15	0.14	0.014
30	12.96	14.85	0.16	0.18	0.17	0.014
40	12.96	14.85	0.17	0.18	0.17	0.007
50	13.97	14.85	0.17	0.18	0.175	0.007
60	13.97	14.85	0.17	0.18	0.175	0.007
70	13.97	14.85	0.17	0.18	0.175	0.007
80	12.96	14.85	0.16	0.18	0.175	0.007
90	12.96	13.77	0.16	0.17	0.175	0
100	12.96	13.77	0.16	0.17	0.17	0
110	12.96	13.77	0.16	0.17	0.17	0.007
120	12.96	13.77	0.16	0.17	0.17	0.007
130	12.96	13.77	0.16	0.17	0.17	0.007
140	12.96	13.77	0.16	0.17	0.17	0.007
150	12.96	13.77	0.16	0.17	0.17	0.007

4.1.2 Permeate Flux After Chemical Cleaning

Time (min)	Run 1 Qp ($ml.min^{-1}$)	Run 2 Qp ($ml.min^{-1}$)	$J_w = \frac{Q_p}{A}$ ($ml.cm^{-2}.min^{-1}$)	$J_w = \frac{Q_p}{A}$ ($ml.cm^{-2}.min^{-1}$)	Average Flux ($ml.cm^{-2}.min^{-1}$)	Standard Deviation
0	0	0	0	0	0	0
5	1.62	1.62	0.02	0.02	0.02	0
10	6.48	5.67	0.06	0.07	0.075	0.007
15	8.1	9.72	0.1	0.09	0.095	0.007
20	10.53	11.34	0.13	0.12	0.125	0.007
25	12.15	13.7	0.15	0.14	0.145	0.007
30	14.58	13.7	0.18	0.17	0.175	0.007
40	14.58	13.7	0.18	0.17	0.175	0.007
50	14.58	13.7	0.18	0.17	0.175	0.007
60	14.58	14.58	0.18	0.17	0.175	0.007
70	14.58	14.58	0.18	0.18	0.18	0
80	14.58	14.58	0.18	0.18	0.18	0
90	14.58	14.58	0.18	0.18	0.18	0
100	14.58	14.58	0.18	0.18	0.18	0.007
110	13.77	13.77	0.17	0.18	0.175	0.007
120	13.77	13.77	0.17	0.18	0.175	0
130	13.77	13.77	0.17	0.17	0.175	0
140	13.77	13.77	0.17	0.17	0.175	0
150	13.77	13.77	0.17	0.17	0.175	0

4.2 Toray SWRO Membranes

4.2.1 Permeate Flux Before Chemical Cleaning

Time (min)	Run 1 Qp ($ml.min^{-1}$)	Run 2 Qp ($ml.min^{-1}$)	$J_w = \frac{Q_p}{A}$ ($ml.cm^{-2}.min^{-1}$)	$J_w = \frac{Q_p}{A}$ ($ml.cm^{-2}.min^{-1}$)	Average Flux ($ml.cm^{-2}.min^{-1}$)	Standard Deviation
0	0	0	0	0	0	0
5	2.43	2.43	0.03	0.03	0.03	0
10	6.48	5.67	0.08	0.07	0.075	0.007
15	7.78	8.1	0.096	0.1	0.098	0.007
20	8.91	8.1	0.11	0.1	0.105	0.007
25	11.34	10.53	0.14	0.13	0.135	0.014
30	13.7	12.15	0.17	0.15	0.16	0.014
40	12.96	12.15	0.16	0.15	0.155	0.007
50	12.96	12.15	0.16	0.15	0.155	0.007
60	12.96	12.96	0.16	0.16	0.16	0.007
70	11.25	12.96	0.15	0.16	0.155	0.007
80	11.25	12.15	0.15	0.15	0.155	0.007
90	11.25	12.15	0.15	0.15	0.155	0.007
100	11.25	12.15	0.15	0.15	0.155	0.007
110	11.25	12.15	0.15	0.15	0.155	0.007
120	11.25	12.15	0.15	0.15	0.155	0.007
130	11.25	12.15	0.15	0.15	0.155	0.007
140	11.25	12.15	0.15	0.15	0.155	0.007
150	11.25	12.15	0.15	0.15	0.155	0.007

4.2.2 Permeate Flux after Chemical Cleaning

Time (min)	Run 1 Qp ($ml.min^{-1}$)	Run 2 Qp ($ml.min^{-1}$)	$J_w = \frac{Q_p}{A}$ ($ml.cm^{-2}.min^{-1}$)	$J_w = \frac{Q_p}{A}$ ($ml.cm^{-2}.min^{-1}$)	Average Flux ($ml.cm^{-2}.min^{-1}$)	Standard Deviation
0	0	0	0	0	0	0
5	3.24	3.24	0.04	0.04	0.04	0.007
10	4.05	4.86	0.05	0.06	0.055	0.003
15	8.1	8.91	0.1	0.11	0.105	0.007
20	8.91	9.72	0.11	0.12	0.12	0.007
25	9.72	11.39	0.12	0.14	0.13	0.007
30	12.15	13.77	0.15	0.17	0.165	0.007
40	12.96	13.77	0.16	0.17	0.165	0.014
50	12.96	13.77	0.16	0.17	0.165	0.007
60	12.96	13.77	0.16	0.17	0.165	0.007
70	12.15	12.96	0.15	0.16	0.155	0
80	12.15	12.96	0.15	0.16	0.155	0.007
90	12.15	12.96	0.15	0.16	0.155	0
100	12.15	12.96	0.15	0.16	0.155	0
110	12.15	12.96	0.15	0.16	0.155	0
120	12.15	12.96	0.15	0.16	0.155	0
130	12.15	12.96	0.15	0.16	0.155	0
140	12.15	12.96	0.15	0.16	0.155	0
150	12.15	12.96	0.15	0.16	0.155	0

5 - Membrane Autopsy

5.1 Fluid Systems SWRO Membrane

5.1.1 Membrane Visualisation

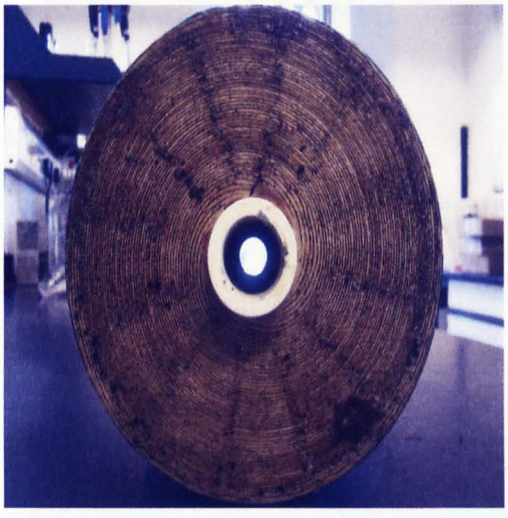

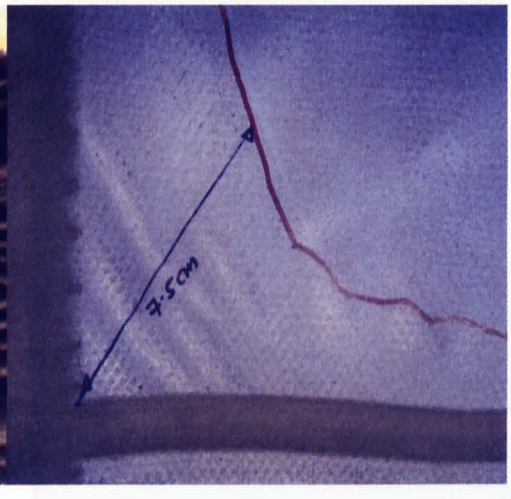

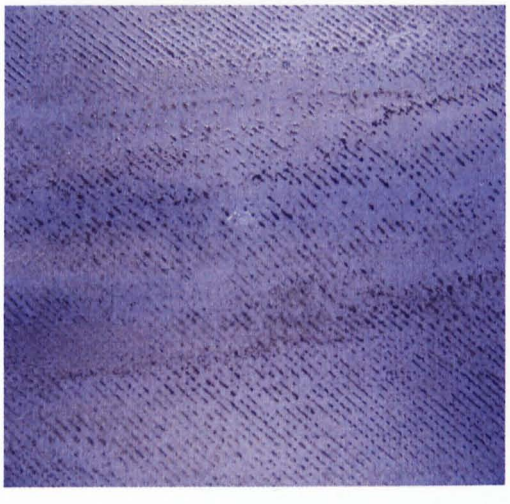

5.1.2 AFM and SEM Images (Fluid Systems Membrane)

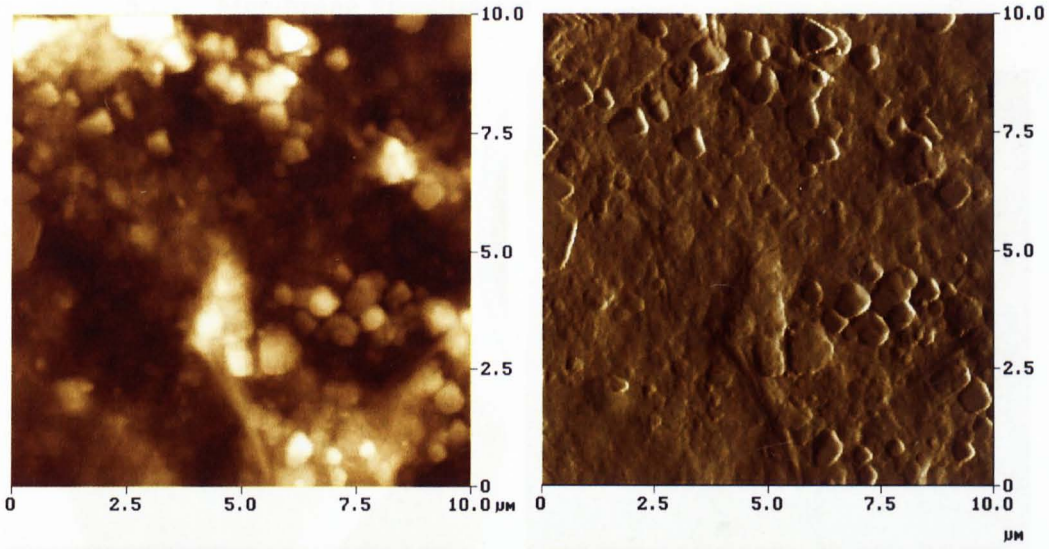

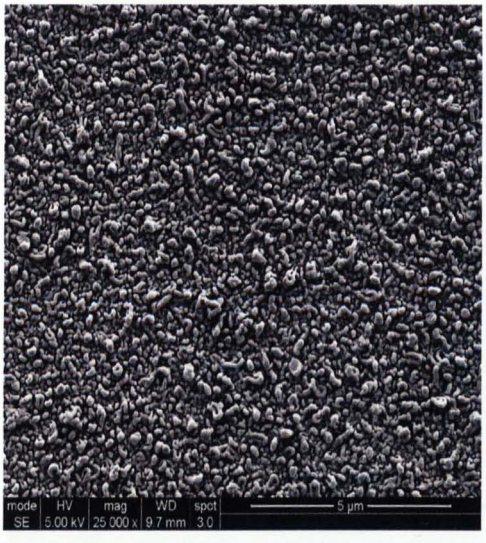

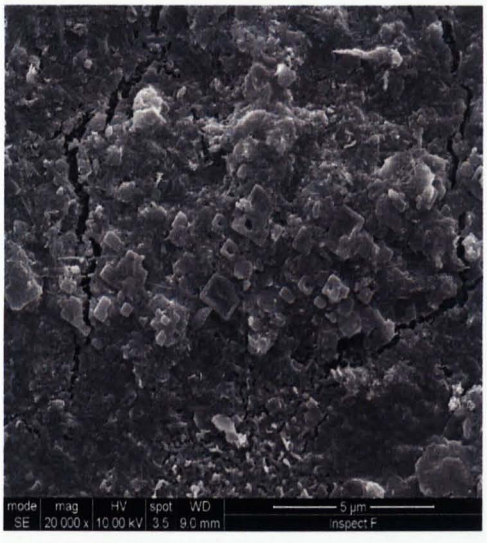

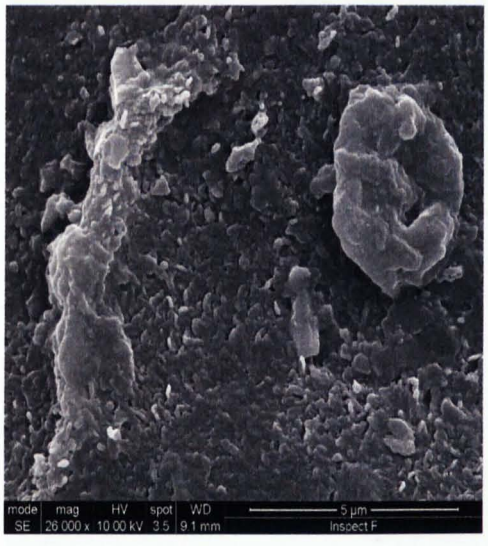

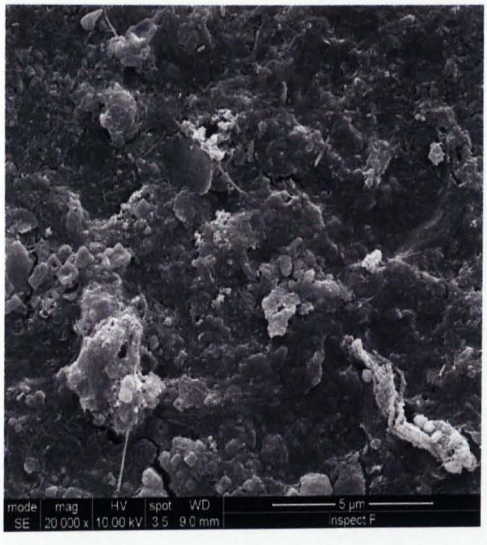

5.2 Toray SWRO Membrane

5.2.1 Membrane Visualisation

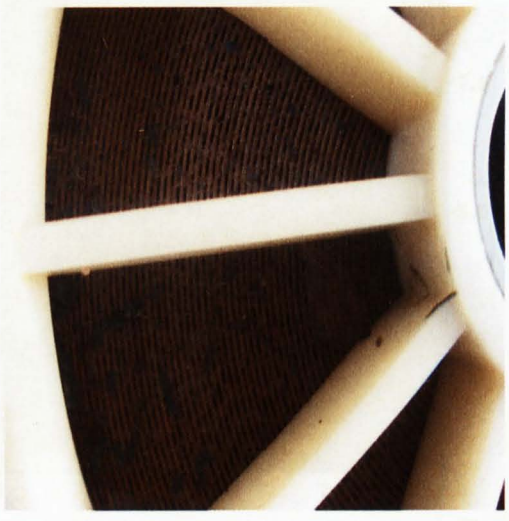


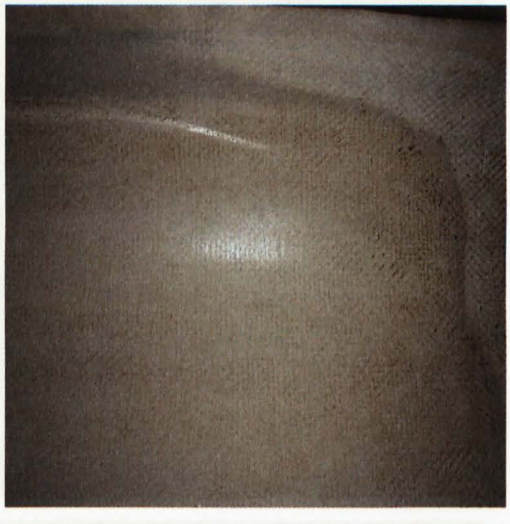

5.2.1 AFM and SEM Images (Toray Membrane)

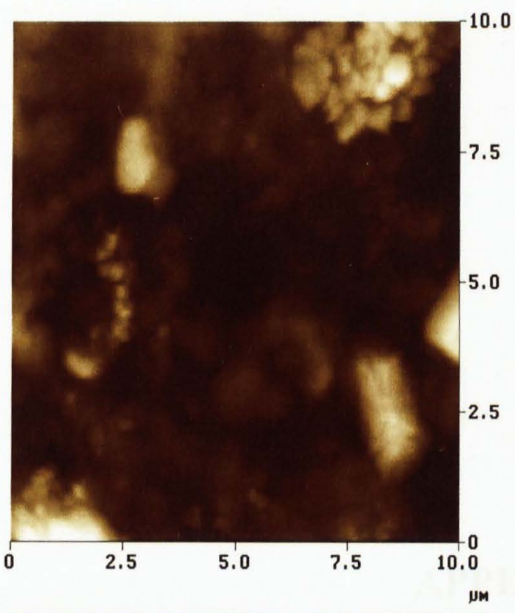

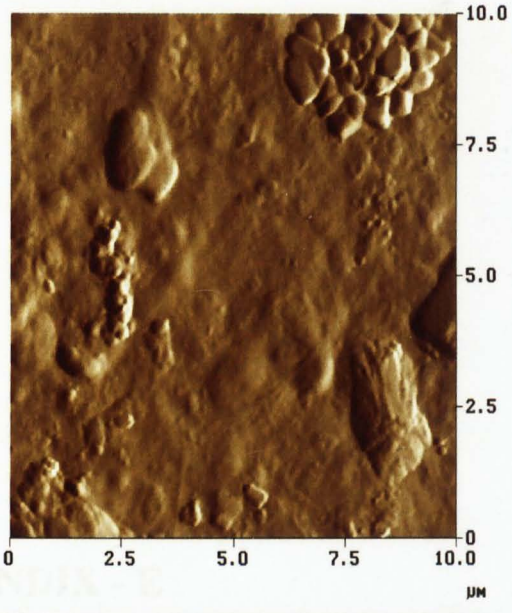

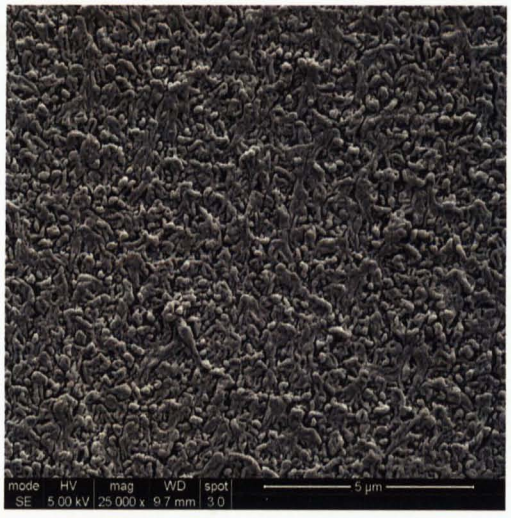

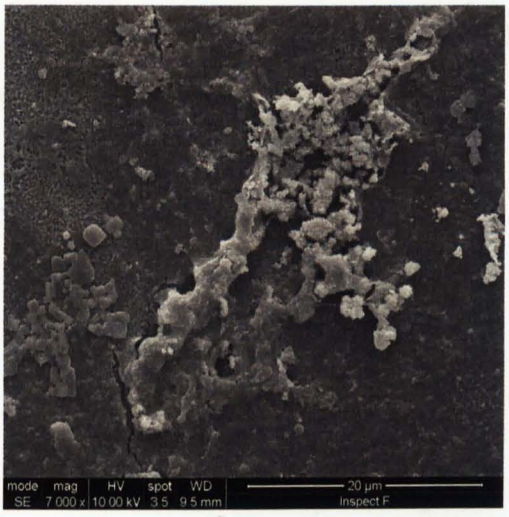

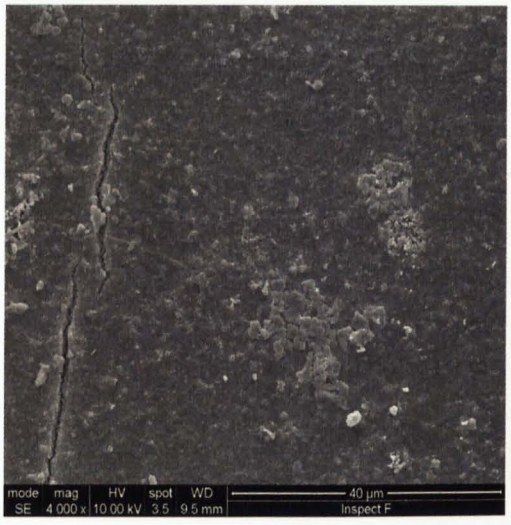

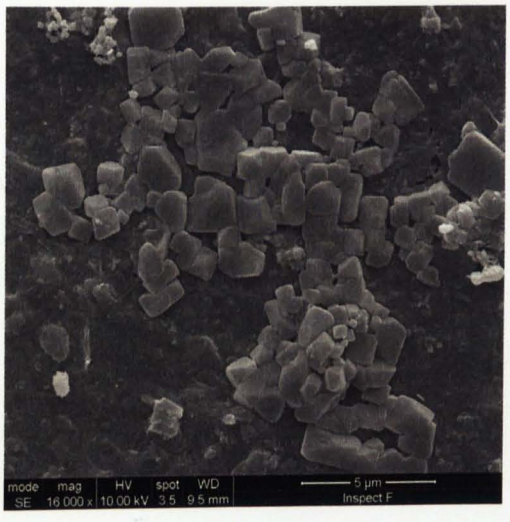

APPENDIX - E

EFFECT OF COMPOSITE FOULING ON THE PERMEATE FLUX OF SWRO MEMBRANE

APPENDIX - E

EFFECT OF COMPOSITE FOULING ON THE PERMEATE FLUX OF SWRO MEMBRANE

1. Pure Water

1.1 Permeate flow

Time (min)	Run 1 Permeate Flow (Q_p) ($ml.min^{-1}$)	Run 2 Permeate Flow (Q_p) ($ml.min^{-1}$)	Average Permeate Flow (Q_p) ($ml.min^{-1}$)
0	0	0	0
5	5.99	5.35	5.66 ± 0.452
10	14.58	13.77	14.67 ± 0.573
15	21.87	21.10	21.48 ± 0.544
20	29.97	25.92	27.87 ± 2.63
25	37.26	34.02	35.6 ± 2.29
30	44.55	44.55	44.55 ± 0
60	40.50	39.69	40.10 ± 0.573
90	39.69	38.10	38.89 ± 1.124
120	36.45	37.26	36.85 ± 0.573
150	35.64	37.26	36.44 ± 1.146
180	34.83	36.45	35.63 ± 1.146
210	34.02	35.64	34.82 ± 1.146
240	34.02	35.64	34.82 ± 1.146
270	34.02	35.64	34.82 ± 1.146
300	33.21	35.64	34.40 ± 1.718
330	33.21	35.64	34.40 ± 1.718
360	33.21	35.64	34.40 ± 1.718

1.2 Permeate flux

Time (min)	Run 1 Permeate flux (J) $J = \frac{Q_p}{A}$ (ml.cm^{-2}.min^{-1})	Run 2 Permeate flux (J) $J = \frac{Q_p}{A}$ (ml.cm^{-2}.min^{-1})	Average Permeate flux (J) $J = \frac{Q_p}{A}$ (ml.cm^{-2}.min^{-1})
0	0	0	0
5	0.07	0.06	0.07 ± 0.006
10	0.18	0.17	0.18 ± 0.007
15	0.27	0.26	0.27 ± 0.007
20	0.37	0.32	0.34 ± 0.035
25	0.46	0.42	0.44 ± 0.028
30	0.55	0.55	0.55 ± 0
60	0.50	0.49	0.50 ± 0.007
90	0.49	0.47	0.48 ± 0.0141
120	0.45	0.46	0.45 ± 0.007
150	0.44	0.46	0.44 ± 0.0141
180	0.43	0.45	0.43 ± 0.0141
210	0.42	0.44	0.43 ± 0.0141
240	0.42	0.44	0.43 ± 0.141
270	0.42	0.44	0.43 ± 0.141
300	0.41	0.44	0.43 ± 0.212
330	0.41	0.44	0.43 ± 0.212
360	0.41	0.44	0.43 ± 0.212

1.3 Mass transfer coefficient of Pure water (K_w)

- Feed pressure = 41 bar
- Membrane surface area = 81 cm^2.
- Average permeate flux (J)

$$J = \frac{Q_p}{A} = \frac{34.4}{81} = 0.43 \text{ (ml.cm}^{-2}\text{.min}^{-1}\text{)}$$

The feed water and retentate contain pure water and osmotic pressure difference across the membrane is zero and the feed pressure is equal the net driven pressure (P_f = NDP).

- Mass transfer coefficient for pure water (K_w)

$$K_w = \frac{J}{NDP} = \frac{0.43}{41} = 10.5 \times 10^{-3} \text{ (ml.cm}^{-2}\text{.min}^{-1}\text{ .bar}^{-1}\text{)}$$

2. The Mediterranean Sea Seawater

2.1 Permeate Flow, Permeate Flux and Normalised Permeate Flux

Time (min)	Run 1 Qp ($ml.min^{-1}$)	Run 2 Qp ($ml.min^{-1}$)	$J = \frac{Q_p}{A}$ ($ml.cm^{-2}.min^{-1}$)	$J = \frac{Q_p}{A}$ ($ml.cm^{-2}.min^{-1}$)	Average $J = \frac{Q_p}{A}$ ($ml.cm^{-2}.min^{-1}$)
0	7.65	7.85	0.096	0.097	1.0 ± 0.0010
30	7.57	7.62	0.095	0.094	1.0 ± 0.0010
60	7	7.04	0.086	0.087	0.087 ± 0.0010
90	6.84	6.91	0.085	0.085	0.085 ± 0
120	6.39	6.78	0.079	0.084	0.082 ± 0.0335
150	6.33	6.2	0.078	0.077	0.078 ± 0.0010
180	6.35	5.22	0.066	0.064	0.065 ± 0.0014
210	5.25	5.2	0.065	0.064	0.065 ± 0.0010
240	5.13	5.16	0.063	0.064	0.064 ± 0.0010
270	4.64	5.08	0.057	0.063	0.060 ± 0.0042
300	4.58	4.43	0.057	0.055	0.056 ±0.0014
330	4.42	4.3	0.055	0.053	0.054 ± 0.0014
360	4.36	4.12	0.054	0.051	0.053 ±0.0021

2.2 Average Normalised Permeate Flux

Time (min)	Temperature (°C)	Average of normalised permeate flux (J_a/J_0)
0	24	1.0 ± 0.0010
30	24.8	1.0 ± 0.0010
60	25.2	0.87 ± 0.0010
90	25.5	0.85 ± 0
120	25.3	0.82 ± 0.0335
150	25.1	0.78 ± 0.0010
180	25.4	0.65 ± 0.0014
210	25.5	0.65 ± 0.0010
240	25.8	0.64 ± 0.0010
270	25.3	0.60 ± 0.0042
300	25.1	0.56 ±0.0014
330	25.4	0.54 ± 0.0014
360	25.3	0.53 ±0.0021

2.3 Feed and Permeate Concentration

Time (min)	Run 1 C_f ($mg.l^{-1}$)	Run 2 C_f ($mg.l^{-1}$)	Average C_f ($mg.l^{-1}$)	Run 1 C_p ($mg.l^{-1}$)	Run 2 C_p ($mg.l^{-1}$)	Average C_p ($mg.l^{-1}$)
0	37100	37100	37100 ± 0	5000	4500	4750 ±353.55
30	37100	37100	37100 ± 0	3500	3800	3650 ± 212.13
60	37100	37100	37100 ± 0	3150	3500	3050 ± 247.48
90	37100	37100	37100 ± 0	2830	3300	2825 ± 282.82
120	37100	37100	37100 ± 0	2700	3100	2725 ± 282.82
150	37110	37100	37105 ± 7.07	2500	2900	2580 ± 212.13
180	37130	37110	37120 ± 14.14	2390	2550	2495 ± 113.14
210	37150	37120	37135 ± 21.21	2300	2450	2380 ± 176.78
240	37160	37140	37150 ± 14.14	2240	2350	2270 ± 176.78
270	37180	37190	37185 ± 7.07	2150	2300	2185 ± 176.78
300	37220	37200	37210 ± 4.14	2230	2280	2255 ± 127.279
330	37240	37230	37235 ± 7.07	2250	2300	2285 ± 106.07
360	37250	37260	37255 ± 7.07	2300	2350	2350 ± 106.07

2.4 Average Salt Rejection and Salt Passage (%)

Time (min)	Average C_f ($mg.l^{-1}$)	Average C_p ($mg.l^{-1}$)	Salt Rejection (%) $SR(\%) = \frac{(C_f - C_p)}{C_f}$	Salt Passage (%) $SP(\%) = 100 - SR$
0	37100 ± 0	4750 ±353.6	87.2 ± 0.990	12.8 ± 0.990
30	37100 ± 0	3650 ± 212.1	90.2 ± 0.566	9.8 ± 0.566
60	37100 ± 0	3325 ± 247.5	91.1 ± 0.636	8.9 ± 0.636
90	37100 ± 0	3100 ± 282.8	92.2 ± 0.353	7.8 ± 0.353
120	37100 ± 0	2900 ± 282.8	92.6 ± 0.141	7.4 ± 0.141
150	37105 ±7. 071	2750 ± 212.1	93.2 ± 0.212	6.8 ± 0.212
180	37120 ± 14.14	2470 ± 113.1	93.5 ± 0.212	6.5 ± 0.212
210	37135 ± 21.21	2325 ± 176.8	93.9 ± 0.212	6.1 ± 0.212
240	37150 ± 14.14	2225 ± 176.8	94.2 ± 0.071	5.8 ± 0.071
270	37185 ± 7.071	2175 ± 176.8	94.2 ± 0.071	5.8 ± 0.071
300	37210 ± 14.14	2190 ± 127.3	94.0 ± 0.071	6.0 ± 0.071
330	37235 ± 7.071	2225 ± 106.1	93.9 ± 0.141	6.1 ± 0.141
360	37255 ± 7.071	2275 ± 106.1	93.8 ± 0.071	6.2 ± 0.071

2.5 - Mass transfer coefficient of Mediterranean Sea seawater (K_w)

- TDS = 37100 $mg.L^{-1}$
- Feed pressure = 41bar
- Recovery = 0.1% (Very low)
- Area = 81 cm^2

The same equations present in Section 1.4 were used to calculate mass transfer coefficient for the Mediterranean Sea seawater. Results are shown in Table 2.5 and Table 2.6, respectively.

Table 2.5: Calculation of osmotic pressure (π) and net driven pressure (NDP)

Time (min)	P_f (bar)	P_c (bar)	P_C (bar)	Avg. P_c (bar)	ΔP (bar)	π_{fc} (bar)	π_p (bar)	NDP (bar)
0	41	41	41	41	0	29.68	3.80	7.52
30	41	41	41	41	0	29.68	2.92	8.4
60	41	41	41	41	0	29.68	2.66	8.7
90	41	41	41	41	0	29.68	2.48	8.84
120	41	40.65	41	40.83	0.2	29.68	2.32	8.90
150	41	40.65	40.65	40.65	0.35	29.68	2.20	9.0
180	41	40.14	40.14	40.14	0.86	29.70	1.98	9.10
210	41	39.97	40.31	40.14	0.86	29.72	1.86	9.0
240	41	39.97	39.97	39.97	1.03	29.72	1.74	9.11
270	41	39.60	39.60	39.60	1.4	29.75	1.72	8.77
300	41	39.60	39.60	39.60	1.4	29.77	1.75	8.78
330	41	39.60	39.60	39.60	1.4	29.79	1.78	8.73
360	41	39.60	39.60	39.60	1.4	29.8	1.82	8.68

Table 2.6: Calculation of mass transfer coefficient (k_w)

Time (min)	Permeate flux (J) ($ml.cm^{-2}.min^{-1}$)	Net Driven Pressure NDP (bar)	$K_w = \frac{J}{NDP}$ ($ml.cm^{-2}.min^{-1}.bar^{-1}$)
0	0.10	7.52	13.3×10^{-3}
30	0.10	8.4	11.9×10^{-3}
60	0.090	8.7	10.4×10^{-3}
90	0.085	8.84	9.6×10^{-3}
120	0.082	8.90	9.2×10^{-3}
150	0.078	9.0	8.7×10^{-3}
180	0.065	9.10	7.1×10^{-3}
210	0.065	9.0	7.2×10^{-3}
240	0.064	9.11	7.0×10^{-3}
270	0.061	8.77	7.0×10^{-3}
300	0.056	8.78	6.4×10^{-3}
330	0.054	8.73	6.2×10^{-3}
360	0.053	8.68	6.1×10^{-3}

2.7 Permeate flux verses operating pressure (Pressure increase)

Feed Pressure (psi)	Feed Pressure (bar)	Pressure increase		Average Permeate flux (J) ($ml.cm^{-2}.min^{-1}$)
		Run 1 Permeate flux (J) ($ml.cm^{-2}.min^{-1}$)	Run 2 Permeate flux (J) ($ml.cm^{-2}.min^{-1}$)	
0	0	0	0	0
100	7	0	0	0
200	14	0	0	0 ± 0
300	20	0.018	0.016	0.017 ± 0.001
400	27	0.034	0.033	0.034 ± 0.001
500	34	0.066	0.062	0.064 ± 0.003
600	41	0.094	0.092	0.093 ± 0.001

2.8 Permeate flux verses operating pressure (Pressure decrease)

Feed Pressure (psi)	Feed Pressure (bar)	Pressure decrease		Average Permeate flux (J) ($ml.cm^{-2}.min^{-1}$)
		Run 1 Permeate flux (J) ($ml.cm^{-2}.min^{-1}$)	Run 2 Permeate flux (J) ($ml.cm^{-2}.min^{-1}$)	
600	41	0.054	0.051	0.053 ± 0.002
500	35	0.031	0.027	0.029 ± 0.003
400	28	0.020	0.015	0.018 ± 0.004
300	21	0.006	0.003	0.005 ± 0.002
200	14	0	0	0
100	7	0	0	0
0	0	0	0	0

3. The North Sea Seawater

3.1. Permeate Flow (Q_p) and Permeate Flux (J) verses Time .

Time (min)	Run 1 (Q_p) ($ml.min^{-1}$)	Run 1 (Q_p) ($ml.min^{-1}$)	$J = \frac{Q_p}{A}$ ($ml.cm^{-2}.min^{-1}$)	$J = \frac{Q_p}{A}$ ($ml.cm^{-2}.min^{-1}$)	Average $J = \frac{Q_p}{A}$ ($ml.cm^{-2}.min^{-1}$)
0	11.4	11.34	0.14	0.14	0.14 ± 0
30	11.45	11.34	0.14	0.14	0.14 ± 0
60	10.64	10.53	0.13	0.13	0.13 ± 0
90	10.63	10.53	0.13	0.13	0.13 ± 0
120	9.8	9.72	0.12	0.12	0.12 ± 0
150	9.82	9.72	0.12	0.12	0.12 ± 0
180	9	8.91	0.11	0.11	0.11 ± 0
210	8.97	8.91	0.11	0.11	0.11 ± 0
240	8.18	8.1	0.099	0.1	0.10 ± 0.0010
270	8	7.94	0.097	0.099	0.098 ± 0.0014
300	7.78	7.7	0.094	0.096	0.095 ± 0.0014
330	7.36	7.29	0.089	0.091	0.090 ± 0.0014
360	7.3	7.21	0.088	0.09	0.089 ± 0.0014

3.2 Average Normalised Permeate Flux

Time (min)	Temperature (°C)	Average of normalised permeate flux (J_a/J_0)
0	25	1 ± 0
30	25	1 ± 0
60	25.1	0.93 ± 0
90	25.3	0.93 ± 0
120	25.5	0.86 ± 0
150	24.8	0.86 ± 0
180	25.4	0.79 ± 0
210	24.7	0.79 ± 0
240	25.1	0.71 ± 0.0010
270	25	0.70 ± 0.0014
300	25.4	0.68 ± 0.0014
330	25.2	0.65 ± 0.0014
360	24.8	0.64 ± 0.0014

3.3 Feed and Permeate Concentration

Time (min)	Run 1 C_f ($mg.L^{-1}$)	Run 2 C_f ($mg.L^{-1}$)	Average C_f ($mg.L^{-1}$)	Run 1 C_p ($mg.L^{-1}$)	Run 2 C_p ($mg.L^{-1}$)	Average C_p ($mg.L^{-1}$)
0	25500	25500	25500 ± 0	3850	4000	3925 ±106.07
30	25500	25500	25500 ± 0	3500	3700	2600 ± 141.42
60	25500	25500	25500 ± 0	3100	3300	3200 ± 141.42
90	25500	25500	25500 ± 0	2800	2900	2850 ± 70.71
120	25500	25500	25500 ± 0	2600	2750	2675 ± 106.07
150	25500	25500	25500 ± 0	2300	2500	2400 ± 141.42
180	25500	25500	25500 ± 0	2150	2250	2200 ± 70.71
210	25520	25500	25510 ± 14.142	2050	2200	2125 ± 106.07
240	25550	25530	25540 ±14.142	2000	2150	2075 ± 106.07
270	25570	25550	25560 ± 4.142	2100	2200	2150 ± 70.71
300	25600	25610	25605 ± 7.071	2100	2230	2165 ± 91.92
330	25630	25650	25640 ±14.142	2120	2280	2185 ± 91.92
360	25650	25650	25650 ± 0	2150	2300	2225 ± 106.07

3.4 Average Salt Rejection and Salt Passage (%) (The North Sea).

Time (min)	Average C_f ($mg.l^{-1}$)	Average C_p ($mg.l^{-1}$)	Salt Rejection (%) $SR(\%) = \frac{(C_f - C_p)}{C_f}$	Salt Passage (%) $SP(\%) = 100 - SR$
0	25500 ± 0	3925 ±106.07	84.6 ±0.424	15.4 ±0.212
30	25500 ± 0	2600 ± 141.42	85.9 ± 0.566	14.1 ± 0.283
60	25500 ± 0	3200 ± 141.42	88.2 ± 0.566	11.8 ± 0.238
90	25500 ± 0	2850 ± 70.71	89.1 ± 0.141	10.9 ± 0.71
120	25500 ± 0	2675 ± 106.07	90 ± 0.283	10.0 ± 0.141
150	25500 ± 0	2400 ± 141.42	91.1 ± 0.141	8.9 ± 0.071
180	25500 ± 0	2200 ± 70.711	91.5 ± 0.141	8.5 ± 0.071
210	25510 ± 14.14	2125 ± 106.07	91.8 ± 0.283	8.2 ± 0.141
240	25540 ± 14.14	2075 ± 106.07	91.8 ± 0.566	8.2 ± 0.283
270	25560 ± 4.14	2150 ± 70.711	91.6 ± 0.354	8.5 ± 0.177
300	25605 ± 7.071	2165 ± 91.923	91.6 ± 0.354	8.5 ± 0.177
330	25640 ± 14.14	2185 ± 91.923	91.5 ± 0.354	8.6 ± 0.177
360	25650 ± 0	2225 ± 106.07	91.3 ± 0.414	8.7 ± 0.212

3.5 Feed (P_f), Concentrate (P_c) and Osmotic (π) Pressure Verses Time

Time (min)	P_f (bar)	P_c (bar)	P_c (bar)	Avg. P_c (bar)	ΔP (bar)	π_{fc} (bar)	π_p (bar)	NDP (bar)
0	41	41	41	41	0	20.4	3.14	15.9
30	41	41	41	41	0	20.4	2.80	17.5
60	41	41	41	41	0	20.4	2.56	16.8
90	41	41	41	41	0	20.4	2.28	17.2
120	41	40.98	40.98	40.98	0.20	20.4	2.14	17.4
150	41	40.31	41	40.66 ± 0.014	0.35	20.4	1.92	17.7
180	41	40.31	39.97	40.14 ± 0.014	0.86	20.42	1.76	18.0
210	41	40.31	39.97	40.14 ± 0.014	0.86	20.43	1.7	18.0
240	41	39.97	39.97	39.97 ± 0	1.03	20.5	1.66	18.1
270	41	39.6	39.6	39.6 ± 0	1.4	20.5	1.72	17.9
300	41	39.6	39.6	39.6 ± 0	1.4	20.51	1.73	17.9
330	41	39.6	39.6	39.6 ± 0	1.4	20.52	1.75	17.9
360	41	39.6	39.6	39.6 ± 0	1.4	20.52	1.78	17.8

3.6 Permeate flux (J), Net Driven Pressure (NDP) and Mass Transfer Coefficient for Water (K_w) verses Time

Time (min)	Permeate flux (J) ($ml.cm^{-2}.min^{-1}$)	Net Driven Pressure NDP (bar)	$K_w = \frac{J}{NDP}$ ($ml.cm^{-2}.min^{-1}.bar^{-1}$)
0	0.14 ± 0	15.9	8.8×10^{-3}
30	0.14 ± 0	17.5	8.0×10^{-3}
60	0.13 ± 0	16.8	7.76×10^{-3}
90	0.13 ± 0	17.2	7.57×10^{-3}
120	0.12 ± 0	17.4	6.96×10^{-3}
150	0.12 ± 0	17.7	6.77×10^{-3}
180	0.11 ± 0	18.0	6.13×10^{-3}
210	0.11 ± 0	18.0	6.10×10^{-3}
240	0.10 ± 0.001	18.1	5.53×10^{-3}
270	0.099 ± 0.0014	17.9	5.53×10^{-3}
300	0.096 ± 0.0014	17.9	5.36×10^{-3}
330	0.091 ± 0.0014	17.9	5.10×10^{-3}
360	0.09 ± 0.0014	17.8	5.10×10^{-3}

3.7 Permeate Flux Verses Operating Pressure (Pressure Increase).

Feed Pressure (psi	Feed Pressure (bar)	Pressure Increase		Average Permeate flux (J_w) ($ml.cm^{-2}.min^{-1}$)
		Run 1 Permeate flux (J_w) ($ml.cm^{-2}.min^{-1}$)	Run 2 Permeate flux (J_w) ($ml.cm^{-2}.min^{-1}$)	
0	0	0	0	0
100	7	0	0	0
200	14	0	0	0
300	20	0.02	0.015	0.018 ± 0.001
400	27	0.041	0.039	0.040 ± 0.002
500	34	0.091	0.92	0.092 ± 0.001
600	41	0.14	0.14	0.14 ± 0

3.8 Permeate Flux Verses Operating Pressure (Pressure Decrease).

Feed Pressure (psi)	Pressure Decrease		Average Permeate flux (J_w) ($ml.cm^{-2}.min^{-1}$)
	Run 1 Permeate flux (J_w) ($ml.cm^{-2}.min^{-1}$)	Run 2 Permeate flux (J_w) ($ml.cm^{-2}.min^{-1}$)	
600	0.12	0.11	0.115 ± 0
500	0.073	0.07	0.0715 ± 0.003
400	0.030	0.028	0.029 ± 0.004
300	0.004	0.003	0.0035 ± 0.001
200	0	0	0
100	0	0	0
0	0	0	0

APPENDIX - F

CALCULATION OF REYNOLDS NUMBER

APPENDIX - F

CALCULATION OF REYNOLDS NUMBER

1. **The following equations were used to calculate the velocity and the Reynolds number (Ng and Elimelech, 2004; Hoek *et al.*, (2002):**

$$u = \frac{Q_f}{A}$$

$$\mathrm{Re} = \frac{\rho \times u \times d_h}{\mu}$$

$$d_h = 4 \times \frac{Cross-section\ Area}{Total\ wetted\ perimeter} = \frac{4(w \times h)}{2(w+h)}$$

Where:

u - is the cross flow velocity ($m.s^{-1}$)

Q_f - is the volumetric feed flow rate ($ml.min^{-1}$) =

A - is the channel cross section area = 81 cm^2

d_h - is the hydraulic diameter (mm)

w- is the width of the duct (mm)

h – is the highest of the duct (mm)

μ - is the dynamic viscosity ($kg.m^{-1}.s^{-1}$)

2. **Calculation Procedure:**

Feed flow (Q_f) = 4.2 ($l.min^{-1}$)

$$Q_f = \frac{4.2 \times 10^{-3}}{60} = 7 \times 10^{-5}\ (m^3.s^{-1})$$

Dynamic viscosity = 1.08×10^{-3} ($kg.m^{-1}.s^{-1}$)

Channel weighted (W) = 10.16 cm

Channel highest (h) = 0.2 cm

Hydraulic diameter dh = $\frac{2 \times W \times h}{W+h} = \frac{2 \times 10.16 \times 0.2}{10.16+0.2} = 3.9 \times 10^{-3}\ (m)$

Cross section area (A) = W × h = 0.002 × 0.1016 = 20.32×10^{-5} (m^2)

$$u = \frac{Q_f}{A} = \frac{7.0\times10^{-5}(m^3.s^{-1})}{20.32\times10^{-5}\ (m^2)} = 0.35\ (m.s^{-1})$$

$$\mathrm{Re} = \frac{u\times\rho\times dh}{\mu} = \frac{0.35\ (m.s^{-1})\times1000\ (kg.m^{-3})\times(3.9\times10^{-3})\ m}{1.08\times10^{-3}\ (kg.m^{-1}.s^{-1})} = 1264$$

Table 1: Operating conditions for fouling experiments.

Feed flow (Q_f) ($L.min^{-1}$)	Velocity (u) ($m.s^{-1}$)	Dynamic viscosity (μ) ($kg.m^{-1}.s^{-1}$)	Water density (ρ) ($kg.m^{-3}$)	Reynolds Number (Re)
4.2	0.35	1.08×10^{-3}	1000	1264

APPENDIX - G

CALCULATION OF CONCENTRATION POLARISATION

APPENDIX - G

CALCULATION OF CONCENTRATION POLARISATION

Average feed-concentrate osmotic pressure (bar) $\Delta\pi = \pi_{fc} - \pi_p$

Average feed-concentrate pressure (bar) $\Delta P = \dfrac{P_f - P_c}{2}$

Feed-concentrate osmotic pressure (bar) $\pi_{fc} = \dfrac{0.8 \times C_{fc}}{1000}$

Permeate osmotic pressure (bar) $\pi_p = \dfrac{0.8 \times C_p}{1000}$

Average feed-concentrate concentration ($mg.L^{-1}$) $C_{fc} = c_f \left(\dfrac{\ln\left(\dfrac{1}{1-Y}\right)}{Y} \right)$

Mass transfer coefficient (K) $K = \dfrac{(J_W)_{Salt}}{\ln\left\{\dfrac{\Delta P}{\pi_{fc} - \pi_p} \times \left[1 - \dfrac{(J_w)_{salt}}{(J_w)_{H_2O}}\right]\right\}}$

Concentration Polarisation $CP = \dfrac{C_s}{C_b} = \exp\left(\dfrac{J_w}{K}\right)$

1 - Raw seawater (The Mediterranean Sea)

Parameter	0	30	60	90	120	150	180	210	240	270	300	330	360
$J_w(H_2O)$ ($ml.cm^{-2}.min^{-1}$)	0.34	0.34	0.34	0.34	0.34	0.34	0.34	0.34	0.34	0.34	0.34	0.34	0.34
J_w(Salt) ($ml.cm^{-2}.min^{-1}$)	0.096	0.094	0.087	0.085	0.082	0.078	0.065	0.065	0.064	0.060	0.056	0.054	0.053
C_f ($mg.L^{-1}$)	37100	37100	37100	37100	37100	37105	37120	37135	37150	37185	37210	37235	37258
π_{fc} (bar)	29.68	29.68	29.68	29.68	29.68	29.68	29.70	29.72	29.72	29.75	29.77	29.79	29.80
π_p (bar)	3.8	2.92	2.66	2.48	2.32	2.2	1.98	1.96	1.74	1.72	1.75	1.78	1.82
$(\Delta\pi_{fc}- \Delta\pi_p)$ (bar)	25.9	26.8	27	27.2	27.4	27.5	27.7	27.9	28	28	28	28	28
P_f (bar)	41	41	41	41	41	41	41	41	41	41	41	41	41
P_c (bar)	41	41	41	41	40.83	40.65	40.14	40.14	39.97	39.6	36.9	39.6	39.6
ΔP (bar)	0	0	0	0	0.20	0.35	0.86	0.86	1.03	1.4	1.4	1.4	1.4
$\Delta P=(p_f+p_c)/2$ (bar)	41	41	41	41	40.92	40.83	40.57	40.57	40.49	40.3	40.3	40.3	40.3
K	0.512	0.617	0.456	0.447	0.429	0.398	0.256	0.258	0.261	0.239	0.215	0.203	0.197
CP	1.2	1.2	1.2	1.21	1.22	1.22	1.29	1.29	1.28	1.29	1.30	1.31	1.31

2 - Raw seawater (The North Sea)

Parameter	0	30	60	90	120	150	180	210	240	270	300	330	360
$J_w(H_2O)$ ($ml.cm^{-2}.min^{-1}$)	0.34	0.34	0.34	0.34	0.34	0.34	0.34	0.34	0.34	0.34	0.34	0.34	0.34
J_w(Salt) ($ml.cm^{-2}.min^{-1}$)	0.14	0.14	0.135	0.130	0.125	0.120	0.115	0.110	0.105	0.099	0.097	0.093	0.090
C_{fc} ($mg.L^{-1}$)	25500	25500	25500	25500	25500	25500	25500	25510	25540	25560	25605	25640	25650
π_f (bar)	20.4	20.4	20.4	20.4	20.4	20.4	20.42	20.43	20.5	20.5	20.51	20.52	20.52
P_f (bar)	41	41	41	41	41	41	41	41	41	41	41	41	41
$(\Delta\pi_{fc}- \Delta\pi_p)$ (bar)	17.3	17.6	17.8	18.1	18.3	18.5	18.7	18.7	18.8	18.8	18.8	18.8	18.7
P_c (bar)	41	41	41	41	40.98	40.66	40.14	40.14	39.7	39.6	39.6	39.6	39.6
ΔP (bar)	0	0	0	0	0.2	0.35	0.86	0.86	1.03	1.4	1.4	1.4	1.4
$\Delta P=(p_f+p_c)/2$ (bar)	41	41	41	41	40.96	40.92	40.79	40.79	40.75	40.65	40.65	40.65	40.65
K	0.30	0.31	0.28	0.29	0.25	0.26	0.23	0.23	0.20	0.19	0.18	0.17	0.16
CP	1.6	1.6	1.6	1.61	1.61	1.62	1.63	1.63	1.66	1.67	1.69	1.71	1.72

APPENDIX - H

PREVENTION OF SWRO MEMEBRANE FOULING USING NANA-ALUMINA DEPTH FILTER (DISRUPTOR^{TM})

APPENDIX - H

PREVENTION OF SWRO MEMEBRANE FOULING USING NANA-ALUMINA DEPTH FILTER (DISRUPTOR™)

1. Raw Seawater from the North Sea.

1.1 Permeate Flow (Q_p) verses Time.

Time (min)	Run 1 (Q_p) ($ml.min^{-1}$)	Run 1 (Q_p) ($ml.min^{-1}$)	Average (Q_p) ($ml.min^{-1}$)	$J = \frac{Q_p}{A}$ ($ml.cm^{-2}.min^{-1}$)	$J = \frac{Q_p}{A}$ ($ml.cm^{-2}.min^{-1}$)	Average (J) ($ml.cm^{-2}.min^{-1}$)
0	11.4	11.34	11.37 ± 0.042	0.14	0.14	0.14 ± 0
30	11.45	11.34	11.4 ± 0.078	0.14	0.14	0.14 ± 0
60	10.64	10.53	10.59 ± 0.078	0.13	0.13	0.13 ± 0
90	10.63	10.53	10.58 ± 0.71	0.13	0.13	0.13 ± 0
120	9.8	9.72	9.76 ± 0.057	0.12	0.12	0.12 ± 0
150	9.82	9.72	9.77 ± 0.071	0.12	0.12	0.12 ± 0
180	9	8.91	9.0 ± 0.064	0.11	0.11	0.11 ± 0
210	8.97	8.91	8.94 ± 0.042	0.11	0.11	0.11 ± 0
240	8.18	8.1	8.14 ± 0.057	0.099	0.1	0.10 ± 0.001
270	8	7.94	7.97 ± 0.042	0.097	0.099	0.099 ± 0.0014
300	7.78	7.7	7.74 ± 0.057	0.094	0.096	0.096 ± 0.0014
330	7.36	7.29	7.33 ± 0.05	0.089	0.091	0.091 ± 0.0014
360	7.3	7.21	7.26 ± 0.064	0.088	0.09	0.09 ± 0.0014

1.2 Feed (P_f), Concentrate (P_c) and Osmotic (π) Pressure Verses Time

Time (min)	P_f (bar)	P_c (bar)	P_c (bar)	ΔP (bar)	ΔP (bar)	Average ΔP (bar)	π_{fc} (bar)	π_p (bar)	NDP (bar)
0	41	41	41	0	0	0	20.3	0.20	20.5
30	41	41	41	0	0	0	20.3	0.20	20.5
60	41	40.7	40.7	0.3	0.3	0.3 ± 0	20.3	0.20	20.35
90	41	40.7	40.3	0.3	0.3	0.3 ± 0	20.3	0.20	20.35
120	41	40.7	40.5	0.3	0.5	0.4 ± 0.141	20.3	0.20	20.25
150	41	40.3	40.5	0.7	0.5	0.6 ± 0.141	20.3	0.20	20.20
180	41	40.3	40.3	0.7	0.7	0.7 ± 0	20.3	0.20	20.15
210	41	40.3	40.3	0.7	0.7	0.7 ± 0	20.3	0.20	20.15
240	41	40	40.3	1.0	0.7	0.85 ± 0.212	20.3	0.20	20.10
270	41	40	40	1.0	1.0	1.0 ± 0	20.3	0.20	20.0
300	41	40	40	1.0	1.4	1.2 ± 0.283	20.3	0.20	19.9
330	41	39.6	39.6	1.4	1.4	1.4 ± 0	20.3	0.20	19.8
360	41	39.6	39.6	1.4	1.4	1.4 ± 0	20.3	0.20	19.8

1.3 Permeate flux (J), Net Driven Pressure (NDP) and Mass Transfer Coefficient for Water (K_w) verses Time

Time (min)	Permeate flux (J) ($ml.cm^{-2}.min^{-1}$)	Net Driven Pressure NDP (bar)	$K_w = \frac{J}{NDP}$ ($ml.cm^{-2}.min^{-1}.bar^{-1}$)
0	0.14 ± 0	20.5	6.8×10^{-3}
30	0.14 ± 0	20.5	6.8×10^{-3}
60	0.13 ± 0	20.35	6.4×10^{-3}
90	0.13 ± 0	20.35	6.4×10^{-3}
120	0.12 ± 0	20.25	5.9×10^{-3}
150	0.12 ± 0	20.20	5.9×10^{-3}
180	0.11 ± 0	20.15	5.5×10^{-3}
210	0.11 ± 0	20.15	5.5×10^{-3}
240	0.10 ± 0.001	20.10	5.0×10^{-3}
270	0.099 ± 0.0014	20.0	5.0×10^{-3}
300	0.096 ± 0.0014	19.9	4.8×10^{-3}
330	0.091 ± 0.0014	19.8	4.6×10^{-3}
360	0.09 ± 0.0014	19.8	4.5×10^{-3}

1.4 Permeate Flux Verses Operating Pressure (Pressure Increase).

Feed Pressure (psi	Feed Pressure (bar)	Pressure Increase		Average Permeate flux (J_w) ($ml.cm^{-2}.min^{-1}$)
		Run 1 Permeate flux (J_w) ($ml.cm^{-2}.min^{-1}$)	Run 2 Permeate flux (J_w) ($ml.cm^{-2}.min^{-1}$)	
0	0	0	0	0
100	7	0	0	0
200	14	0	0	0
300	20	0.02	0.015	0.018 ± 0.001
400	27	0.041	0.039	0.040 ± 0.002
500	34	0.091	0.92	0.092 ± 0.001
600	41	0.14	0.14	0.14 ± 0

1.5 Permeate Flux Verses Operating Pressure (Pressure Decrease).

Feed Pressure (psi)	Feed Pressure (bar)	Pressure decrease		Average Permeate flux (J) ($ml.cm^{-2}.min^{-1}$)
		Run 1 Permeate flux (J) ($ml.cm^{-2}.min^{-1}$)	Run 2 Permeate flux (J) ($ml.cm^{-2}.min^{-1}$)	
600	41	0.12	0.11	0.115 ± 0
500	35	0.073	0.07	0.0715 ± 0.003
400	28	0.030	0.028	0.029 ± 0.004
300	21	0.004	0.003	0.0035 ± 0.001
200	14	0	0	0
100	7	0	0	0
0	0	0	0	0

2 Pre-filtered Raw Seawater Though Nano-alumina Filter (The North Sea).

2.1 Permeate Flow and Permeate Flux Verses Time.

Time (min)	Run 1 Q_p ($ml.min^{-1}$)	Run 2 Q_p ($ml.min^{-1}$)	Average Q_P ($ml.min^{-1}$)	$J = \frac{Q_p}{A}$ ($ml.cm^{-2}.min^{-1}$)	$J = \frac{Q_p}{A}$ ($ml.cm^{-2}.min^{-1}$)	Average J ($ml.cm^{-2}.min^{-1}$)
0	12.15	12.10	12.13 ± 0.035	0.15	0.15	0.15 ± 0
30	12.15	12.10	12.13 ± 0.035	0.15	0.15	0.15 ± 0
60	12.10	12	12.10 ± 0.071	0.15	0.15	0.15 ± 0
90	12.0	11.9	11.95 ± 0.071	0.15	0.147	0.149 ± 0.001
120	11.9	11.7	11.80 ± 0.141	0.147	0.14	0.144 ± 0.003
150	11.5	11.34	11.42 ± 0.113	0.14	0.14	0.14 ± 0
180	11.3	10.8	11.0 ± 0.354	0.13	0.13	0.13 ± 0
210	10.5	10.10	10.35 ± 0.085	0.13	0.125	0.128 ± 0.002
240	10.3	10.0	10.15 ± 0.212	0.13	0.12	0.123 ± 0.002
270	10.12	10	10.10 ± 0.085	0.125	0.12	0.12 ± 0
300	10	9.90	9.95 ± 0.021	0.12	0.12	0.12 ± 0
330	9.76	9.81	9.79 ± 0.035	0.12	0.12	0.12 ± 0
360	9.33	9.5	9.42 ± 0.120	0.115	0.12	0.118 ± 0.002

2.2 Feed (P_f), Concentrate (P_c) and Osmotic (π) Pressure Verses Time

Time (min)	P_f (bar)	P_c (bar)	P_c (bar)	ΔP (bar)	ΔP (bar)	Average ΔP bar)	π_{fc} (bar)	π_p (bar)	NDP (bar)
0	41	41	41	0	0	0	20.3	0.20	20.50
30	41	41	41	0	0	0	20.3	0.20	20.50
60	41	41	41	0	0	0	20.3	0.20	20.50
90	41	41	41	0	0	0	20.3	0.20	20.50
120	41	41	41	0	0	0	20.3	0.20	20.50
150	41	40.7	40.7	0.3	0.3	0.3 ± 0	20.3	0.20	20.35
180	41	40.7	40.7	0.3	0.3	0.3 ± 0	20.3	0.20	20.35
210	41	40.7	40.7	0.3	0.3	0.3 ± 0	20.3	0.20	20.35
240	41	40.5	40.5	0.3	0.5	0.5 ± 0	20.3	0.20	20.25
270	41	40.5	40.5	0.5	0.5	0.5 ± 0	20.3	0.20	20.25
300	41	40.5	40.5	0.5	0.5	0.5 ± 0	20.3	0.20	20.25
330	41	40.5	40.5	0.5	0.5	0.5 ± 0	20.3	0.20	20.25
360	41	40.5	40.3	0.5	0.7	0.6 ± 0.141	20.3	0.20	20.20

2.3 Permeate flux (J), Net Driven Pressure (NDP) and Mass Transfer Coefficient for Water (K_w) verses Time

Time (min)	Permeate flux (J) ($ml.cm^{-2}.min^{-1}$)	Net Driven Pressure NDP (bar)	$K_w = \frac{J}{NDP}$ ($ml.cm^{-2}.min^{-1}.bar^{-1}$)
0	0.15 ± 0	20.50	7.3×10^{-3}
30	0.15 ± 0	20.50	7.3×10^{-3}
60	0.15 ± 0	20.50	7.3×10^{-3}
90	0.149 ± 0.001	20.50	7.3×10^{-3}
120	0.144 ± 0.003	20.50	7.0×10^{-3}
150	0.14 ± 0	20.35	6.9×10^{-3}
180	0.13 ± 0	20.35	6.4×10^{-3}
210	0.128 ± 0.002	20.35	6.3×10^{-3}
240	0.123 ± 0.002	20.25	6.1×10^{-3}
270	0.12 ± 0	20.25	5.9×10^{-3}
300	0.12 ± 0	20.25	5.9×10^{-3}
330	0.12 ± 0	20.25	5.9×10^{-3}
360	0.118 ± 0.002	20.20	5.8×10^{-3}

2.4 Permeate Flux Verses Operating Pressure (Pressure Increase).

Feed Pressure (psi	Feed Pressure (bar)	Pressure Increase		Average Permeate flux (J_w) ($ml.cm^{-2}.min^{-1}$)
		Run 1 Permeate flux (J_w) ($ml.cm^{-2}.min^{-1}$)	Run 2 Permeate flux (J_w) ($ml.cm^{-2}.min^{-1}$)	
0	0	0	0	0
100	7	0	0	0
200	14	0	0	0
300	20	0.016	0.015	0.0155 ± 0.001
400	27	0.060	0.057	0.059 ± 0.002
500	34	0.096	0.98	0.097 ± 0.001
600	41	0.15	0.15	0.15 ± 0

2.5 Permeate Flux Verses Operating Pressure (Pressure Decrease).

Feed Pressure (psi)	Feed Pressure (bar)	Pressure decrease		Average Permeate flux (J) ($ml.cm^{-2}.min^{-1}$)
		Run 1 Permeate flux (J) ($ml.cm^{-2}.min^{-1}$)	Run 2 Permeate flux (J) ($ml.cm^{-2}.min^{-1}$)	
600	41	0.12	0.12	0.12 ± 0
500	35	0.084	0.080	0.082 ± 0.003
400	28	0.051	0.054	$0.052.5 \pm 0.004$
300	21	0.004	0.003	0.004 ± 0.001
200	14	0	0	0
100	7	0	0	0
0	0	0	0	0

3.0 Pre-filtered North Sea seawater through 5μm Cartridge filter.

3.1 Permeate flow and permeate flux verses time.

3.2

Time (min)	Run 1 (Q_p) ($ml.min^{-1}$)	Run 1 (Q_p) ($ml.min^{-1}$)	Average (Q_p) ($ml.min^{-1}$)	$J = \frac{Q_p}{A}$ ($ml.cm^{-2}.min^{-1}$)	$J = \frac{Q_p}{A}$ ($ml.cm^{-2}.min^{-1}$)	Average **(J)** ($ml.cm^{-2}.min^{-1}$)
0	12.1	12.1	12.1 ± 0	0.15	0.15	0.15 ± 0
30	12.1	12.1	12.1 ± 0	0.15	0.15	0.15 ± 0
60	12	12	12 ± 0	0.15	0.15	0.15 ± 0
90	11.95	11.9	11.93 ± 0.034	0.148	0.147	0.148 ± 0.001
120	11.7	11.55	11.63 ± 0.106	0.14	0.14	0.14 ± 0
150	10.9	10.8	10.85 ± 0.071	0.135	0.13	0.133 ± 0.004
180	10.5	10.4	10.45 ± 0.071	0.13	0.13	0.13 ± 0
210	10.1	9.95	10.03 ± 0.106	0.125	0.12	0.123 ± 0.004
240	9.75	9.63	9.69 ± 0.085	0.12	0.118	0.119 ± 0.001
270	9.3	9.2	9.2 ± 0.141	0.115	0.115	0.115 ± 0.001
300	9.0	8.9	8.95 ± 0.071	0.11	0.11	0.11 ± 0.0014
330	8.25	8.28	8.27 ± 0.021	0.10	0.10	0.10 ± 0.0014
360	8.15	8.10	8.13 ± 0.035	0.10	0.10	0.10 ± 0.0014

3.2 Feed (P_f), Concentrate (P_c) and Osmotic (π) Pressure Verses Time

Time (min)	P_f (bar)	P_c (bar)	P_c (bar)	ΔP (bar)	ΔP (bar)	Average ΔP bar)	π_{fc} (bar)	π_p (bar)	NDP (bar)
0	41	41	41	0	0	0	20.3	0.20	20.50
30	41	41	41	0	0	0	20.3	0.20	20.50
60	41	41	41	0	0	0	20.3	0.20	20.50
90	41	40.7	40.7	0.3	0.3	0.3 ± 0	20.3	0.20	20.35
120	41	40.7	40.5	0.3	0.4	0.35 ± 0.071	20.3	0.20	20.33
150	41	40.5	40.5	0.5	0.5	0.5 ± 0	20.3	0.20	20.25
180	41	40.5	40.5	0.5	0.5	0.5 ± 0	20.3	0.20	20.25
210	41	40.5	40.3	0.5	0.7	0.6 ± 0.141	20.3	0.20	20.15
240	41	40.3	40.5	0.5	0.5	0.6 ± 0.141	20.3	0.20	20.15
270	41	40.3	40.3	0.7	0.7	0.7 ± 0	20.3	0.20	20.15
300	41	40.3	40.3	0.7	0.7	0.7 ± 0	20.3	0.20	20.15
330	41	40	40	1.0	1.0	1.0 ± 0	20.3	0.20	20
360	41	40	40	1.0	1.0	1.0 ± 0	20.3	0.20	20

3.3 Permeate flux (J), Net Driven Pressure (NDP) and Mass Transfer Coefficient for Water (K_w) verses Time

Time (min)	Permeate flux (J) ($ml.cm^{-2}.min^{-1}$)	Net Driven Pressure NDP (bar)	$K_w = \frac{J}{NDP}$ ($ml.cm^{-2}.min^{-1}.bar^{-1}$)
0	0.15 ± 0	20.50	7.3×10^{-3}
30	0.15 ± 0	20.50	7.3×10^{-3}
60	0.15 ± 0	20.50	7.3×10^{-3}
90	0.149 ± 0.001	20.35	7.3×10^{-3}
120	0.144 ± 0.003	20.33	7.1×10^{-3}
150	0.14 ± 0	20.25	6.9×10^{-3}
180	0.13 ± 0	20.25	6.5×10^{-3}
210	0.128 ± 0.002	20.15	6.4×10^{-3}
240	0.123 ± 0.002	20.15	6.1×10^{-3}
270	0.12 ± 0	20.15	6.0×10^{-3}
300	0.12 ± 0	20.15	6.0×10^{-3}
330	0.12 ± 0	20	6.0×10^{-3}
360	0.118 ± 0.002	20	5.9×10^{-3}

3.4 Permeate Flux Verses Operating Pressure (Pressure Increase).

Feed Pressure (psi	Feed Pressure (bar)	Pressure Increase		Average Permeate flux (J_w) ($ml.cm^{-2}.min^{-1}$)
		Run 1 Permeate flux (J_w) ($ml.cm^{-2}.min^{-1}$)	Run 2 Permeate flux (J_w) ($ml.cm^{-2}.min^{-1}$)	
0	0	0	0	0
100	7	0	0	0
200	14	0	0	0
300	20	0.014	0.014	0.014 ± 0
400	27	0.041	0.057	0.085± 0.003
500	34	0.091	0.090	0.097 ± 0.001
600	41	0.15	0.15	0.15 ± 0

3.5 Permeate Flux Verses Operating Pressure (Pressure Decrease).

Feed Pressure (psi)	Feed Pressure (bar)	Pressure decrease		Average Permeate flux (J) ($ml.cm^{-2}.min^{-1}$)
		Run 1 Permeate flux (J) ($ml.cm^{-2}.min^{-1}$)	Run 2 Permeate flux (J) ($ml.cm^{-2}.min^{-1}$)	
600	41	0.11	0. 11	0.11 ± 0
500	35	0.073	0.067	0.07 ± 0.004
400	28	0.035	0.040	0.0038 ± 0.004
300	21	0.004	0.003	0.004 ± 0.001
200	14	0	0	0
100	7	0	0	0
0	0	0	0	0

4.0 Pre-filtered North Sea seawater through 1 μm filter.

4.1 Permeate flow and permeate flux verses time.

Time (min)	Run 1 Q_p ($ml.min^{-1}$)	Run 2 Q_p ($ml.min^{-1}$)	Average Q_P ($ml.min^{-1}$)	$J_w = \frac{Q_p}{A}$ ($ml.cm^{-2}.min^{-1}$)	$J_w = \frac{Q_p}{A}$ ($ml.cm^{-2}.min^{-1}$)	Average J_w ($ml.cm^{-2}.min^{-1}$)
0	12.3	12.2	12.25 ± 0.071	0.15	0.15	0.15 ± 0
30	12.3	12.2	12.25 ± 0.071	0.15	0.15	0.15 ± 0
60	12.2	12	12.10 ± 0.141	0.15	0.15	0.15 ± 0
90	12.0	12	12.0 ± 0	0.148	0.148	0.148 ± 0
120	11.9	11.6	11.75 ± 0.212	0.147	0.143	0.145 ± 0.0013
150	11.6	11.3	11.45 ± 0.212	0.14	0.14	0.14 ± 0
180	11.4	11	11.20 ± 0.283	0.14	0.13	0.138 ± 0.0017
210	10.8	10.6	10.7 ± 0.141	0.13	0.13	0.13 ± 0
240	10.5	10.1	10.3 ± 0.283	0.13	0.125	0.127 ± 0.0017
270	10	9.8	9.9 ± 0.141	0.12	0.12	0.12 ± 0
300	9.7	9.6	9.65 ± 0.071	0.12	0.12	0.12 ± 0
330	9.2	9	9.1 ± 0.141	0.11	0.11	0.11 ± 0
360	9	8.9	8.95 ± 0.071	0.11	0.11	0.11 ± 0

4.2 Feed (P_f), Concentrate (P_c) and Osmotic (π) Pressure Verses Time

Time (min)	P_f (bar)	P_c (bar)	P_c (bar)	ΔP (bar)	ΔP (bar)	Average ΔP bar)	π_{fc} (bar)	π_p (bar)	NDP (bar)
0	41	41	41	0	0	0	20.3	0.20	20.50
30	41	41	41	0	0	0	20.3	0.20	20.50
60	41	41	41	0	0	0	20.3	0.20	20.50
90	41	41	41	0	0	0	20.3	0.20	20.50
120	41	41	41	0	0	0	20.3	0.20	20.50
150	41	40.3	41	0.3	0.3	0.3 ± 0	20.3	0.20	20.35
180	41	40.3	40.3	0.3	0.3	0.3 ± 0	20.3	0.20	20.35
210	41	40.3	40.3	0.3	0.3	0.3 ± 0	20.3	0.20	20.35
240	41	40	40.3	0.5	0.5	0.5 ± 0	20.3	0.20	20.25
270	41	40	40	0.5	0.5	0.5 ± 0	20.3	0.20	20.25
300	41	40	40	0.5	0.7	0.6 ± 0.141	20.3	0.20	20.2
330	41	39.6	39.6	0.7	0.7	0.7 ± 0	20.3	0.20	20.15
360	41	39.6	39.6	0.7	0.7	0.7 ± 0	20.3	0.20	20.15

4.3 Permeate flux (J), Net Driven Pressure (NDP) and Mass Transfer Coefficient for Water (K_w) verses Time

Time (min)	Permeate flux (J) ($ml.cm^{-2}.min^{-1}$)	Net Driven Pressure NDP (bar)	$K_w = \frac{J}{NDP}$ ($ml.cm^{-2}.min^{-1}.bar^{-1}$)
0	0.15 ± 0	20.50	7.3×10^{-3}
30	0.15 ± 0	20.50	7.3×10^{-3}
60	0.15 ± 0	20.50	7.3×10^{-3}
90	0.149 ± 0.001	20.50	7.3×10^{-3}
120	0.144 ± 0.003	20.50	7.0×10^{-3}
150	0.14 ± 0	20.35	6.9×10^{-3}
180	0.13 ± 0	20.35	6.4×10^{-3}
210	0.128 ± 0.002	20.35	6.3×10^{-3}
240	0.123 ± 0.002	20.25	6.1×10^{-3}
270	0.12 ± 0	20.25	5.9×10^{-3}
300	0.12 ± 0	20.2	5.9×10^{-3}
330	0.12 ± 0	20.15	5.9×10^{-3}
360	0.118 ± 0.002	20.15	5.9×10^{-3}

4.4 Permeate Flux Verses Operating Pressure (Pressure Increase).

Feed Pressure (psi	Feed Pressure (bar)	Pressure Increase		Average Permeate flux (J_w) ($ml.cm^{-2}.min^{-1}$)
		Run 1 Permeate flux (J_w) ($ml.cm^{-2}.min^{-1}$)	Run 2 Permeate flux (J_w) ($ml.cm^{-2}.min^{-1}$)	
0	0	0	0	0
100	7	0	0	0
200	14	0	0	0.015 ± 0.0021
300	20	0.012	0.013	0.022 ± 0.0028
400	27	0.050	0.055	0.049 ± 0.0113
500	34	0.094	0.095	0.101 ± 0.0134
600	41	0.15	0.15	0.15 ± 0

4.5 Permeate Flux Verses Operating Pressure (Pressure Decrease).

Feed Pressure (psi)	Feed Pressure (bar)	Pressure decrease		Average Permeate flux (J) ($ml.cm^{-2}.min^{-1}$)
		Run 1 Permeate flux (J) ($ml.cm^{-2}.min^{-1}$)	Run 2 Permeate flux (J) ($ml.cm^{-2}.min^{-1}$)	
600	41	0.12	0.12	0.12 ± 0
500	35	0.075	0.072	0.070 ± 0.0042
400	28	0.040	0.045	0.03 ± 0
300	21	0.004	0.003	0.0035 ± 0.0016
200	14	0	0	0
100	7	0	0	0
0	0	0	0	0

5.0 Pre-filtered North Sea seawater through 1 μm filter followed by nano-alumina filter.

5.1 Permeate flow and permeate flux verses time.

Time (min)	Run 1 Q_p ($ml.min^{-1}$)	Run 2 Q_p ($ml.min^{-1}$)	Average Q_P ($ml.min^{-1}$)	$J_w = \frac{Q_p}{A}$ ($ml.cm^{-2}.min^{-1}$)	$J_w = \frac{Q_p}{A}$ ($ml.cm^{-2}.min^{-1}$)	Average J_w ($ml.cm^{-2}.min^{-1}$)
0	12.47	12.5	12.49 ± 0.021	0.15	0.15	0.15 ± 0
30	12.47	12.5	12.49 ± 0.021	0.15	0.15	0.15 ± 0
60	12.3	12.4	12.35 ± 0.071	0.15	0.15	0.15 ± 0
90	12.2	12.3	12.25 ± 0.071	0.15	0.15	0.15 ± 0
120	12.2	12.1	12.15 ± 0.071	0.15	0.15	0.15 ± 0
150	11.46	11.7	11.58 ± 0.170	0.14	0.14	0.14 ± 0
180	11.31	11.35	11.43 ± 0.170	0.14	0.14	0.14 ± 0
210	11.27	11.3	11.29 ± 0.021	0.14	0.14	0.14 ± 0
240	11.2	11.2	11.2 ± 0	0.138	0.138	0.138 ± 0
270	11.2	11.1	11.15 ± 0.071	0.138	0.137	0.138 ± 0.001
300	11.1	11.0	11.05 ± 0.071	0.137	0.136	0.137 ± 0.001
330	10.9	10.8	10.8 ± 0	0.135	0.13	0.13 ± 0
360	10.8	10.7	10.7 ± 0.071	0.13	0.13	0.13 ± 0

5.2 Feed (P_f), Concentrate (P_c) and Osmotic (π) Pressure Verses Time

Time (min)	P_f (bar)	P_c (bar)	P_c (bar)	ΔP (bar)	ΔP (bar)	Average ΔP bar)	π_{fc} (bar)	π_p (bar)	NDP (bar)
0	41	41	41	0	0	0	20.3	0.20	20.50
30	41	41	41	0	0	0	20.3	0.20	20.50
60	41	41	41	0	0	0	20.3	0.20	20.50
90	41	41	41	0	0	0	20.3	0.20	20.50
120	41	41	41	0	0	0	20.3	0.20	20.50
150	41	40.7	40.7	0.3	0.3	0.3 ± 0	20.3	0.20	20.35
180	41	40.7	40.7	0.3	0.3	0.3 ± 0	20.3	0.20	20.35
210	41	40.7	40.7	0.3	0.3	0.3 ± 0	20.3	0.20	20.35
240	41	40.7	40.7	0.3	0.3	0.3 ± 0	20.3	0.20	20.35
270	41	40.7	40.5	0.3	0.5	0.4 ± 0.141	20.3	0.20	20.30
300	41	40.5	40.5	0.5	0.5	0.5 ± 0	20.3	0.20	20.25
330	41	40.5	40.5	0.5	0.5	0.5 ± 0	20.3	0.20	20.25
360	41	40.5	40.5	0.5	0.5	0.5 ± 0	20.3	0.20	20.25

5.3 Permeate flux (J), Net Driven Pressure (NDP) and Mass Transfer Coefficient for Water (K_w) verses Time

Time (min)	Permeate flux (J) ($ml.cm^{-2}.min^{-1}$)	Net Driven Pressure NDP (bar)	$K_w = \frac{J}{NDP}$ ($ml.cm^{-2}.min^{-1}.bar^{-1}$)
0	0.15 ± 0	20.50	7.3×10^{-3}
30	0.15 ± 0	20.50	7.3×10^{-3}
60	0.15 ± 0	20.50	7.3×10^{-3}
90	0.15 ± 0	20.50	7.3×10^{-3}
120	0.15 ± 0	20.50	7.3×10^{-3}
150	0.14 ± 0	20.35	6.9×10^{-3}
180	0.14 ± 0	20.35	6.9×10^{-3}
210	0.14 ± 0	20.35	6.8×10^{-3}
240	0.138 ± 0	20.35	6.8×10^{-3}
270	0.138 ± 0.001	20.30	6.8×10^{-3}
300	0.137 ± 0.001	20.25	6.8×10^{-3}
330	0.13 ± 0	20.25	6.4×10^{-3}
360	0.13 ± 0	20.25	6.4×10^{-3}

5.4 Permeate Flux Verses Operating Pressure (Pressure Increase).

Feed Pressure (psi	Feed Pressure (bar)	Pressure Increase		Average Permeate flux (J_w) ($ml.cm^{-2}.min^{-1}$)
		Run 1 Permeate flux (J_w) ($ml.cm^{-2}.min^{-1}$)	Run 2 Permeate flux (J_w) ($ml.cm^{-2}.min^{-1}$)	
0	0	0	0	0
100	7	0	0	0
200	14	0	0	0
300	20	0.016	0.016	0.016 ± 0
400	27	0.065	0.068	0.067 ± 0.0021
500	34	0.097	0.099	0.098 ± 0.0021
600	41	0.15	0.15	0.15 ± 0

5.5 Permeate Flux Verses Operating Pressure (Pressure Decrease).

Feed Pressure (psi)	Feed Pressure (bar)	Pressure decrease		Average Permeate flux (J) ($ml.cm^{-2}.min^{-1}$)
		Run 1 Permeate flux (J) ($ml.cm^{-2}.min^{-1}$)	Run 2 Permeate flux (J) ($ml.cm^{-2}.min^{-1}$)	
600	41	0.13	0.13	0.13 ± 0
500	35	0.086	0.090	0.088 ± 0.003
400	28	0.055	0.060	0.058 ± 0.004
300	21	0.005	0.004	0.0045 ± 0.001
200	14	0	0	0
100	7	0	0	0
0	0	0	0	0

6.0 Pre-filtered North Sea seawater through 5 µm filter followed by nano-alumina filter.

6.1 Permeate flow and permeate flux verses time.

Time (min)	Run 1 Q_p ($ml.min^{-1}$)	Run 2 Q_p ($ml.min^{-1}$)	Average Q_P ($ml.min^{-1}$)	$J_w = \frac{Q_p}{A}$ ($ml.cm^{-2}.min^{-1}$)	$J_w = \frac{Q_p}{A}$ ($ml.cm^{-2}.min^{-1}$)	Average J_w ($ml.cm^{-2}.min^{-1}$)
0	12.53	12.4	12.47 ± 0.092	0.15	0.15	0.15 ± 0
30	12.46	12.4	12.43 ± 0.042	0.15	0.15	0.15 ± 0
60	12.23	12.4	12.22 ± 0.021	0.15	0.15	0.15 ± 0
90	12.2	12	12.1 ± 0.141	0.15	0.148	0.15 ± 0
120	11.8	11.9	11.85 ± 0.071	0.146	0.147	0.147 ± 0.003
150	11.7	11.8	11.75 ± 0.071	0.14	0.146	0.14 ± 0
180	11.6	11.65	11.66 ± 0.141	0.14	0.14	0.14 ± 0
210	11.53	11.4	11.47 ± 0.092	0.14	0.14	0.14 ± 0
240	11.41	11.3	11.36 ± 0.078	0.14	0.14	0.139 ± 0.004
270	11.14	11.1	11.12 ± 0.078	0.138	0.137	0.138 ± 0.001
300	11	10.9	10.95 ± 0.071	0.136	0.136	0.136 ± 0
330	10.94	10.8	10.87 ± 0.099	0.135	0.13	0.133 ± 0.004
360	10.74	10.65	10.70 ± 0.064	0.13	0.13	0.13 ± 0

6.2 Feed (P_f), Concentrate (P_c) and Osmotic (π) Pressure Verses Time

Time (min)	P_f (bar)	P_c (bar)	P_c (bar)	ΔP (bar)	ΔP (bar)	Average ΔP bar)	π_{fc} (bar)	π_p (bar)	NDP (bar)
0	41	41	41	0	0	0	20.3	0.20	20.50
30	41	41	41	0	0	0	20.3	0.20	20.50
60	41	41	41	0	0	0	20.3	0.20	20.50
90	41	41	41	0	0	0	20.3	0.20	20.50
120	41	41	41	0	0	0	20.3	0.20	20.50
150	41	40.7	40.7	0.3	0.3	0.3 ± 0	20.3	0.20	20.35
180	41	40.7	40.7	0.3	0.3	0.3 ± 0	20.3	0.20	20.35
210	41	40.7	40.7	0.3	0.3	0.3 ± 0	20.3	0.20	20.35
240	41	40.7	40.7	0.3	0.3	0.3 ± 0	20.3	0.20	20.35
270	41	40.7	40.5	0.3	0.5	0.4 ± 0.141	20.3	0.20	20.30
300	41	40.5	40.5	0.5	0.5	0.5 ± 0	20.3	0.20	20.25
330	41	40.5	40.5	0.5	0.5	0.5 ± 0	20.3	0.20	20.25
360	41	40.5	40.5	0.5	0.5	0.5 ± 0	20.3	0.20	20.25

6.3 Permeate flux (J), Net Driven Pressure (NDP) and Mass Transfer Coefficient for Water (K_w) verses Time

Time (min)	Permeate flux (J) ($ml.cm^{-2}.min^{-1}$)	Net Driven Pressure NDP (bar)	$K_w = \frac{J}{NDP}$ ($ml.cm^{-2}.min^{-1}.bar^{-1}$)
0	0.15 ± 0	20.50	7.3×10^{-3}
30	0.15 ± 0	20.50	7.3×10^{-3}
60	0.15 ± 0	20.50	7.3×10^{-3}
90	0.15 ± 0	20.50	7.3×10^{-3}
120	0.15 ± 0	20.50	7.3×10^{-3}
150	0.14 ± 0	20.35	6.9×10^{-3}
180	0.14 ± 0	20.35	6.9×10^{-3}
210	0.14 ± 0	20.35	6.8×10^{-3}
240	0.138 ± 0	20.35	6.8×10^{-3}
270	0.138 ± 0.001	20.30	6.8×10^{-3}
300	0.137 ± 0.001	20.25	6.8×10^{-3}
330	0.13 ± 0	20.25	6.4×10^{-3}
360	0.13 ± 0	20.25	6.4×10^{-3}

6.4 Permeate Flux Verses Operating Pressure (Pressure Increase).

Feed Pressure (psi	Feed Pressure (bar)	Pressure Increase		Average Permeate flux (J_w) ($ml.cm^{-2}.min^{-1}$)
		Run 1 Permeate flux (J_w) ($ml.cm^{-2}.min^{-1}$)	Run 2 Permeate flux (J_w) ($ml.cm^{-2}.min^{-1}$)	
0	0	0	0	0
100	7	0	0	0
200	14	0	0	0
300	20	0.016	0.015	0.016 ± 0
400	27	0.060	0.055	0.045 ± 0.004
500	34	0.098	0.11	0.104 ± 0.006
600	41	0.15	0.15	0.15 ± 0

6.5 Permeate Flux Verses Operating Pressure (Pressure Decrease).

Feed Pressure (psi)	Feed Pressure (bar)	Pressure decrease		Average Permeate flux (J) ($ml.cm^{-2}.min^{-1}$)
		Run 1 Permeate flux (J) ($ml.cm^{-2}.min^{-1}$)	Run 2 Permeate flux (J) ($ml.cm^{-2}.min^{-1}$)	
600	41	0.13	0.13	0.13 ± 0
500	35	0.086	0.080	0.083 ± 0.004
400	28	0.050	0.055	0.055 ± 0.007
300	21	0.005	0.004	0.0045 ± 0.001
200	14	0	0	0
100	7	0	0	0
0	0	0	0	0

7.0 Normalised Permeate Flux (J/J_0)

$$J_N = \left(1 - \frac{J}{J_0}\right)$$

Where:

J_N – is the actual permeate flux ($ml.cm^{-2}.min^{-1}$)

J – is the actual permeate flux ($ml.cm^{-2}.min^{-1}$)

J0 – is the initial permeate flux ($ml.cm^{-2}.min^{-1}$)

7.1 – Normalised permeate flux for raw and pre-filtered seawater

Time	RSW	Pre-filtered Nano-alumina filter	Pre-filtered 5µm filter	Pre-filtered 1µm filter	Pre-filtered 5µm + nano-alumina filter	Pre-filtered 1 µm nano-alumina filter
0	1	1	1	1	1	1
30	1	1	1	1	1	1
60	0.93	1	1	1	1	1
90	0.93	0.99	0.99	0.99	0.99	1
120	0.86	0.96	0.93	0.96	0.98	1
150	0.86	0.93	0.89	0.93	0.93	0.93
180	0.79	0.87	0.87	0.92	0.93	0.93
210	0.79	0.85	0.82	0.87	0.93	0.93
240	0.71	0.82	0.79	0.85	0.93	0.92
270	0.71	0.8	0.77	0.8	0.92	0.92
300	0.69	0.8	0.73	0.8	0.91	0.91
330	0.65	0.8	0.67	0.73	0.87	0.87
360	0.64	0.79	0.67	0.73	0.87	0.87

8.0 Culturable Plate Count

$$Concentration\ of\ bacteria\ in\ water\ sample = \frac{Average\ plate\ count \times Overall\ diluution\ factor}{volume\ (0.1\ ml)} = CFU.ml^{-1}$$

Water sample	Plate 1	Plate 2	Plate 3	Average
Raw seawater	73	71	90	78 ± 10.44
Pre-filtered (Nano-alumina filter)	2	1	3	2 ± 1.0

- **Raw seawater**

$$CFU = \frac{78}{0.1} = 780 = CFU.ml^{-1}$$

- **Pre-filtered through nano-alumina filter**

$$CFU = \frac{2}{0.1} = 20 = CFU.ml^{-1}$$

9.0 – TEP Measurements

Water sample	Number of TEP particles in 20 images
Raw seawater	120
Pre-filtered (Nano-alumina filter)	24

$$R(\%) = \frac{N_{(RSW)} - N_{(PSW)}}{N_{(RSW)}} \times 100\%$$

Where:

R (%) – rejection of TEP particles

N(RSW) – is the number of TEP particles in raw seawater

N(PSW) – is the number of TEP particles in pre-filtered seawater through the nano-alumina filter

$$R(\%) = \frac{120 - 24}{120} \times 100\% = 80\%$$

10.0 Contact Angle Measurements

10.1 New Toray SWRO Membrane

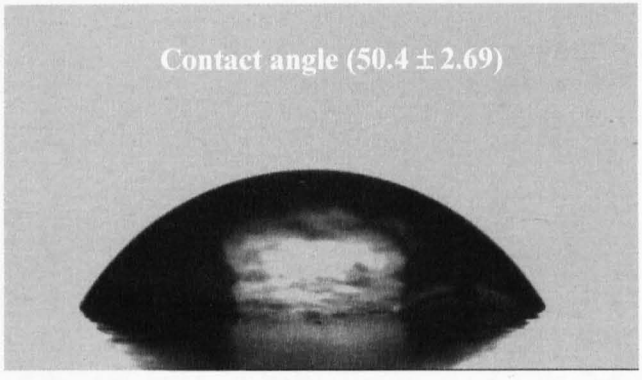

10.2 Fouled Toray SWRO Membrane by Raw Seawater (The North Sea)

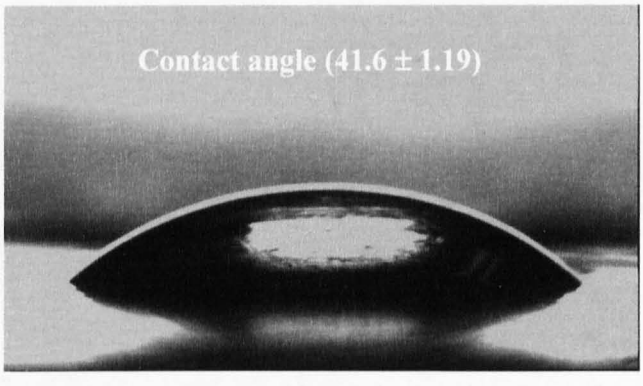

10.3 Fouled Toray SWRO Membrane by Pre-filtered Seawater through nano-alumina filter (The North Sea).